

**The biosynthesis of plant and fungal sesquiterpenoids in *Ustilago maydis*  
and discovery of a bioactive compound from *Fistulina hepatica***

Inaugural-Dissertation

Zur Erlangung des Doktorgrades  
der Mathematisch-Naturwissenschaftlichen Fakultät  
der Heinrich-Heine-Universität Düsseldorf

vorgelegt von

**Jungho Lee**  
aus Daegu

Düsseldorf, September 2020

aus dem Institut für Mikrobiologie  
der Heinrich-Heine-Universität Düsseldorf

Gedruckt mit der Genehmigung der  
Mathematisch-Naturwissenschaftlichen Fakultät der  
Heinrich-Heine-Universität Düsseldorf

Referent: Prof. Dr. Michael Feldbrügge  
Korreferent : Prof. Dr. Julia Frunzke  
Tag der mündlichen Prüfung: 26. Oktober 2020

### **Eidesstattliche Erklärung**

Ich versichere an Eides Statt, dass die Dissertation von mir selbständig und ohne unzulässige fremde Hilfe unter Beachtung der „Grundsätze zur Sicherung guter wissenschaftlicher Praxis an der Heinrich-Heine-Universität Düsseldorf“ erstellt worden ist. Die Dissertation wurde in ihrer jetzigen oder einer ähnlichen Form noch bei keiner anderen Hochschule eingereicht. Ich habe zuvor keine erfolglosen Promotionsversuche unternommen.

---

Ort, Datum

---

Unterschrift

Die Untersuchungen zur vorliegenden Arbeit wurden von Oktober 2016 bis September 2020 in Düsseldorf an der Heinrich-Heine-Universität in dem Institut für Mikrobiologie unter der Betreuung von Herrn Prof. Dr. Michael Feldbrügge durchgeführt.

Teile dieser Arbeit wurden veröffentlicht in:

Lee, J., Hilgers, F., Loeschke, A., Jaeger, K. E., Feldbrügge, M., 2020, *Ustilago maydis* serves as a novel production host for the synthesis of plant and fungal sesquiterpenoids. *Frontiers in Microbiology* 11, 1655.

Lee, J., Shi, Y., Grün, P., Gube, M., Feldbrügge, M., Bode, H. B., Hennicke, F., 2020, Identification of feldin, an antifungal polyine from the beefsteak fungus *Fistulina hepatica*. *Biomolecules* 10, 1502.



## Summary

Sesquiterpenoids are important secondary metabolites with various pharma- and nutraceutical properties. The precursor of all terpenoids is isopentenyl diphosphate (IPP) and can be, e.g., obtained through the mevalonate (MVA) pathway in higher basidiomycetes. From an industrial point of view, there is a high interest in using microbial systems to produce these bioactive compounds. In particular, higher basidiomycetes possess a versatile biosynthetic repertoire for sesquiterpenoids. A promising production host is the model fungus *Ustilago maydis*. It offers the advantage of metabolic compatibility and potential tolerance for substances toxic to other microorganisms. Therefore, the development of the cell factory concept to expand the production repertoire in *U. maydis* was the objective of this study.

*U. maydis* was established as a novel production host for the synthesis of plant and fungal sesquiterpenoids. Investigation of the genes encoding enzymes of the MVA pathway revealed that the relevant enzyme Aat1 localizes to the peroxisomes despite the absence of a canonical peroxisomal targeting signal. Overexpressing MVA pathway genes resulted in increased lycopene levels. Therefore, a heterologous pathway was successfully implemented to produce lycopene that served as a straightforward read-out for precursor pathway engineering. By expressing heterologous genes encoding the plant (+)-valencene synthase CnVS and the basidiomycete sesquiterpenoid synthase Cop6, (+)-valencene and  $\alpha$ -cuprenene were successfully produced, respectively. Notably, the fungal compound yielded about tenfold higher titers in comparison to the plant substance. This proof of principle demonstrates that *U. maydis* can serve as a promising novel chassis for the production of terpenoids.

To expand the production repertoire in *U. maydis*, fungal bioactive compounds were explored. Mushroom-forming basidiomycetes from the subphylum Agaricomycotina evolve efficient chemical defense mechanisms to maintain their ecological fitness against antagonists. A plethora of bioactive compounds have been characterized from Agaricomycotina. However, a few of them are made it into development as agrochemicals or pharmaceutical lead structures. It was hypothesized that some of their antimicrobial compounds might be more active against ascomycetes like *Saccharomyces cerevisiae* than against *U. maydis* due to its relatedness with higher basidiomycetes. To identify fungal bioactive compounds against which *U. maydis* may possess a higher tolerance, initially, ethyl acetate crude extracts from mycelial cultures of thirty-five basidiomycete mushroom species were screened for antifungal bioactivity. By this, one extract from the mycelial culture of the wood-decaying edible mushroom *Fistulina hepatica* inhibited the growth of *S. cerevisiae* much stronger than the one of *U. maydis*. To identify the respective bioactive compound(s), bioactivity-guided HPLC/MS fractionation and purification were performed. NMR-based structure elucidation of a bioactive isolate yielded a new polyene displaying prominent antifungal bioactivity against *S. cerevisiae*.

### Zusammenfassung

Sesquiterpenoide sind wichtige Sekundärmetaboliten mit zahlreichen pharmazeutischen und nutrazeutischen Eigenschaften. Der Vorläufer aller Terpenoide ist Isopentenylidiphosphat (IPP) und wird z. B. im Mevalonat (MVA)-Pfad der höheren Basidiomyceten synthetisiert. Aus industrieller Hinsicht besteht ein großes Interesse mikrobielle Systeme zur Herstellung von bioaktiven Verbindungen zu nutzen. Insbesondere höhere Basidiomyceten besitzen ein vielseitiges biosynthetisches Repertoire für Terpenoide. Ein vielversprechender Produktionswirt ist der Modellpilz *Ustilago maydis*. Dieser Pilz hat den Vorteil der metabolischen Kompatibilität und der potentiellen Toleranz gegenüber Substanzen, die für andere Mikroorganismen toxisch sind. Aus diesem Grund war die Entwicklung des Zellfabrikkonzepts zur Erweiterung des Produktionsrepertoires in *U. maydis* das Ziel der vorliegenden Studie.

Zunächst wurde *U. maydis* als neuartiger Produktionswirt für die Synthese von pflanzlichen und pilzlichen Sesquiterpenoiden etabliert. Die Untersuchung der Gene die für die Enzyme des MVA-Weges kodieren ergab, dass sich das relevante Enzym Aat1, trotz des Fehlens eines peroxisomalen Zielsignals, in den Peroxisomen lokalisierte. Die Überexpression der Gene des MVA-Weges, führten zu Erhöhung des Lycopinspiegels. Durch die Implementierung eines heterologen Pfades, konnte diese Erhöhung zum Auslesen der Überexpression der Vorläufergene genutzt werden. Die Expression der Gene, die für die pflanzliche (+)-Valencensynthase CnVS und die Basidiomyceten Sesquiterpenoidsynthase Cop6 kodieren, führten sowohl zur Produktion von (+)-Valencen als auch  $\alpha$ -Cuprenen. Im Vergleich zu der pflanzlichen Verbindung, war der Titer der pilzlichen Verbindung etwa zehnmal höher. Somit konnte gezeigt werden, dass *U. maydis* als ein vielversprechender, neuartiger Wirt für die Herstellung von Terpenoiden dienen kann.

Um das Produktionsrepertoire in *U. maydis* zu erweitern, wurden bioaktive Pilzverbindungen untersucht. Fruchtkörper-bildende Basidiomyceten aus dem Subphylum der Agaricomycotina nutzen chemische Abwehrmechanismen, um ihre ökologische Fitness gegen Antagonisten aufrechtzuerhalten. Aus Agaricomycotina ist daher eine Vielzahl von diesen bioaktiver Verbindungen charakterisiert, wovon einige wenige zu Agrochemikalien oder pharmazeutischen Leitstrukturen entwickelt wurden. Aufgrund ihrer Basidiomyceten-spezifischen Herkunft wurde vermutet, dass einige antimikrobielle Verbindung aktiver gegen Ascomyceten wie z. B. *Saccharomyces cerevisiae* sein als gegenüber *U. maydis* sein sollten. Um solche bioaktiven Pilzverbindungen zu identifizieren, wurden zunächst Ethylacetat-Rohextrakte, aus Myzelkulturen von 35 Basidiomyceten-Pilzarten, auf ihre antimykotische Aktivität hin untersucht. Dabei hemmte ein Extrakt, aus der Myzelkultur des Eichen-Leberreischlings *Fistulina hepatica*, das Wachstum von *S. cerevisiae* viel stärker als das von *U. maydis*. Die Identifizierung dieser Verbindung erfolgte mittels einer bioaktivitätsgesteuerter HPLC/MS-Fraktionierung und Reinigung. Die NMR-basierte Strukturaufklärung eines bioaktiven Isolats ergab ein neues Polyin mit ausgeprägter antimykotischer Bioaktivität gegen *S. cerevisiae*.

## List of abbreviations

$\alpha$	Anti or alpha	kb	Kilobases
aa	Amino acid	kDa	Kilodalton
ATCC	American Type Culture Collection	L	Liter
ATP	Adenosine triphosphate	LB	Lysogeny broth
AMP	Adenosine monophosphate	M	Molar
Amp	Ampicillin	m	Meter
bp	Basepair	MEP	Methylethritol phosphate
BSA	Bovine serum albumin	mg	Milligram
°C	Degree Celsius	min	Minute
CAZymes	Carbohydrate-active enzymes	$\mu$ L	Microliter
cbx	Carboxin	$\mu$ m	Micrometer
C-terminus	Carboxyl-terminus	mL	Milliliter
CM	Complete medium	mM	Millimolar
CHO	Chinese hamster ovary	mol	Mole
$\Delta$	Deletion	mRNA	Messenger RNA
ddH <sub>2</sub> O	Double distilled water	MVA	Mevalonate
DF	Downstream flank	NADPH	Nicotinamide adenine dinucleotide phosphate
DIC	Differential interference contrast	NatR	Nourseothricin resistance
DIG	Digoxigenin	NES	Nuclear export signal
DNA	Deoxyribonucleic acid	NM	Nitrate minimal medium
dNTP	Doxynucleotide triphosphate	NMR	Nuclear magnetic resonance
eGfp	Enhanced green fluorescent protein	N-terminus	Amino-terminus
et al.	And others	OD	Optical density
ER	Endoplasmic reticulum	ORF	Open reading frame
FLP	Flippase recombinase	PCR	Polymerase chain reaction
FPP	Farnesyl-PP	PDA	Potato dextrose agar
FRT	FLP recognition target	ppm	Parts per million
fw	Forward	PTS	Peroxisomal targeting signal
g	Gram	RFU	Relative fluorescence unit(s)
GC-FID	Gas Chromatography-Flame Ionization Detector	RNA	Ribonucleic acid
GC-MS	Gas Chromatography-Mass Spectrometry	rpm	Rounds per minute
gDNA	Genomic DNA	rv	Reverse
Gent	Gentamycin	s	Second
Glc	Glucose	SDS	Sodium dodecyl sulfate
GOI	Gene-of-interest	UF	Upstream flank
h	Hour	UV	Ultraviolet
HA	Hemagglutinin	V	Voltage
HPLC	High Performance Liquid Chromatography	v/v	Volume by volume
Hyg	Hygromycin B	$\lambda$	Wavelength
Hz	Hertz	$\lambda_{\max}$	Wavelength of maximum absorption
i.e.	That is	w/v	Weight by volume
ip	Iron-sulfur protein	wt	Wildtype

**Table of contents**

Summary .....	I
Zusammenfassung .....	II
List of abbreviations .....	III
1 Introduction .....	1
1.1 Terpenoids and relevant biosynthetic pathways.....	1
1.1.1 Carotenoids and the biosynthesis .....	2
1.1.1.1 Fungal carotenoid pathway .....	4
1.1.1.2 Opsins in fungi .....	5
1.2 Production of natural terpenoids .....	7
1.2.1 Plant terpenoids and biotechnology .....	7
1.2.2 Value-added fungal terpenoids and their biosynthesis in higher basidiomycetes .....	9
1.2.3 Fungal terpenoid production in biotechnology and its challenges .....	12
1.3 Importance of discovery of novel bioactive compounds and elevation of the demands .....	15
1.3.1 Basidiomycota, rich sources for discovery of bioactive compounds .....	16
1.3.2 The basidiomycete fungus <i>Fistulina hepatica</i> .....	17
1.4 <i>Ustilago maydis</i> , a model organism from basic research to biotechnological applications.....	17
1.4.1 From a natural producer to a cell factory of value-added compounds.....	19
1.5 Aim of this study .....	22
2 Results.....	23
2.1 Part 1 <i>U. maydis</i> serves as a novel production host for the synthesis of plant and fungal sesquiterpenoids.....	23
2.1.1 <i>U. maydis</i> contains an evolutionarily conserved FPP pathway.....	23
2.1.2 Establishing the production of lycopene in <i>U. maydis</i> as an indicator of carotenoid precursors .....	31
2.1.3 Metabolic engineering of the mevalonate module monitored by lycopene production .....	33
2.1.4 The subcellular localization of enzymes involved in FPP synthesis.....	36
2.1.5 The heterologous production of the plant sesquiterpenoid synthase CnVS in <i>U. maydis</i> ..	38
2.1.6 The recombinant production of the plant sesquiterpenoid (+)-valencene in <i>U. maydis</i> .....	39
2.1.7 The heterologous production of the fungal sesquiterpenoid synthase Cop6 in <i>U. maydis</i> ..	41
2.1.8 The recombinant production of the fungal sesquiterpenoid $\alpha$ -cuprenene in <i>U. maydis</i> ....	42
2.2 Part 2 Identification of feldin, an antifungal polyine from the beefsteak fungus <i>Fistulina hepatica</i> .....	44
2.2.1 Bioactivity tests with ethyl acetate extracts from 35 basidiomycete mushroom species ...	44
2.2.2 Characteristics of <i>Fistulina hepatica</i> .....	45
2.2.3 Identification of the new antifungal polyine feldin from basidiomycete extract BE05 .....	47
3 Discussion .....	49
3.1 Part 1 <i>U. maydis</i> serves as a novel production host for the synthesis of plant and fungal sesquiterpenoids.....	49
3.1.1 Establishing lycopene production as molecular read-out, reflecting internal FPP levels...	49

## Table of contents

3.1.2 Genetic engineering for higher biosynthesis of FPP .....	50
3.1.3 Subcellular localization of the mevalonate pathway enzymes .....	51
3.1.4 The heterologous production of plant and fungal sesquiterpenoids in <i>U. maydis</i> .....	53
3.1.4.1 Two main strategies to improve sesquiterpenoid production .....	54
3.1.4.2 Essential metabolic engineering to increase FPP levels for sesquiterpenoid production .....	56
3.1.4.3 Future study to produce value-added sesquiterpenoid scaffolds in <i>U. maydis</i> .....	56
3.2 Part 2 Identification of feldin, an antifungal polyine from the beefsteak fungus <i>Fistulina hepatica</i> .....	57
3.2.1 High potentials of bioactive polyines from plants and fungi for drug discovery .....	57
3.2.2 Instability of polyines and a possible solution for stabilizing .....	58
3.2.3 A potential biosynthetic route for feldin and <i>U. maydis</i> as a novel heterologous production host .....	59
3.3 Conclusion and outlook.....	60
4 Materials and Methods.....	62
4.1 Materials .....	62
4.1.1 Chemicals, enzymes, and kits .....	62
4.1.1.1 Chemicals .....	62
4.1.1.2 Enzymes and kits .....	62
4.1.2 Solutions and media .....	63
4.1.2.1 For cultivation of <i>E. coli</i> .....	63
4.1.2.2 For cultivation of <i>U. maydis</i> .....	64
4.1.2.3 Strain maintenance .....	65
4.1.3 Oligonucleotides .....	65
4.1.4 Plasmids for <i>U. maydis</i> strain generation.....	66
4.1.5 Strains .....	73
4.2 Methods.....	76
4.2.1 Molecular biology methods .....	76
4.2.2 Microbiological methods .....	80
4.2.2.1 Microbiological work with <i>E. coli</i> .....	80
4.2.2.2 Microbiological work with <i>U. maydis</i> .....	81
4.2.2.3 Microbiological work with higher basidiomycete fungi .....	84
4.2.3 Biochemical methods .....	86
4.2.4 Bioinformatics .....	90
4.2.5 Computer programs.....	91
5 References .....	92
6 Appendix.....	113

## 1 Introduction

### 1.1 Terpenoids and relevant biosynthetic pathways

Terpenoids (isoprenoids) constitute the largest class of natural products and an important class of secondary metabolites in the three domains of life (bacteria, archaea, and eukaryotes; Lombard and Moreira, 2011). In nature, over 40,000 structurally diverse terpenoids have been found that have a wide range of attractive ecological, physiological, and structural functions (McGarvey and Croteau, 1995; Withers and Keasling, 2007). Terpenoids exhibit a plethora of biological functions like photoprotection, hormone signaling, and defense against pathogens (Schmidt-Dannert, 2015; Troost et al., 2019). Because of these diverse bioactivities, they are also of interest to biotechnology. Artemisinin, for example, functions as an anti-malarial drug (Paddon et al., 2013). In addition, diverse carotenoids are found in natural sources and used as natural food additives (Schempp et al., 2018).

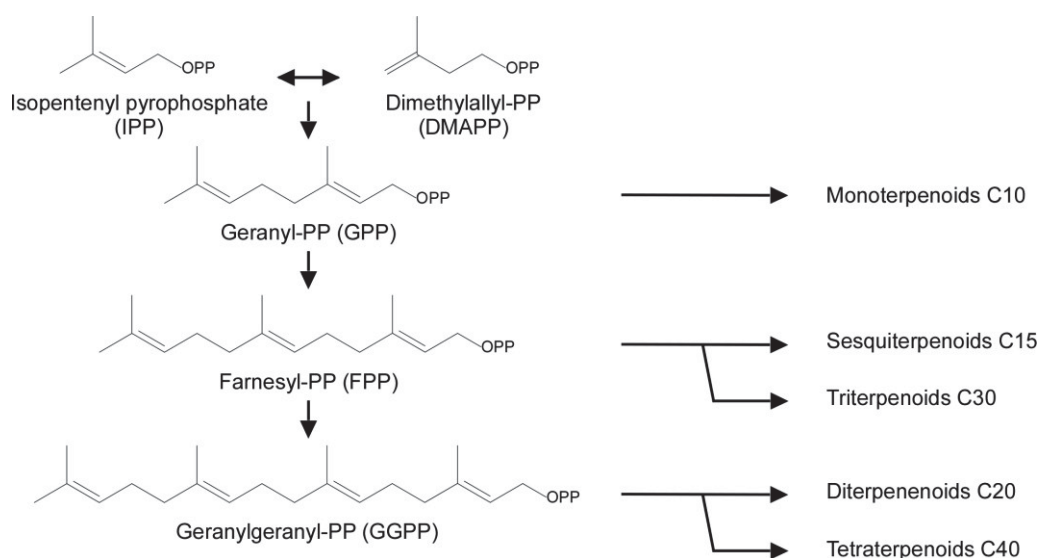


**Figure 1.1 Schematic representation of terpenoid classification and the biosynthesis.**

The secondary metabolites are indicated with the arrowheads representing the reactions. The numbers of carbon in each class of terpenoids are indicated in the round brackets. Monoterpenoids are derived from geranyl-PP (GPP). Farnesyl-PP (FPP) is the precursor of sesquiterpenoids and triterpenoids. Diterpenoids and tetraterpenoids (mainly carotenoids) are derived from geranylgeranyl-PP (GGPP). The figure is modified from Frohwitter et al., 2014.

Various terpenoids are classified according to the number of C5 scaffold isopentenyl diphosphate (IPP) building blocks. Sesquiterpenoids, for example, contain three and diterpenoids consist of four of such building blocks, forming C15 and C20 scaffolds, respectively (Figure 1.1; Withers and Keasling, 2007; Frohwitter et al., 2014). Two independent metabolic pathways can synthesize two terpenoid precursors, IPP and dimethylallyl diphosphate (DMAPP). Evolutionarily eukaryotes and prokaryotes have developed and adapted either the mevalonate (MVA) pathway or the methylerythritol phosphate (MEP) pathway to synthesize terpenoids and diverse secondary metabolites (Lombard and Moreira, 2011). In general, the MVA pathway is found in eukaryotes and archaea, whereas the MEP pathway is considered characteristic in bacteria (Boucher et al., 2004;



Lange et al., 2000; Lombard and Moreira, 2011). However, there are exceptions. For example, some bacteria possess the MVA pathway as the primary route of IPP and DMAPP synthesis (Voynova et al., 2004; Steussy et al., 2006). In addition, plants and photosynthetic eukaryotes contain the MEP pathway together with the MVA pathway (Sapir-Mir et al., 2008; Lombard and Moreira, 2011). Although the final metabolites are IPP and DMAPP in both pathways, the starting points are different. The MVA pathway starts from the condensation reaction of two molecules of acetyl-CoA to synthesize acetoacetyl-CoA by acetyl-CoA C-acetyltransferase. In contrast, the MEP pathway begins the conversion reaction of glyceraldehyde-3-phosphate (GAP) and pyruvate to 1-deoxy-D-xylulose 5-phosphate (DXP) and carbon dioxide, which is catalyzed by DOXP synthase (DXS; Troost et al., 2019; Li et al., 2020). Two biosynthetic pathways were compared in terms of carbon stoichiometry for synthesizing 1 mol of IPP from glucose (Figure 1.2; Gruchattka et al., 2013).

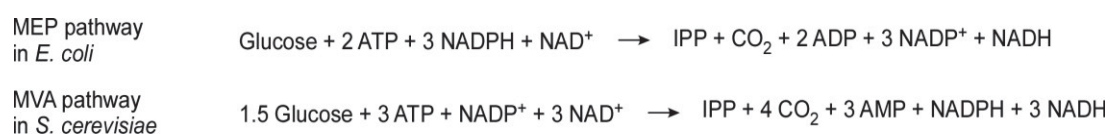


**Figure 1.2 Carbon stoichiometry of MEP pathway and MVA pathway.**

Comparison of carbon stoichiometry for synthesizing 1 mol of IPP from glucose between two microbial model organisms having either the MEP pathway (*E. coli*) or the MVA pathway (*S. cerevisiae*). The information is adapted from Gruchattka et al., 2013 and Schempp et al., 2018.

The MEP pathway in *E. coli* consumes 1 mol of glucose to generate 1 mol of IPP and only releases 1 mol of CO<sub>2</sub>. However, the MVA pathway in *S. cerevisiae* needs 1.5 mol of glucose to generate 1 mol of IPP and releases 4 mol of CO<sub>2</sub>. According to this calculation, the MEP pathway has a higher carbon efficiency, whereas the MVA pathway is more energy efficient. The MVA pathway regenerates a higher amount of NADPH and NADH (Gruchattka et al., 2013). In addition, the MEP pathway requires flavodoxin or ferredoxin as an additional cofactor for its enzymatic reactions. In contrast, NADPH is the only cofactor required for the activity of the MVA pathway (Orsi et al., 2020).

### 1.1.1 Carotenoids and the biosynthesis

Most carotenoids are tetraterpenoids (C<sub>40</sub>). About 850 natural carotenoids have been identified by 2018 (Maoka, 2020). The global market size of carotenoids has grown annually. It is predicted that the market will reach 2.0 billion US dollars in 2020 due to the high demands for food and beverages, pharmaceuticals, cosmetics, animal feed, and dietary supplements (McWilliams, 2018; Ram et al., 2020). 80-90% of carotenoids have been produced through chemical synthesis. Nevertheless, the number of naturally produced carotenoids in the global market has increased as a result of rising concerns about health issues (Saini and Keum, 2019).

Carotenoids consist of the basic unit, isoprenoid, which is linked with a double or single bond. The structures are linear and symmetrical. At the light-absorbing conjugated double bonds, the strong electronic transition from ground energy level to the S<sub>2</sub> state results in the specific absorption

between 400-500 nm (Fish et al., 2002; Zigmantas et al., 2002). Therefore, carotenoids have different color ranges from yellow to red (Britton, 1995). Due to the high hydrophobicity, the solubility of carotenoids in water is very low. With this chemical property, carotenoids are associated in hydrophobic areas of membranes, interacting with proteins to maintain the membrane flexibility and rigidity (Kirti et al., 2014; Ram et al., 2020; Wang et al., 2019). In plants and bacteria, the carotenoid pathway enzymes are translocated to the membrane to access their hydrophobic substrates (Sandmann, 2009; Ruiz-Sola and Rodríguez-Concepción, 2012; Wang et al. 2019).

Carotenoids are natural and lipophilic pigments synthesized by a wide range of photosynthetic and some non-photosynthetic organisms. Various carotenoids play different functions in many organisms. Carotenoids are essential compounds for generating yellow, orange, and red color in plants, algae, fungi, and bacteria. In addition, carotenoids mainly function as photoreceptors in photosynthetic organisms (Maoka, 2020). In contrast, the physiological functions of carotenoids in non-photosynthetic microorganisms are unclear. However, some evidence supports another physiological role of carotenoids is protection against ultraviolet (UV) radiation, reactive oxygen species (ROS), and antioxidants (Avalos and Limón, 2015). Furthermore, more complex functions related to tolerance and adaptation to specific stress conditions, such as salinity, pH, and temperature, are found in bacteria (Fong et al., 2001; Montero-Lobato et al., 2018). In general, animals can not synthesize carotenoids. Therefore, their main source of carotenoids is from their diets. In animals, carotenoids have health benefits as antioxidants and as vitamin A precursors (Avalos and Limón, 2015). Astaxanthin, for example, is an orange xanthophyll mostly produced by microalga and bacteria and in aquatic environments. Through the food chain, astaxanthin is accumulated in fish flesh and shells of crustaceans. It is currently used as an antioxidant and a feed additive for salmon pigmentation (Avalos and Limón, 2015; de Carvalho and Caramujo, 2017). For humans, astaxanthin has shown various health benefits with its properties, such as antioxidant function, UV-light protection, and anti-inflammatory (Guerin et al., 2003).

The carotenoid pathway for different carotenoids has been investigated (Avalos and Limón, 2015; Maoka, 2020). Geranylgeranyl pyrophosphate (GGPP) synthesis is an enzymatic condensation step of farnesyl pyrophosphate (FPP) and isopentyl pyrophosphate (IPP) by GGPP synthase. Two molecules of GGPP are further condensed to form phytoene by a bifunctional enzyme functioning as a phytoene synthase and lycopene cyclase (Estrada et al., 2009). Lycopene is the product of the desaturation of phytoene by a phytoene desaturase. The bifunctional enzyme cyclizes both ends of lycopene to form  $\beta$ -ionone rings for the synthesis of  $\beta$ -carotene, which is the precursor of retinal. A carotenoid cleavage enzyme specifically recognizes the  $\beta$ -ionone ring of  $\beta$ -carotene and symmetrically cleaves the central 15-15' double bond to form retinal (Prado-Cabrero et al., 2007; Estrada et al., 2009).



### 1.1.1.1 Fungal carotenoid pathway

The carotenoid pathway is investigated using several filamentous fungi, which are natural producers of carotenoids (Avalos and Limón, 2015).  $\beta$ -carotene, for example, is accumulated in the zygomycetes *Phycomyces blakesleeanus* and *Mucor circinelloides*. In the ascomycetes, *Aspergillus nidulans*, and *Saccharomyces cerevisiae*, which are well-known fungal model organisms that have no genes for the carotenoid pathway (Avalos and Limón, 2015). However, other ascomycetes *Neurospora crassa* and *Fusarium fujikuroi* are studied for the production of neurosporaxanthin (Avalos and Limón, 2015). The basidiomycete fungus *Xanthophyllomyces dendrorhous* is a natural producer of astaxanthin through the intrinsic carotenoid pathway and industrially engineered to increase the yields (Melillo et al., 2013). Furthermore, the carotenoid pathway and retinal production in *F. fujikuroi* are deeply studied (Figure 1.3A; Prado-Cabrero et al., 2007). The four genes (*carB*, *carRA*, *carO*, *carX*) of the carotenoid pathway are located in a gene cluster, and the transcription levels are increased by illumination (Figure 1.3B; Prado et al., 2004).

In *U. maydis*, the carotenoid pathway enzymes have been predicted because of their high amino acid sequence similarity to carotenoid enzymes from other fungi (Figure 1.3B). Car3 is identified as a GGPP synthase. Car2 is predicted as a bifunctional enzyme functioning as a phytoene synthase and lycopene cyclase like CarRA from *F. fujikuroi* and *P. blakesleeanus* (Linnemannstöns et al., 2002; Prado et al., 2004; Estrada et al. 2009; Sanz et al., 2011). The two functional domains of CarRA from the zygomycete fungus *Blakeslea trispora* are well-characterized, and CarA is a phytoene synthase producing the natural product lycopene (Rodríguez-Sáiz et al., 2004; Wang et al., 2017b) Car1 has high similarity to phytoene desaturase, which converts phytoene to lycopene. The transcription level of *car1* is increased by light exposure (Estrada et al., 2009). Photoinduction of transcriptional levels within the carotenoid pathway in other fungi has been reported. In *M. circinelloides*, for example, the mRNA levels of *carB* and *carRP* are highly induced by blue light (Velayos et al., 2000a-b). This light induction of the fungal carotenoid pathway increases the accumulation of carotenoids. Neurosporaxanthin, for example, is highly accumulated by light exposure in *F. fujikuroi*. The carotenoid photoinduction in fungi is White Collar complex-mediated (Avalos and Limón, 2015; Avalos et al., 2017). The WC complex is a heterodimer consisting of WC-1 containing a LOV flavin-binding domain and WC-2 (He and Liu, 2005; Sanz et al., 2009). The enzymatic conversion from lycopene to  $\beta$ -carotene is the second function of Car2. The biological function of the carotenoid pathway in *U. maydis* is most likely to provide a precursor of retinal. A carotenoid oxygenase Cco1 in *U. maydis* is a homolog of CarX from *F. fujikuroi* and BCMO1 from *H. sapiens* (Prado-Cabrero et al., 2007; Estrada et al., 2009). The *cco1* deletion mutant of *U. maydis* accumulates a tiny amount of  $\beta$ -carotene, and a similar phenotype of *F. fujikuroi* suggests that  $\beta$ -carotene is used in retinal biosynthesis (Estrada et al., 2009; Avalos and Limón, 2015).

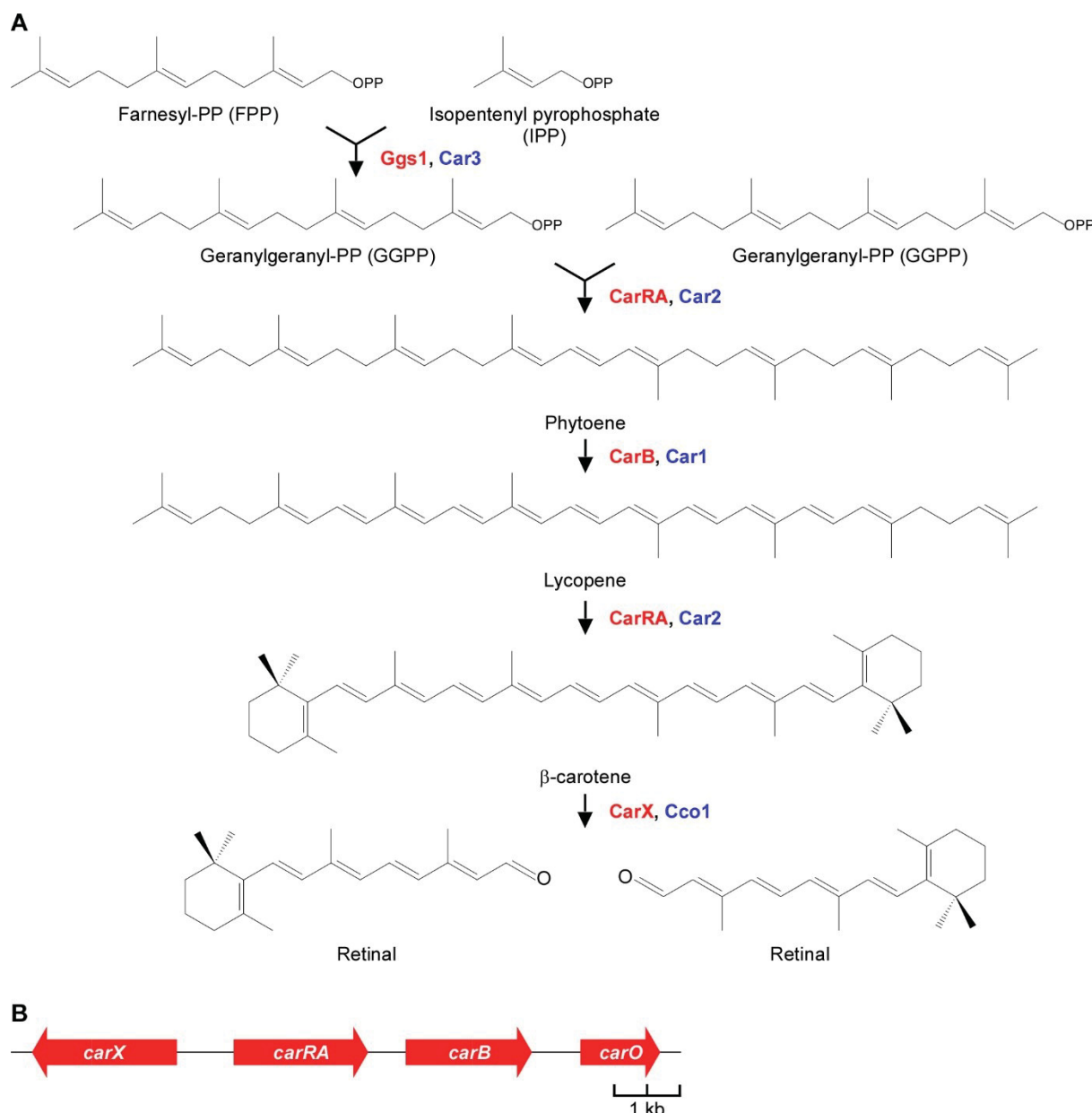


**Figure 1.3 The carotenoid pathway in *F. fujikuroi* and *U. maydis*.**

(A) The carotenoid pathway enzymes from *F. fujikuroi* and *U. maydis*. The enzymes from *F. fujikuroi* and *U. maydis* are indicated in red and blue, respectively. The enzymes from *U. maydis* are predicted except Cco1 (Estrada et al., 2009). Ggs1 and Car3 are geranylgeranyl pyrophosphate synthases. The bifunctional enzyme functioning as a phytoene synthase and lycopene cyclase in *F. fujikuroi* is CarRA, and the homolog in *U. maydis* is Car2. CarB and Car1 are phytoene desaturases. A cleavage reaction of  $\beta$ -carotene generates retinals. CarX and Cco1 are carotenoid oxygenases in *F. fujikuroi* and *U. maydis*, respectively. (B) Schematic representation of the gene cluster for the carotenoid pathway in *F. fujikuroi*. Four genes encoding essential enzymes for retinal production are located in a gene cluster. CarO is an opsin in *F. fujikuroi*. In contrast, the carotenoid pathway genes in *U. maydis* are not located in a gene cluster. The figure is modified from Estrada et al., 2009. The biosynthetic pathway enzymes and genetic information are adapted from Estrada et al., 2009 and Avalos et al., 2017.

### 1.1.1.2 Opsins in fungi

Opsins are a family of photoactive proteins and contain seven-transmembrane helices. Retinal is a chromophore of opsin and binds at a conserved lysine residue of the opsins. The light-mediated isomerization of 11-*cis*-retinal to all-*trans*-retinal activates the opsins to function as ion pumps for sensing light (Figure 1.4A-B; Terakita, 2005; Zhang et al., 2011). In fungi, there is a three-type

classification of the green-light sensing rhodopsins based on the photocycle's speed and the conserved amino acids. For example, Nop-1 from *N. crassa* is a slow photocycle rhodopsin, and LR from *Leptosphaeria maculans* shows a fast photocycle ability. CarO-like rhodopsins also show a fast photocycle ability, but the lysine residue for retinal binding via Schiff base is conserved (Fan et al., 2011; Wang et al., 2018). Previously, a genetic study has found that CarO is a putative opsin like protein, which is suggested to be a photoreceptor in *F. fujikuroi*. However, there is a lack of evidence to determine the function of CarO. Even though the gene is located in the carotenoid gene cluster, and the light exposure changes the transcription level, the deletion mutant did not show any apparent phenotypes (Prado et al., 2004).

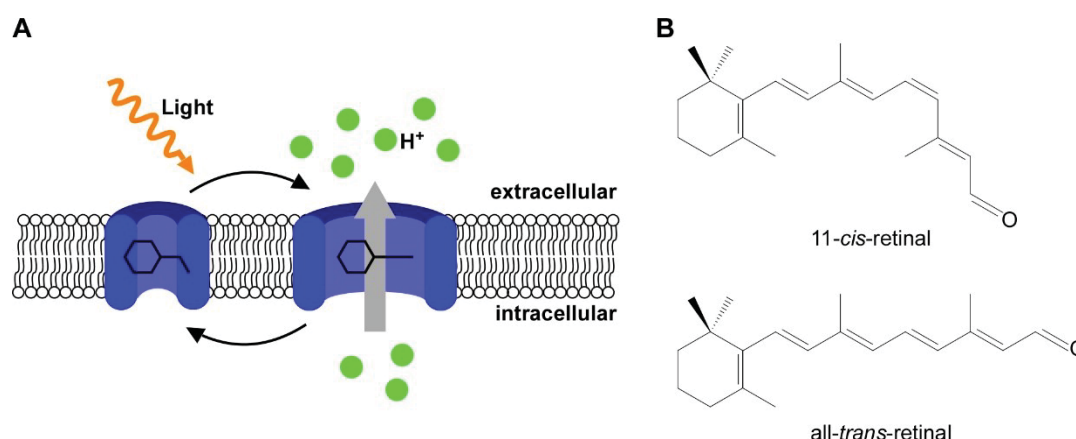


**Figure 1.4 Schematic representation of the proton pumping mechanism of opsin and isoforms of retinal.**

(A) Light response of opsin and the role of retinal. Covalent binding of 11-*cis*-retinal at the lysine residue of opsin inactivates the proton pump activity. Illumination isomerizes 11-*cis*-retinal to all-*trans*-retinal, which changes the conformation of opsin to pump out protons to extracellular space. (B) The two isoforms of retinal as the chromophores of opsins. The information of the light-mediated proton pump by opsins is adapted from Terakita, 2005 and Zhang et al., 2011.

There are three putative opsins (Ops1, UMAG\_02629; Ops2, UMAG\_00371; Ops3, UMAG\_04125) in *U. maydis* (Estrada et al. 2009). The transcription level of *ops3* is induced during plant infection, whereas the transcriptional level of the gene encoding Ops1 is highly induced by blue light (Ghosh et al., 2014; Brych et al., 2016; Lanver et al., 2018; Panzer et al., 2019). An electrophysical study with patch-clamp experiments has proven that Ops1 and Ops2 are green light-driven proton pumps (Panzer et al., 2019). In addition, the conserved amino acids have been found as retinal binding sites (Ops1, K247; Ops2, K245), as proton acceptors (Ops1, D118; Ops2, D115), and as proton donors (Ops1, E129; Ops2, D126; Panzer et al., 2019). Similarly, CarO has proton pumping activity in *F. fujikuroi* (García-Martínez et al., 2015; Panzer et al., 2019). Ops1 is localized in the plasma membrane, and Ops2 is localized in the vacuolar membranes (Panzer et al., 2019). The pump activity of Ops1 is influenced by the concentrations of acetate, indole-3-acetic acid (IAA), indole-3-propionic acid (IPA), and pH. The biological function of rhodopsins in fungi during infection is still unclear, but it is suggested that it has a significant role in the plant-fungus interaction (Panzer et al., 2019).

## 1.2 Production of natural terpenoids

Traditionally, terpenoids are extracted from plant or fungal materials (Hennicke et al., 2016; Jiang et al., 2016). Extraction of diverse terpenoids from natural sources has been exercised to obtain essential oils containing terpenoids for traditional remedies (Hunter and Brogden 1965a; Jirovetz et al., 2006). Natural sources typically have low concentrations of terpenoids, meaning that supplying large amounts of natural oils by the traditional methods is unsustainable and costly (Morser and Pichler, 2019). Moreover, this extraction exercise is often profoundly affected by seasonal and geographical variations (Morser and Pichler, 2019).

### 1.2.1 Plant terpenoids and biotechnology

Some naturally obtained essential oils used in traditional remedies may become hardly accessible in the near future. Sandalwood oil, for example, has been extracted from the East Indian sandalwood tree (*Santalum album*), which only grows in tropical climate regions, such as Southern India and Southeast Asia (Burdock and Carabin, 2008). This essential oil has been marketed as a remedy material, and it has been reported as a chemotherapeutic and chemopreventive agent against skin cancer and as additional bioactive agents (Benencia and Courrèges, 1999; Dwivedi et al., 2003; Jrovetz et al., 2006). In addition,  $\alpha$ -santalol in the East Indian sandalwood is responsible for a long-lasting distinctive soft and woody scent. Therefore, sandalwood has been considered as a valuable natural source for fragrance industries (Baldovini et al., 2010). Because of the benefits in healthcare and fragrance production, sandalwood trees have been recklessly harvested. As a result, these slow-growing trees have suffered because of overexploitation and increasing illegal logging. The sandalwood tree is currently classified as a highly endangered species (Burdock and Carabin, 2008). The potent anticancer drug taxol production is another example of unsustainable terpenoid extraction from natural sources (Morser and Pichler, 2019). It was estimated that 2-3 million mature pacific yew trees would have to be sacrificed per year to obtain taxol for cancer treatment in the United States of America (Suffness, 1995; Morser and Pichler, 2019).

An alternative way to obtain terpenoids is chemical synthesis, which can meet the demand and reduce production costs (Hunter and Brogden, 1965b; García-Cabeza et al., 2014). However, the number of natural terpenoids produced via this approach is limited because the tremendous terpenoids have complex chemical structures, and many of their chemical reactions have not been discovered (Xiao and Zhong, 2016). Extensive efforts are made to heterologously produce these compounds in microorganisms to increase sustainability and expand chemical diversity via modification of near-to-natural versions (Ro et al., 2006; Ignea et al., 2018; Schempp et al., 2018). Several companies, such as Amyris, Evolva, Isobionics (now BASF), and Firmenich, have already marketed diverse terpenoids produced in engineered microorganisms (Schempp et al., 2018). One of the successful plant-derived fragrance compounds in industrial levels is (+)-valencene, which is present in various citrus species. Due to its woody citrus characteristic, (+)-valencene has been used for citrus flavoring in drinks and fragrances. The market volume in 2014 was 10,000 kg/year, and

half of that amount was used for the production of (+)-nootkatone, which is an oxidized sesquiterpenoid. The biosynthetic gene, *CnVS*, was found in *Callitropsis nootkatensis*, also known as Alaska yellow cedar (Figure 1.5; Beekwilder et al., 2014). It is predicted that *CnVS* cyclizes FPP to (+)-valencene in the cytosol (Sharon-Asa et al., 2003; Beekwilder et al., 2014).

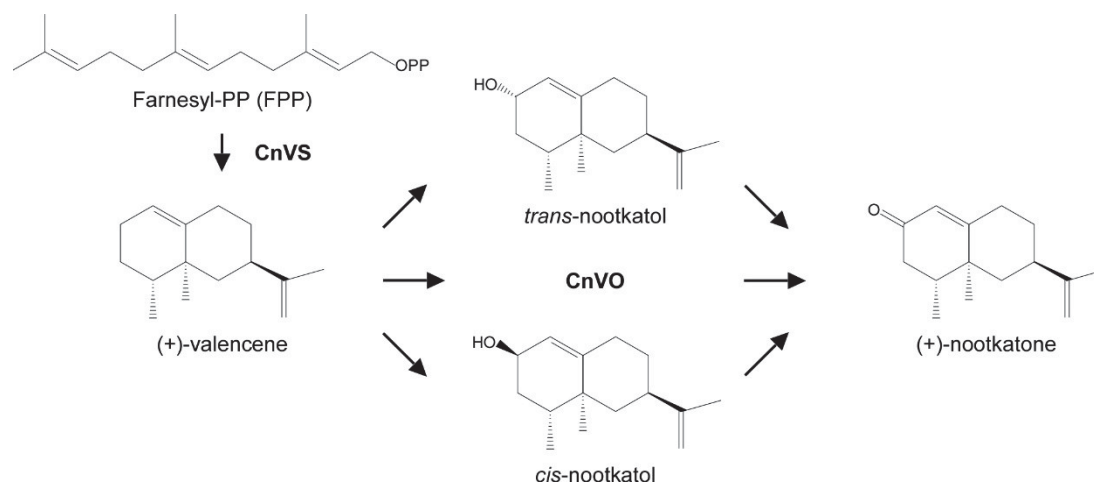


**Figure 1.5 Schematic representation of the biosynthetic pathway for (+)-valencene and (+)-nootkatone.** The first enzymatic reaction to cyclize farnesyl-PP (FPP) to (+)-valencene is catalyzed by a valencene synthase (*CnVS*). The proposed steps to convert (+)-valencene to (+)-nootkatone are hydroxylation and oxidation catalyzed by a valencene oxidase (*CnVO*). The hydroxylation results in the formation of two isoforms of nootkatol (*trans*-nootkatol and *cis*-nootkatol). The enzymes indicated here are from *C. nootkatensis*. The figure is modified from Cankar et al., 2014.

Different microorganisms have been established to produce (+)-valencene by heterologous expression of *CnVS* and pathway engineering. Isobionics (now BASF) engineered a *Rhodobacter sphaeroides* strain by introducing the mevalonate pathway enzymes from *Paracoccus zeaxanthinifaciens* and marketed biotechnologically produced (+)-valencene. Further optimization of the cultivation process increased its highest titer to 352 mg/L (Hümbelin et al., 2002; Beekwilder et al., 2014; Troost et al., 2019). Engineered *Rhodobacter capsulatus* confirmed the advantage of the highly efficient synthesis of IPP and DMAPP via the heterologous mevalonate pathway, which led to a titer of 18 mg/L (Troost et al., 2019). The heterologous production of (+)-valencene in *S. cerevisiae* has been developed since the heterologous expression of *CnVS* was successful, and it reached a titer of 1.36 mg/L (Beekwilder et al., 2014; Chen et al., 2019; Ouyang et al., 2019; Meng et al., 2020). The highest titer of 539.3 mg/L was achieved by overexpressing genes of the intrinsic mevalonate pathway, down-regulating the squalene pathway, knocking out a gene encoding Rox1, and optimizing fed-batch fermentation conditions in a bioreactor (Chen et al., 2019). Rox1 is a transcriptional factor that inhibits the expression of hypoxia-induced genes in the MVA pathway and ergosterol biosynthesis (Montañés et al., 2011; Chen et al., 2019). The heterologous production of (+)-valencene in the basidiomycete fungus *Schizophyllum commune*, which is a natural producer of fungal sesquiterpenoids and whose MVA pathway enzymes are annotated, was successful (Ohm et al., 2010; Scholtmeijer et al., 2014). Engineering a *thn* gene mutant, which secretes less



schizophyllan in the culture medium, by introducing the valencene synthase gene from *Chamaecyparis nootkatensis* reached a titer of 16.6 mg/L (Scholtmeijer et al., 2014).

The next two steps of enzymatic reactions, regioselective allylic hydroxylation and oxidation, lead to the bioconversion from (+)-valencene to (+)-nootkatone, which is depended on for flavor and fragrance applications. It is also known to have a high potential for use as an insect repellent (Zhu et al., 2001; Flor-Weiler et al., 2011). Recent reports of (+)-nootkatone proved that it could be a good medicinal compound for cancer treatments as an activator of AMP-activated protein kinase (AMPK) inhibiting the KRAS pathway or autophagy, ROS production, cell cycle arrest, and inhibition of the NF- $\kappa$ B signaling pathway (Hung et al., 2019; Zhu et al., 2020). However, only a trace amount of (+)-nootkatone is found in grapefruit oil (Hunter and Brogden, 1965a-b). Isolation and functional determination of valencene oxidase CYP706M1 (CnVO) from *Callitropsis nootkatensis* revealed the biosynthetic pathway of (+)-nootkatone (Figure 1.5; Cankar et al., 2014). The co-production of CnVS and CnVO in *S. cerevisiae* reached the titer of 144  $\mu$ g/L (Cankar et al., 2014). Further production improvement was achieved with combinatorial overexpression of (+)-nootkatone biosynthetic pathway genes from different origins, for example, a premnaspirodiene oxygenase (HPO) from *Hyoscyamus muticus*, a cytochrome P450 reductase (AtCRP) from *A. thaliana* and an alcohol dehydrogenase (Adh1p) from *S. cerevisiae*. Moreover, additional engineering strategies to increase the carbon flux within the MVA pathway in *S. cerevisiae* improved the titer of 53.7 mg/L (Ouyang et al., 2019). A similar approach to increase the oxidation rate from  $\beta$ -nootkatol to (+)-nootkatone by screening various dehydrogenases has been tested, and two short-chain dehydrogenase/reductase (SDR) superfamily dehydrogenases, ZSD1 from *Zingiber zerumbet* and ABA2 from *Citrus sinensis* effectively oxidized  $\beta$ -nootkatol to (+) nootkatone (Meng et al., 2020). However, achieving a high yield of (+)-nootkatone from the bioconversion of (+)-valencene in *S. cerevisiae* is challenging. The viability of the cells is low in the presence of  $\beta$ -nootkatol and (+)-nootkatone at concentrations exceeding 100 mg/L, and the majority amount of  $\beta$ -nootkatol is accumulated in the endomembranes. Furthermore, there is a feedback loop inhibiting the hydroxylation reaction of CYP71D51v2, a P450 that converts (+)-valencene to  $\beta$ -nootkatol, by the product (Gavira et al., 2013).

### 1.2.2 Value-added fungal terpenoids and their biosynthesis in higher basidiomycetes

Mushroom (fruiting body)-forming basidiomycetes (subphylum Agaricomycotina, especially from the class of Agaricomycetes) are a rich source of terpenoids (Xiao and Zhong, 2016; Zhao et al., 2017; Sandargo et al., 2019). In East Asia, *Ganoderma* spp., so-called Ling-zhi or Reishi mushrooms, have been preciously consumed as the mushroom of immortality in traditional medicine for many centuries (Pegler, 2002; Shiao, 2003). Due to their long-known medicinal benefits, the estimated annual worldwide market volume of *Ganoderma* spp. exceeds 2.5 billion US dollars (Li et al., 2013). Extensive research on *Ganoderma* spp. has revealed different biological properties, such as anti-hypertensive, immunomodulatory anticancer, antiviral, and antimicrobial activities (Boh et al., 2007). Biochemical studies support these medicinal benefits of *Ganoderma* spp. with diverse terpenoids,

such as genoderic acids, ganoderiols, ganolucidic acids, lucidones, and lucidenic acids (Cole et al., 2003; Hennicke et al., 2016).

Higher basidiomycetes have been attracted in the discovery of novel bioactive terpenoids. Prominent examples are derivatives of the sesquiterpenoid illudin S from *Omphalotus olearius* that exhibit strong anti-tumor activity (Jaspers et al., 2002; see below) and the diterpenoid pleuromutilin from *Clitopilus passeckerianus* that can be applied as an antibacterial antibiotic since it inhibits protein synthesis by targeting the peptidyl transferase component of the 50S subunit of prokaryotic ribosomes (Hartley et al., 2009; de Mattos-Shipley et al., 2017; see below).

Studies of volatile organic compounds (VOC) in higher basidiomycete fungi have also significantly expanded the knowledge on fungal sesquiterpenoid diversity (Wu et al., 2005, 2007; Campos Ziegenbein et al., 2006; Agger et al., 2009; Engels et al., 2011; Orban et al., 2020). With edible mushrooms, such as the poplar mushroom *Cyclocybe aegerita* (syn. *Agrocybe aegerita*), such studies also advance an understanding of the contribution of VOCs to the aroma of such mushrooms as comestibles (Rapior et al., 1998; Kleofas et al., 2014; Costa et al., 2015). Analyzing VOC profiles at different fruiting stages of *C. aegerita* reveals approximately 150 substances are produced, and an alteration of the VOC profile composition with ongoing fruiting body development where significant amounts of sesquiterpenoids were detected, especially during sporulation (Orban et al., 2020). A later study discovered 11 putative sesquiterpenoid synthases in *C. aegerita* (Zhang et al., 2020). Biosynthetic gene clusters (BGCs) for fungal bioactive terpenoids from higher basidiomycete fungi have been identified to understand the biosynthetic pathways. *Armillaria* spp. are known as honey mushrooms and regarded as edible mushrooms, but many species are forest parasites (Dörfer et al., 2019). These species naturally produce protoilludene-type sesquiterpenoids known as melleolides, which are structurally diverse, antimicrobial, and cytotoxic natural compounds (Engels et al., 2011). Melleolide B, C, and D, for example, have been reported with significant activities against *Bacillus cereus*, *Bacillus subtilis*, and *Escherichia coli* (Arnone et al., 1986). To date, 71 melleolides from *Armillaria* spp. have been investigated (Dörfer et al., 2019). The main biosynthesis step of melleolides is esterification between the C15 tricyclic protoilludene framework and orsellinic acid (Figure 1.6A; Lackner et al., 2013). The protoilludene determines the structural diversity and chemical properties of melleolides. The sesquiterpenoid synthase Pro1 from *Armillaria gallica* has been functionally studied in so far that Pro1 cyclizes farnesyl pyrophosphate to exclusively produce 6-protoilludene (Figure 1.6A; Engels et al., 2011). The further modification is tailored by cytochrome P450 monooxygenases and other hydroxylases (Dörfer et al., 2019). The other moiety, orsellinic acid, which is derived from acetyl-CoA and malonyl-CoA, could be combined with protoilludene by the polyketide synthase (PKS) ArmB (Figure 1.6A; Lackner et al., 2013). This enzyme contains a thioesterase domain and is responsible for the transesterification of the carboxylic acid functionality of orsellinic acid (Lackner et al., 2013). In *Armillaria mellea*, a melleolide biosynthesis gene cluster has been identified, which consists of 16 genes, including *pro1*, *armB*, and five cytochrome P450 monooxygenase genes (Figure 1.6B; Collins et al., 2013).

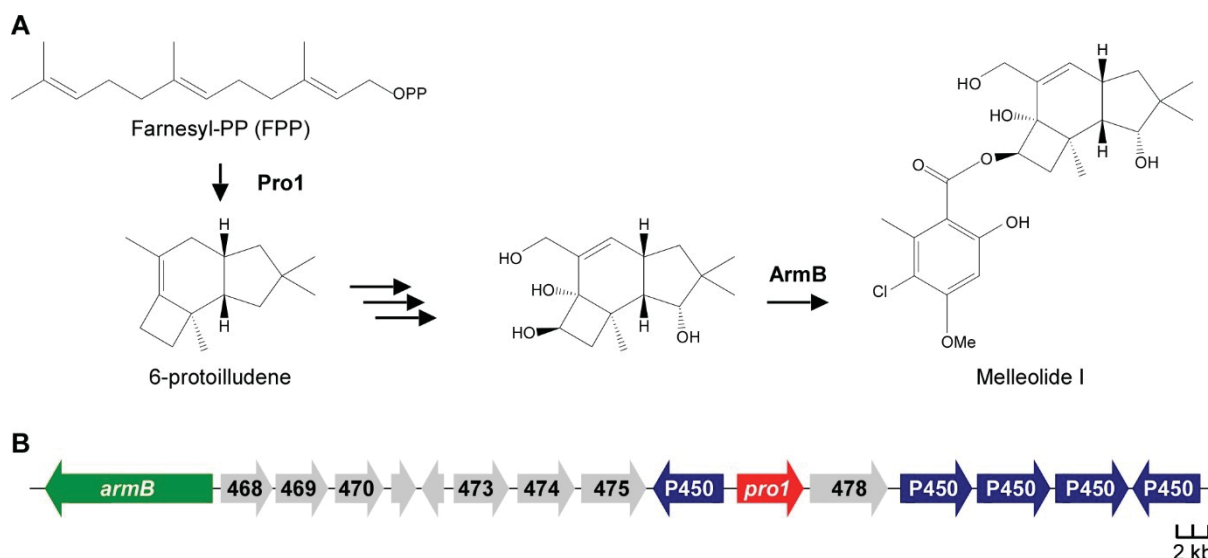


**Figure 1.6 Suggested melleolide biosynthetic pathway in *A. gallica* and the biosynthetic gene cluster for melleolides in *A. mellea*.**

(A) Two biosynthetic enzymes within the melleolide biosynthetic pathway. Pro1 cyclizes FPP to 6-protoilludene and a polyketide synthase (PKS) ArmB is responsible for combining orsellinic acid moiety to an oxidized derivative of 6-protoilludene in *A. gallica*. (B) The biosynthetic gene cluster for melleolides in *A. mellea*. 16 genes are located in the gene cluster encoding enzymes: ArmB, orsellinic acid synthase; 468, NAD(P)-binding dehydrogenase; 469, short-chain dehydrogenase/reductase; 470, NAD-dependent epimerase/dehydratase; 471 and 472, hypothetical proteins; 473, O-methyltransferase; 474, aryl-alcohol dehydrogenase; 475, NAD(P)-binding dehydrogenase; 476, cytochrome P450 monooxygenase; Pro1, protoilludene synthase; 478, short-chain dehydrogenase/reductase; 479-482, cytochrome P450 monooxygenases. The information on the biosynthetic pathway and the gene cluster is modified from Engels et al., 2011, Lackner et al., 2013, and Dörfer et al., 2019.

Another relevant example is the antibacterial sesquiterpenoid lagopodin B, which was chemically characterized and isolated from the basidiomycete mushroom *Coprinopsis cinerea* (Bollinger, 1965; Bu'Lock and Darbyshire, 1976). Still, it took a decades-long search to find the biosynthetic pathway that synthesizes lagopodin B (Agger et al., 2009; Stöckli et al., 2019). Six sesquiterpenoid synthases in *C. cinerea* have been identified (Agger et al., 2009). The heterologous production in *S. cerevisiae* revealed the biosynthesized products of five sesquiterpenoid synthases (Agger et al., 2009). Among the five sesquiterpenoid synthases, Cop6 selectively produces  $\alpha$ -cuprenene, and its gene is located in a mini-gene cluster flanked by two neighboring genes, *cox1* and *cox2*, encoding P450 cytochrome monooxygenases (Figure 1.7A-B; Agger et al., 2009). This study has provided a clue that lagopodin B might be an oxygenated  $\alpha$ -cuprenene derivative. Interestingly, all gene cluster members are transcriptionally activated after co-cultivation with Gram-positive bacteria, and these two P450 cytochrome monooxygenases are responsible for the conversion of  $\alpha$ -cuprenene to lagopodins (Stöckli et al., 2019).



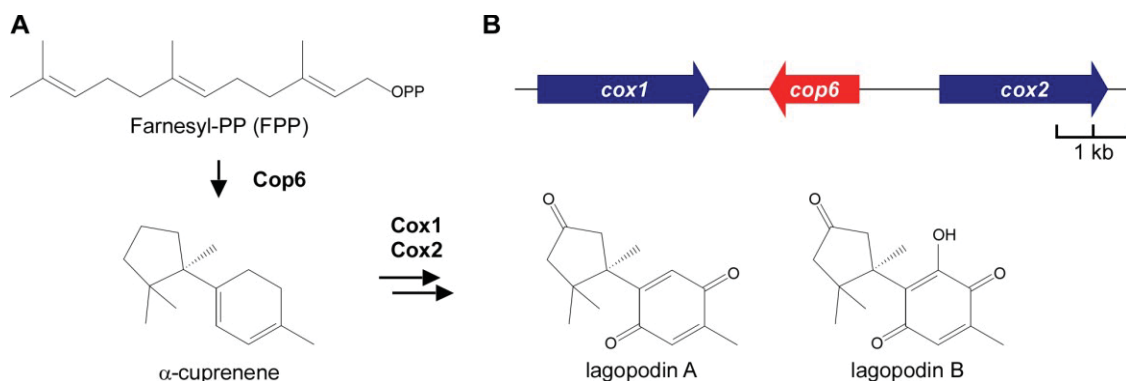


**Figure 1.7 Biosynthesis of  $\alpha$ -cuprenene and the oxygenated derivatives and the *cop6* gene cluster in *C. cinerea*.**

(A) The biosynthetic pathway to produce  $\alpha$ -cuprenene and the suggested enzymatic reaction steps for the antimicrobial sesquiterpenoids, lagopodin A and B in *C. cinerea*. The cyclization reaction of FPP to  $\alpha$ -cuprenene is catalyzed by Cop6. Further modifications by Cox1 and Cox2 might result in the synthesis of lagopodin A and B. (B) Schematic representation of the *cop6* gene cluster in *C. cinerea* genome. Two cytochrome P450 monooxygenase encoding genes, *cox1* and *cox2*, flank *cop6*. The NCBI accession numbers are listed as follows: Cop6 (XP\_001832549), Cox1 (XP\_001832548), and Cox2 (XP\_01832550). The biosynthetic pathway and genetic information are adapted from Agger et al., 2009 and Stöckli et al., 2019.

### 1.2.3 Fungal terpenoid production in biotechnology and its challenges

Heterologous production of most fungal terpenoids has not yet been achieved because several challenges hinder its progress. A significant number of terpenoid synthases are not characterized, and their functional roles are not elucidated (Zhang et al., 2020). 1133 putative terpenoid synthases from 99 basidiomycetes are predicted, indicating that each basidiomycete contains many genes encoding terpenoid synthases (Zhang et al., 2020). Still, this prediction is restricted to basidiomycete genome sequences of which are available (Sandargo et al., 2019; Zhang et al., 2020). Furthermore, the enzymatic functions of the putative terpenoid synthases and the biological function of their products are unknown (Zhang et al., 2020).

Biological knowledge of natural producers of fungal terpenoids is limited. Higher basidiomycete fungi often entail the disadvantage of being difficult to cultivate and that sophisticated molecular tools for pathway engineering are not available. In addition, the nutritional requirements of several mushroom species are underexplored. For example, *Pluteus* and *Lepiota* are difficult to cultivate in the laboratory (Sandargo et al., 2019). Therefore, limited numbers of fungal terpenoids are studied, and most fungal terpenoid production studies are focused on the optimization of fermentation processes (Xiao and Zhong, 2016).

It is difficult to obtain enough pure substances for defined biological assays. A mixture of fungal secondary metabolites can be detected in HPLC and GC profiles, and structure elucidation is the only method to identify and classify the novel compounds in the profiles (Kjer et al., 2010; Engels et al., 2011; Orban et al., 2020). When the concentrations are extremely low, it is challenging to isolate the pure compounds (Koehn and Carter, 2005; Sandargo et al., 2019). Only prominent peaks in the profiles are accessible to isolate. In the case of fungal terpenoids, diverse derivatives could be detected, and their chemical characteristics are similar. Therefore, the isolation process is

more complicated (Hennicke et al., 2016). In addition, the cultivation of fruiting body forming basidiomycetes requires a long time and special cultivation conditions (Sandargo et al., 2019). Different profiles of secondary metabolites were detected in different stages of *C. aegerita* (Orban et al., 2020). Therefore, optimization of sustainable cultivation conditions and large scale cultivation methods should be studied to achieve enough fungal materials to isolate target fungal terpenoids (Sandargo et al., 2019). Furthermore, the establishment of extraction and isolation methods is essential (Kjer et al., 2010; Hennicke et al., 2016). Moreover, the absence of commercial reference compounds to identify and quantify fungal terpenoids is another obstacle (Melillo et al., 2013).

Construction of cDNA libraries to identify fungal genes encoding target terpene synthases and cytochrome P450 monooxygenases and characterization of the genes is laborious. Plant and fungal terpene synthases have low sequence identity (Engels et al., 2011; Zhang et al., 2020). Although conserved motifs have been reported that are present in fungal sesquiterpenoid synthases (metal-binding motifs, DEXXD, and NDxxSxxxE), the acid sequence similarity compared with functionally characterized sesquiterpenoid synthases from plants and the basidiomycete mushroom *C. cinerea* is low (Agger et al., 2009; Lopez-Gallego et al., 2010; Engels et al., 2011).

Only a few biosynthetic gene clusters and pathways for fungal terpenoids have been reported, although numerous bioinformatics algorithms have been developed to discover biosynthetic gene clusters (BGCs; Keller, 2019; Zhang et al., 2020). Many genes encoding cytochrome P450 monooxygenases for the biosynthesis of sesquiterpenoid scaffolds have not yet been identified or enzymatically characterized (Zhang et al., 2020). The biosynthetic pathway elucidation of structurally diverse melleolides from *Armillaria* spp. is challenging (Dörfer et al., 2019). 6-protoilludene could be oxygenated to melleolide I in *A. gallica*, but the full biosynthesis pathway is unknown (Engels et al., 2011). The genome sequence database allows the identification of a melleolide biosynthesis gene cluster consisting of 16 genes, including *pro1* and *armB* in *A. mellea* (Collins et al., 2013). However, only five cytochrome P450 monooxygenase genes are found in the biosynthetic gene cluster, and other tailoring genes encoding hydroxylases positioned outside of the biosynthetic gene cluster for the diverse melleolides are not yet discovered (Dörfer et al., 2019).

Validation of enzymatic functions of putative fungal sesquiterpenoid synthases in heterologous model organisms, such as *E. coli*, is not always successful (Agger et al., 2009; Zhang et al., 2020; Zhang and Hong, 2020). Six potential sesquiterpenoid synthases from *C. cinerea* have been predicted (Agger et al., 2009). However, heterologous expression of *cop5* in *E. coli* has not been successful. It might be that the *cop5* transcript is differently spliced than the annotation in the genome database (Agger et al., 2009). According to the functional validation study of 11 predicted sesquiterpenoid synthases in *C. aegeria*, heterologously produced Agr10 and Agr11 are not functional in *E. coli* (Zhang et al., 2020).

Evolutionary developments of organisms specialize their gene expression mechanisms and cellular events (Vellai and Vida, 1999; Carrascosa et al., 2001; Aylett and Ban, 2017; Macek et al., 2019;

Mojzita et al., 2019); Xu et al., 2019). This fact could explain the challenges of fungal secondary metabolite discovery and production in heterologous systems. As a heterologous host, *S. cerevisiae* might not be well-evolved in expressing heterologous biosynthetic gene clusters for complex fungal secondary metabolites, and it often causes no product (Keller, 2019). The main reasons are seen with different post-transcriptional mechanisms, cellular trafficking, and the lack of precursors (Keller, 2019). These issues may also (at least partially) relate to the main challenge for high-level expression of genes encoding P450s in heterologous systems (Ichinose and Wariishi, 2013; Renault et al., 2014; Moser and Pichler, 2019). The N-terminal hydrophobic transmembrane domain is essential for eukaryotic cytochrome P450s to anchor in the ER membrane. In general, the heterologous production of cytochrome P450s in *E. coli* is limited due to the constraints of the endomembrane system (Zhang and Hong, 2020). Despite significant efforts to modify the N-termini of 304 cDNAs encoding cytochrome P450s from the basidiomycete mushrooms *Phanerochaete chrysosporium* and *Postia placenta* for heterologous expression in *E. coli*, the majority of P450s remain recalcitrant towards heterologous production (Ichinose and Wariishi, 2013).

The low enzymatic activity of P450s in heterologous systems is another challenge. The functional production of cytochrome P450s with high enzymatic activity is crucial for high yields of fungal terpenoids. In addition, the production of cytochrome P450 reductases (CPRs), which are also inserted into the ER membrane, is essential for the successful functionality of cytochrome P450s. The instability of CPR is a major issue for the low enzymatic activity of P450s in *S. cerevisiae* (Renault et al. 2014). In the case of exploring the biosynthetic pathway of lagopodins in *C. cinerea*, despite the heterologous expression of the *cop6* gene cluster containing two cytochrome P450 monooxygenases genes, *cox1* and *cox2*, in *S. cerevisiae* is achievable, the enzymatic activities of the P450s are too low to produce sufficient amounts of the oxidized  $\alpha$ -cuprenene derivatives for isolation (Agger et al., 2009). Heterologous expression levels of genes encoding P450s from *P. chrysosporium* are low in *E. coli* and *S. cerevisiae*, and the enzymes are not functional (Subramanian and Yadav, 2008). This challenge has also been reported during the production of plant-derived terpenoids in microbial production hosts and has caused the major bottleneck for the heterologous production (Moser and Pichler, 2019). The low enzymatic activity of heterologous P450s from the biosynthetic pathways of the antimalarial artemisinin and anticancer drug taxol directly influence the low titers in *E. coli* and *S. cerevisiae* (Croteau et al., 2006; Dejong et al., 2006; Ajikumar et al., 2010; Paddon et al., 2013; Moser and Pichler, 2019).

The toxicity of fungal terpenoids and their intermediates within the biosynthetic pathway is a great challenge for heterologous microorganisms. As a functional characterization procedure of novel fungal biosynthetic pathways, heterologous expression is an easy way to achieve the goal (Agger et al., 2009; Engels et al., 2011; Sandargo et al., 2019; Zhang et al., 2020). However, diverse secondary metabolites derived from fungal biosynthetic pathways might exhibit antibacterial or antifungal bioactivities. The antibacterial sesquiterpenoid lagopodin B isolated from the mushroom *C. cinerea* has shown a strong bioactivity against several Gram-positive bacteria, such as *B. subtilis*

(Stöckli et al., 2019). Furthermore, during understanding the diversity of melleolides from *Armillaria* spp. and their biosynthetic pathway, varying bioactivities of melleolide derivatives have been reported (Obuchi et al., 1990; Dörfer et al., 2019). Therefore, it will be challenging with *E. coli* and *S. cerevisiae* to characterize the respective biosynthesis genes, including P450 monooxygenase genes, since the intermediates or final products are potentially toxic to the heterologous hosts. To circumvent the product toxicity, specific transporters and regulation mechanisms for pumping out the toxic products are necessary. However, these systems are often specialized in higher basidiomycetes (Xiao and Zhong, 2016).

### 1.3 Importance of discovery of novel bioactive compounds and elevation of the demands

Bioactive compounds are natural products that are found in small quantities in nature, especially from plants and fungi (Kris-Etherton et al., 2002; Koehn and Carter, 2005; Kjer et al., 2010; Mickymaray, 2019). These compounds are attractive for the development of potential drugs because of their broad molecular diversity and therapeutic potential as antioxidant, anti-inflammatory, anticancer, and antimicrobial agents (Koehn and Carter, 2005; Kjer et al., 2010; Hyde et al., 2019; Subramaniam et al., 2019). Since the discovery of penicillin in 1928 and its enormous impact on human history, further discovery and production of antibiotics have been the key to curing infectious diseases. However, in modern society, the occurrence rate of infectious diseases is elevated, and multidrug-resistant microbes resulting from natural selection have been reported recurrently (Nikaido, 2009; Magiorakos et al., 2012; Blair et al., 2015; Tyers and Wright, 2019; Ogawara, 2020). For example, sepsis is an extreme immune response to an infection in the bloodstream and a highly lethal syndrome that causes multiple organ dysfunction and is challenging to detect and treat (Caraballo and Jaimes, 2019). The number of global sepsis cases exceeds 30 million, and 5 million deaths from sepsis are annually reported (Fleischmann et al., 2016). Furthermore, as the world population increases, invasive fungal diseases impose a growing threat to human life (Roemer and Krysan, 2014). Invasive fungal infections involve high mortality rates, killing about one and a half million people annually (Brown et al., 2012). The major fungal infections are caused by the genera *Cryptococcus*, *Candida*, *Aspergillus*, and *Pneumocystis* (Brown et al., 2012). The current clinical treatments rely on two classes of antifungal drugs, such as azoles and polyenes, which are mainly targeting the plasma membrane and the ergosterol biosynthetic pathway (Douglas and Konopka, 2016). However, the development of new antifungal drugs lags behind the clinical need to treat patients suffering from fungal infections by *Candida albicans* and *Candida glabrata*, which are resistant to widely-applied antifungal drugs (White et al., 2002; Roemer and Krysan, 2014). Unfortunately, the number of candidates for the development of novel antifungal drugs against human fungal pathogens by the large pharmaceutical companies has been declining over the past decades (Sandargo et al., 2019).

### 1.3.1 Basidiomycota, rich sources for discovery of bioactive compounds

Many species of Basidiomycota, the second-largest division of the kingdom Fungi with currently more than 30,000 described species (He et al., 2019), form conspicuous fruiting bodies (basidiomes, basidiocarps, mushrooms) for the sake of reproduction. As a result, these fungi are commonly often referred to as (basidiomycete) mushrooms. Fruiting bodies are produced by species of the class Agaricomycetes in particular, which is assigned to the Basidiomycota subphylum Agaricomycotina (Sandargo et al., 2019; Zhao et al., 2017). Like other fungi, basidiomycete mushrooms maintain their ecological fitness mainly by efficient chemical defense mechanisms by which they protect their vegetative mycelia and their fruiting bodies against antagonists (Künzler, 2018). Therefore, they produce a cornucopia of diverse, unique bioactive substances. These basidiomycete-derived bioactive secondary metabolites have been attracted in research for new antibiotic discovery (de Mattos-Shipley et al., 2017; Sandargo et al., 2019).

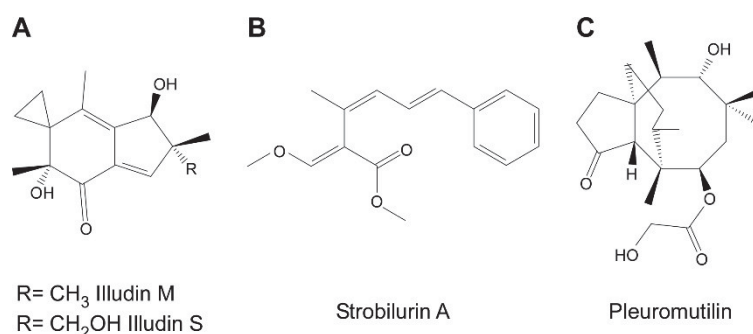


**Figure 1.8 Important bioactive secondary metabolites from Basidiomycota.**

(A) The chemical structure of cytotoxic illudins M and S from species of the genera *Omphalotus* and *Lampteromyces*. (B) The chemical structure of antifungal strobilurin A. (C) The chemical structure of pleuromutilin, a tricyclic diterpenoid from *Clitopilus passeckerianus*. The chemical structures are derived from Sandargo et al., 2019.

A few such compounds have made it into development as agrochemical pesticides or pharmaceutical lead structures (Hyde et al., 2019; Sandargo et al., 2019; Tayyrov et al., 2019). Illudins are fungal sesquiterpenoids exhibiting high cytotoxicity in various tumor cell types and have potentials for anticancer drugs (Figure 1.8A; Jaspers et al., 2002; Sandargo et al., 2019). Strobilurins are successful agrochemical fungicides from the mycelial cultures of *Favolachia*, *Mycena*, *Oudemansiella*, *Strobilurus*, and *Xerula* (Figure 1.8B; Stadler and Hoffmeister, 2015; Sandargo et al., 2019). They target the ubiquinol-oxidation center in the mitochondrial cytochromes and block electron transfer (Sauter et al., 1999). As specified above, pleuromutilin from *C. passeckerianus* exhibits a strong inhibition effect on protein synthesis (Figure 1.8C; Hartley et al., 2009; de Mattos-Shipley et al., 2017; Sandargo et al., 2019). The basidiomycete-derived pleuromutilins are launched on the market as the newest antibacterial antibiotics (Sandargo et al., 2019). In addition, some fungi may produce interesting antifungals that are more active against ascomycetes like the highly adaptive human-pathogenic yeast *Candida albicans* (Costa-de-Oliveira and Rodrigues, 2020) than to basidiomycetes, such as the polyines described by Schlingmann et al., (1995).



### 1.3.2 The basidiomycete fungus *Fistulina hepatica*

The beefsteak fungus *Fistulina hepatica*, formerly assigned to Schizophyllaceae (Matheny et al., 2006), is an edible mushroom *incertae sedis* from the order of Agaricales (He et al., 2019). This wood-decaying species has been genome-sequenced with focus to the brown-rot (heart rot) it causes in *Quercus* spp. and *Castanea* spp. (Floudas et al., 2015; Kaffenberger and Schilling, 2015; Regué et al., 2019). Among several other metabolites with interesting chemical properties or bioactivities, some bioactive polyines ('polyacetylenes') have been described from *F. hepatica* (Jones et al., 1966; Ivanova et al., 2013; Tsuge et al., 1999; Vaz et al., 2011; Wu et al., 2005, 2007). In addition to the above-mentioned fungal secondary metabolites, polyines comprise another important class of fungal bioactive compounds. They are even more well-known in plants, exemplified by the antifungals falcarinol and falcarindiol from carrot roots (Garrod et al., 1979a-b; Minto and Blacklock, 2008).

### 1.4 *Ustilago maydis*, a model organism from basic research to biotechnological applications

*Ustilago maydis* is a basidiomycete and causes a corn smut disease. It has to undergo a morphological change to infect its narrow host range infecting only maize (*Zea mays*) and its progenitor plant teosinte (*Zea mays* subsp. *parviglumis*; Bölker et al., 2001).

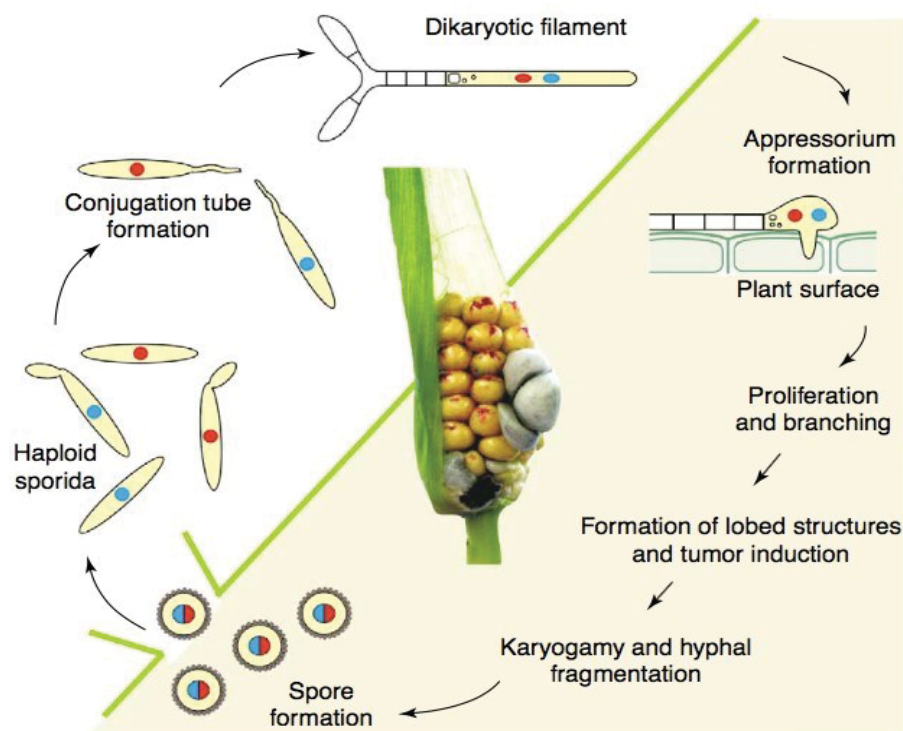


**Figure 1.9. Life cycle of *U. maydis*.**

Different mating types at the *a* and *b* locus are indicated as the blue and red nuclei of the haploid, dikaryotic, and diploid cells. In the middle of the figure, an infected corn ear with tumor formation by *U. maydis* is shown. The figure is derived from Feldbrügge et al., 2004.

To develop the infection stage, two mating types of haploid sporidia recognize its compatible partner via a pheromone/receptor system directed by the *a* mating-type locus and conjugate to form dikaryon (Bölker et al., 1992; Spellig et al., 1994; Szabó et al., 2002; Vollmeister et al., 2012). Afterward, the dikaryon grows in a filamentous form, which possesses pathogenicity. In this stage, the *b* locus encoding a heterodimeric transcription factor, bE/bW directs the PKA/MAPK signaling mediated morphological switch (Kronstad and Leong, 1990; Gillissen et al., 1992; Feldbrügge et al., 2004). The hypha senses plant surface signals that trigger the formation of an appressorium-like structure, a specialized structure at the hypha tip for efficient infection (Mendoza-Mendoza et al., 2009). A number of effector molecules are secreted at the infection zone, and the colonization of the host cells is further processed (Doehlemann et al., 2008). In the intracellular space in the host, *U. maydis* massively proliferates, and fragmentation of hyphae occurs. (Doehlemann et al., 2008). As a result of this colonization, tumors are formed at all aerial parts of the host plants. Within the tumors, black diploid teliospores develop and then germinate under favorable conditions to release haploid cells (Figure 1.9; Vollmeister et al., 2012).

*U. maydis* serves as an excellent model system for basic cell biology and plant pathology (Kahmann and Kämper, 2004; Zarnack and Feldbrügge, 2010; Béthune et al., 2019). The genome is sequenced and well-annotated (Kämper et al., 2006). Transcriptomics and proteomics have been carried out, and sophisticated molecular tools are established (Scherer et al., 2006; Koepke et al., 2011; Olgeiser et al., 2019). Strains can be efficiently generated by homologous recombination, and after stable insertion in the genome, selection markers can be excised using the FLP-FRT system (Brachmann et al., 2004; Khrunyk et al., 2010; Terfrüchte et al., 2014). In addition, CRISPER/Cas9 genome editing technology is established in *U. maydis* and has been applied to delete large-sized biosynthetic gene clusters for metabolic engineering (Schuster et al., 2016; Becker et al., 2020). Moreover, designing synthetic polycistronic mRNAs with viral 2A peptides allows encoding two independent polypeptide chains from a single mRNA in *U. maydis* (Müntjes et al., 2020).

Besides serving as a model for basic research, *U. maydis* is also advancing as a flexible microorganism for biotechnological applications. For this purpose, *U. maydis* has various advantages. Importantly, *U. maydis* have been eaten as a delicacy for centuries in Mexico, indicating that its consumption is not harmful to humans, and the yeast form is non-pathogenic (Brachmann et al., 2001; Feldbrügge et al., 2013). *U. maydis* can utilize a broad range of carbon sources to grow. The yeast form cells consume diverse hexoses and pentoses (Maassen et al., 2014; Cano-Canchola et al., 2000). Furthermore, the list of alternative carbon sources can be expanded during filamentous growth. Since the fungus can proliferate in the host plants, more complex and raw plant materials, such as cellulose, polygalacturonic acid, and homogenized plant tissues, can be catabolized (Cano-Canchola et al., 2000; Doehlemann et al., 2008; Mueller et al., 2008; Couturier et al., 2012; Geiser et al., 2016; Stoffels et al., 2020). As a workhorse platform organism, the duplication time is approximately 2 h during exponential growth in liquid culture. The growth speed is comparable to the ascomycete fungus *S. cerevisiae*, which is well-established in biotechnological applications

(Becht et al., 2005). Different cultivation methods have been deeply established and developed, such as basic baffled shaking flasks and a few liter scale fermenters (Drews and Kraume, 2005, 2007; Klement et al., 2012). The unicellular haploid yeast cells have shown a high hydromechanics stress resistance and the robustness against culture impurities in bioreactors (Klement et al., 2012). Furthermore, bioprocess engineering has been studied to understand cell physiology in *U. maydis* using RAMOS (respiration activity monitoring system). RAMOS is an online monitoring system that stores parameters, such as growth behavior, cultivation medium condition changes, enzymatic activities, and optimal cultivation conditions (Klement et al., 2012; Terfrüchte et al., 2018; Stoffels et al., 2020).

### 1.4.1 From a natural producer to a cell factory of value-added compounds.

*U. maydis* is a natural producer of organic acids (e.g., malate, succinate, itaconic acid, itatartarate, and (S)-2-hydroxyparaconic acid), polyols (erythritol and mannitol), and intracellular triacylglycerols (Guevarra and Tabuchi, 1990; Bölker et al., 2008; Moon et al., 2010). In addition, it naturally produces glycolipids, such as mannosylerythritol lipids (MELs) and ustilagic acids (UAs), which can be used as a basis for sustainable detergents and emulsifiers. These glycolipids are classified as biosurfactants that biologically function for the adhesion to hydrophobic surfaces, allow the bioavailability of water-insoluble substrates, and exhibit bioactivity against different microorganisms (Ron and Rosenberg, 2001). In 1950, ustilagic acid was first described as an insoluble compound with antibiotic activity, secreted from *U. maydis* (Haskins, 1950). The chemical structure has been revealed that the sugar moiety is the disaccharide cellobiose, which is O-glycosidically linked to the  $\omega$ -hydroxyl group of the unusual long-chain fatty acid 15,16-dihydroxyhexadecanoic acid or 2,15,16-trihydroxyhexadecanoic acid (Hewald et al., 2005). By isolating a strain (MB215), which produces a high amount of glycolipid, and creating deletion mutants, key enzymes in the biosynthetic pathway were discovered. Cyp1, a cytochrome P450 monooxygenase, is responsible for the production of cellobiose lipid ustilagic acid. For further modification, another cytochrome P450 monooxygenase Cyp2 is involved in the subterminal hydroxylation of the hexadecanoic acid (Hewald et al., 2005). The biosynthetic genes and Rua1, which is the transcriptional factor containing two C-terminal zinc finger domains within the ustilagic acid biosynthetic gene cluster, have been identified. The transcriptional factor selectively binds to conserved motifs acting as upstream activating sequences (UAS-1 and UAS-2) of promoter sequences for the ustilagic acid biosynthetic genes for the transcriptional activation (Teichmann et al., 2010). Furthermore, optimal conditions, such as nitrogen starvation, have been tested to activate the biosynthetic gene cluster for the higher production of ustilagic acids in *U. maydis* (Hewald et al., 2005; Teichmann et al., 2007; Teichmann et al., 2010; Feldbrügge et al., 2013).

In contrast, the biosynthetic gene cluster for the production of mannosylerythritol lipids is relatively short, containing only five genes (Hewald et al., 2005). The chemical structure of MELs mainly contains a mannosylerythritol disaccharide, and the mannosyl moiety is acylated with different



lengths of fatty acids. MELs are classified depending on the number of acetyl groups. MEL-A is fully acetylated. MEL-B and MEL-C are monoacetylated, whereas MEL-D is deacetylated (Kitamoto et al., 1990). The biosynthetic gene cluster consists of an acetyltransferase gene *mat1*, a major facilitator gene *mnf1*, two putative acyltransferase genes *mac1* and *mac2*, and a glycosyltransferase encoding gene *emt1* (Hewald et al., 2006). The gene cluster of MELs is induced under conditions of nitrogen starvation. Mac1 and Mac2 are essential for the production and secretion of mannosylerythritol lipids by transferring short- and medium-chain fatty acids. Mmf1 plays a significant role in the secretion (Hewald et al., 2006).

Another example of natural products from *U. maydis* is itaconic acid, a versatile building block for tailor-made biofuels (Becker et al., 2020; Wierckx et al., 2020). The applications of itaconic acid and its derivatives are diverse in the industrial production of fibers, plastics, rubbers, and surfactants. Furthermore, itaconic acid has a potential application with bioactivities in agricultural and pharmaceutical areas (Willke and Vorlop, 2001; Okabe et al., 2009; Betancourt et al., 2010; Bera et al., 2015; De Carvalho et al., 2018; Kuenz and Krull, 2018). The production of itaconic acid in *U. maydis* was recently improved by understanding the intrinsic biosynthetic gene clusters for by-products, such as mannosylerythritol lipids (MELs), ustilagic acids (UAs), and triacylglycerols (TAGs), and removing them in the genome to channel carbon source to the desired product efficiently. Additional improvement of gene expression of *ria1*, which encodes the transcription factor in the itaconic acid biosynthetic gene cluster, and optimization of cultivation conditions resulted in the titer 53.5 g/L (Becker et al., 2020).

A recent application is the establishment of *U. maydis* as a novel host for the production of heterologous proteins. This study strongly supports that valuable proteins like antibody formats can be exported in the culture medium by a novel unconventional secretion pathway (Sarkari et al., 2014). In *U. maydis*, the unconventional secretion pathway was first studied when extracellular chitinase Cts1, which contains no classical N-terminal secretion signal, was discovered during basic fungal research on Rrm4 mediated long-distance mRNA transport (Koepke et al., 2011). Through several years of in-depth research on the biological function and its unconventional secretion mechanisms, it was found that Cts1 mediated unconventional secretion prevents undesired *N*-glycosylation of the product that is usually processed during conventional secretion (Stock et al., 2012; Sarkari et al., 2014). As a successful example of pharmaceutical relevant products, an active state of  $\alpha$ BoNTA nanobody ( $\alpha$ BoNTANB), which neutralizes botulinum toxin A (BoNTA) from *Clostridium botulinum*, was produced about 140  $\mu$ g/L via the unconventional secretion manner in *U. maydis* (Terfrüchte et al., 2017).

The utilization of cheap, non-sugar, and non-food carbon sources plays a significant role to practice the economic and sustainable production of value-added products in alternative host microorganisms (Moser and Pichler, 2019). At present, *U. maydis* strains are being optimized to convert plant biomass into valuable products to develop the ecological and economic impact of a biorefinery. As the biotrophic smut fungus, *U. maydis* exhibits filamentous growth during its plant

infection phase and degrades plant cell wall components by transcriptionally activating the intrinsic carbohydrate-active enzymes (CAZymes; Doehlemann et al., 2008). Constitutive activation of two main CAZymes, the endoxylanase Xyn11A and the  $\beta$ -glucosidase Bgl1, improves the saccharification of plant cell wall components during yeast-like growth (Geiser et al., 2016). Furthermore, strains have been successfully engineered to grow on cellulose, xylose, and polygalacturonic acid (Geiser et al., 2016; Stoffels et al., 2020).

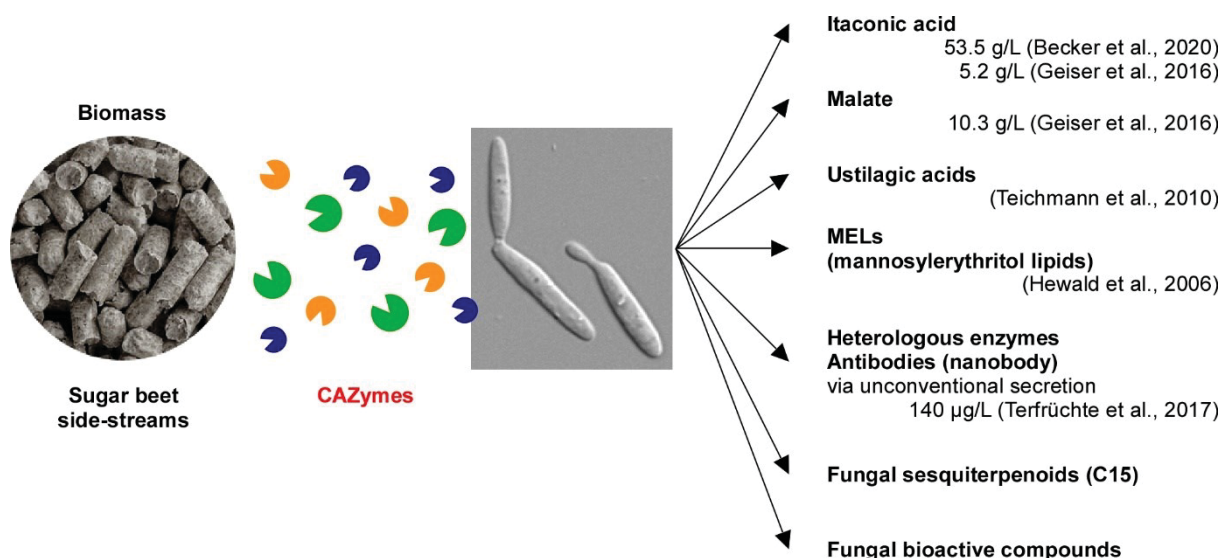


**Figure 1.10 Cell factory concept to produce value-added products via activation of intrinsic CAZymes in *U. maydis* and a blueprint for development.**

Yeast form cells secrete CAZymes to degrade waste biomass, such as sugar beet pulp, and utilize as a carbon source. In the meantime, the engineered strains specifically produce diverse compounds. Itaconic acid, malate, ustilagic acids, and MELs are natural products from *U. maydis*. Further metabolic engineering and optimization of cultivation conditions improved the titers. The established unconventional secretion, an active form of  $\alpha$ BoNTA nanobody was produced (Terfrüchte et al., 2017). Itaconic acid and malate are successful examples of the cell factory concept with CAZymes (Geiser et al., 2016). In the case of itaconic acid, the highest titer was 53.5 g/L up to date (Becker et al., 2020). A further modification is necessary to increase the titer of 5.2 g/L with CAZymes to degrade cellulose (Geiser et al., 2016). Accessibility of the production of fungal sesquiterpenoids and fungal bioactive compounds was tested in this study to expand the list of value-added products by *U. maydis*. Other titers of the value-added products are indicated with the references.

The latter is a major component of pectin. Monomeric galacturonic acid, which is the most abundant sugar in pectin, can be utilized by *U. maydis* to grow on (Müller et al., 2018). However, the polymeric substrate during the saccharification of the plant cell wall is not fully accessible. Genetic activation of hydrolytic enzymes and heterologous production of enzymes, endo- and exo-polygalacturanases allows the yeast form cells to catabolize polygalacturonic acid (Stoffels et al., 2020). Thus, a consolidated bioprocess is being developed, in which complex natural substrates are converted to fermentable sugars and to value-added compounds in the future (Figure 1.10; Geiser et al., 2016).

### 1.5 Aim of this study

In this study, two parts focus on developing the cell factory concept with the basidiomycete fungus *U. maydis* for expanding the production repertoire. The heterologous production of fungal sesquiterpenoids and fungal bioactive compounds in well-established microorganisms, such as *E. coli* and *S. cerevisiae*, is challenging. Thus, this study tackles this challenge to establish a novel basidiomycete model fungus *U. maydis*, which might serve better for the heterologous production.

The first part is the establishment of *U. maydis* as a novel production host for the synthesis of plant and fungal sesquiterpenoids. Bioinformatics analysis should identify the intrinsic mevalonate pathway. Afterward, the accumulation of lycopene in a mutant strain should serve as a molecular read-out of the internal FPP levels, which are crucial for the high production of sesquiterpenoids. Metabolic engineering within the mevalonate pathway should increase the carbon flux to FPP. Since the mevalonate pathway in eukaryotes is compartmentalized, studying the subcellular localization of the limiting step enzymes in *U. maydis* might be informative for future studies to channel the precursor supply within the mevalonate pathway. In the end, the production of (+)-valencene, a well-characterized plant sesquiterpenoid and produced in heterologous systems, will serve as an excellent example to test the capability of *U. maydis* for the production of sesquiterpenoid. Eventually, a fungal sesquiterpenoid synthase Cop6 from *C. cinerea* will be heterologously produced in *U. maydis* to show its potential as a novel basidiomycete model organism to produce fungal sesquiterpenoids.

The second part of the study deals with the whole procedure of identifying novel bioactive compounds from basidiomycete mushrooms for the production of which *U. maydis* might be more suitable than *S. cerevisiae* as a heterologous production organism. A screening of ethyl acetate crude extracts from mycelial cultures of 35 species of basidiomycete mushrooms for differential bioactivity against *S. cerevisiae* and *U. maydis* should help select candidate extracts for further processing. A bioactivity-guided isolation process via HPLC/MS and chemical structure elucidation of bioactive isolate(s) with NMR should then be conducted to identify and isolate the bioactive compound(s) within the crude extract(s).

## 2 Results

### 2.1 Part 1 *U. maydis* serves as a novel production host for the synthesis of plant and fungal sesquiterpenoids

#### 2.1.1 *U. maydis* contains an evolutionarily conserved FPP pathway

To design a strategy for the heterologous production of sesquiterpenoids in *U. maydis*, the underlying metabolic pathways were predicted using bioinformatics analysis (Figure 2.1; Figure 2.2-9). As a starting point, information from the KEGG pathway “terpenoid backbone biosynthesis” was adopted for *U. maydis* (Kyoto Encyclopedia of Genes and Genomes, Kanehisa and Goto, 2000; <https://www.genome.jp/kegg/>). The metabolic network was conceptually divided into four parts: the mevalonate module, the prenyl phosphate module, the carotenoid module, and the recombinant sesquiterpenoid module (Troost et al., 2019). The mevalonate pathway from acetyl-CoA to isopentenyl- and dimethylallyl diphosphate (IPP and DMAPP) is evolutionarily highly conserved in eukaryotes (Miziorko, 2011). Therefore, the detailed knowledge on *S. cerevisiae*, *H. sapiens*, and *A. thaliana* was used as a blueprint (Figure 2.1; Table 2.1; Figure 2.2-9; Nielsen and Keasling, 2016; Ye et al., 2016).

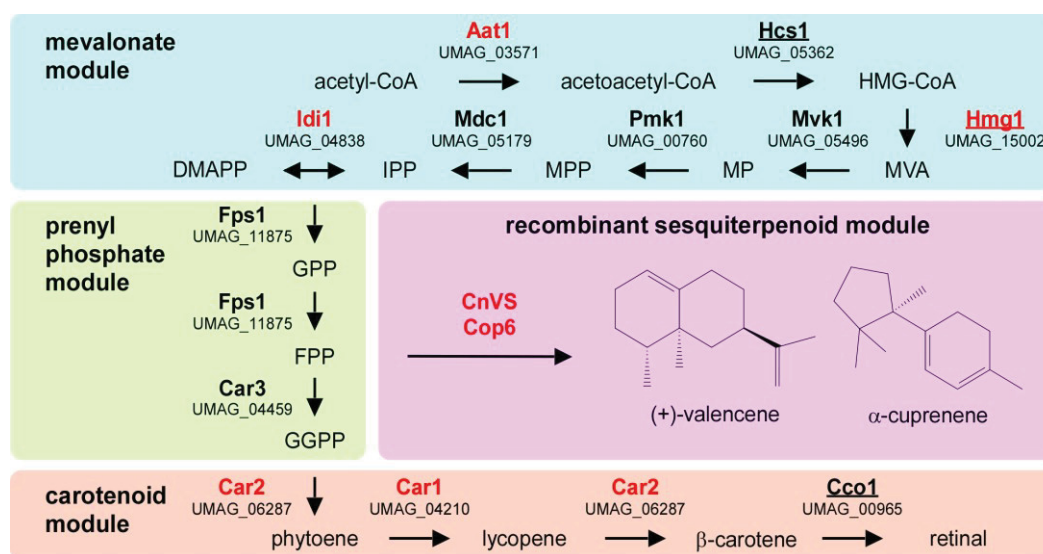


**Figure 2.1 Metabolic network for the heterologous production of sesquiterpenoids.**

Graphical representation of the various modules involved in recombinant sesquiterpenoid synthesis: mevalonate module (blue), prenyl phosphate module (green), carotenoid module (orange), and recombinant sesquiterpenoid module (pink). Enzyme names are given in Table 2.1. Enzymes studied in this study are indicated in red, and those that were already studied in *U. maydis* are underlined (HMG-CoA, 3-hydroxy-3-methylglutaryl-CoA; MVA, mevalonate; MP, mevalonate-5-phosphate; MPP, mevalonate-pyrophosphate; IPP, isopentenyl-pyrophosphate; DMAPP, dimethylallyl-pyrophosphate, GPP, geranyl-pyrophosphate; FPP, farnesyl-pyrophosphate GGPP, geranylgeranyl-pyrophosphate). This figure is derived from Lee et al., 2020a (Figure 1).

The enzymatic functions of enzymes Hcs1 (3-hydroxy-3-methylglutaryl-CoA synthase) and Hmg1 (3-hydroxy-3-methylglutaryl-CoA reductase) have been previously studied in *U. maydis* (Croxen et al., 1994; Winterberg et al., 2010). Hcs1 is essential to synthesize 3-hydroxy-3-methylglutaryl-CoA, which is also a precursor of ferrichrome A biosynthesis for iron-chelating (Winterberg et al., 2010). Hmg1 is the homolog of Hmg1p and Hmg2p from *S. cerevisiae*. The domain architecture of Hmg1 from *U. maydis* is highly conserved with the architectures from its homologs in different organisms (Figure 2.2-9).

**Table 2.1 Putative or experimentally verified enzymes of the mevalonate pathway in different organisms**

<i>U. maydis</i>			<i>S. cerevisiae</i>			<i>H. sapiens</i>		
Name	UMAG	NCBI annotation	Name	Identities (%)	e-value	Name	Identities (%)	e-value
Aat1	03571	Acetyl-CoA C-acetyltransferase	Erg10p	209 (52)	2e-128	ACAT1	240 (59)	4e-166
						ACAT2	175 (45)	7e-104
Hcs1	05362	Probable hydroxymethylglutaryl-CoA synthase	Erg13p	219 (48)	1e-154	HMGCS1	234 (50)	3e-154
						HMGCS2	228 (49)	1e-147
Hmg1	15002	Probable 3-hydroxy-3-methylglutaryl-CoA reductase	Hmg1p	273 (62)	1e-179	HMGCR	258 (60)	8e-172
			Hmg2p	278 (60)	0			
Mvk1	05496	Mevalonate-5-kinase	Erg12p	147 (37)	1e-60	MVK	148 (38)	3e-53
Pmk1	00760	Phosphomevalonate kinase	Erg8p	150 (29)	2e-40	PMVK	No homologs found	
Mdc1	05179	Mevalonate-5-pyrophosphate decarboxylase	Mvd1p	198 (50)	2e-119	MVD	200 (49)	3e-112
Idi1	04838	Isopentenyl diphosphate isomerase	Idi1p	137 (52)	2e-77	IDI1	116 (53)	3e-68
						IDI2	98 (42)	2e-51
Fps1	11875	Putative bifunctional (2E,6E)-farnesyl diphosphate synthase/dimethylallyl transferase	Erg20p	211 (69)	9e-155	FDPS	169 (50)	8e-103

This table is derived from Lee et al., 2020a (Table 1).

The heterologous production of Hmg1 from *U. maydis* in *E. coli* has revealed the enzymatic activity and the catalytic function of the C-terminal domain (Croxen et al., 1994). The remaining enzymes (acetyl-CoA C-acetyltransferase Aat1, mevalonate kinase Mvk1, phosphomevalonate kinase Pmk1, mevalonate diphosphate decarboxylase Mdc1, isopentenyl diphosphate isomerase Idi1, and farnesyl pyrophosphate synthase Fps1) were identified by high amino acid sequence similarity and the presence of conserved domains when compared to well-studied fungal, human and plant versions (Figure 2.1; Table 2.1; Figure 2.2-9). Furthermore, highly conserved amino acids forming active sites of the enzymes were identified during matching known active site forming amino acids of previously studied crystal structures.

Acetyl-CoA C-acetyltransferase Aat1 (acetoacetyl-CoA thiolase) contains the conserved cysteine and histidine, forming an active site of acetoacetyl-CoA thiolase from *Zoolea ramigera*. The structural analysis of the enzyme from *Z. ramigera* revealed that Cys-89 is the site of reaction to form intermediate during the enzymatic reaction, and Cys-378 is a base deprotonating the second acetyl-CoA substrate for condensation. His-348 is suggested to interact with the thioester carbonyl of acetyl-CoA to stabilize the carbanion produced after proton abstraction (Miziorko, 2011). These



essential amino acids in the active site are also found in the homologs from *S. cerevisiae*, *H. sapiens*, and *A. thaliana* (Figure 2.2).

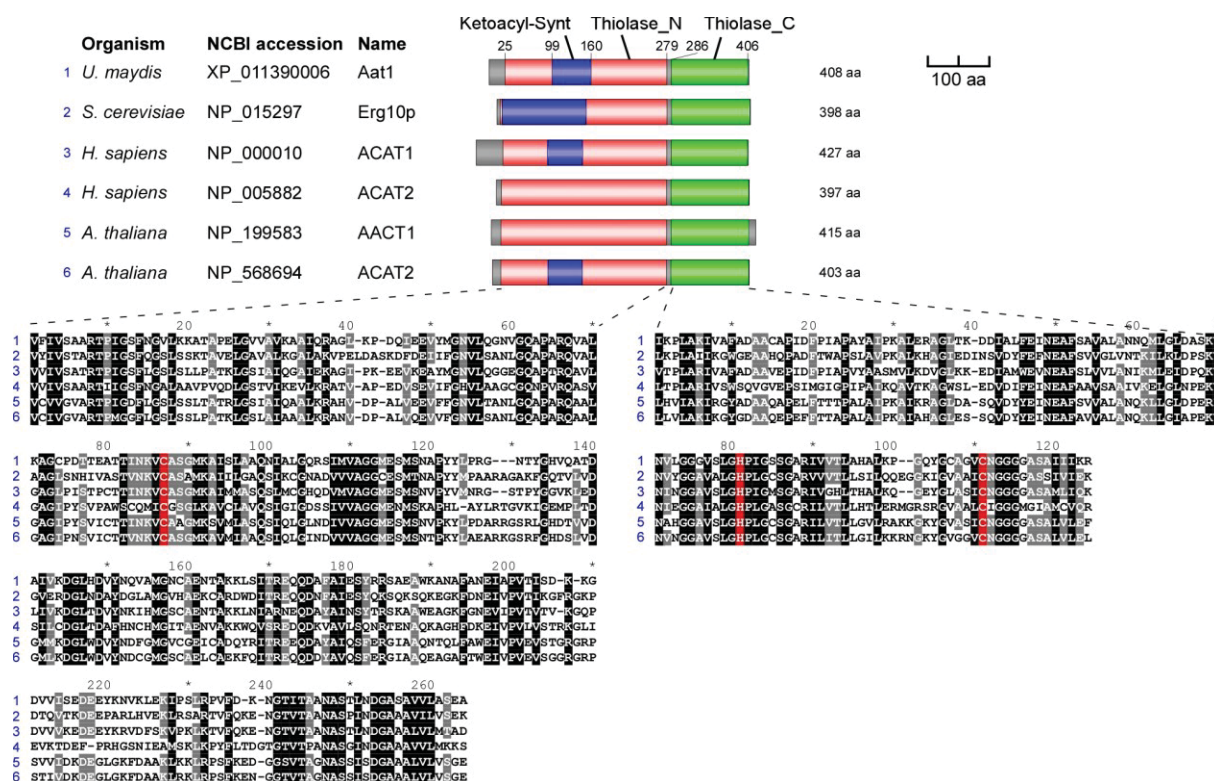


**Figure 2.2** Amino acid sequence comparison of acetyl-CoA C-acetyltransferase Aat1 with homologs in *S. cerevisiae*, *H. sapiens*, and *A. thaliana*.

Domain architecture, according to SMART is given on the top (Ketoacyl-Synt, protein families Pfam identifier PF00109; Thiolase\_N, PF00108; Thiolase\_C, PF02803), and a sequence alignment of the corresponding domains is given at the bottom. Essential amino acids in the active site of the enzyme from the bacterium *Zoogloea ramigera* are given in red (Miziorko, 2011). This figure is derived from Lee et al., 2020a (Supplementary Figure S1A).

The structure of HMG-CoA synthase (MvaS) from the Gram-positive bacterium *Staphylococcus aureus* has been previously elucidated and the active site forming amino acids, Cys-111, His-233, and Glu79 are highly conserved in the homologs from *U. maydis*, *S. cerevisiae*, *H. sapiens*, and *A. thaliana* (Figure 2.3). Within the active site of HMG-CoA synthase from *S. aureus*, Cys-111 and Glu-79 are catalytic base, forming the acetyl-enzyme reaction intermediate and involving in the condensation step with the carboxylate oxygen abstracting a proton from the methyl carbon of acetylcysteine, respectively. Acetoacetyl-CoA is bound with His233 (Miziorko, 2011).

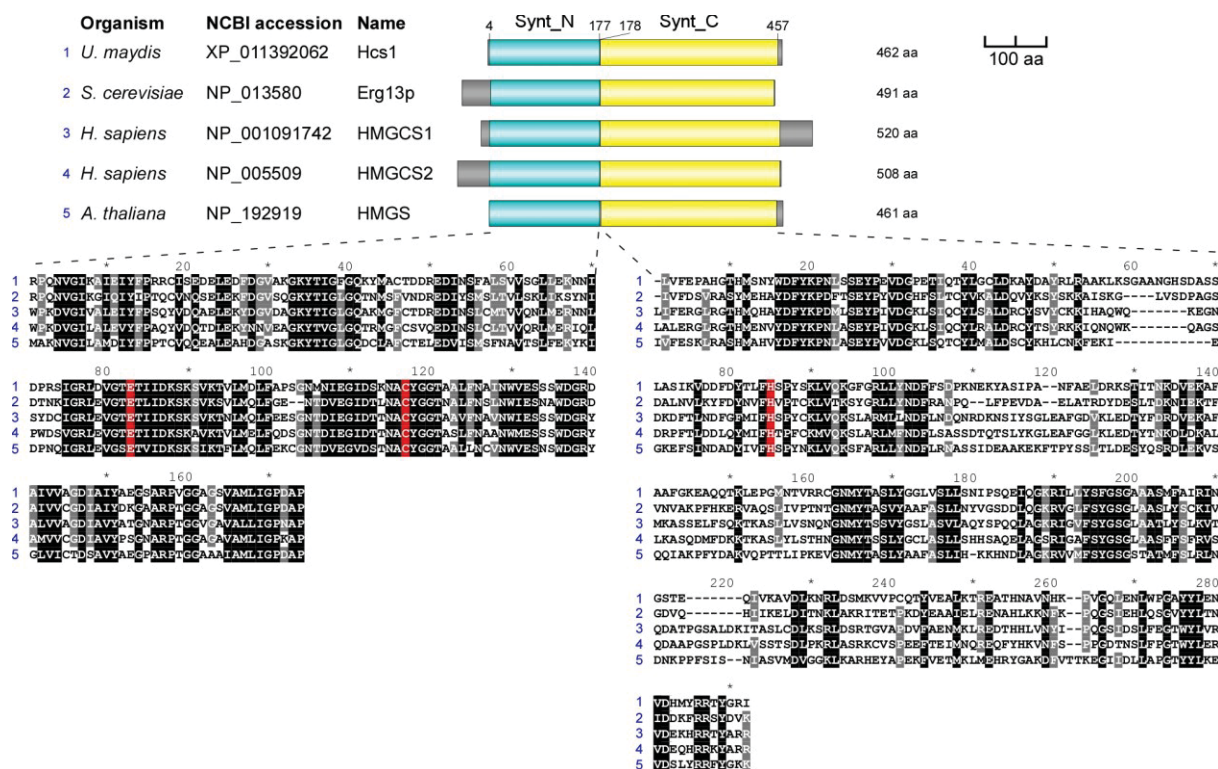


**Figure 2.3 Amino acid sequence comparison of 3-hydroxy-3-methylglutaryl-CoA synthases with homologs in *S. cerevisiae*, *H. sapiens*, and *A. thaliana*.**

Domain architecture, according to SMART is given on the top (Synt\_N, protein families Pfam identifier PF01154; Synt\_C, PF08540), and a sequence alignment of the corresponding domains is given at the bottom. Essential amino acids in the active site of the enzyme from the bacterium *Staphylococcus aureus* are given in red (Miziorko, 2011). This figure is derived from Lee et al., 2020a (Supplementary Figure S1B).

The catalytic domain, HMG-CoA red domain, is highly conserved in 3-hydroxy-3-methylglutaryl-CoA synthase Hmg1 and its homologs in *S. cerevisiae*, *H. sapiens*, and *A. thaliana* (Figure 2.4). Asp-767, Lys-691, and Glu-559 form the active site of human HMG-CoA reductase (Miziorko, 2011). Asp-767 involves in a hydrogen bond network with Lys-691. Both Lys-691 and Glu-559 are in close proximity to the thioester carbonyl of HMG-CoA and involves in two reductive steps to form mevalonate (Miziorko, 2011). These three key residues are also found in the homologs from *U. maydis*, *S. cerevisiae*, *H. sapiens*, and *A. thaliana* (Figure 2.4).

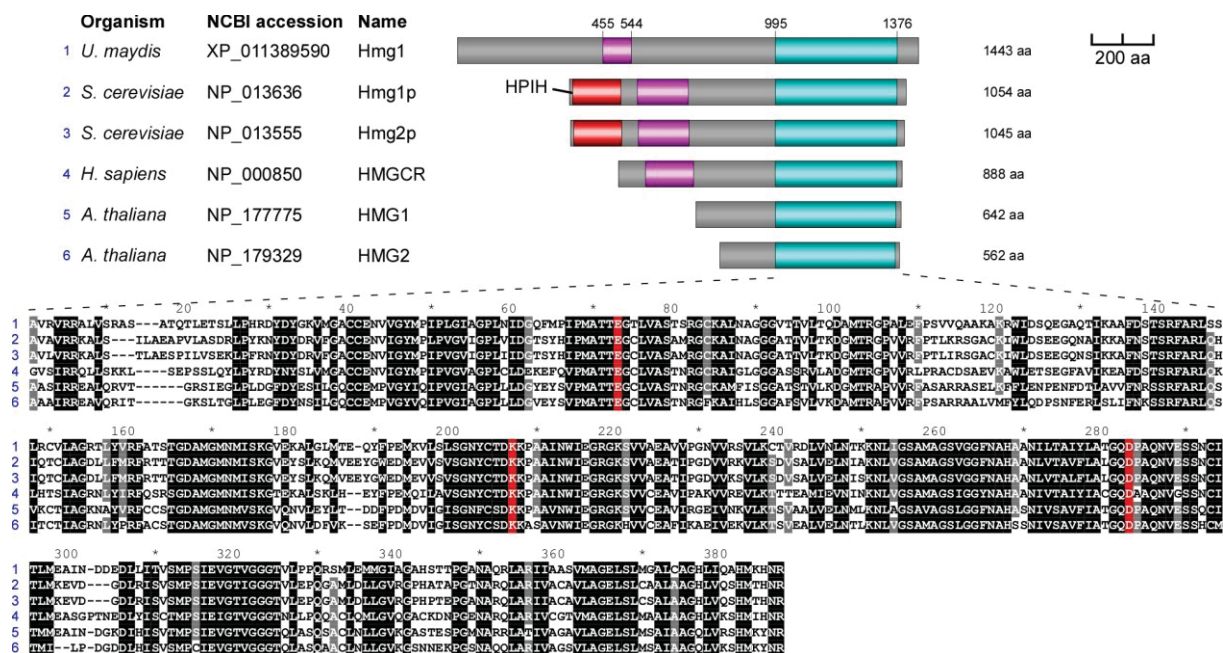


**Figure 2.4 Amino acid sequence comparison of 3-hydroxy-3-methylglutaryl-CoA synthase Hmg1 with homologs in *S. cerevisiae*, *H. sapiens*, and *A. thaliana*.**

Domain architecture, according to SMART is given on the top (Sterol sensing, protein families Pfam identifier PF12349; HMG-CoA red, PF00368; HPIH, PF13323), and a sequence alignment of the corresponding domains are given at the bottom. Essential amino acids in the active site of the enzyme from *H. sapiens* are given in red (Miziorko, 2011). This figure is derived from Lee et al., 2020a (Supplementary Figure S1C).

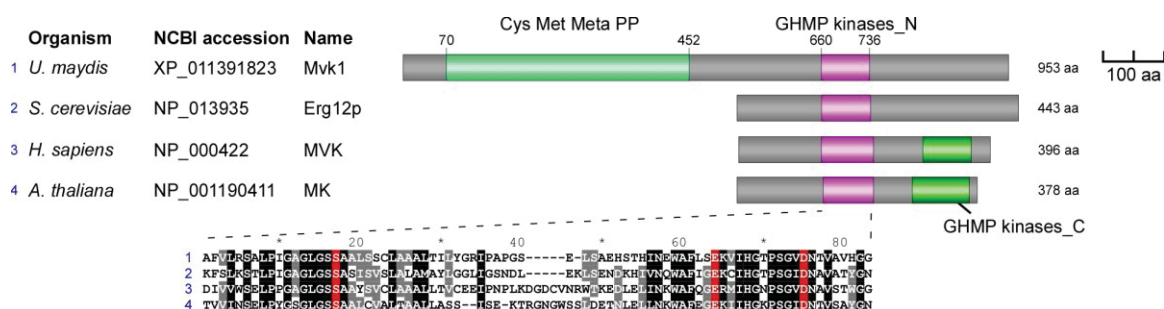


**Figure 2.5 Amino acid sequence comparison of mevalonate kinase Mvk1 with homologs in *S. cerevisiae*, *H. sapiens*, and *A. thaliana*.**

Domain architecture, according to SMART is given on the top (Cys Met Meta PP, protein families Pfam identifier PF01053; GHMP kinases\_N, PF00288; GHMP kinases\_C, PF08544), and a sequence alignment of the corresponding domains is given at the bottom. Essential amino acids in the active site of the enzyme from *Rattus norvegicus* are given in red (Miziorko, 2011). This figure is derived from Lee et al., 2020a (Supplementary Figure S1D).

Mevalonate kinase from *U. maydis* was the only enzyme not predicted in the KEGG pathway database. A previous structural study with mevalonate kinase from *Rattus norvegicus* has demonstrated that Glu-193 and Ser-146 coordinate to bound a magnesium ion, and Lys-13 interacts with the gamma phosphoryl group of ATP and forms a salt bridge with Asp-204, which is positioned to support the transfer of the gamma phosphoryl group of ATP to an acceptor substrate (Fu et al., 2002; Miziorko, 2011). The conserved amino acid residues in the active site of Rat mevalonate kinase were found in the homologs from *U. maydis*, *S. cerevisiae*, *H. sapiens*, and *A. thaliana* (Figure 2.5).



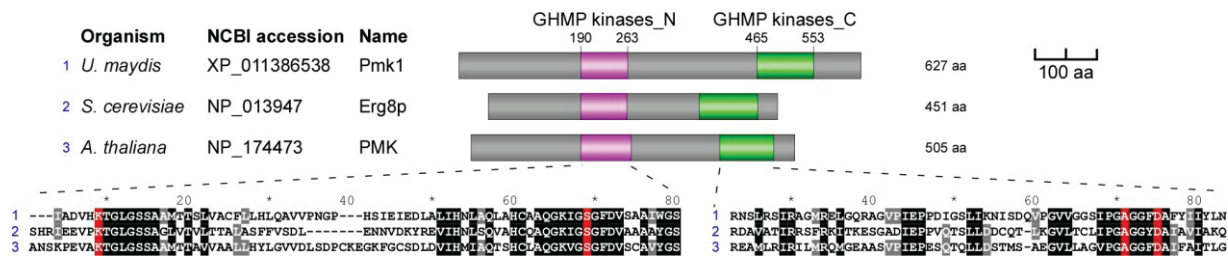


**Figure 2.6 Amino acid sequence comparison of phosphomevalonate kinase Pmk1 with homologs in *S. cerevisiae*, *H. sapiens*, and *A. thaliana*.**

Domain architecture, according to SMART is given on the top (GHMP kinases\_N, protein families Pfam identifier PF00288; GHMP kinases\_C, PF08544), and a sequence alignment of the corresponding domains is given at the bottom. Essential amino acids in the active site of the enzyme from the bacterium *Streptococcus pneumoniae* are given in red (Andreassi et al., 2009). This figure is derived from Lee et al., 2020a (Supplementary Figure S1E).

Phosphomevalonate kinases in invertebrates have low similarity with phosphomevalonate kinases from plants, fungi, and bacteria (Miziorko, 2011). The crystal structure from *S. pneumoniae* has revealed that Lys-101 and Ser-147 serve to bind with the carboxyl group of mevalonate-5-phosphate via a hydrogen bond in the active site. In addition, Ala-293 and Asp-297 are responsible for binding with the phosphoryl group of mevalonate-5-phosphate (Andreassi et al., 2009). The essential amino acid residues for mevalonate-5-phosphate binding were highly conserved in phosphomevalonate kinases from *U. maydis*, *S. cerevisiae*, and *A. thaliana* (Figure 2.6).

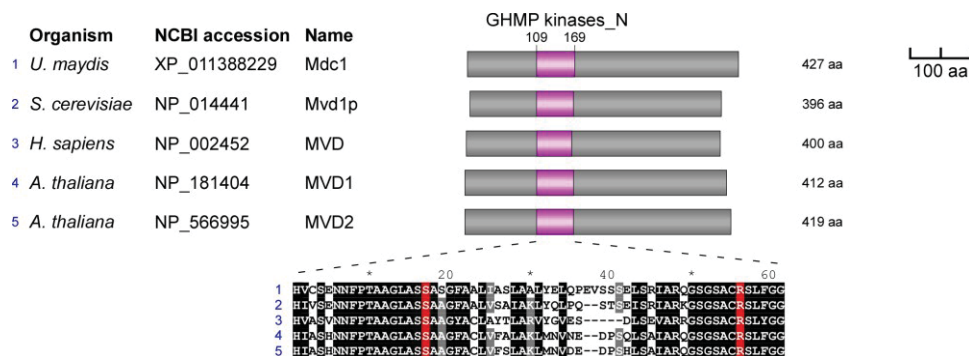


**Figure 2.7 Amino acid sequence comparison of mevalonate diphosphate decarboxylase Mdc1 with homologs in *S. cerevisiae*, *H. sapiens*, and *A. thaliana*.**

Domain architecture, according to SMART is given on the top (GHMP kinases\_N, protein families Pfam identifier PF00288), and a sequence alignment of the corresponding domains is given at the bottom. Essential amino acids in the active site of the enzyme from *H. sapiens* are given in red (Miziorko, 2011). This figure is derived from Lee et al., 2020a (Supplementary Figure S1F).

The conserved GHMP kinases\_N domains were found in mevalonate diphosphate decarboxylases in *U. maydis*, *S. cerevisiae*, *H. sapiens*, and *A. thaliana* (Figure 2.7). Ser-127 and Arg-161 positioning in the active site of human mevalonate diphosphate decarboxylase are highly conserved in the homologs from other organisms (Miziorko, 2011). Ser-127 interacts with the phosphoryl chain of ATP and transfer the gamma phosphoryl group of ATP to mevalonate diphosphate. Arg-161 interacts with the carboxyl group of the substrate (Miziorko, 2011). During the amino acid sequence comparison, the conserved amino acid residues in the active site of human mevalonate diphosphate

decarboxylase were also found in the homologs from *U. maydis*, *S. cerevisiae*, and *A. thaliana* (Figure 2.7).

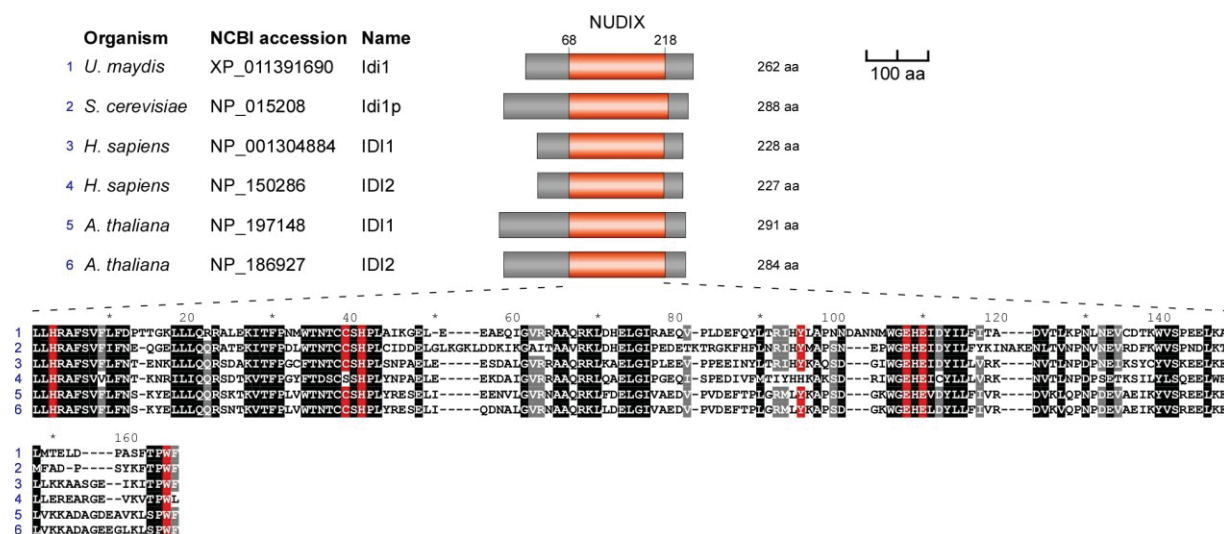


**Figure 2.8 Amino acid sequence comparison of isopentenyl diphosphate isomerase Idi1 with homologs in *S. cerevisiae*, *H. sapiens*, and *A. thaliana*.**

Domain architecture, according to SMART is given on the top (NUDIX, protein families Pfam identifier PF00293), and a sequence alignment of the corresponding domains is given at the bottom. Essential amino acids in the active site of the enzyme from *H. sapiens* are given in red (Zheng et al., 2007). This figure is derived from Lee et al., 2020a (Supplementary Figure S1G).

The same strategy was applied to identify the enzymes of the prenyl phosphate module, producing geranylgeranyl diphosphate (GGPP) via chain elongation from IPP and DMAPP (Figure 2.1; Table 2.1; Figure 2.8). IPP isomerases contain highly conserved NUDIX domains. The active site amino acid residues in two isoforms of human IPP isomerases (IDI1 and IDI2) were also found in the homologs' NUDIX domains. In the NUDIX domain from human IPP isomerases, Cys-87, Tyr-137, Glu-149, and Trp-197 form the active site. Cys-87 and Glu-149 protonate the carbon-carbon double bond of IPP. Tyr-137, which is directly hydrogen-bound to Glu-149, is responsible for the catalytic or substrate binding. His-41, His-52, Glu-147, and Glu-149 coordinate a magnesium ion, and the water molecule is hydrogen-bonded with His-89. (Zheng et al., 2007). The amino acid sequence comparison of isopentenyl diphosphate isomerase Idi1 with homologs in *S. cerevisiae*, *H. sapiens*, and *A. thaliana* also revealed the highly conserved amino acid residues forming the active sites (Figure 2.8).

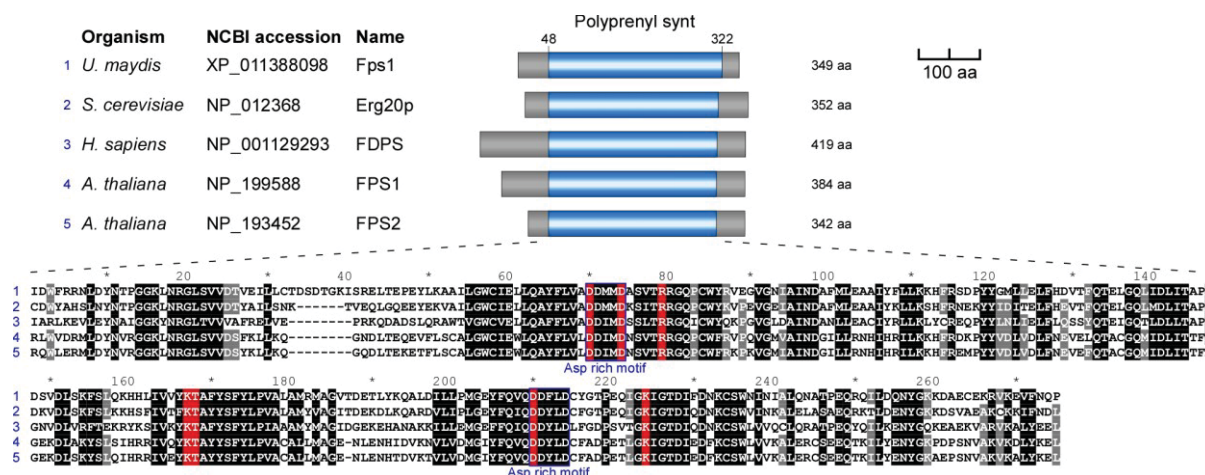


**Figure 2.9 Amino acid sequence comparison of farnesyl diphosphate Fps1 with homologs in *S. cerevisiae*, *H. sapiens*, and *A. thaliana*.**

Domain architecture, according to SMART is given on the top (Polyprenyl synt, protein families Pfam identifier PF00348), and a sequence alignment of the corresponding domains is given at the bottom. Essential amino acids in the active site of the enzyme from *H. sapiens* are given in red (Kavanagh et al., 2006). This figure is derived from Lee et al., 2020a (Supplementary Figure S1H).

Farnesyl diphosphate synthase/dimethylallyl transtransferases synthesize farnesyl pyrophosphate. Aspartate-rich motifs (DDIMD and DDYLD) were conserved in the polyprenyl synt domains of farnesyl diphosphate synthase/dimethylallyl transtransferases from *U. maydis*, *S. cerevisiae*, *H. sapiens*, and *A. thaliana* (Figure 2.9). In addition, amino acid residues of the active site from FDPS in *H. sapiens* are highly conserved. Thr-201 and Lys-200 are the geranyl pyrophosphate binding sites. Arg-112 and Lys-257 are positioned in the flexible loop shielding the active site (Kavanagh et al., 2006). These essential amino acid residues were also found in Fps1 from *U. maydis* (Figure 2.9). The carotenoid module has been predicted before, and its primary function is the production of retinal that serves as a chromophore for photoactive opsin channels Ops1-3 (Estrada et al., 2009; Panzer et al., 2019). The cleavage reaction of  $\beta$ -carotene into two retinal molecules is catalyzed by Cco1 ( $\beta$ -carotene cleavage oxygenase; Estrada et al., 2009). It was already shown that the deletion of *cco1* resulted in the accumulation of  $\beta$ -carotene (Estrada et al., 2009). Loss of retinal synthesis causes no mutant phenotype under standard growth conditions or during pathogenic development. Thus, the biological function of opsins in *U. maydis* during infection is as yet unclear. However, it is suggested that the opsins may play an important role in the plant-fungus interaction (Estrada et al., 2009; Panzer et al., 2019). In the previous study of the carotenoid module in *U. maydis*, the enzymes are predicted via amino acid sequence similarity with other known fungal carotenoid module enzymes. FPP is condensed with IPP by Car3 (UMAG\_04459) to form GGPP. GGPP is further converted into phytoene by a bifunctional enzyme, Car2 (UMAG\_06287), with its enzymatic activity as a phytoene synthase. Car1 (UMAG\_04210) desaturates phytoene to form lycopene. The bifunctional enzyme, Car2, involves in the lycopene cyclization reaction to convert lycopene to  $\beta$ -carotene. Within the carotenoid module, only Cco1 has been functionally characterized (Figure 2.1; Estrada et al., 2009).

For the recombinant sesquiterpenoid module, the key precursor FPP from the prenyl phosphate module is branched off by the plant (+)-valencene synthase from *Callitropsis nootkatensis* (Beekwilder et al., 2014; CnVS; Troost et al., 2019) and the fungal  $\alpha$ -cuprenene synthase Cop6 from *Coprinopsis cinerea* (Agger et al., 2009) to synthesize (+)-valencene and  $\alpha$ -cuprenene, respectively (Figure 2.1). In essence, (+)-valencene served as a benchmarking product for a new approach as it has been the target in multiple studies on microbial sesquiterpenoid production before, while  $\alpha$ -cuprenene served as an example of basidiomycete sesquiterpenoids that has been well-studied before (Agger et al., 2009; Beekwilder et al., 2014; Frohwitter et al., 2014; Stöckli et al., 2019; Troost et al., 2019). These two plant and fungal sesquiterpenoids were used to show the direct proof that the genetically engineered *U. maydis* strains can serve as an alternative platform organism to produce sesquiterpenoids, especially fungal sesquiterpenoids in the future.

### 2.1.2 Establishing the production of lycopene in *U. maydis* as an indicator of carotenoid precursors

For the production of recombinant sesquiterpenoids, improvement of activities of the mevalonate module is required in order to obtain higher levels of the key precursor FPP (Figure 2.1). However, FPP is a toxic intermediate, and the detection of intracellular FPP levels is not trivial (Dahl et al., 2013). Therefore, the intrinsic carotenoid module was modified to accumulate lycopene, a colored FPP-derived product that can be easily detected and quantified (Figure 2.10A-B). Carotenoid synthesis should serve as an easy read-out system for the activity of the underlying metabolic pathway and a safety valve for high FPP levels.

As mentioned above, the carotenoid module was previously studied in *U. maydis* (Figure 2.1; Figure 2.10A). Lycopene is naturally produced by desaturation of phytoene and then further converted into two steps, i.e., cyclization forming  $\beta$ -carotene and the cleavage of this intermediate to retinals. Notably, in *U. maydis*, Car2 is a bifunctional enzyme, serving as phytoene synthase and lycopene cyclase (Estrada et al., 2009). In preparation for lycopene production, *car2* was deleted in the wild type, which abolished carotenoid accumulation due to the bifunctionality of the encoded enzyme (Figure 2.10A-B). The resulting strains exhibited no growth defects. It is consistent with the observation that *cco1* $\Delta$  strains and opsins are dispensable for normal growth of *U. maydis* (Estrada et al., 2009).

To synthesize lycopene in the *car2* $\Delta$  strain, a heterologous phytoene synthase from *Agrobacterium aurantiacum* (AaCrtB; Chen et al., 2016) was produced. It should enable heterologous reconstruction of the process and efficient visual detection of the red color of lycopene (Figure 2.10A-B). The corresponding bacterial open reading frame was codon-optimized for *U. maydis* (see Materials and Methods), and the constitutively active promoter  $P_{rpl40}$  controlled the expression. The respective promoter region was derived from *rpl40*, encoding a ribosomal protein of the large subunit.



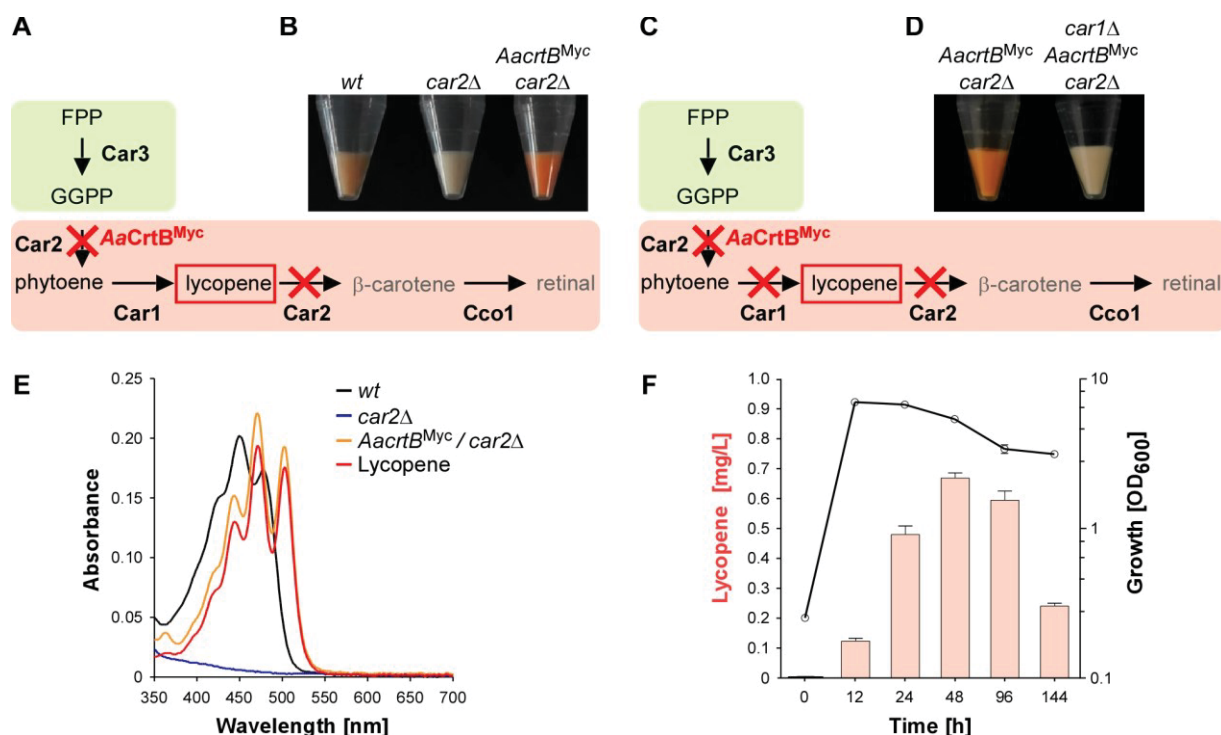


**Figure 2.10 Lycopene production in *U. maydis*.**

(A) Schematic representation of the carotenoid module given in Figure 2.1 and generation of a strain for lycopene production (red cross indicates gene deletion; AacrB<sup>Myc</sup> is the phytoene synthase from *Agrobacterium aurantiacum* containing a triple Myc epitope tag). (B) Cell pellets of strains indicated above the image. (C) Schematic representation of the carotenoid module given in Figure 2.1 and the functionality of Car1 (red cross indicates gene deletion). (D) Cell pellets of strains indicated above the image. (E) Absorption spectrum of various *U. maydis* strains. (F) Analysis of lycopene concentrations (left, orange bars) in relation to the growth phase of strain producing AacrB<sup>Myc</sup> and carrying a deletion of *car2* (OD<sub>600</sub>, black line). Three independent biological experiments (*n*=3) were carried out. Error bars indicate the standard deviation of the mean (SD). This figure is derived from Lee et al., 2020a (Figure 2; Supplementary Figure S2A-B).

The resulting construct was inserted at the *car2* locus of the *car2*Δ strain by homologous recombination. A triple Myc epitope tag was fused at the C-terminus to confirm the heterologous production of the full-length protein. The production was verified by Western blot analysis (see below). Car1 is predicted as a phytoene desaturase (Estrada et al., 2009). The heterologous production of AacrB<sup>Myc</sup> in a *car1* and *car2* double deletion strain resulted in no production of carotenoids and confirmed the necessity of Car1 for the implementation of lycopene as the end product in this strategy (Figure 2.10C-D).

Analyzing the AacrB<sup>Myc</sup> producing strain demonstrated the production of lycopene (Figure 2.10E). Recording an absorption spectrum of cell extracts in *n*-hexane showed that the spectrum was shifted in comparison to the wild type from β-carotene- to lycopene-specific maxima (λ<sub>max</sub> 450 nm and 503 nm, respectively; Figure 2.10E; Fish et al., 2002), as measured with a commercially available lycopene standard (see Materials and Methods). Studying the production in shake flasks over time revealed that the lycopene titer increased during cell proliferation. Lycopene was still produced in the stationary phase, and maximal amounts were detected after 48 h of culturing (Figure 2.10F; 0.7 mg/L; see Materials and Methods). In summary, the heterologous production of a bacterial

phytoene synthase in a genetically engineered strain resulted in the efficient production of lycopene as a molecular read-out for intracellular FPP levels.

### 2.1.3 Metabolic engineering of the mevalonate module monitored by lycopene production

To increase the activity of the metabolic pathways leading to higher FPP levels, the expression of three biosynthetic genes that were known to encode enzymes with limiting activity in other well-studied systems was altered (Nielsen and Keasling, 2016; Ye et al., 2016; Troost et al., 2019): Aat1, Hmg1, and Idi1 (Figure 2.1; Table 2.1).

Aat1 was predicted as an acetyl-CoA C-acetyltransferase for acetyl-CoA condensation in the mevalonate module and had high amino acid sequence similarities with the homologs in *S. cerevisiae* (Erg10p, 52%) and *H. sapiens* (ACAT1, 59%; ACAT2, 45%; Table 2.1). Furthermore, the domain architecture is similar to the homologs in *S. cerevisiae*, *H. sapiens*, and *A. thaliana*, and Aat1 contains the highly conserved amino acid residues forming the active site (Figure 2.2). The substrate for the enzymatic reaction is acetyl-CoA, which is a product of glycolysis and the precursor for the TCA cycle and fatty acid biosynthesis (Galdieri et al., 2014). In addition, acetyl-CoA is also the substrate of lysine acetyltransferases (KATs) for protein acetylation, which is important for numerous biological roles, such as transcription, replication, DNA repair, cell cycle, and aging (Galdieri et al., 2014; Krivoruchko et al., 2015). Thus, the first carbon flux step into the mevalonate module is limited.

In the case of Hmg1, an N-terminal truncated version of the reductase designated Hmg1<sup>NA1-932</sup> was generated (Figure 2.4). This enzyme is known to be a rate-limiting enzyme in other organisms for mevalonate synthesis, whose production is under tight control (DeBose-Boyd, 2008). It contains a targeting peptide in the N-terminal extension for insertion into the ER membrane, and the deletion of this region resulted in cytoplasmic localization and higher activity (Donald et al., 1997; Polakowski et al., 1998; Kampranis and Makris, 2012). The domain architecture of Hmg1 from *U. maydis* is highly similar to the architecture of the homologs in *S. cerevisiae*, *H. sapiens*, and *A. thaliana* (Figure 2.4). The sterol sensing domain at the N-termini is responsible for the sensing high accumulation of sterol in the ER and the ubiquitin-mediated degradation of the C-terminal catalytic domain (Figure 2.4; DeBose-Boyd, 2008). In contrast to *S. cerevisiae*, *U. maydis* contains a single Hmg1 enzyme (Table 2.1), and its activity was already investigated in *E. coli* (Croxen et al., 1994). Idi1 from *U. maydis* was predicted as an isopentenyl diphosphate isomerase, which contains a NUDIX domain and highly conserved amino acid residues in the active site of the homologs in *S. cerevisiae*, *H. sapiens*, and *A. thaliana* (Figure 2.8). Isopentenyl diphosphate isomerase is a key-rate-limiting enzyme, and DMAPP and IPP levels are important for the isoprenoid unit condensation to increase the FPP pool (Berthelot et al., 2012; Troost et al., 2019). It is attributed to the fact that the low expression level, enzymatic activity, short half-life, and weak substrate affinity limit the enzymatic function in the MVA pathway (Ramos-Valdivia et al., 1997).



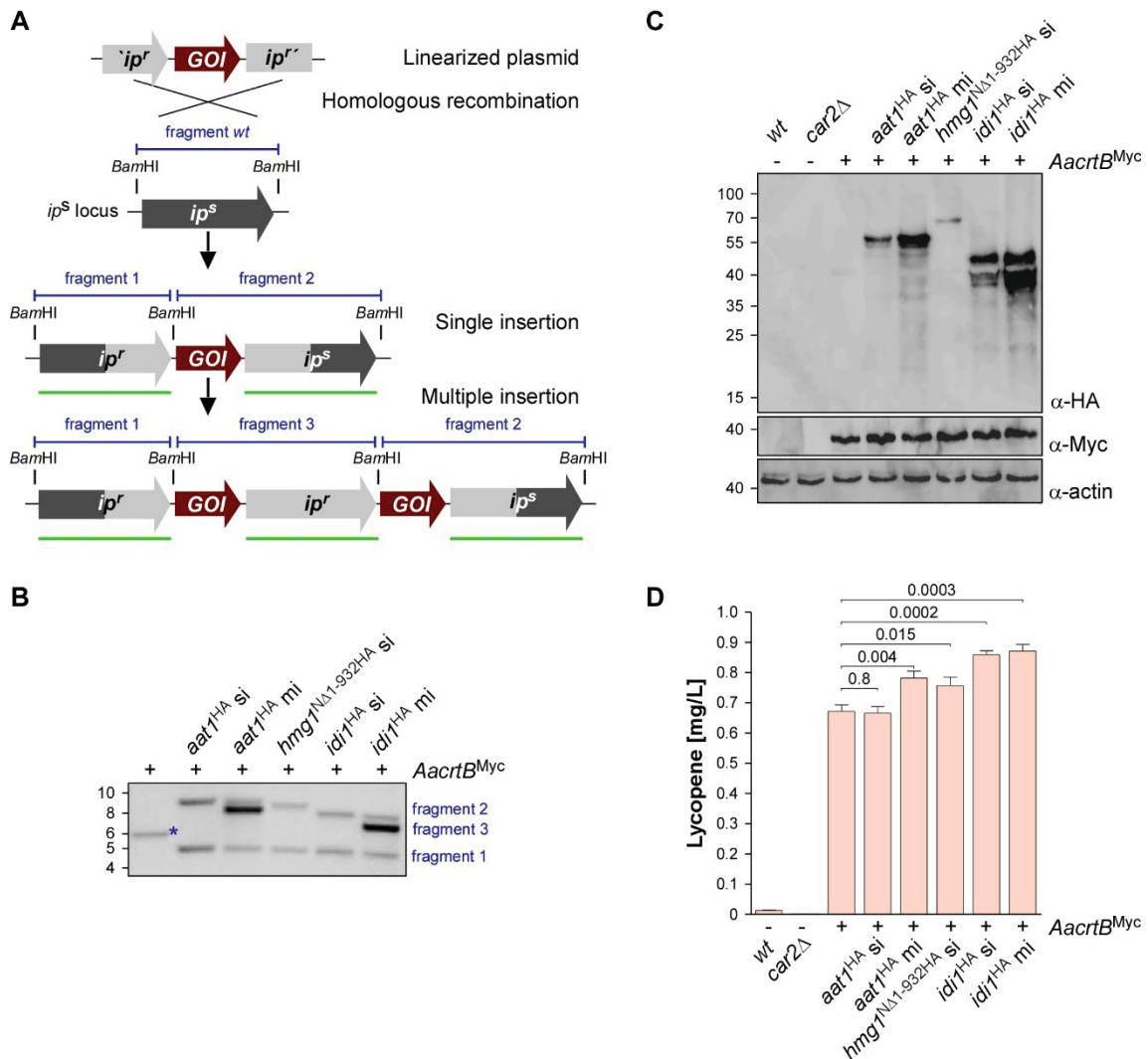


**Figure 2.11 Genetic engineering of the mevalonate pathway.**

(A) Graphical representation of the genetic modification at the *ip<sup>s</sup>* locus encoding an iron-sulfur protein conferring carboxin resistance. The wild type (*wt*) version encoding a sensitive version *ip<sup>s</sup>* is given in dark grey. The corresponding resistant version is given in light grey (*ip<sup>r</sup>*). The gene-of-interest (*GOI*) and fragments expected in Southern blot analysis (shown in B) are given in red and blue, respectively. The probe used for hybridization is indicated as a green line. A more detailed view is shown in Appendix Figure 6.1 (B) Southern blot analysis of strains indicated above the lanes. The wild type band is indicated by a blue asterisk (size marker in kb, left). (C) Western blot analysis of strains indicated above the lanes. The expected molecular weight is 47 kDa for Aat1<sup>HA</sup>, 58 kDa for Hmg1<sup>NA1-932HA</sup>, 34 kDa for Idi1<sup>HA</sup>, 37 kDa for AaCrtB<sup>Myc</sup>, and 42 kDa for actin (UMAG\_11232). Antibodies are given in the lower right corner (size marker in kDa, left). Note that the AaCrtB<sup>Myc</sup> producing strains carried a deletion of *car2*. (D) Analysis of lycopene concentrations in strains given at the bottom. Three independent biological experiments (*n*=3) were carried out. Error bars indicate the standard deviation of the mean (SD). Statistical significance was calculated using the unpaired two-tailed *t*-test, and *p*-values were indicated above. Note that the AaCrtB<sup>Myc</sup> producing strains carried a deletion of *car2*. This figure is derived from Lee et al., 2020a (Figure 3).

To generate *U. maydis* strains with different levels of gene expression, the *ip<sup>s</sup>* locus was chosen (Loubradou et al., 2001). The expression was controlled by the strong constitutively active promoter *P<sub>otef</sub>* and the respective open reading frames were fused at their N-termini with a triple HA epitope tag for detection (Brachmann et al., 2004). Transformation of linearized plasmids resulted in two types of homologous recombination events: (i) single or (ii) multiple insertions (Figure 2.11A). The type of homologous insertion was verified by Southern blot analysis (Figure 2.11B). The detection of

the insertion event was designed in such a way that in the case of a single insertion of the gene-of-interest, the wild type fragment was replaced by two fragments of the predicted size. In the case of a multiple insertion, a third fragment of intermediary size was detected (Figure 2.11A-B; Appendix Figure 6.1). To confirm heterologous production of the full-length protein AaCrtB as a necessity for lycopene accumulation in the tested strains, a triple Myc epitope tag was fused at the C-terminus. The production was verified by Western blot analysis (Figure 2.11C). In addition, as expected, multiple insertions resulted in higher protein amounts (Figure 2.11C). In the case of Hmg1<sup>NA1-932HA</sup>, only single insertion events were obtained, although 30 transformants were screened. It suggests that a strong overproduction of a truncated Hmg1 interferes with growth.

Assaying the lycopene concentration after 48 h of incubation in shake flasks revealed in all cases of additional production of Aat1<sup>HA</sup>, Hmg1<sup>NA1-932HA</sup>, and Idi1<sup>HA</sup>, a statistically significant increase (Figure 2.11D). In the case of Aat1<sup>HA</sup> producing strains, multiple insertions led to a higher lycopene production than a single insertion, indicating that mRNA and protein amounts were limiting. In the case of Hmg1<sup>NA1-932HA</sup>, a slight increase in lycopene yield was observed (Figure 2.11D). A titer of up to 0.9 mg/L could be achieved in strains overproducing Idi1<sup>HA</sup>. The amount of lycopene in the strain with multiple insertions of *idi1*<sup>HA</sup> was not higher, indicating that most likely, the enzyme activity, not the protein amount, is limiting in the strain (Figure 2.11D).

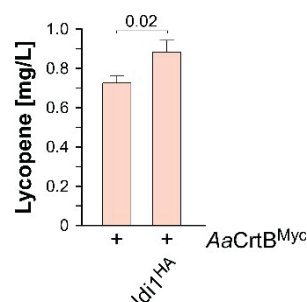


**Figure 2.12 Overexpression of *idi1* in a stable locus for lycopene production in *U. maydis*.**

Lycopene concentrations in strains given at the bottom. Three independent biological experiments ( $n=3$ ) were carried out. Error bars indicate the standard deviation of the mean (SD). Statistical significance was calculated using the unpaired two-tailed *t*-test, and *p*-values were indicated above. Note that the AaCrtB<sup>Myc</sup> producing strains carry a deletion of *car2*. This figure is derived from Lee et al., 2020a (Supplementary Figure S3D).

For additional metabolic engineering and heterologous production of sesquiterpenoid synthases, expression of *idi1*<sup>HA</sup> at the stable locus *cco1* under control of the constitutively active promoter  $P_{rp110}$  was attempted. The promoter region was derived from *rp110*, encoding ribosomal protein 10 of the large subunit. The lycopene titer was increased to 0.9 mg/L (Figure 2.12), which is comparable to the values obtained when *Idi1*<sup>HA</sup> was expressed at the *ip<sup>s</sup>* locus (Figure 2.11D; Figure 2.12).

Thus, by addressing known bottlenecks of the mevalonate pathway, it was possible to alter terpenoid production, which was easily measured as lycopene production. Hence, lycopene is a good indicator and an efficient and robust read-out system for tuning the precursor biosynthetic pathway.

### 2.1.4 The subcellular localization of enzymes involved in FPP synthesis

In eukaryotes, it has been reported that the mevalonate pathway is compartmentalized (Olivier et al., 2000; Sapir-Mir et al., 2008). Peroxisome is the main organelle containing the mevalonate pathway enzymes in mammalian and plant cells (Olivier and Krisans, 2000; Kovacs and Krisans, 2003; Sapir-Mir et al., 2008). The entire mevalonate pathway from the synthesis of acetoacetyl-CoA to IPP and DMAPP is compartmentalized in the peroxisomes in mammalian cells (Olivier et al., 2000). In contrast, the late mevalonate pathway enzymes are localized in the peroxisome in plant cells (Clastre et al., 2011). However, identification of isoforms and signal peptide sequences of the mevalonate pathway enzymes reveals more complex compartmentalization of the mevalonate pathway. Aat1 homologs, for example, are found in peroxisomes and the cytoplasm (Reumann et al., 2007; Simkin et al., 2011; Wang et al., 2017a). 3-hydroxy-3-methylglutaryl-CoA reductase (HMGR) is known to be endoplasmic reticulum (ER) membrane-bound with the N-terminal transmembrane and sterol sensing domains, and the C-terminal catalytic domain is exposed to the cytosol. In mouse brain cells, HMGR is also found in the peroxisomes (Kovacs et al., 2001, 2002; Kovacs and Krisans, 2003). Isopentenyl diphosphate isomerase (IDI1) isoforms in plants contain a conserved peroxisomal targeting signal PTS1 for localization in the peroxisomes (Sapir-Mir et al., 2008; Clastre et al., 2011). To study the subcellular localization of the respective enzymes within the mevalonate module of *U. maydis*, Gfp was fused at their N-termini (enhanced version of the green fluorescent protein, Clontech). The respective genes were inserted at the *ip<sup>s</sup>* locus and the constitutively active promoter *P<sub>ter</sub>* was used for the expression. Measuring green fluorescence revealed that the production of Gfp fusion proteins was detectable (Figure 2.13A). In Western blot analysis, the expected protein size of the full-length fusion proteins was verified (Figure 2.13B).

Fluorescence microscopy showed that the truncated version Hmg1<sup>Δ1-932</sup>-Gfp, missing the predicted ER membrane-spanning region, localized mainly in the cytoplasm, like unfused Gfp. Idi1-Gfp also exhibited mainly cytoplasmic localization (Figure 2.13C). Thus, in contrast to plants (Simkin et al., 2011), geranyl pyrophosphate (GPP) appears to be synthesized in the cytoplasm. Idi1-Gfp also localized to a certain extent to the nucleus (Figure 2.13C). The same holds true for Gfp and it is known that a small proportion of Gfp and small Gfp fusion proteins mislocalize to the nucleus in *U. maydis* (Figure 2.13C).

Microscopic observation of Aat1-Gfp revealed the accumulation of fluorescence signals in distinct foci (Figure 2.13C). This localization pattern is specific for peroxisomes, as indicated by the localization of Gfp carrying a C-terminal SKL localization signal or of peroxisomal protein Pex3-Gfp (Figure 2.13C-D). A second characteristic for peroxisomes in *U. maydis* is their microtubule-dependent transport during hyphal growth (Figure 2.13D; Guimaraes et al., 2015). Fluorescence signals of Aat1-Gfp moved processively along the hypha, as is known for peroxisomes (comparison with movement of Gfp-SKL shown in Figure 2.13D). Thus, either the initial reaction of the mevalonate pathway takes place in peroxisomes or an alternative enzyme is acting during FPP synthesis in the cytosol. In essence, studying the subcellular localization of enzymes of the mevalonate module is

highly informative to devise future metabolic engineering strategies for more efficient precursor supply within specific compartments.

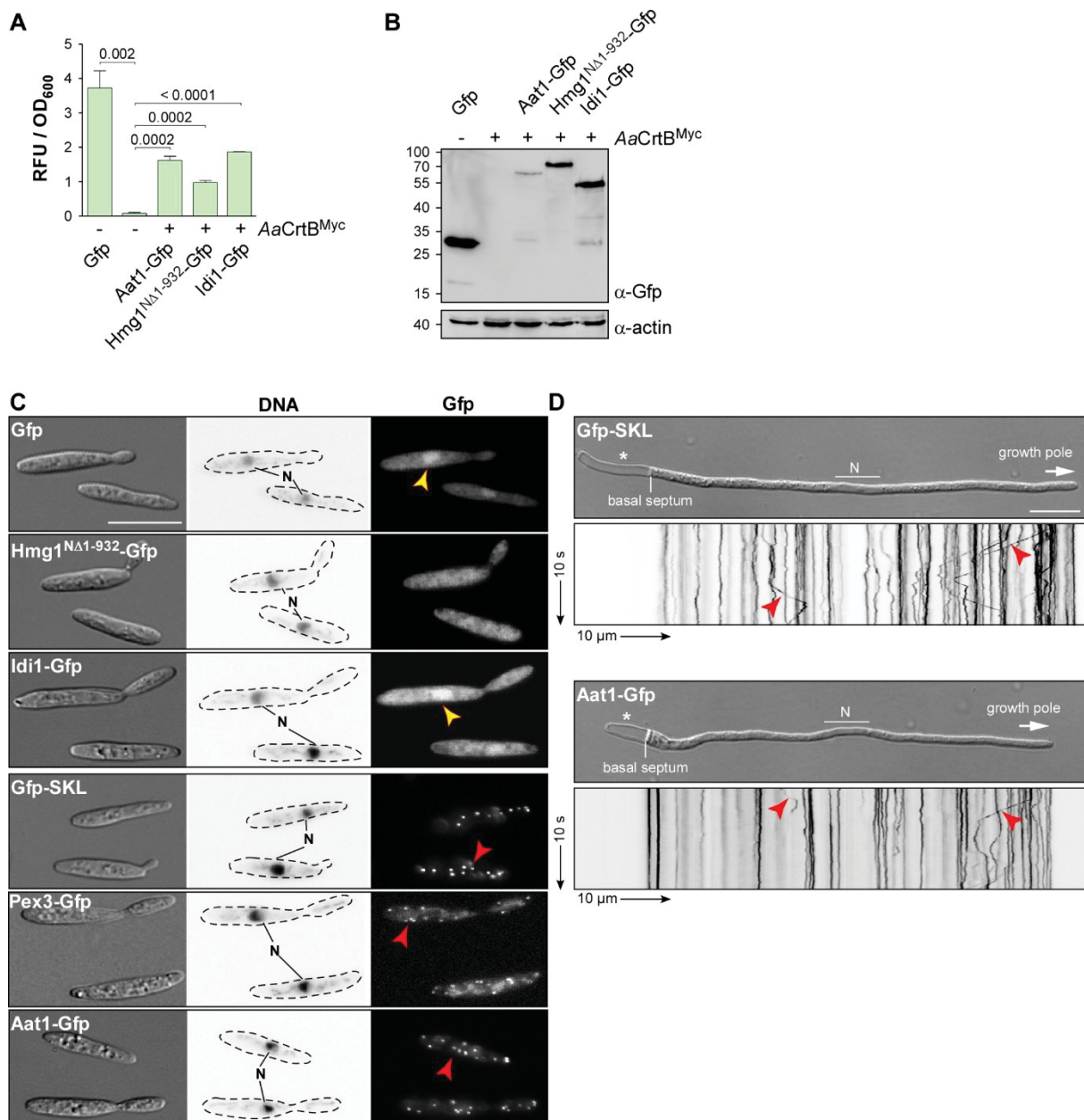


**Figure 2.13 Subcellular localization of enzymes of the mevalonate pathway.**

(A) Quantification of Gfp production using fluorimeter measurements. Relative fluorescence units are given relative to the optical density (OD<sub>600</sub>). At least three independent biological experiments ( $n=3$ ) were performed with three technical replicates per strain. Error bars indicate the standard error of the mean (SEM). Statistical significance was calculated using the unpaired two-tailed  $t$ -test, and  $p$ -values were indicated above. Note that the AaCrtB<sup>Myc</sup> producing strains carried a deletion of *car2*. (B) Western blot analysis of strains indicated above the lanes. The expected molecular weight is 70 kDa for Aat1-Gfp, 81 kDa for Hmg1<sup>NA1-932</sup>-Gfp, 57 kDa for Idi1-Gfp, 37 kDa for AaCrtB<sup>Myc</sup>, and 57 kDa for actin (UMAG\_11232). Antibodies are given in the lower right corner (size marker in kDa given on the left). Note that the AaCrtB<sup>Myc</sup> expressing strains carry a deletion of *car2*. (C) Microscopic analysis showing DIC images of fixed cells on the left (size bar, 10  $\mu$ m). Corresponding staining of DNA with Hoechst 33342 (middle panel; N, nucleus; inverted image) and green fluorescence (Gfp) on the right (yellow and red arrowheads indicate nuclei and peroxisomes, respectively). (D) Microscopic analysis showing DIC images of AB33 hyphae (6 h.p.i.) on top (size bar, 10  $\mu$ m; N, nucleus) and corresponding kymographs at the bottom; genetic background as indicated (arrow length on the left and bottom indicates time and distance, respectively). The bidirectional movement of peroxisomes is visible as diagonal lines (red arrowheads). This figure is derived from Lee et al., 2020a (Figure 4; Supplementary Figure S2D-F).



### 2.1.5 The heterologous production of the plant sesquiterpenoid synthase CnVS in *U. maydis*

As proof of principle for sesquiterpenoid production in *U. maydis*, the plant (+)-valencene synthase CnVS, converting FPP to (+)-valencene was chosen for the heterologous production (Figure 2.1; Beekwilder et al., 2014; Troost et al., 2019). For efficient detection of the protein production, CnVS was fused with Gfp at the N-terminus, as C-terminal fusions were reported to affect enzyme activity (Kampranis and Makris, 2012). The constitutively active promoter  $P_{otef}$  was selected and the gene was inserted at the *upp3* locus of a strain producing  $AaCrtB^{Myc}$  and carrying a deletion of *car2*. The heterologous production was verified by fluorimeter measurements and Western blot analysis (Figure 2.14A-B). Studying the subcellular localization showed the presence of CnVS-Gfp in the cytoplasm in order to ensure substrate access, but also to some extent in the nucleus (Figure 2.14C).

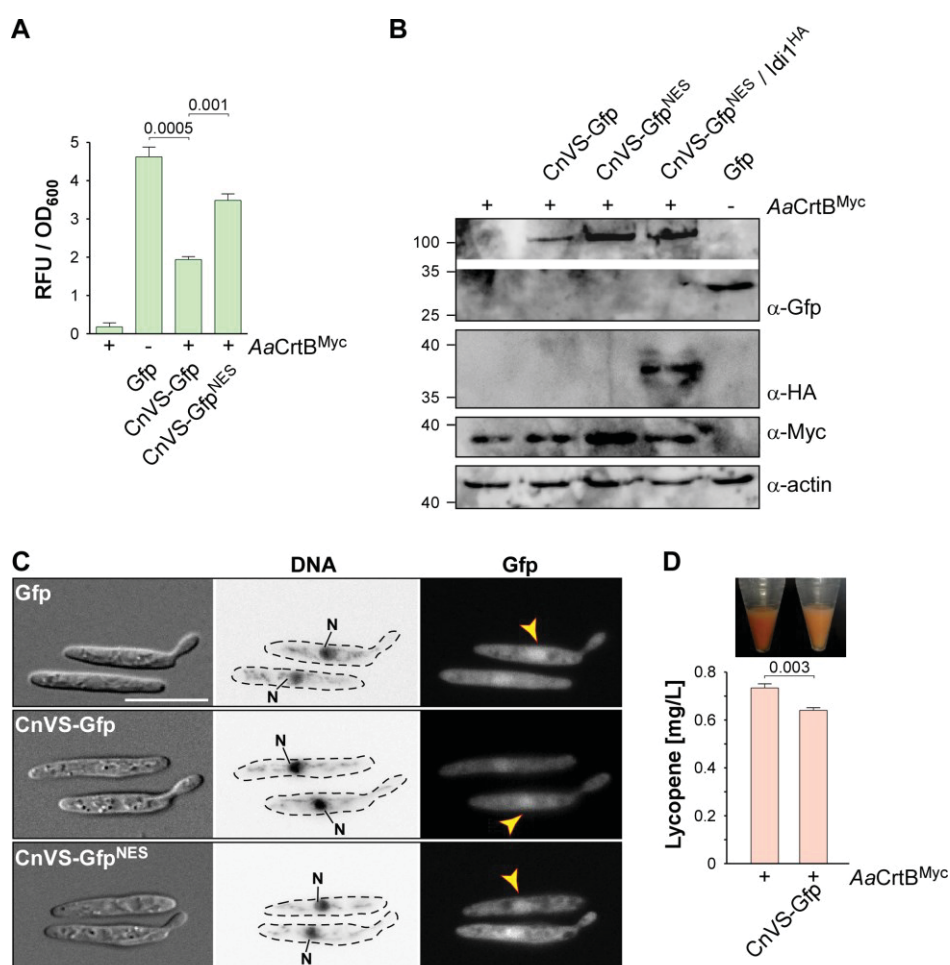


**Figure 2.14 Expression of a heterologous gene encoding (+)-valencene synthase CnVS in *U. maydis*.**

(A) Quantification of Gfp production using fluorimeter measurements. Relative fluorescence units are given relative to the optical density (OD<sub>600</sub>). At least three independent biological experiments ( $n=3$ ) were performed with three technical replicates per strain. Error bars indicate the standard error of the mean (SEM). Statistical significance was calculated using the unpaired two-tailed *t*-test, and *p*-values were indicated above. Note that the  $AaCrtB^{Myc}$  producing strains carried a deletion of *car2*. (B) Western blot analysis of strains indicated above the lanes. The expected molecular weight is 96 kDa for CnVS-Gfp, 97 kDa for CnVS-Gfp<sup>NES</sup>, 27 kDa for Gfp, 37 kDa for  $AaCrtB^{Myc}$ , and 42 kDa for actin (UMAG\_11232). Antibodies are given in the lower right corner (size marker in kDa given on the left). Note that the  $AaCrtB^{Myc}$  producing strain carried a deletion of *car2*. (C) Microscopic analysis showing DIC images of fixed cells on the left (size bar, 10μm). Corresponding staining of nuclear DNA with Hoechst 33342 (middle panel; N, nucleus; inverted image) and green fluorescence (Gfp) on the right (yellow arrowheads indicate nuclei). (D) Cell pellets and lycopene concentrations (orange bars) of



strains given at the bottom. Three independent biological experiments ( $n=3$ ) were carried out. Error bars indicate the standard deviation of the mean (SD). Statistical significance was calculated using the unpaired two-tailed  $t$ -test, and  $p$ -values were indicated above. Note that the AaCrtB<sup>Myc</sup> producing strains carried a deletion of *car2*. This figure is derived from Lee et al., 2020a (Figure 5A-C; Supplementary Figure S3A).

To enhance cytoplasmic localization, a nuclear export signal (NES) from the murine minute virus (MTKKFGTLTI; Engelsma et al., 2008) was fused to the N-terminus of Gfp resulting in CnVS-Gfp<sup>NES</sup>. Fluorescence microscopy revealed that the protein was also produced in this form, but its nuclear localization was only slightly reduced (Figure 2.14C). Hence, the heterologous NES did not function efficiently in *U. maydis*. However, the protein amount of CnVS-Gfp<sup>NES</sup> was significantly higher than CnVS-Gfp (Figure 2.14A-C). The N-terminal NES sequence most likely improved the expression or protein stability as a side effect. Measuring the lycopene titer of the strain co-producing CnVS-Gfp and AaCrtB<sup>Myc</sup> (*car2*Δ background) showed a significant decrease of lycopene accumulation compared to the progenitor strain, which can also be detected by visual inspection (Figure 2.14D). Apparently, a proportion of the FPP is no longer available for lycopene synthesis, suggesting the functionality of the heterologous CnVS-Gfp. In essence, enzymatic cyclization of FPP to (+)-valencene by the heterologously produced CnVS was indirectly observed via the established molecular read-out for intracellular FPP levels.

### 2.1.6 The recombinant production of the plant sesquiterpenoid (+)-valencene in *U. maydis*

To measure the volatile (+)-valencene, CnVS producing strains were incubated with *n*-dodecane to collect the product (see Material and Methods). After 48 h of incubation in shake flasks, (+)-valencene in the *n*-dodecane phase was measured by gas chromatography (Figure 2.15A). A prominent peak was detected in GC-MS analysis with an identical retention time of 7.3 min to the commercial reference (+)-valencene. Importantly, this peak was absent in the negative control strain (Figure 2.15A). Furthermore, analyzing a fragmentation pattern in mass spectrometry (MS) identified a pattern of peaks characteristic for (+)-valencene (Figure 2.15B; Troost et al., 2019). Thus, the identified substance is most likely the desired product. Using a commercial reference (Merck), a standard calibration curve was generated to quantify the titer via GC-FID analysis (Figure 2.15C). Up to 5.5 mg/L (+)-valencene could be obtained from the CnVS-Gfp<sup>NES</sup> producing strain (AaCrtB<sup>Myc</sup> / *car2*Δ; Figure 2.15D). Finally, it was tested whether the overproduction of Idi1<sup>HA</sup>, which improved the carbon flux within the mevalonate pathway (see above), can improve the titer of (+)-valencene. To this end, the corresponding gene was inserted at the *cco1* locus of the strain producing CnVS-Gfp<sup>NES</sup>. For *idi1*<sup>HA</sup> expression, the constitutively active promoter P<sub>rp110</sub> was used. The promoter region was derived from *rp110*, encoding ribosomal protein 10 of the large subunit. In contrast to the improvement of lycopene titer by the overproduction of Idi1<sup>HA</sup>, (+)-valencene production was not increased in this strain (Figure 2.12; Figure 2.14B; Figure 2.15D). To verify whether the N-terminal fusion of Gfp interferes drastically with the enzyme activity, the (+)-valencene titer from a CnVS-Gfp expressing strain (3.3 mg/L) with that of a strain producing an untagged

version (4.8 mg/L; Figure 2.15E) was compared. Hence, the Gfp fusion only slightly reduced the enzyme activity. However, it would be advisable to use an untagged CnVS for an improved production strain. For future attempts, it might be advantageous to downregulate the production of AaCrtB<sup>Myc</sup> or Car3 to redirect more FPP to sesquiterpenoids. In essence, it was successful for the heterologous production of the widely produced plant sesquiterpenoid (+)-valencene, which was chosen here as a common model compound, by reengineering the intrinsic FPP pathway.

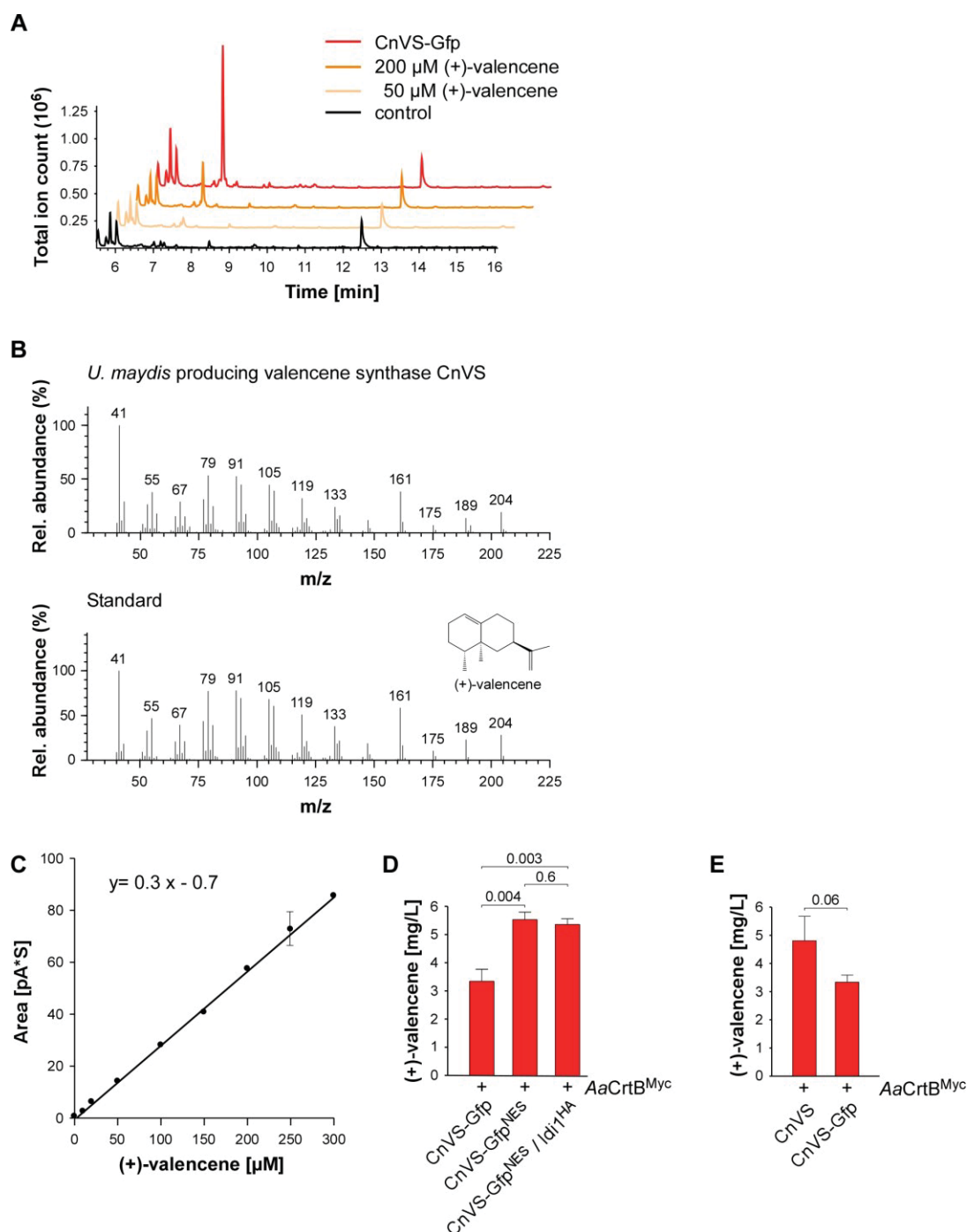


**Figure 2.15 (+)-valencene synthesis in *U. maydis*.**

(A) GC-MS chromatogram of (+)-valencene from CnVS producing strain and the corresponding standard diluted in *n*-dodecane samples of the negative control. (B) Fragmentation pattern of (+)-valencene peak at 7.3 min (shown in A). (C) Calibration curve of the peak derived from GC-FID measurements versus

(+)-valencene concentrations. **(D-E)** The concentration of (+)-valencene produced in the culture, determined by GC-FID according to commercial reference compound. Three independent biological experiments ( $n=3$ ) were carried out. Error bars indicate the standard deviation of the mean (SD). Statistical significance was calculated using the unpaired two-tailed  $t$ -test, and  $p$ -values were indicated above. Note that the  $AaCrtB^{Myc}$  producing strains carried a deletion of *car2*. This figure is derived from Lee et al., 2020a (Figure 5D-F; Supplementary Figure S3B-C).

### 2.1.7 The heterologous production of the fungal sesquiterpenoid synthase Cop6 in *U. maydis*

As pointed out above, the basidiomycete *U. maydis* might serve as a suitable production platform for the synthesis of sesquiterpenoids from higher basidiomycete fungi. For this purpose, a heterologous gene encoding sesquiterpenoid synthase Cop6 from the basidiomycete mushroom *C. cinerea* was expressed in *U. maydis*.

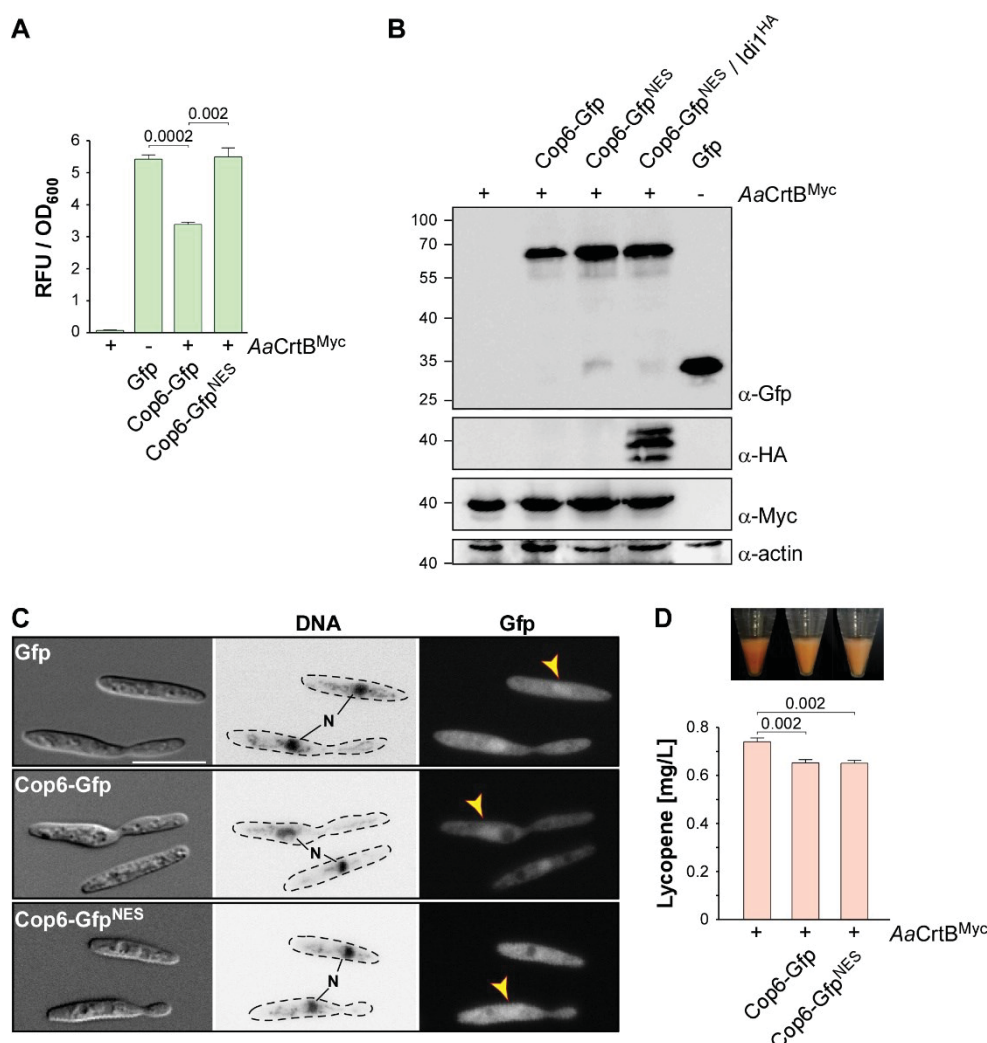


**Figure 2.16** Expression of a heterologous gene encoding  $\alpha$ -cuprenene synthase Cop6 in *U. maydis*.

**(A)** Quantification of Gfp production using fluorimeter measurements. Relative fluorescence units (RFU) are given relative to the optical density (OD<sub>600</sub>). At least three independent biological experiments ( $n=3$ ) were performed with three technical replicates per strain. Error bars indicate the standard error of the mean (SEM). Statistical significance was calculated using the unpaired two-tailed  $t$ -test, and  $p$ -values were indicated above. Note that the  $AaCrtB^{Myc}$  producing strains carried a deletion of *car2*. **(B)** Western blot analysis of strains indicated above the lanes. The expected molecular weight is 65 kDa for Cop6-Gfp, 66 kDa for Cop6-Gfp<sup>NES</sup>, 27 kDa for Gfp, 37 kDa for  $AaCrtB^{Myc}$ , and 42 kDa for actin (UMAG\_11232). Antibodies are given in the lower right corner (size marker in kDa given on the left). Note that the  $AaCrtB^{Myc}$  producing strains carried a deletion

of *car2*. **(C)** Microscopic analysis showing DIC images of fixed cells on the left (size bar, 10  $\mu$ m). Corresponding staining of DNA Hoechst 33342 (middle panel; N, nucleus, inverted image) and green fluorescence (Gfp) on the right (yellow arrowheads indicate nuclei). **(D)** Cell pellets and lycopene concentrations (orange bars) of strains given at the bottom. Three independent biological experiments ( $n=3$ ) were carried out. Error bars indicate the standard deviation of the mean (SD). Statistical significance was calculated using the unpaired two-tailed *t*-test, and *p*-values were indicated above. Note that the AaCrtB<sup>Myc</sup> producing strains carried a deletion of *car2*. This figure is derived from Lee et al., 2020a (Figure 6A-C; Supplementary Figure S4A).

A previous study of six potential sesquiterpenoid synthases from *C. cinerea* showed that Cop6 is highly selective to produce  $\alpha$ -cuprenene, and the gene encoding Cop6 is located in a mini-gene cluster containing two cytochrome P450 monooxygenases encoding genes, *cox1* and *cox2* (Agger et al., 2009). Together with a similar backbone structure like  $\alpha$ -cuprenene, it is suggested that lagopodins, which have antimicrobial activity, could be the oxidized products of Cox1 and Cox2 (Agger et al., 2009; Stöckli et al. 2019). Thus, biosynthesis of  $\alpha$ -cuprenene is well-studied among fungal sesquiterpenoids from higher basidiomycetes, and  $\alpha$ -cuprenene is a value-added product.

For the heterologous production of  $\alpha$ -cuprenene in *U. maydis*, Gfp or Gfp<sup>NES</sup> was fused to the N-terminus of Cop6. To express the gene, the constitutively active promoter *P<sub>oter</sub>* was selected, and the corresponding construct was targeted to the *upp3* locus of a strain producing AaCrtB<sup>Myc</sup> and carrying a deletion of *car2*. The heterologous production was confirmed via fluorimeter measurements and Western blot analysis (Figure 2.16A-B). Analysis of the subcellular localization revealed that Cop6-Gfp localized to the cytoplasm (Figure 2.16C). Consistent with the aforementioned localization of CnVS-Gfp<sup>NES</sup>, the NES version did not prevent the nuclear accumulation but resulted in higher protein amounts (Figure 2.16A-C). As was the case with heterologous production of CnVS described above, the amount of lycopene was reduced in strains co-producing the sesquiterpenoid synthase and AaCrtB<sup>Myc</sup> (*car2* $\Delta$  background), suggesting that part of the FPP was redirected to the recombinant sesquiterpenoid (Figure 2.16D). Thus, the heterologous production of a sesquiterpenoid synthase from the basidiomycete mushroom *C. cinerea* was tested in *U. maydis* and measuring the enzymatic functionality of Cop6 was possible via the FPP competence with the intrinsic carotenoid module.

### 2.1.8 The recombinant production of the fungal sesquiterpenoid $\alpha$ -cuprenene in *U. maydis*

To directly verify the enzymatic reaction of Cop6 in *U. maydis*, Cop6 producing strains were incubated for 48 h in shake flasks, and the  $\alpha$ -cuprenene was trapped in *n*-dodecane (see Materials and Methods). The GC-MS analysis of the organic phase showed an additional peak at a retention time of 7.4 min that was absent in the negative control (Figure 2.17A). The total ion count was slightly higher in the NES version, most likely due to the higher enzyme amount in the Cop6-Gfp<sup>NES</sup> expressing strain (Figure 2.17A). To confirm  $\alpha$ -cuprenene production, the fragmentation pattern of this peak was analyzed in mass spectrometry (Figure 2.17B). The fragmentation pattern was consistent with reported data for  $\alpha$ -cuprenene (Figure 2.17B; Agger et al., 2009). Finally, the yield of  $\alpha$ -cuprenene production was estimated. Due to the absence of a commercial reference for

$\alpha$ -cuprenene, a standard calibration curve was generated with a similar reference sesquiterpenoid  $\beta$ -caryophyllene (Merck) and compared the intensity of the electrically charged particles via GC-FID (Figure 2.17C). The highest amount of  $\alpha$ -cuprenene in the Cop6-Gfp<sup>NES</sup> producing strain was estimated as the titer of 0.1 g/L (Figure 2.17D). The overexpression of *Idi1*<sup>HA</sup> at the *cco1* locus did not increase the titer further (Figure 2.16B; Figure 2.17 D).

In summary, biosynthesis of the fungal sesquiterpenoid  $\alpha$ -cuprenene in *U. maydis* was successful, in addition to the plant-derived (+)-valencene, demonstrating that *U. maydis* serves as a promising novel host for the production of such specific sesquiterpenoids.

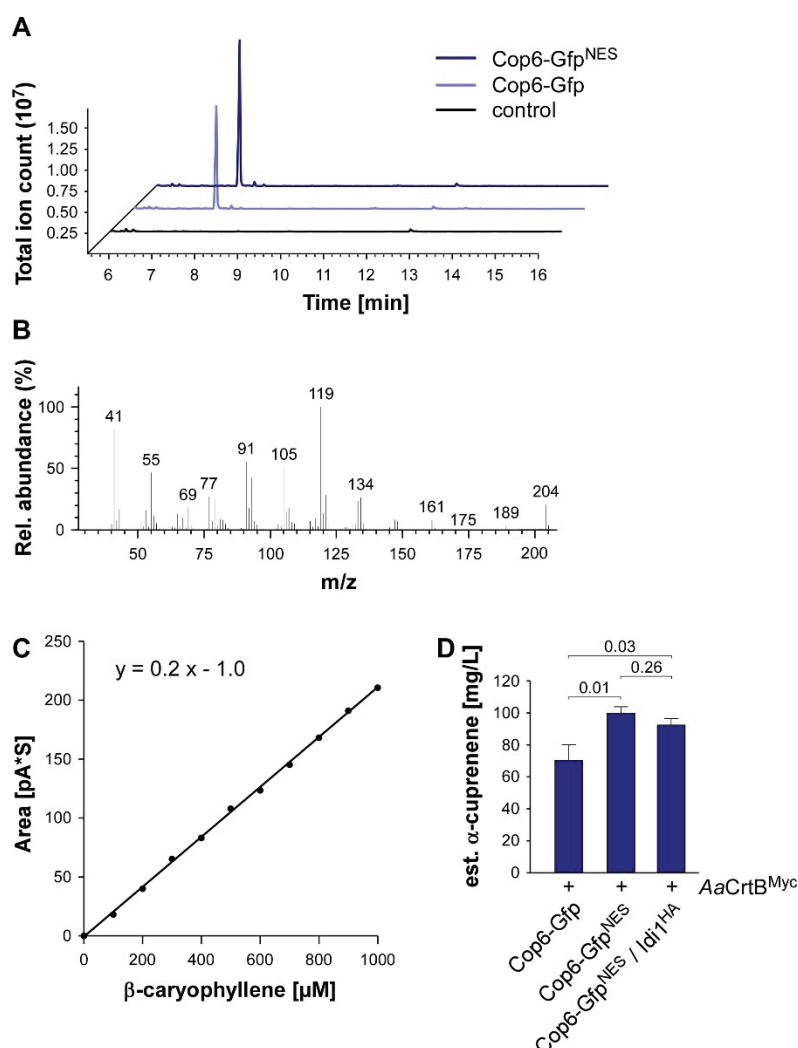


**Figure 2.17  $\alpha$ -cuprenene synthesis in *U. maydis*.**

(A) GC-MS chromatogram of  $\alpha$ -cuprenene from Cop6 producing strains. (B) Fragmentation pattern of peaks at 7.4 min given in (A). (C) Calibration curve of the peak derived from GC-FID measurements versus the chemically related compound  $\beta$ -caryophyllene. (D) Estimated concentration of  $\alpha$ -cuprenene determined via GC-FID using the reference compound  $\beta$ -caryophyllene (Supplementary Figure S4B). Three independent biological experiments ( $n=3$ ) were carried out. Error bars indicate the standard deviation of the mean (SD). Statistical significance was calculated using the unpaired two-tailed *t*-test, and *p*-values were indicated above. Note that the AaCrtB<sup>Myc</sup> producing strains carried a deletion of *car2*. This figure is derived from Lee et al., 2020a (Figure 6D-F; Supplementary Figure S4B).



## 2.2 Part 2 Identification of feldin, an antifungal polyine from the beefsteak fungus *Fistulina hepatica*

### 2.2.1 Bioactivity tests with ethyl acetate extracts from 35 basidiomycete mushroom species

Due to the high bioactivity of fungal secondary metabolites, the heterologous production in many model microorganisms has not yet been established (Xiao and Zhong, 2016). Therefore, the establishment of novel platform microorganisms, which have a higher tolerance for fungal bioactive compounds, is advantageous for understanding the biosynthetic pathways and high heterologous production levels. The basidiomycete fungus *U. maydis* might be more suitable than *S. cerevisiae* as a heterologous production microorganism for diverse fungal compounds from basidiomycete mushrooms. To identify novel bioactive secondary metabolites, ethyl acetate extracts from mycelial cultures of wild strains of 35 basidiomycete mushroom species were tested (Figure 2.18; Appendix Figure 6.3; Appendix Table 6.2). Their antifungal activity was analyzed in an antimicrobial assay against the yeast *S. cerevisiae* and the yeast form of *U. maydis*.

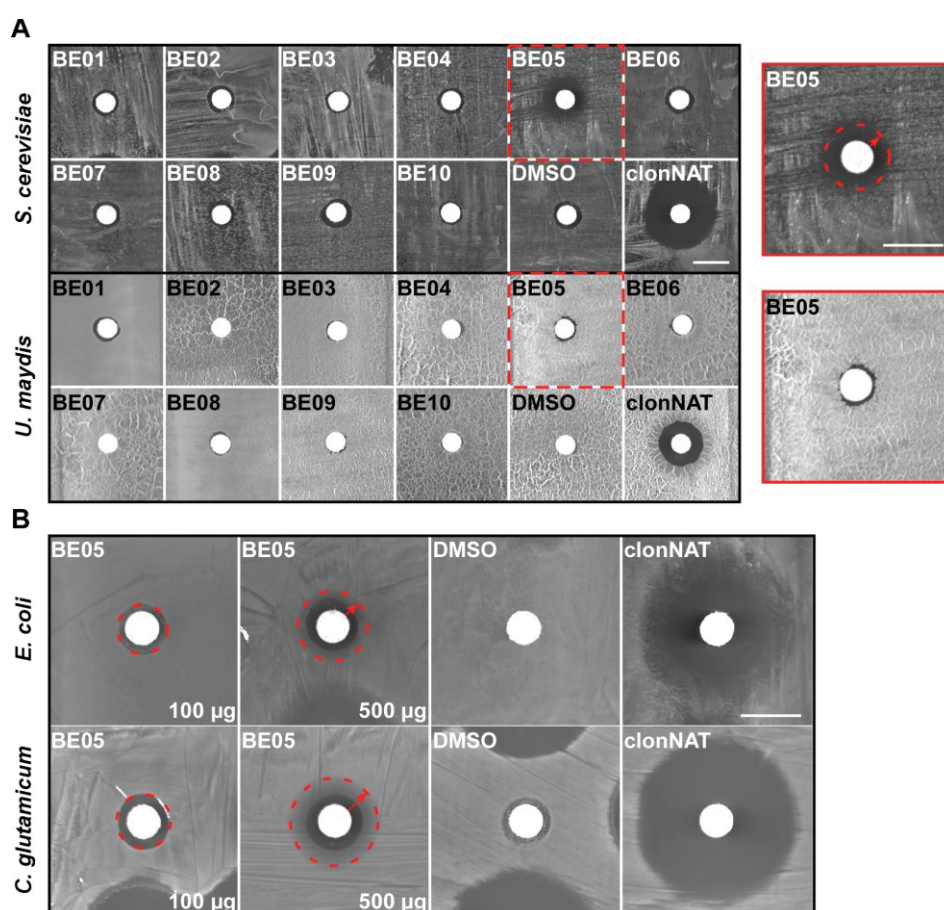


**Figure 2.18 Bioactivity test of the basidiomycete ethyl acetate crude extracts.**

(A) Bioactivity test of the basidiomycete ethyl acetate crude extracts BE01-10 against *S. cerevisiae* and *U. maydis*. 100 µg of each crude extract was dissolved in DMSO to impregnate the filter paper disk centrally placed on each agar plate. DMSO was used instead of such an extract as the negative control, and 200 µg of clonNAT dissolved in ddH<sub>2</sub>O was used as the positive control, respectively. The size bar represents 1 cm. Three independent biological experiments ( $n=3$ ) were carried out. The images in the red-framed panel on the right show magnified photographs of the biotests with extract BE05 from the left panel (highlighted by a dashed

frame), which yielded a zone of growth inhibition (halo, red circle with arrow) with *S. cerevisiae*. (B) Bioactivity test with crude extract BE05 against *E. coli* and *C. glutamicum*. 100 µg or 500 µg of BE05 crude extract were dissolved in DMSO to impregnate the filter paper disk. DMSO was used instead of such an extract as the negative control, and 200 µg of clonNAT dissolved in ddH<sub>2</sub>O was used as the positive control, respectively. The dashed red circle and arrow indicate the size of the growth inhibition zone (halo) with both bacterial strains caused by 500 µg of BE05. This halo comprises an inner zone clearly delimited by its dark color from the agar medium below (no bacterial biofilm), and an outer zone (still some bacterial biofilm) which appears brighter than the inner halo but darker than the surrounding bacterial biofilm beyond the dashed circle. The size bar represents 1 cm. Three independent biological experiments ( $n=3$ ) were carried out. This figure is derived from Lee et al., 2020b (Figure 1; Supplementary Figure S1-2).

The vast majority of extracts showed no activity under these conditions (Figure 2.18A; Appendix Figure 6.3; Appendix Table 6.2). However, the bioactivity of the crude extract BE05 from *Fistulina hepatica* against *S. cerevisiae* was detected. The same extract was hardly active against *U. maydis* (Figure 2.18A). The antifungal crude extract BE05 was further tested against Gram-positive *Corynebacterium glutamicum* and the Gram-negative *Escherichia coli* bacteria. With both bacteria, the application of 500 µg of BE05 extract resulted in the formation of a two-zone halo, the inner zone of which completely lacked bacterial growth. In the adjacent outer halo zone that appears optically brighter than the inner halo, the bacterial lawn was still formed but at a lower density compared to the surrounding biofilm (Figure 2.18B). Compared to *S. cerevisiae* (see Figure 2.18A), where halo formation was already striking with 100 µg of BE05 extract, *C. glutamicum*, as well as *E. coli* exhibited a slight growth inhibition when challenged with BE05 extract (Figure 2.18B).

### 2.2.2 Characteristics of *Fistulina hepatica*

The fungal strain from which the basidiomycete extract BE05 originates has been isolated from basidiomes of *Fistulina hepatica* exhibiting unambiguous ecological and morphological features of this species as described by Knudsen and Vesterholt (2008) and Krieglsteiner, (2000): tongue-shaped basidiome, upper surface reddish-brown, hymenophore light yellowish, consisting of individual tubules, context very soft, reddish-brown, with lighter streaks, exuding a dull red liquid when cut, grown on *Quercus* sp. (Figure 2.19A).

After isolation by sterile explanting of hyphal tufts from freshly harvested fruiting bodies and subcultivation for clean-up, *F. hepatica* mycelium was cultivated for four weeks at 25°C on potato dextrose agar (PDA). PDA was selected over other suitable media for the sake of simplifying the laborious process of identification and isolation of novel bioactive compounds since cultivation on PDA yields reduced pigmentation with various fungi (Griffith et al., 2007).

The previously recorded mycelial characteristics reappeared with our strain of *F. hepatica* grown on PDA: the mycelium displays a whitish wooly to cottony texture that peripherally collapses into a velutinous yellowish colored mat (Figure 2.19B; Stalpers and Vlug, 1983). The less intense yellow pigmentation on PDA, in contrast to the cultures by Stalpers and Vlug, (1983), is in agreement with the work of Griffith et al., (2007), even though the latter work only included ascomycetes.

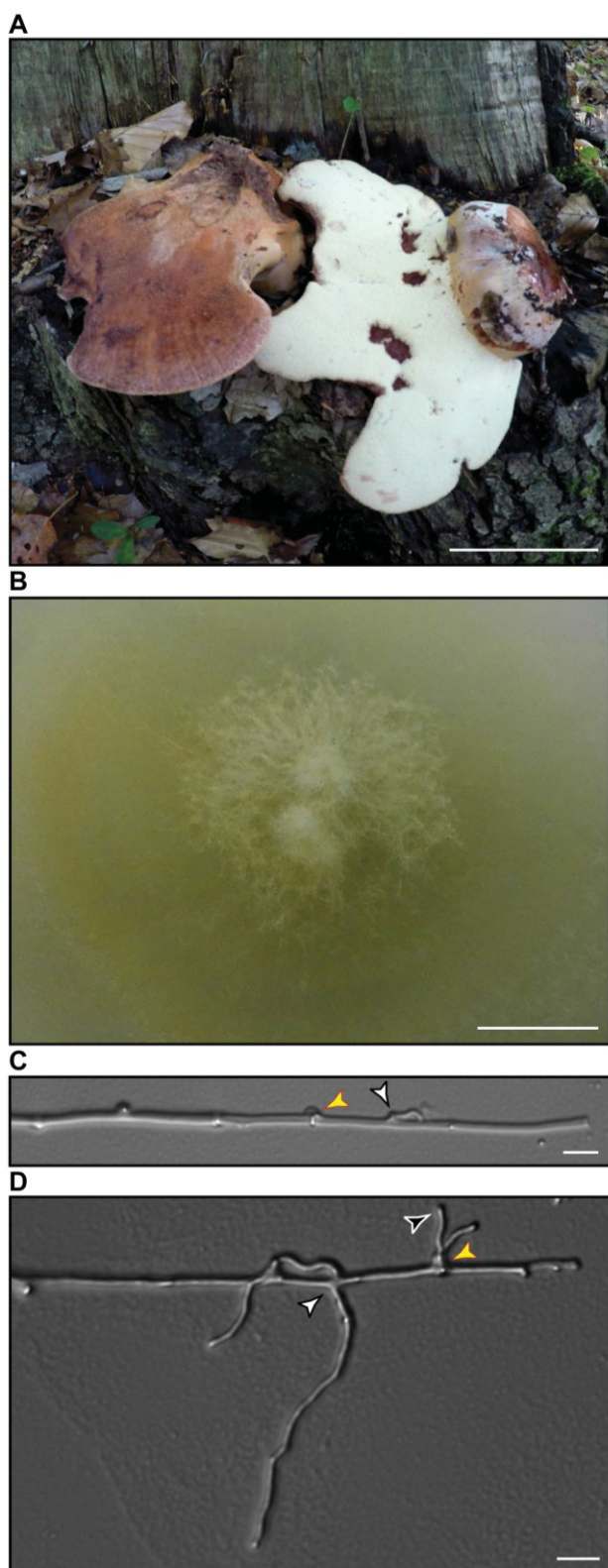


**Figure 2.19 Basidiocarp and mycelial morphology of the *F. hepatica* wild strain the mycelial culture of which served to generate basidiomycete ethyl acetate crude extract BE05.**

(A) Pileal surface (left specimen) as well as stipe and pore surface (right specimen) of two fruiting bodies growing from a stump of an oak tree in a mixed *Fagus sylvatica* forest close to the city of Jena (Germany). The size bar represents 5 cm. (B) Mycelial colony morphology of *F. hepatica* growing on PDA at 25°C. The size bar represents 1 cm. (C-D) Typical hyphal morphology of *F. hepatica* indicating a clamp connection (red-framed yellow arrowhead) at a septum between two dikaryotic hyphal segments of aerial mycelium at the colony margin. Such clamp connections may grow out to form new hyphae (D, white-framed black arrowhead). Side-branch formation on *F. hepatica* hyphae normally occurs via outgrowth of side branches in acute angles (C-D, black-framed white arrowheads). Such a side branch is either more or less equally-sized to the hypha from which it grows out (D, black-framed white arrowheads), or it branches off as a very narrow hypha (C, black-framed white arrowhead) from a wide hypha. The size bar represents 10  $\mu\text{m}$ . This figure is derived from Lee et al., 2020b (Figure 2).

In further agreement with its identity, microscopy of *F. hepatica* mycelium of the here-employed strain on PDA yielded typical features of *F. hepatica* cultures described by Stalpers and Vlug, (1983). Clamp connections were noticed on a regular basis on dikaryotic hyphae (Figure 2.19C). Some clamps grow out to form new hyphae (Figure 2.19D). Also, the typical branching of hyphae was noticed, which normally takes place in acute angles (Figure 2.19D) or happens as branching-off of



very narrow hyphae growing from wide hyphae (see Figure 2.19C). In essence, the morphological characteristics of basidiocarp and mycelial culture *F. hepatica* were confirmed.

### 2.2.3 Identification of the new antifungal polyine feldin from basidiomycete extract BE05

According to the encouraging bioactivity results (see Figure 2.18), the cultivation of *F. hepatica* on PDA was largely upscaled, which was followed by ethyl acetate extraction, LC-MS-based fractionation, and subfractionation of a large amount of BE05 (see Materials and Methods). All fractions were retested for their antifungal activity against *S. cerevisiae* and *U. maydis*. Fractions showing inhibition of *S. cerevisiae* but hardly against *U. maydis*, such as fraction 8.2, were further processed (Figure 2.20A). Via LC-MS-mediated clean-up, purification of one bioactive fraction was possible (fraction 8.2.6) containing only one promising mass signal.

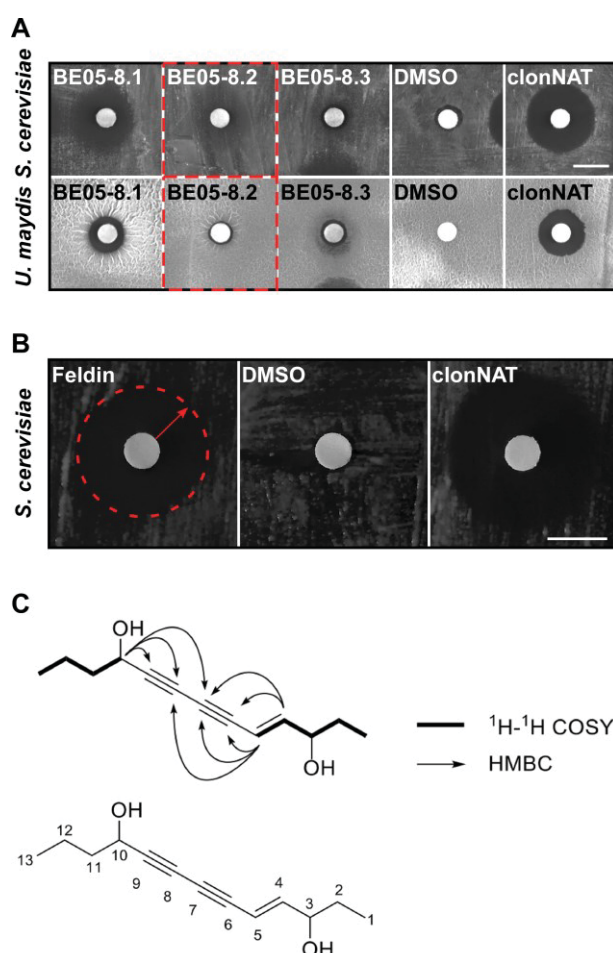


**Figure 2.20 Bioactivity-guided fractionation from the basidiomycete ethyl acetate crude extract BE05, bioactivity of the freshly isolated bioactive compound against *S. cerevisiae*, and structure of the compound (feldin).**

(A) Bioactivity test of the subfraction 8.2. from basidiomycete ethyl acetate crude extract BE05 against *S. cerevisiae* and *U. maydis*. 100  $\mu\text{g}$  of this subfraction was dissolved in DMSO to impregnate the filter paper disk. DMSO was used instead of such an extract as the negative control, and 200  $\mu\text{g}$  of clonNAT dissolved in ddH<sub>2</sub>O was used as the positive control, respectively. The size bar represents 1 cm. Three independent biological experiments ( $n=3$ ) were carried out. (B) Bioactivity of the new polyine against *S. cerevisiae* and *U. maydis*. 100  $\mu\text{g}$  of the new *F. hepatica* polyine feldin was dissolved in DMSO to impregnate the filter paper disk. DMSO was used instead of such an extract as the negative control, and 200  $\mu\text{g}$  of clonNAT dissolved in ddH<sub>2</sub>O was used as the positive control, respectively. The size bar represents 1 cm. Three independent

biological experiments ( $n=3$ ) were carried out. (C) Structure of the new *F. hepatica* polyine feldin. This figure is derived from Lee et al., 2020b (Figure 3).

Structure elucidation of the isolate was carried out via NMR. To possibly obviate potential substance instability, a known feature with polyines, a subsample when freshly obtaining fraction 8.2.6, was immediately sidelined. This subsample has been directly applied to biotesting at least against *S. cerevisiae* (Figure 2.20B) to leave just enough amount of fraction 8.2.6 to execute NMR analysis for structure elucidation, i.e., 2 mg.

**Table 2.2 NMR data assignment of feldin**

No.	$^1\text{H}$ (mult., J)	$^{13}\text{C}$ , mult.
1	0.95 (t, 6.8)	8.6, $\text{CH}_3$
2	1.53 (m)	29.3, $\text{CH}_2$
3	4.06 (td, 7.1, 1.5)	72.4, CH
4	6.32 (15.9, 5.6)	149.8, CH
5	5.78 (ddd, 15.9, 1.7, 0.7)	107.3, CH
6	-	76.0, C
7	-	72.8, C
8	-	68.0, C
9	-	83.2, C
10	4.41 (t, 6.7)	61.5, CH
11	1.68 (m)	39.5, $\text{CH}_2$
12	1.48 (m)	18.1, $\text{CH}_2$
13	0.98 (t, 6.7)	12.6, $\text{CH}_3$

This table is derived from Lee et al., 2020b (Table 2).

The molecular formula of the corresponding compound (Figure 2.20C), designated as feldin, was established from the quasimolecular  $[\text{M} + \text{Na}]^+$  ion peak at  $m/z$  229.1178 (calcd for  $\text{C}_{13}\text{H}_{18}\text{O}_2\text{Na}$ , 229.1199,  $\Delta\text{ppm}$  9.2), which indicated five unsaturated degrees. All proton signals were associated with their respective carbons via analysis of the HSQC spectrum. The resemblance of the NMR data of feldin (Table 2.2) and 4-dodecene-6,8-diyne-1,3,10-triol (Bohlmann and Knoll, 1978), a polyine, suggested that they were structurally similar except that C-1 hydroxymethyl in 4-dodecene-6,8-diyne-1,3,10-triol is replaced by a methyl group ( $\delta_{\text{C}} = 8.6$ ) in feldin. In addition, feldin has one more methylene at C-12 ( $\delta_{\text{C}} = 18.1$ ) than 4-dodecene-6,8-diyne-1,3,10-triol. These structural differences were determined by 2D NMR data (Appendix Figure 6.4). In essence, it was successful for solving the structure of the novel compound feldin from the basidiomycete *F. hepatica* that exhibits antimicrobial activity against the ascomycete *S. cerevisiae*.



### 3 Discussion

#### 3.1 Part 1 *U. maydis* serves as a novel production host for the synthesis of plant and fungal sesquiterpenoids

This study presents a straightforward strategy to engineer the terpenoid metabolism and produce the carotenoid lycopene as well as plant and fungal sesquiterpenoids in *U. maydis*. The establishment of lycopene production functioned as an efficient read-out for the activity of the FPP-dependent pathway. It allowed initial pathway engineering and the production of plant (+)-valencene and fungal  $\alpha$ -cuprenene as proof of principle.

##### 3.1.1 Establishing lycopene production as molecular read-out, reflecting internal FPP levels

To establish a terpenoid producing strain, an advantageous early step is the establishment of a simple read-out system for the activity of the FPP-based metabolic network. To this end, the intrinsic carotenoid pathway was redirected towards lycopene production by deletion of *car2* and the heterologous production of the phytoene synthase *AaCrtB* (Chen et al., 2016). Importantly, loss of retinal biosynthesis does not affect the growth of cells, and currently, no light-regulated biological function could be assigned to retinal-dependent opsins (Estrada et al., 2009). This strategy enabled visual and quantitative detection of the carotenoid lycopene used for initial pathway engineering (see below). The red cell pellet color indicated the available FPP levels, which could be converted to the target sesquiterpenoids (Figure 2.1). This molecular read-out system also successfully played a role in the indication of the functionality of the plant and fungal sesquiterpenoid synthases in *U. maydis* (Figure 2.14D; Figure 2.16D). The heterologous production of sesquiterpenoid synthases consuming FPP reduced lycopene amounts. Thus, the intracellular FPP levels correlated with lycopene yields. Similar strategies have been followed in *S. cerevisiae*, where GGPP was used as a metabolic branching point to synthesize carotenoids. The resulting strains were successfully used to improve terpenoid production by carotenoid-based screening of mutants or by automated lab evolution (Özaydın et al., 2013; Reyes et al., 2014; Triikka et al., 2015). Redirecting naturally occurring carotenoid pathways towards sesquiterpenoids was successfully achieved in *C. glutamicum* and the red yeast *X. dendrorhous*. In contrast to *S. cerevisiae*, both microorganisms are natural producers of carotenoids (Melillo et al., 2013; Frohwitter et al., 2014).

For future advancement of the system, regulation of GGPP synthase *Car3* production is advantageous since high FPP concentrations are toxic for microorganisms, and FPP is the precursor for essential secondary metabolite biosynthesis, such as ergosterol, farnesol, heme A, and ubiquinone (Dahl et al., 2013; Hu et al., 2017). Therefore, increased pathway activity resulting in higher FPP levels could even limit production (Dahl et al., 2013). In *E. coli*, this problem was addressed by using stress-responsive promoters that respond to high FPP levels. The identified promoters were used to create a functional FPP biosensor, and it improved the production of

amorphadiene (Dahl et al., 2013). Thus, lycopene production serves as a safety valve for excess FPP.

Finally, besides the use of lycopene as a read-out system, *U. maydis* might offer the possibility to serve as an alternative host for lycopene production. A sustainable biotechnological approach in *U. maydis* prevents the use of nutrient-rich food like tomatoes for lycopene extraction and avoids the risk of contamination by bacterial toxins when produced in bacteria, such as *E. coli*. The lycopene production titer of the current system is rather low. However, pathway engineering in other fungal microorganisms like *S. cerevisiae* resulted in strains producing 0.3 g/L of lycopene in shake flask fermentation (Shi et al., 2019). Thus, comparable pathway engineering in *U. maydis* could result in similar yield increases.

### 3.1.2 Genetic engineering for higher biosynthesis of FPP

The initial bioinformatics analysis allowed us to annotate the mevalonate, prenyl phosphate, and carotenoid modules in *U. maydis* (Figure 2.1; Table 2.1; Figure 2.2-9). The metabolic engineering of the mevalonate pathway was carried out at three different points: overproduction of Aat1, Idi1, and a truncated version of Hmg1 containing only the catalytic domain (Figure 2.11). In each case, the accumulation of lycopene was higher, supporting the accuracy of the pathway prediction (Figure 2.11D). The most successful approach was the transcriptional upregulation of *idi1*, indicating that this key step is a bottleneck of the pathway in *U. maydis*. Idi1 is also known as the bottleneck in other systems like *S. cerevisiae*, where it was also initially tackled by *IDI1* overexpression or the production of heterologous plant enzymes with better performances (Ramos-Valdivia et al., 1997; Ignea et al., 2011; Ye et al., 2016). However, multiple insertions of the Idi1 production construct in *U. maydis* did not increase lycopene levels further, suggesting that the Idi1 mRNA amount is no longer the limiting factor.

According to the bioinformatics analysis, Aat1 functions as an acetyl-CoA C-acetyltransferase at the first step in the mevalonate pathway in *U. maydis*. (Figure 2.1; Table 2.1; Figure 2.2). The substrate acetyl-CoA is known for various enzymatic reactions (Galdieri et al., 2014; Krivoruchko et al., 2015). Therefore, increasing acetyl-CoA channeling into the mevalonate pathway was attempted by overexpression of *aat1*<sup>HA</sup> at the *ip<sup>s</sup>* locus (Figure 2.11). The titer of lycopene was increased as a result of the higher transcription level by the multiple insertion event (Figure 2.11B-D). The first branching point of the mevalonate pathway in *U. maydis* was engineered for higher lycopene production. Similar outcomes of metabolic engineering to supply higher acetyl-CoA levels entering the mevalonate pathway for high terpenoid production in other heterologous systems have been observed (Lv et al., 2016; Rodriguez et al., 2016; Werner et al., 2016; Moser and Pichler, 2019; Zhang and Hong, 2020).

The production of the truncated version of Hmg1 was inspired by work in *S. cerevisiae*, where removing the N-terminal domain resulted in cytoplasmic localization due to detachment from the ER membrane and increased protein stability (Donald et al., 1997; Kampranis and Makris, 2012;

Hu et al., 2017). Consistently, the overproduction of Hmg1<sup>NA1-932</sup> resulted in higher lycopene amounts (Figure 2.11D). In this case, multiple insertions of the *hmg1*<sup>NA1-932</sup> allele at the *ip<sup>s</sup>* locus were not obtained, suggesting that high levels of Hmg1<sup>NA1-932</sup> cause growth defects (Figure 2.11B). These alterations should be combined in a single production strain to improve the performance of the underlying metabolic network.

### 3.1.3 Subcellular localization of the mevalonate pathway enzymes

Since the mevalonate pathway is compartmentalized in eukaryotes, understanding the subcellular sites of enzymatic reactions in the MVA pathway to connect the precursor supply chain and to avoid limiting steps during the carbon flux is crucial for terpenoid production (Zhang and Hong, 2020). It was proposed in mammalian cells that the complete mevalonate pathway is in peroxisomes (Kovacs et al., 2007; Olivier et al., 2000; Olivier and Krisans, 2000). In contrast to mammalian cells, the lower mevalonate pathway of plants is in peroxisomes (Simkin et al., 2011). This study focused on three key enzymes within the mevalonate module and verified the subcellular localization in *U. maydis*.

The catalytic reaction to generate mevalonate is by 3-hydroxy-3-methylglutaryl-CoA reductase Hmg1 with its C-terminal catalytic domain projecting into the cytoplasm (Croxen et al., 1994). In this study, the fluorescence microscopy verified the subcellular localization of the N-terminal truncated Hmg1 (Hmg1<sup>NA1-932</sup>) in the cytoplasm with a fluorescent signal (Figure 2.13C). Interestingly, the well-known ER bound 3-hydroxy-3-methylglutaryl-CoA reductase (HMGR) is also found in peroxisomes, which suggests a critical role of peroxisome in the cholesterol biosynthesis pathway of mouse brain cells (Kovacs et al., 2001, 2002; Kovacs and Krisans, 2003). However, there is no canonical peroxisomal targeting signal (PTS1) in Hmg1 as the truncation version is localized to the cytoplasm (Figure 2.13C).

In *U. maydis*, Idi1 localized in the cytoplasm as expected. The eGFP tagging at the N-terminus of Idi1 allowed us to visualize the subcellular localization in the cytoplasm (Figure 2.13C). The Idi1 homolog in *S. cerevisiae* (Idi1p) has shown that it is localized to the cytoplasm (Natter et al. 2005). In addition, there was no apparent peroxisomal targeting signal within Idi1 in *U. maydis*. Since it is observed that Idi1 appears to be cytoplasmic in *U. maydis*, the late steps of the pathway most likely take place in the cytoplasm. Thus, in basidiomycetes, the subcellular compartmentalization of the mevalonate pathway might be different.

The accessibility of high amounts of acetyl-CoA reflects the yields of the mevalonate pathway derived secondary metabolites (Rodriguez et al., 2016; Moser and Pichler, 2019; Zhang and Hong, 2020). In the mevalonate pathway, acetyl-CoA is the starting precursor metabolite to be condensed by acetyl-CoA C-acetyltransferase to form acetoacetyl-CoA (Figure 2.1; Troost et al., 2019). In *S. cerevisiae*, acetyl-CoA is present in the cytosol, mitochondria, peroxisomes, and nucleus (Chen et al., 2012; Galdieri et al., 2014). However, the majority of acetyl-CoA is compartmentalized in mitochondria and peroxisomes (Hammer and Avalos, 2017; Zhang and Hong, 2020). Peroxisomal targeting of acetoacetyl-CoA thiolases is reminiscent of the subcellular localization in mammalian

and plant cells (Kovacs et al., 2007; Simkin et al., 2011). As the initial step of the cholesterol biosynthesis, acetoacetyl-CoA thiolase containing an N-terminus mitochondrial targeting signal and a PTS1 (QKL) showed its activity and localization in peroxisomes of CHO cells (Olivier et al., 2000). Other acetoacetyl-CoA thiolases are found in cytosol and mitochondria (Thompson and Krisans., 1990; Olivier et al., 2000). In *A. thaliana*, a peroxisomal acetoacetyl-CoA thiolase (AACT1) contains a PTS1 (SAL) motif, while ACAT2 localizes into the cytosol (Reumann et al., 2007; Sapir-Mir et al., 2008; Simkin et al., 2011). In *S. cerevisiae*, an acetyl-CoA C-acetyltransferase (Erg10p) related to the mevalonate pathway is localized to the cytosol, and 3-ketoacyl-CoA thiolase for the  $\beta$ -oxidation of fatty acids is localized in the peroxisomes (Peretó et al., 2005; Werner et al., 2016). However, to our surprise, Aat1 exhibited a peroxisomal localization, although no conventional peroxisomal targeting signals were detectable (Figure 2.13C-D). Interestingly, four additional enzymes are annotated as putative acetoacetyl-CoA thiolases in the proteome of *U. maydis* (UMAG\_03298, 01843, 01090, and 02715). In principle, these enzymes could participate in the MVA pathway in the cytoplasm. Therefore, it is interesting to investigate the biological function of peroxisomal localization of the acetyl-CoA C-acetyltransferase (Aat1) in *U. maydis*. In peroxisomes, fatty acids are converted to acetyl-CoA via  $\beta$ -oxidation and then the acetyl unit leaves the peroxisomes in the form of acetyl-carnitine (Chen et al., 2015; Galdieri et al., 2015). From the observation of peroxisomal Aat1, it might be possible that peroxisomal acetyl-CoA is condensed by Aat1 to acetoacetyl-CoA to be transported into the cytosol or further converted to HMG-CoA by Hcs1 to exit the peroxisomes. There are two HMG-CoA synthases in rat. One localizes in mitochondria for ketogenesis (Ayté et al., 1990). The other one has been considered as a cytosolic enzyme, but a later finding of PTS2 in the HMG-CoA supports the localization to peroxisomes in CHO cells (Olivier et al. 2000). To fully link the precursor transport from the peroxisomes to the cytosol, the first prerequisite is an observation of Hcs1 localization in *U. maydis*.

Subcellular engineering to relocate acetyl-CoA into the cytosol is advantageous for terpenoid biosynthesis (Chen et al., 2015; Lv et al., 2016; Yee et al., 2019; Liu et al., 2020). Thus, understanding and improving the transport routes of acetyl units from the peroxisomes to the cytosol or from the mitochondria to the cytosol in *U. maydis* might increase the cytosolic acetyl unit levels for further enzymatic reactions within the mevalonate pathway. Since acetyl-CoA is impermeable across the mitochondrial inner membrane, acetyl unit transport routes are crucial for the subcellular engineering (Chen et al., 2015). The citrate/malate shuttle and citrate transporter transfer acetyl units from the mitochondria to the cytosol in eukaryotes (Hynes and Murray, 2010). In the mitochondria, acetyl-CoA is converted to citrate, and it is transported to the cytosol. Afterward, the cytosolic citrate is converted by ATP-citrate lyase to acetyl-CoA in fungi (Hynes and Murray, 2010; Rodriguez et al., 2016). In *U. maydis*, for example, UMAG\_01005 contains the three conserved domains, such as ATP grasp domain, CoA ligase domain, and citrate synthase domain, that might function as an ATP-citrate lyase (Hynes and Murray, 2010). In *S. cerevisiae*, pyruvate is converted to acetaldehyde by pyruvate decarboxylase (Pdc1p) to continuously form acetate, which is later converted by two

cytosolic acetyl-CoA synthetases (Acs1 and Acs2) to acetyl-CoA in the cytosol (Galdieri et al., 2014; Chen et al., 2015; Bu et al., 2017). On the other hand, pyruvate enters mitochondria to form acetyl-CoA by pyruvate dehydrogenase for the TCA cycle (Galdieri et al., 2014). Acetyl-CoA in the mitochondrial matrix can be converted to acetate by Ach1, which has a high activity of the CoA transfer from succinyl-CoA to acetate (Chen et al., 2015). The mitochondrial acetate is transported to the cytosol and further converted by the cytosolic acetyl-CoA synthetases to acetyl-CoA instead of the ATP-citrate lyase mediated route in other fungi (Chen et al., 2015). As a novel concept of developing a cell factory for terpenoid production, knowledge of subcellular localization of acetyl-CoA is essential for metabolic engineering (Chen et al., 2015; Moser and Pichler, 2019). For example, the dual-utilization of acetyl-CoA in mitochondria and cytosol significantly improved the production of isoprenoid by compartmentalization of the entire mevalonate pathway in *S. cerevisiae* (Lv et al., 2016).

Thus, the subcellular localization study of the key enzymes within the mevalonate pathway in *U. maydis* lays a solid foundation for subcellular engineering. The efficiency of the utilization of peroxisomal acetyl-CoA for the mevalonate module in *U. maydis* might give a hint of an alternative route of high acetyl-CoA supply for terpenoid biosynthesis. In addition, understanding of acetyl unit transport routes from the mitochondria to the cytosol in *U. maydis* will play a significant role in the issue of acetyl-CoA supply for the MVA pathway.

### 3.1.4 The heterologous production of plant and fungal sesquiterpenoids in *U. maydis*

To demonstrate the possibility of the heterologous production of sesquiterpenoids in *U. maydis*, synthesis of plant (+)-valencene and fungal  $\alpha$ -cuprenene was chosen. (+)-valencene is extensively used in the flavor and fragrance industries, but also shows antagonistic activity against the plant pathogenic nematode *Heterodera schachtii* (Troost et al., 2019; Schleker et al., manuscript in preparation). High titers of 352 mg/L and 540 mg/L were reached in optimized *R. sphaeroides* and *S. cerevisiae* strains, respectively (Beekwilder et al., 2014; Chen et al., 2019). Currently, a sustainable production process is implemented by the companies, Evolva and Isobionics (now BASF), using the aforementioned microorganisms (Schempp et al., 2018; Chen et al., 2019). Therefore, this target compound was chosen as a very prominent representative of heterologously produced sesquiterpenoids to benchmark in this study. The fluorescent microscopy revealed the cytoplasmic localization of CnVS in *U. maydis* (Figure 2.14C). This observation supports the assumption that plant sesquiterpenoid synthases are localized in the plant cytosol (Sapir-Mir et al., 2008). The first time in the basidiomycete model fungus *U. maydis*, the functional production of a sesquiterpenoid synthase was determined with lycopene as the molecular read-out for intracellular FPP levels (Figure 2.14D). The heterologous production of the plant (+)-valencene synthase CnVS in *U. maydis* alone resulted in (+)-valencene levels of 5.5 mg/L in shake flask fermentation, without extensive pathway engineering (Figure 2.15D). To put it into perspective, the heterologous production of CnVS in *S. cerevisiae* resulted in an initial titer of 1.3 mg/L (Cankar et al., 2014).



Thus, the initial yield of (+)-valencene in *U. maydis* is a promising starting point but needs further improvement.

$\alpha$ -cuprenene is originally synthesized by the sesquiterpenoid synthase Cop6 from the basidiomycete mushroom *C. cinerea* (Agger et al., 2009). The corresponding gene is part of a mini-gene cluster flanked by *cox1* and *cox2* encoding cytochrome P450 monooxygenases.  $\alpha$ -cuprenene is converted by these enzymes to lagopodin B with antibacterial activity against Gram-positive bacteria (Agger et al., 2009; Stöckli et al., 2019). Interestingly, all members of the cluster are transcriptionally activated after co-cultivation with Gram-positive bacteria (Stöckli et al., 2019). This target compound was chosen as a representative of basidiomycete specialty chemicals, which are not yet widely accessible by other heterologous organisms, to test applicability in *U. maydis*. Cop6 was localized in the cytoplasm, where the substrate FPP might be present in *U. maydis* (Figure 2.16C). The functionality of the fungal sesquiterpenoid synthase Cop6 in *U. maydis* was successfully determined via lycopene bleaching (Figure 2.16D). Therefore, the initially established FPP read-out system served as a simple tool for testing the functional production of a fungal sesquiterpenoid synthase. The heterologous production of  $\alpha$ -cuprenene in *U. maydis* reached an estimated titer of 0.1 g/L in shake flask fermentation (Figure 2.17D). Consistently,  $\alpha$ -cuprenene was also produced in the basidiomycete yeast *X. dendrorhous*, using a similar strategy where Cop6 was heterologously produced to redirect FPP towards  $\alpha$ -cuprenene. A comparable titer of 0.08 g/L was obtained after four days of cultivation, and strains were able to produce  $\alpha$ -cuprenene and astaxanthin simultaneously, indicating that, like in this study, the wild type FPP pool was not limited in sesquiterpenoid synthesis (Melillo et al., 2013).

Notably, the titer of the fungal sesquiterpenoid was ten times higher than the plant sesquiterpenoid. It is consistent with the initial hypothesis that the basidiomycete *U. maydis* might serve as a promising host for the production of sesquiterpenoids from higher basidiomycetes.

### 3.1.4.1 Two main strategies to improve sesquiterpenoid production

In this study, two main strategies were applied to improve sesquiterpenoid production. First, understanding the heterologous production of the sesquiterpenoid synthases with a fluorescent protein guided an approach to apply a nuclear export signal to rescue their mislocalization into the nucleus. Surprisingly, the additional NES tagging did not significantly improve the localization into the cytoplasm (Figure 2.14C; Figure 2.16C). However, the amounts of the enzymes available for the bioconversion of FPP were higher compared to the strains without NES tagging (Figure 2.14A-B; Figure 2.16A-B). The effect of the NES is most likely on the stability of protein as the N-end rule pathway. Now, this term is called N-degron pathways. Ubiquitin (Ub)-proteasome system (UPS) mediated protein degradation mechanisms for determination of protein lifespan to protect cells from misfolded, aggregated, and abnormal proteins have been thoroughly investigated in other model systems, such as in mammalian cell lines, in *S. cerevisiae*, and in bacteria (Varhavsky, 1996; Varhavsky, 2011). The target protein is labeled with a poly-Ub chain at an internal lysine by

Ub ligases (E1-3). The poly-Ub chain is recognized and processively degraded by 26S proteasome (Varhavsky, 2011). In this ATP-dependent processive proteolysis, N-terminal modification, for example, acetylation, is crucial for the selection of degradation pathways. The Arg/N-end rule pathway targets specifically unacetylated N-terminal amino acids. In contrast, the Ac/N-end rule pathway recognizes N-terminally acetylated proteins (Varhavsky, 2011). In eukaryotes, different patterns of the second amino acids are recognized (Varhavsky, 2011; Kim et al., 2014; Tran, 2019; Varhavsky, 2019). The specific amino acids in N-end rule pathways that serve as N-terminal degradation signals in *U. maydis* have not yet been fully understood. Interestingly, the second amino acid sequence of the NES is threonine (Thr), while valine (Val) is the second amino acid of the eGfp for N-terminal tagging to visualize the heterologous production and localization of both sesquiterpenoid synthases in this study. Threonine (Thr) plays a significant role in the improvement of protein stability as the N-end rule pathway in *S. cerevisiae*, while Val is unable to rescue proteins from the degradation by the Ubr1 QC pathway (Tran, 2019). Therefore, it might be possible that threonine (Thr) from the NES might stabilize the sesquiterpenoid synthases in *U. maydis*. To investigate the stabilization functions of N-terminal amino acid residues, inhibition of translation in protein synthesis by cycloheximide (CHX) could be applied, and the half-life of target proteins could be monitored (Kim et al., 2014). In addition, testing different NES variants to obtain a high-performance exportation of the sesquiterpenoid synthases from the nucleus in *U. maydis* could be a promising future task. A combination of a biologically functional NES and the N-end rule pathway in *U. maydis* might offer a synergistic effect on the higher sesquiterpenoid production with high enzyme levels for bioconversion of FPP at the cytoplasm.

Second, *Idi1* was selected for the overproduction to improve the carbon flux within the mevalonate pathway as the overproduction improved the yield of lycopene (Figure 2.12). However, this *Idi1* overproduction did not have the same effect on the production of sesquiterpenoids (Figure 2.15D; Figure 2.17D). Previous studies have shown that combinatorial metabolic engineering with different enzymes could effectively improve the carbon flux to FPP for the higher production of (+)-valencene in *S. cerevisiae* and *C. glutamicum* (Frohwitter et al., 2014; Chen et al., 2019). Another combinatorial overexpression was attempted during the production of germacrene A in *S. cerevisiae*. The highest titer, 191 mg/L of germacrene A, is achieved when truncated Hmg1p and fusion protein of FPP synthase (Erg20p) and germacrene A synthase (GAS) are overproduced together, since FPP can be converted into different essential metabolites (Hu et al., 2017). Furthermore, different combinations of precursor biosynthetic genes in the intrinsic MEP pathway and the heterologous MVA pathway in *R. capsulatus* result in the different production levels of two plant sesquiterpenoids, (-)-patchoulol and (+)-valencene (Troost et al., 2019). It is worth trying different overexpression combinations within the mevalonate pathway for sesquiterpenoid production, avoiding precursor limiting steps.

### 3.1.4.2 Essential metabolic engineering to increase FPP levels for sesquiterpenoid production

According to the findings in this study, it is necessary to focus engineering at the branching point where FPP is converted to desired sesquiterpenoids. Both sesquiterpenoid production strains were generated with AaCrtB<sup>Myc</sup> overproducing strains. As a result, part of the FPP pool could be converted to the sesquiterpenoids, but still reduced amount of lycopene was synthesized (Figure 2.14D; Figure 2.16D). The transcriptional strength of the promoter P<sub>otef</sub> is high for the sesquiterpenoid synthases, but there might still be room to improve the gene expression levels with a stronger promoter to channel more FPP to sesquiterpenoids. A similar result has been found for the heterologous gene expression in *U. maydis* when the promoter P<sub>otef</sub> was used to activate intrinsic CAZymes (Geiser et al., 2016). The transcription level is unexpectedly low, and exchanging the promoter to a stronger promoter P<sub>oma</sub> significantly increases the transcription level to observe the enzymatic activity (Geiser et al., 2016). In parallel, applying the multiple insertion events at *ip<sup>s</sup>* locus for the heterologous expression of genes encoding sesquiterpenoid synthases might help select an appropriate promoter strength. As different lycopene titers were measured when the overproduction of the key mevalonate pathway enzymes at the *ip<sup>s</sup>* locus was tested, the occurrence of multiple insertion at the *ip<sup>s</sup>* locus and simultaneous improvement of the titer indicate a possibility of further transcription level improvement (Figure 2.11; Appendix Figure 6.1).

An alternative approach is blocking the carotenoid module so that more FPP is available for sesquiterpenoids. Deletion of *car3* encoding GGPP synthase in *U. maydis* was attempted to channel more FPP to sesquiterpenoid in an  $\alpha$ -cuprenene producing strain. However, despite numerous transformants were screened, it was not successful. A similar difficulty was observed in another basidiomycete fungus *X. dendrorhous* that knocking out both *crtE* alleles was not successful (Niklitschek et al., 2008). These observations in two different basidiomycete systems agree that FPP levels are not limited. FPP is well-known to be a toxic secondary metabolite in many microorganisms, and it might be attributed to high amounts of FPP that enter the carotenoid module. Therefore, blocking the carotenoid module causes high levels of FPP, which is lethal to cells. With this assumption, it is worth trying to reduce the expression level of *car3* with genetic tools or regulatable promoters, such as the promoter P<sub>arg1</sub>, which inactivates transcription in the presence of glucose and activates it upon arabinose induction. This promoter exchange could allow us to obtain a strain with an adjustable expression level of *car3* during the cell growth. Furthermore, this approach might let us understand the FPP conversion rate between the carotenoid module and the recombinant sesquiterpenoid module for further metabolic engineering.

### 3.1.4.3 Future study to produce value-added sesquiterpenoid scaffolds in *U. maydis*

In the future, Cop6 may be co-produced with the cytochrome P450 monooxygenases Cox1 and Cox2 for the production of lagopodin A and B in *U. maydis* (Agger et al., 2009; Stöckli et al., 2019). It is advantageous to establish a platform organism to produce lagopodin B. It has been reported as

a fungal bioactive compound against many microorganisms, and the bioconversion of  $\alpha$ -cuprenene to lagopodin B increases the economic value as a potential antibiotic (Agger et al., 2009; Stöckli et al., 2019). For studying the functional production of fungal cytochrome P450 monooxygenases, *U. maydis* might be suitable. Only 23 genes in *U. maydis* are annotated as genes encoding P450s in the genome database (Hewald et al., 2005). *U. maydis* has relatively fewer P450s than that of other filamentous fungi (Hewald et al., 2005). In addition, a functional study of these endogenous cytochrome P450 monooxygenases in *U. maydis* might allow us to set up exclusive production conditions for heterologous cytochrome P450 monooxygenases. Cyp1, an endogenous cytochrome P450 monooxygenase, is functionally well-characterized for the production of ustilagic acids (Hewald et al., 2005). To introduce heterologous cytochrome P450 monooxygenases, such as Cox1 and Cox2, the genetic and biological information of Cyp1 will play an important role in future study.

### 3.2 Part 2 Identification of feldin, an antifungal polyine from the beefsteak fungus *Fistulina hepatica*

In the present study, a bioactive compound from mycelial cultures of basidiomycete mushrooms has been characterized via a bioactivity-guided isolation process chiefly employing the model ascomycete *S. cerevisiae* and the model basidiomycete *U. maydis* as test microorganisms. Pure bioactive compound isolation and structure elucidation revealed a novel bioactive polyine ('polyacetylene') designated feldin.

#### 3.2.1 High potentials of bioactive polyines from plants and fungi for drug discovery

Although known from fungi, polyines are even more well-studied from plants, such as falcarinol and falcarindiol from oil-filled channels within the periderm/pericyclic parenchyma tissue running parallel to the length of the root of carrot plants. Falcarindiol exhibits antifungal bioactivity protecting the young roots, supposedly via alteration or damage of the plasma membrane or other membrane functions (Garrod et al., 1979a-b; Minto and Blacklock, 2008), which is also a proposed mode of action of certain bacterial polyines (Fritsche et al., 2014). In addition, certain falcarindiol isoforms display antibacterial bioactivities (Kobaisy et al., 1997; Lechner et al., 2004). Being potent antibacterials, some such polyines have been the source of several unique pharmacophores like phomallenic acid C identified from a *Phoma* sp. (Ascomycota). Phomallenic acid C exhibits a 20-fold higher potency than thiolactomycin or cerulenin against the Gram-positive human-pathogenic bacterium *Staphylococcus aureus* (Ondeyka et al., 2006).

So far, a couple of polyines have been described from *F. hepatica* (Jones et al., 1966; Tsuge et al., 1999) as well as from *Fistulina pallida*, including a polyine glycoside (Ahmed et al., 1974). The two structurally similar polyines classified as triacetylene derivatives, cinnatriacetins A and B, were isolated from *F. hepatica* basidiomes and reported to exhibit bioactivity against Gram-positive bacteria, but none against Gram-negative bacteria and *S. cerevisiae* (Tsuge et al., 1999). This, and the fact that the new polyine feldin from *F. hepatica* mycelium shows activity against *S. cerevisiae*,

supports the notion that *F. hepatica* may employ a versatile arsenal of polyines to equip its chemical defense system against antagonists, including fungal ones. Well-known with cultivated mushroom species like the button mushroom (*Agaricus bisporus*), mushroom-parasitic bacteria, and microfungi impose a severe threat to mushrooms colonizing their substrate or producing their basidiomes. Blotch-disease-causing pseudomonads (Frey-Klett et al., 2011) or the ascomycetous button mushroom pathogen *Lecanicillium fungicola* (Berendsen et al., 2010) are certainly among the most economically relevant examples of such mushroom parasites. Thus, in nature, polyines accumulating in *F. hepatica* mycelium and fruiting bodies may potentially help the fungus keep such antagonists at bay. In contrast to induced mushroom defense systems, such as the antifungal strobilurin A of *Oudemansiella mucida* (Kettering et al., 2004), the new polyine feldin described here from *F. hepatica* belongs to the autonomous defense molecules (Künzler, 2018), at least under the tested conditions, as its mycelium constitutively produces it on PDA. It is relatively common to observe the accumulation of such compounds in fungi, in contrast to the situation in plants (Minto and Blacklock, 2008).

Fungal polyines may display broad bioactivity spectra, such as 10-hydroxy-undeca-2,4,6,8-tetraynamide. Besides bioactivity against Gram-negative and Gram-positive bacteria, it also affects a broad spectrum of fungi (several ascomycetes including *S. cerevisiae* as well as the closely related human-pathogenic yeast *Candida albicans*, and the basidiomycetous yeast *Rhodotorula glutinis*), the oomycete *Phytophthora infestans*, and Ehrlich ascites tumor cells (Bäuerle et al., 1982). Other fungal polyines like the allenic fungal polyine of Schlingmann et al., (1995) show a narrower bioactivity spectrum. While basidiomycetes like *U. maydis* and *Rhodotorula rubra* are hardly affected, it is strongly active against Gram-positive bacteria and *C. albicans*. The latter pathogen is notorious for adapting quickly to adverse conditions derived from its environment, including prolonged exposure to antifungals (Costa-de-Oliveira and Rodrigues, 2020), making a permanent search for new selective drugs against it essential. Fungal polyines have been studied as potential drugs of high potency like the tuberculosis cure mycomycin (Celmer and Solomons, 1952), the cholesterol biosynthesis inhibitors from the silver fir wood-decomposer *Xerula melanotricha* (Kuhnt et al., 1990), or 10-hydroxy-undeca-2,4,6,8 tetraynamide from *Mycena viridimarginata* (Bäuerle et al., 1982).

### 3.2.2 Instability of polyines and a possible solution for stabilizing

Polyines tend to be unstable, succumbing to oxidative, photolytic, or pH-dependent decomposition (Minto and Blacklock, 2008). Other polyines are damaged after NMR solvent evaporation, and it was hypothesized to potentially face the same effect with feldin (Parish et al., 2004; Fritsche et al., 2014; Kai et al., 2018). To prevent such hypothetical damage from affecting bioactivity, the bioactivity of feldin against *S. cerevisiae* was ascertained with a subsample of fresh feldin sidelined before NMR (see Figure 2.20B). Similarly, the antibacterial polyine isolated from the basidiomycete *Baeospora myosura* proved to be very unstable, i.e., it polymerized when the solvent was removed (Parish et al. 2004). Likewise, Schlingmann et al., (1995) reported the 3,4,5,6-tetrahydro-6-hydroxy-



derivative of the tuberculosis cure mycomycin (reported as potent but unstable by Celmer and Solomons, 1952), they dealt with was too unstable to isolate in a pure form. Moreover, bacterial polyines can also be unstable for the same or similar reasons. Thus, careful handlings by avoiding light, oxygen, and solvent evaporation have been advised for bioactivity assessment (Fritsche et al., 2014; Kai et al., 2018).

A possible solution for stabilizing bioactive polyines like feldin may come from a (temporary) derivatization, e.g., creating a polyine glycoside. Such derivatives may be found in fungi and plants and can exhibit antibacterial and anti-inflammatory activities (Pan et al., 2009; He et al., 2011; Konovalov, 2014). Even in a very close relative of *F. hepatica*, a natural polyine glycoside is known (Ahmed et al., 1974). Consisting of a conjugation of a sugar moiety and a polyine, polyine glycosides are judged as more stable than pure polyines, interestingly with no bioactivity reported in the one described by Ahmed et al., (1974). The latter may relate to one suggested mode of action of polyines. Bäuerle et al., (1982) discussed the activity of 10-hydroxy-undeca-2,4,6,8-tetraynamide to be correlated to its high chemical reactivity due to carbon-carbon triple bonds making such compounds, according to Walsh et al., (1972), inactivate enzymes by alkylation. Pan et al., (2009) suggest that the carbohydrate part of polyine glycosides may play a “protecting” role in either stabilizing the polyine moiety or in masking its biological activity until cleavage of the carbohydrate moiety by a glycosidase. Otherwise, it may increase solubility and facilitate the delivery of these molecules to specific cell types (e.g., via binding to certain sugar transporters).

### 3.2.3 A potential biosynthetic route for feldin and *U. maydis* as a novel heterologous production host

In *Daucus carota* and the basidiomycete fungus *Cantharellus formosus*, biosynthesis of a variety of polyines shares the same route from the condensation of acetyl-CoA and malonyl-CoA to enter the crepenynic acid pathway (Blacklock et al., 2010; Dawid et al., 2015). To form the unique carbon-carbon triple bond within the backbone structure of polyines, desaturation steps are required for the bioconversion from oleic acid to crepenynic acid. Further desaturation results in dehydropenynic acid (Minto and Blacklock, 2008). Six fatty acid desaturase 2 (FAD2) enzymes from *D. carota* were experimentally evaluated for the enzymatic functions within the crepenynic acid pathway (Busta et al., 2018). When the heterologous production of *F. hepatica* polyines in *U. maydis* is considered due to its higher tolerance as a basidiomycete host, a derivatization approach might be advisable. After identifying potential polyine biosynthesis genes in the *F. hepatica* genome sequence of Floudas et al., (2015), the next step is to attempt overexpression of respective candidate genes, in a method similar to the proof of principle approach to producing plant and fungal sesquiterpenoids in *U. maydis* as shown earlier (Lee et al., 2020a). Ultimately, the heterologous production of plant enzymes for a coupling approach would be easily feasible in *U. maydis*. Such modification might be an option to engineer polyine-derivatives, which are relatively stable and secreted into the culture medium by *U. maydis*. Eventually, the conjugation could be cleaved by a glycosidase to release the

polyine moiety. The present results verified the presence of bioactive mushroom compounds that are more active against the ascomycete platform microorganism *S. cerevisiae* than basidiomycetes. It provides a starting ground to try out heterologous production of polyine (polyine glycoside) in *U. maydis*.

### 3.3 Conclusion and outlook

This study followed the microbial cell factory concept to establish the model basidiomycete fungus *U. maydis* as a novel chassis for the production of a broad range of terpenoids. In parallel, novel bioactive compounds from higher basidiomycete fungi were explored, which are potentially suitable for expanding the production repertoire of *U. maydis* as a platform microorganism.

As proof of concept, two different sesquiterpenoids have been successfully produced in *U. maydis* by modifying the existing mevalonate pathway and introducing heterologous enzymes. Additional sesquiterpenoid synthases from higher basidiomycetes like *Omphalotus olearius* could be heterologously produced for illudins and other compounds (Schmidt-Dannert, 2015; Xiao and Zhong, 2016). Notably, the mevalonate pathway in *U. maydis* is also partially compartmentalized like in other eukaryotic systems (Olivier et al., 2000; Olivier and Krisans, 2000; Reumann et al., 2007; Sapir-Mir et al., 2008). Moreover, the tested plant and fungal sesquiterpenoid synthases were localized in the cytoplasm. Therefore, future studies of the subcellular localization of the remaining mevalonate pathway enzymes will provide evidence of the necessity of subcellular engineering (Zhang and Hong, 2020).

There are several straightforward strategies to increase the yield of the desired fungal sesquiterpenoids (Kampranis and Makris, 2012; Zhang and Hong, 2020). The upregulation of the desired pathway would be possible by the heterologous production of enzymes with higher activity like the optimized versions of bacterial Aat1 (Shiba et al., 2007). In addition, the introduction of the heterologous mevalonate pathway via synthetic polycistronic mRNAs with viral 2A peptides might be advantageous (Müntjes et al., 2020). It avoids the regulatory networks within the intrinsic mevalonate pathway in *U. maydis* and might improve the carbon flux from acetyl-CoA to sesquiterpenoids (Troost et al., 2019; Orsi et al., 2020). Competing pathways, such as that for ergosterol biosynthesis, could be reduced by downregulation of Erg9 squalene synthase production or by treating chemical inhibitors, which block the biosynthesis of ergosterol (Asadollahi et al., 2010). Alternatively, deletion of *fer4*, encoding an enoyl-CoA hydratase, will prevent the consumption of 3-hydroxy-3-methylglutaryl-CoA during ferrichrome A synthesis (Asadollahi et al., 2010). Finally, the fusion of FPP synthase (Erg20p) and germacrene A synthase (GAS) has been shown to increase sesquiterpenoid yield, as FPP was directly funneled into product formation (Hu et al., 2017).

Cytochrome P450s further modify diverse plant and fungal sesquiterpenoids, and this modification is responsible for the bioactivity of sesquiterpenoid scaffolds (Agger et al., 2009; Engels et al., 2011; Gavira et al., 2013; Lackner et al., 2013; Paddon et al., 2013; Dörfer et al., 2019; Stöckli et al., 2019). This study successfully provided evidence that *U. maydis* has capabilities to produce (+)-valencene

and  $\alpha$ -cuprenene. In the future, heterologous expression of genes encoding cytochrome P450s for the production of (+)-nootkatone and lagopodins will be carried out. This attempt might suggest that *U. maydis* can be a novel platform microorganism to produce bioactive plant and fungal sesquiterpenoid scaffolds, which are challenging for other model microorganisms to produce. Furthermore, this fungus might serve to identify the functions of unknown biosynthetic enzymes, assisting with the discovery of new biosynthetic gene clusters from higher basidiomycete fungi. Eventually, a sustainable and consolidated strategy for next-generation bioengineering of terpenoid production will include the use of alternative carbon sources generated from the enhanced biomass-degrading ability of *U. maydis* (Geiser et al., 2016; Stoffels et al., 2020).

To meet the high demands of antibiotics for clinical purposes, discovering new bioactive compounds and developing large-scale production methods are essential (Koehn and Carter, 2005). Compared to the scenario in ascomycetes, a major problem is the complexity of genetics in the basidiomycete species producing such bioactive compounds (Sandargo et al., 2019). To date, biosynthesis of a few Agaricomycotina molecules has been evaluated, and the heterologous production of the tricyclic diterpenoid pleuromutilin and the polyketide strobilurins in the ascomycete fungus *Aspergillus oryzae* has been accomplished (Alberti et al., 2017; Nofiani et al., 2018). However, the heterologous production in ascomycetous hosts might not always work with any of the numerous metabolite families that were hitherto obtained from mushrooms. The present work has provided an established procedure of bioactive-guided fractionation and isolation of a novel bioactive compound from the higher basidiomycete fungus *F. hepatica*. The strong bioactivity of the new polyine feldin from *F. hepatica* against *S. cerevisiae* suggests that, to some extent, it would be very challenging for *S. cerevisiae* to produce fungal bioactive compounds of such kind, which might have high potentials to be new antibiotics in the future. Therefore, the establishment of a closely related basidiomycete fungus *U. maydis* as a novel cell factory might be an alternative solution.

For the higher production, bioinformatics analysis and prediction of the biosynthetic gene clusters for these fungal bioactive compounds are prerequisites (Keller, 2019; Sandargo et al., 2019). Functional expression of the biosynthetic genes in a heterologous platform organism, such as *U. maydis*, must be then confirmed, ultimately by the detection of the desired intermediates or final products. To establish such a heterologous platform organism, understanding of available precursor supplies and intrinsic biosynthetic pathways to connect to the heterologous biosynthetic pathways is necessary.

In essence, based on the data from the present work, the basidiomycete fungus *U. maydis* exhibits a promising potential to serve as a novel platform microorganism for the production of basidiomycete sesquiterpenoids. Future studies will evaluate whether *U. maydis* may prospectively serve as a platform microorganism for the laborious production of valuable bioactive compounds from basidiomycete mushrooms.

## 4 Materials and Methods

### 4.1 Materials

#### 4.1.1 Chemicals, enzymes, and kits

##### 4.1.1.1 Chemicals

The chemicals used in this study were purchased from the following companies unless specified otherwise: Thermo Fisher Scientific, Merck, TCI Deutschland GmbH, Roche, Fluka, Difco, BioRad, GE Healthcare, Pharmacia, BioWorld, Invitrogen, Serva, Carl Roth, Caelo, Applichem, Acros Organics, and VWR Chemicals.

##### 4.1.1.2 Enzymes and kits

The following tables indicate the lists of enzymes, protease inhibitors, kits, and size standards used in this study.

**Table 4.1 Enzymes used in this study**

Name	Application	Company
Lysozyme (muraminidase)	Plasmid isolation	Merck
Glucanex (Trichoderma Lysing Enzymes)	Protoplasting of <i>U. maydis</i> sporidia	Merck
Phusion-HF DNA polymerase	DNA amplification	Thermo Fisher Scientific
Restriction enzymes	Restriction of DNA molecules	New England Biolabs
T4 DNA ligase	Ligation of DNA molecules	Roche
T5 exonuclease	Gibson Assembly®	New England Biolabs
Taq DNA ligase	Gibson Assembly®	Roche
Alkaline phosphatase	Dephosphorylation of DNA fragments	Roche
RNAse A	Plasmid isolation, genomic DNA isolation	Boehringer Ingelheim

**Table 4.2 Protease inhibitors used in this study**

Name	Application	Company
Benzamidine	Preparation of cell extracts for Western blot analysis	Merck
cOmplete™ EDTA-free Protease Inhibitor Cocktail	Preparation of cell extracts for Western blot analysis	Roche
Phenylmethylsulfonyl fluoride (PMSF)	Preparation of cell extracts for Western blot analysis	Serva

Table 4.3 Kits used in this study

Name	Application	Company
Plasmid mini Kit	Isolation of plasmid DNA	Macherey-Nagel
Monarch® PCR & DNA Cleanup Kit	Purification of DNA fragments	New England Biolabs
Monarch® DNA Gel Extraction Kit	Elution and purification of DNA fragments from agarose gels	New England Biolabs
PCR DIG Labeling Mix	Digoxigenin labeling of PCR products (generation of Southern blot probes)	Roche
CDP-Star®	Chemiluminescent substrate for alkaline phosphatase in Southern blot analysis	Roche
Amersham™ ECL™ prime detection reagent	Chemiluminescent substrate for horseradish peroxidase (HRP)	GE Healthcare Life Sciences

Table 4.4 Protein and DNA size standards used in this study

Name	Application	Company
PageRuler™ Prestained Protein Ladder (10-180 kDa)	SDS-PAGE	Thermo Fisher Scientific
GeneRuler 1 kb DNA Ladder	DNA Gel electrophoresis	Thermo Fisher Scientific
2-Log DNA Ladder (0.1-10.0 kb)	DNA Gel electrophoresis	New England Biolabs
$\lambda$ PstI (PstI digested Enterophage $\lambda$ DNA)	DNA Gel electrophoresis	own preparation

#### 4.1.2 Solutions and media

##### 4.1.2.1 For cultivation of *E. coli*

For cloning purposes, media for the cultivation of *E. coli* were prepared as below (Sambrook et al., 1989). If necessary, the medium was supplemented with ampicillin 100 µg/mL or gentamycin 40 µg/mL after cooling down.

dYT-medium (liquid) for 1 L	YT-medium (solid) for 1 L
16 g tryptone 10 g yeast extract 5 g NaCl Add ddH <sub>2</sub> O and then autoclave	8 g tryptone 5 g yeast extract 5 g NaCl 15 g Agar Add ddH <sub>2</sub> O and then autoclave

Table 4.5 Antibiotics used for *E. coli* cultivation

Antibiotic	Final concentration (µg/mL)
Ampicillin	100
Gentamycin	40



#### 4.1.2.2 For cultivation of *U. maydis*

Media for the cultivation of *U. maydis* were prepared (Banuett and Herskowitz, 1989; Holiday, 1974; Scherer et al., 2006). Autoclaving of the media was conducted for sterilization at 121°C for 5 min. For preparing agar-containing plates, 2.0% (w/v) Bacto-agar (Difco) was added to the medium before autoclaving. As an alternative way to sterilize media or solutions, a 0.22 µm Filtropur BT 50 bottle top filter (Sarstedt) was used.

CM (complete medium) for 1 L
2.5 g casamino acids 1.5 g NH <sub>4</sub> NO <sub>3</sub> 0.5 g DNA degr. Free acid (Merck, D-3159) 1 g yeast extract 10 mL of vitamin solution 62.5 mL of salt solution Add ddH <sub>2</sub> O, adjust pH 7.0 with NaOH, and autoclave The medium is supplemented with 10 g/L (f.c.) glucose

NM (Nitrate minimal medium) for 1 L
3 g KNO <sub>3</sub> 62.5 mL of salt solution Add ddH <sub>2</sub> O, adjust pH 7.0 with KOH, and autoclaved The medium is supplemented with 10 g/L (f.c.) glucose

Vitamin solution for 1 L
200 mg thiamine hydrochloride 100 mg riboflavin 100 mg pyridoxine monohydrochlorate 400 mg Ca-panthotenate 100 mg aminobenzoic acid 400 mg nicotinic acid 400 mg cholinchloride 2 g <i>myo</i> -inositol Add ddH <sub>2</sub> O

Salt solution for 1 L
16 g KH <sub>2</sub> PO <sub>4</sub> 4 g Na <sub>2</sub> SO <sub>4</sub> 8 g KCl 1.32 g CaCl <sub>2</sub> *2H <sub>2</sub> O 8 mL trace element solution 2 g MgSO <sub>4</sub> Add ddH <sub>2</sub> O and then filter for sterilization

Trace element solution
60 mg H <sub>3</sub> BO <sub>3</sub> 140 mg MnCl*4H <sub>2</sub> O 400 mg ZnCl <sub>2</sub> 40 mg Na <sub>2</sub> MoO <sub>4</sub> *2H <sub>2</sub> O 100 mg FeCl <sub>3</sub> *6H <sub>2</sub> O 40 mg CuSO <sub>4</sub> *5H <sub>2</sub> O Add ddH <sub>2</sub> O and then autoclave

Regeneration agar light (RegLight) for 1 L
10 g yeast extract 4 g peptone 4 g sucrose 182.2 g sorbitol 15 g agar Add ddH <sub>2</sub> O and then autoclave Supplemented with different concentrations of antibiotics for selection of <i>U. maydis</i> transformants

#### 4.1.2.3 Strain maintenance

Overnight culture in 3 mL of CM-glc was mixed with NSY-glycerol and stored at -80°C to store *U. maydis* strains for an extended period.

NSY-glycerol for 1 L
3 g beef extract
5 g peptone
1 g yeast extract
5 g sucrose
800 mL of glycerol (87% [v/v])
Add ddH <sub>2</sub> O and then autoclave

#### 4.1.3 Oligonucleotides

The oligonucleotides used in this study were synthesized by Metabion GmbH (Planegg-Steinkirchen, Germany) or Integrated DNA Technologies Inc. (Coralville, IA, USA).

**Table 4.6 List of oligonucleotides used in this study**

Designation	Nucleotide sequence (5'→ 3')	Remarks
oMB980	GCAGTCTTGGCGAGCTATTC	<i>cco1</i> U1
oMB981	GGTCTCGCCTGCAATATTTACCATTATTCTTCACTTACTG	<i>cco1</i> U2
oMB982	GGTCTCCAGGCCCGGGCAAATGCCTATCGAG	<i>cco1</i> U3
oMB983	GGTCTCCGGCCGCGAGATGGAAGTGCTCGC	<i>cco1</i> D1
oMB984	GGTCTCGCTGCAATATTTCTTGCTAGGACTGAAAGCG	<i>cco1</i> D2
oMB985	GACAATGGTGCTTGCAGGG	<i>cco1</i> D3
oMB986	CTAGGTCTCGTGTCTGAACTCGCACCCAAAGTTG	<i>cco1</i> UF_fw
oMB987	CTAGGTCTCAGACACCCTCCGAATGACTATTTGTAC	<i>cco1</i> UF_rv
oUP054	CCGCGATTCAAGTCAGGTCAG	<i>cco1</i> P1
oUP055	GAATCTATCAGTGACGGCAC	<i>cco1</i> P2
oMB996	GCATCTGTGCGCAGCAACATC	<i>car1</i> U1
oUP134	GGTCTCGCCTGCAATATTGATGAATAGCCTCTTTGCCG	<i>car1</i> U2
oMB998	CTAGGTCTCCAGGCCCTTGACCAAGACAAGAACCTCCG	<i>car1</i> U3
oMB999	CTAGGTCTCCGGCCGGAGCGTCTACACAACCGGG	<i>car1</i> D1
oUP009	CTAGGTCTCGCTGCAATAATTTGACTTCCATACAATGCTCGC	<i>car1</i> D2
oUP010	AAGCTGCTGATGCCGCCTTG	<i>car1</i> D3
oUP011	CTAGGTCTCGTGTGAGGCGAGGTATAAGCAATG	<i>car1</i> DF_fw
oUP012	CTAGGTCTCAGACACCAAGTTGACGTTCTTGTCTC	<i>car1</i> DF_rv
oUP013	TCTCCCTGCATGGTAGTAGC	<i>car2</i> U1
oUP014	GGTCTCGCCTGCAATAATACAATAATAAATCGAAGCGGTTAC	<i>car2</i> U2
oUP015	GGTCTCCAGGCCGACTGGCACTGATTGGTCAAC	<i>car2</i> U3
oUP016	GGTCTCCGGCCAGCATGCACACATGCATCATC	<i>car2</i> D1
oUP017	GGTCTCGCTGCAATATTCACTGCGAAGCGGAGGATC	<i>car2</i> D2
oUP018	CGAAACACAGAAGCGATGAG	<i>car2</i> D3
oUP056	GACAACGCCATGGGACAATC	<i>car2</i> P1
oUP057	CATAGACGGCGTCGACAATG	<i>car2</i> P2
oUP186	CTAGGCGCGCCCCAGCTTTCTACCAAACCGCC	<i>aat1</i> _fw
oUP187	CTACCGCGGTTAGTTCTCACGCTTGATAATGATAG	<i>aat1</i> _rv
oUP266	CTAGGCGCGCCCTGCAGGATGCTACCTATGTTAC	<i>hmg1</i> <sup>NA1-932</sup> _fw

oUP267	CTACCGCGGCTATGTGAGAGAAGATGCTCGAC	<i>hmg1</i> <sup>NA1-932</sup> _rv
oUP268	CTAGGCGCGCCTCGACCGCCACCGTCACCGAG	<i>idi1</i> _fw
oUP269	CTACCGCGGTCAGAGGAGGCGGTGAATGC	<i>idi1</i> _rv
oDD527	GGTCTCGCCTGCAATATTGCCAATGGCACTAC	<i>Upa9</i> U2
oDD605	GGTCTCGTGGCCAAAGAAGACCAGGCAGCATAG	<i>Upa9</i> U3
oDD634	GGTCTCCGGCCTAGTAGGGTCCAACGTCTAC	<i>Upa9</i> D1
oDD635	GGTCTCCCTGCCAATATTGACCTCGAGGCCGAG	<i>Upa9</i> D2
oMB935	GATCCCATGGTGAGCAAGGGCGAGGAG	SKL_fw
oMB936	GCGGCCGCTTTAGAGCTTGGACTTGTACAGCTCGTCCAT	SKL_rv
oUM123	CTACCTGCAGGGTATGTGTAGAGGTGGCCTTG	<i>Prp10</i> _fw
oUM124	CTACCATGGCTTGAATACTGTTGGATGGGAGG	<i>Prp10</i> _rv
oAB049	CATGACCAAGAAGTTTGGCACGCTCACCATCT	NES_fw
oAB050	CCGGAGATGGTGAGCGTGCCAAACTTCTGGT	NES_rv

This table is derived from Lee et al., 2020a (Supplementary Table S4).

#### 4.1.4 Plasmids for *U. maydis* strain generation

Plasmid generation was performed by standard molecular cloning techniques (Sambrook et al., 1989; Sambrook and Russell, 2001), Golden Gate cloning (Terfrüchte et al., 2014), or Gibson Assembly® (Gibson et al., 2009). More details of the cloning method are described below. For amplification of the desired DNA fragments via polymerase chain reaction (PCR), the oligonucleotides (Table 4.6) were used. For efficient expression of heterologous genes, the codon usage was optimized using online tools from Integrated DNA Technologies, Coralville, IA, USA in the case of AaCrtB or tailor-made context-dependent codon usage tools (Zarnack et al., 2006; Zhou et al., 2018; <http://dicodon-optimization.appspot.com/>) in the case of CnVS and Cop6. The codon-optimized synthetic genes were synthesized by Integrated DNA Technologies, Coralville, IA, USA. The DNA sequences are described in Appendix Table 6.1. Confirmation of the construct sequences was performed at the Institute for Genetics in Ludwig Maximilians University München, Martinsried, Germany (see below).

##### pTC-Cbx(+) (pUMa260)

This plasmid contains genes encoding the iron-sulfur protein *ip<sup>S</sup>*, which results in carboxin resistance, and the  $\beta$ -lactamase enzyme, for selection on ampicillin containing media for cloning with *E. coli*. The expression of the carboxin resistance gene is under control of the native promoter, and the transcription termination is facilitated by the native terminator (Brachmann, 2001). The open reading frame of the iron-sulfur protein *ip<sup>S</sup>* served as a template to generate the *ip<sup>S</sup>* locus Southern blot probe by PCR using oMF502 and oMF503 (Brachmann, 2001; Loubradou et al., 2001).

##### pDest (pUMa1467)

This plasmid is a pUC57 derivative used in Golden Gate cloning approaches. It served as a destination vector for the final ligation construct. It contains the sequence for a multiple cloning site and *BsaI* recognition sites. In addition, a gene encoding the  $\beta$ -lactamase enzyme is for selection on ampicillin containing media for cloning with *E. coli* (Terfrüchte et al., 2014).

### **pStor (pUMa1522)**

This plasmid contains the hygromycin B resistance cassette and *Bsa*I recognition sites for the Golden Gate cloning purpose. The hygromycin B resistance gene *hpt* encodes HygB phosphotransferase from *E. coli* (Wang et al., 1988). The expression is under control of the native promoter and terminator of *U. maydis hsp70* (UMAG\_03791). In addition, the plasmid contains a gentamycin resistance gene for selection on gentamycin containing media (GentR) for cloning with *E. coli* (Terfrüchte et al., 2014).

### **pCco1Δ\_HygR (pUMa3281)**

This plasmid is for generating deletion mutants of *cco1* (UMAG\_00965). The plasmid is generated via Golden Gate cloning method, and pUMa1467 (pDest) and pUMa1522 (pStor) were used (Terfrüchte et al., 2014). The hygromycin B resistance cassette contains FRT sites (GAAGTTCCTATTCTCTAGAAAGTATAGGAACTTC) at both ends for recycling by Flp recombinase (Khrunyk et al., 2010). The cassette is flanked by the regions, 1.1 kb upstream and 0.8 kb downstream of *cco1*. The flanking regions were amplified by PCR using oMB981/oMB982, oMB983/oMB984, and UM521 wild type DNA as a template. For cloning with *E. coli*, the plasmid contains a gene encoding  $\beta$ -lactamase enzyme for selection on ampicillin containing media. (This study)

### **pCar1Δ\_HygR (pUMa3286)**

This plasmid is for generating deletion mutants of *car1* (UMAG\_04210). The plasmid is generated via Golden Gate cloning method, and pUMa1467 (pDest) and pUMa1522 (pStor) were used (Terfrüchte et al., 2014). The hygromycin B resistance cassette contains FRT sites at both ends for recycling by Flp recombinase (Khrunyk et al., 2010). The cassette is flanked by the regions, 0.9 kb upstream and 0.6 kb downstream of *car1*. The flanking regions were amplified by PCR using oUP134/oMB998, oMB999/oUP009, and UM521 wild type DNA as a template. For cloning with *E. coli*, the plasmid contains a gene encoding  $\beta$ -lactamase enzyme for selection on ampicillin containing media. (This study)

### **pCar2Δ\_HygR (pUMa3287)**

This plasmid is for generating deletion mutants of *car2* (UMAG\_06287). The plasmid is generated via Golden Gate cloning method, and pUMa1467 (pDest) and pUMa1522 (pStor) were used (Terfrüchte et al., 2014). The hygromycin B resistance cassette contains FRT sites at both ends for recycling by Flp recombinase. The cassette is flanked by the regions, 0.9 kb upstream and 0.9 kb downstream of *car2*. The flanking regions were amplified by PCR using oUP014/oUP015, oUP016/oUP017, and UM521 wild type DNA as a template. For cloning with *E. coli*, the plasmid contains a gene encoding  $\beta$ -lactamase enzyme for selection on ampicillin containing media. (This study)

### **pUpp3Δ\_HygR (pUMa1556)**

This plasmid is for generating deletion mutants of *upp3* (UMAG\_11908). The hygromycin B resistance cassette contains FRTm3 sites (GAAGTTCCTATTCTCCAGA AAGTATAGGAACTTC) at both ends for recycling by Flp recombinase (Khrunyk et al., 2010). The cassette is flanked by the regions, 1.5 kb upstream and 1.9 kb downstream of *upp3*. The flanking regions were amplified by PCR using UM521 wild type as a template. The plasmid is generated via Golden Gate cloning method, and pUMa1467 (pDest) and pUMa1525 (pStor) were used (Sarkari et al., 2014; Terfrüchte et al., 2014).

### **pFLPexpC (pUMa1446)**

This plasmid is for producing a codon-optimized Flp recombinase from *S. cerevisiae* in *U. maydis*. The expression is under the control of the promoter  $P_{crg1}$  and induced in the presence of arabinose. The termination is facilitated by the terminator  $T_{nos}$  from *Agrobacterium tumefaciens*. The Flp recombinase specifically recognizes FRT sites. In addition, it contains the carboxin resistance cassette for giving a selection pressure to the transformed *U. maydis* strains, an autonomously replicating sequence (ARS), and the origins of replication (ori), and a gene encoding  $\beta$ -lactamase enzyme for selection on ampicillin containing media for cloning purpose (Khrunyk et al., 2010).

### **peGfp\_NatR (pUMa3132)**

This plasmid is for producing eGfp (enhanced green 463 fluorescent protein; Clontech, Mountain View, CA, USA) with the nourseothricin resistance cassette at the *upp3* locus. The expression of the nourseothricin resistance gene derived from *Streptomyces noursei* is under the control of  $P_{gap1}$  derived from UMAG\_00343, and the transcription termination is facilitated by the terminator  $T_{cyc1}$  from *S. cerevisiae* (Brachmann, 2001). To integrate into the *upp3* locus, the construct for the *egfp* expression and the nourseothricin resistance is flanked by the regions, 1.5 kb upstream and 1.9 kb downstream of *upp3*. The flanking regions are derived from pUpp3Δ\_HygR (pUMa1556) as a vector backbone. For exchanging the flanking regions to integrate into different loci, *SfiI* cutting sites are present at both ends of the construct. The expression of *egfp* is under the control of the promoter  $P_{otef}$  and the terminator  $T_{nos}$ . For cloning with *E. coli*, the plasmid contains a gene encoding  $\beta$ -lactamase enzyme for selection on ampicillin containing media. (This study)

### **pAacrB<sup>Myc</sup>\_NatR<sup>FRTm7</sup> (pUMa3707)**

This plasmid is for producing codon-optimized AaCrtB from *A. aurantiacum*. The heterologous phytoene synthase was C-terminally fused to 3× Myc tag for verifying the production via Western blot analysis. The expression of *AacrB<sup>Myc</sup>* is under the control of the promoter  $P_{rpl40}$  (1 kb upstream of the ORF of UMAG\_02440) and the terminator  $T_{nos}$ . In addition, it contains the nourseothricin resistance cassette containing FRTm7 (GAAGTTCCTATTCTCTATAAAGTATAGGAACTTC) at both ends for recycling the resistance cassette by Flp recombinase. The expression cassette is integrated



at the *car2* locus by homologous recombination. The flanking regions for the integration into the *car2* locus are derived from pCar2 $\Delta$ \_HygR (pUMa3287). For cloning with *E. coli*, the plasmid contains a gene encoding  $\beta$ -lactamase enzyme for selection on ampicillin containing media. (This study)

### **pAat1<sup>HA</sup>\_CbxR (pUMa3379)**

This plasmid is for producing Aat1 N-terminally fused to 3 $\times$  HA tag at the *ip<sup>s</sup>* locus. The nucleotide sequence of *U. maydis aat1* (UMAG\_03571) was amplified by PCR with oUP186/oUP187 and UM521 wild type DNA as a template. The 3 $\times$  HA tag was used for verification of the production via Western blot analysis. The gene expression is under the control of the promoter P<sub>otef</sub> and the terminator T<sub>nos</sub>. For cloning with *E. coli*, the plasmid contains a gene encoding  $\beta$ -lactamase enzyme for selection on ampicillin containing media. (This study)

### **pHmg1<sup>NA1-932HA</sup>\_CbxR (pUMa3381)**

This plasmid is for producing N-terminally truncated from aa 1 to 932 of Hmg1, which is N-terminally fused to 3 $\times$  HA tag, at the *ip<sup>s</sup>* locus. The desired nucleotide sequence of *U. maydis hmg1* (UMAG\_15002) was amplified by PCR with oUP266/oUP267 and UM521 wild type DNA as a template. The 3 $\times$  HA tag was used for verification of the production via Western blot analysis. The gene expression is under the control of the promoter P<sub>otef</sub> and the terminator T<sub>nos</sub>. For cloning with *E. coli*, the plasmid contains a gene encoding  $\beta$ -lactamase enzyme for selection on ampicillin containing media. (This study)

### **pIdi1<sup>HA</sup>\_CbxR (pUMa3382)**

This plasmid is for producing Idi1 N-terminally fused to 3 $\times$  HA tag at the *ip<sup>s</sup>* locus. The nucleotide sequence of *U. maydis idi1* (UMAG\_04838) was amplified by PCR with oUP268/oUP269 and UM521 wild type DNA as a template. The 3 $\times$  HA tag was used for verification of the production via Western blot analysis. The gene expression is under the control of the promoter P<sub>otef</sub> and the terminator T<sub>nos</sub>. For cloning with *E. coli*, the plasmid contains a gene encoding  $\beta$ -lactamase enzyme for selection on ampicillin containing media. (This study)

### **pAat1G\_CbxR (pUMa4230)**

This plasmid is for producing Aat1 N-terminally fused to eGfp at the *ip<sup>s</sup>* locus. The nucleotide sequence of *aat1* is derived from pAat1<sup>HA</sup>\_CbxR (pUMa3379). The gene encoding eGfp is from pEGfp\_NatR (pUMa3132). The gene expression is under the control of the promoter P<sub>tef</sub> and the terminator T<sub>nos</sub>. For cloning with *E. coli*, the plasmid contains a gene encoding  $\beta$ -lactamase enzyme for selection on ampicillin containing media. (This study)

### **pHmg1<sup>NA1-932</sup>G\_CbxR (pUMa4231)**

This plasmid is for producing N-terminally truncated from aa 1 to 932 of Hmg1, which is N-terminally fused to eGfp, at the *ip<sup>s</sup>* locus. The nucleotide sequence of *hmg1*<sup>NA1-932</sup> is derived from pHmg1<sup>NA1-932HA</sup>\_CbxR (pUMa3381). The gene encoding eGfp is from peGfp\_NatR (pUMa3132). The gene expression is under the control of the P<sub>tef</sub> and the terminator T<sub>nos</sub>. For cloning with *E. coli*, the plasmid contains a gene encoding β-lactamase enzyme for selection on ampicillin containing media. (This study)

### **pIdi1G\_CbxR (pUMa4232)**

This plasmid is for producing Idi1 N-terminally fused to eGfp at the *ip<sup>s</sup>* locus. The nucleotide sequence of *idi1* is derived from pIdi1<sup>HA</sup>\_CbxR (pUMa3382). The gene encoding eGfp is from peGfp\_NatR (pUMa3132). The gene expression is under the control of the promoter P<sub>tef</sub> and the terminator T<sub>nos</sub>. For cloning with *E. coli*, the plasmid contains a gene encoding β-lactamase enzyme for selection on ampicillin containing media. (This study)

### **pUpa9mC\_HygR (pUMa2722)**

This plasmid is for producing Upa9 C-terminally fused to mCherry with the hygromycin B resistance cassette at the *upa9* locus. The insert construct is flanked by the regions, 1.1 kb of *upa9* (UMAG\_06200) ORF, and 1.0 kb downstream of *upa9*. The flanking regions were amplified by PCR using oDD527/oDD605, oDD634/oDD635, and UM521 wild type DNA as a template. The gene expression is under the control of the native promoter of *upa9* and the terminator T<sub>nos</sub>. For cloning with *E. coli*, the plasmid contains a gene encoding β-lactamase enzyme for selection on ampicillin containing media. (This study)

### **peGfp-skl\_CbxR (pUMa3141)**

This plasmid is for producing eGfp C-terminally fused to SKL at the *ip<sup>s</sup>* locus. To insert the SKL sequence at the C-terminus of eGfp, oMB935 and oMB936 were used to amplify the *egfp-skl* fragment by PCR. The gene expression is under the control of the P<sub>otef</sub> and the terminator T<sub>nos</sub>. For cloning with *E. coli*, the plasmid contains a gene encoding β-lactamase enzyme for selection on ampicillin containing media. (This study)

### **pUpa9G\_NatR (pUMa2938)**

This plasmid is for producing Upa9 C-terminally fused to eGfp with the nourseothricin resistance cassette at the *upa9* locus. The insert construct is flanked by the regions, 1.1 kb of *upa9* ORF and 1.0 kb downstream of *upa9*. The flanking regions were amplified by PCR using oDD527/oDD605 and oDD634/oDD635 and UM521 wild type DNA as a template. The gene expression is under the control of the native promoter and the terminator T<sub>nos</sub>. For cloning with *E. coli*, the plasmid contains a gene encoding β-lactamase enzyme for selection on ampicillin containing media. (This study)

### **pIdi1<sup>HA</sup>\_NatR<sup>FRTm1</sup> (pUMa4082)**

This plasmid is for producing Idi1 N-terminally fused to 3× HA tag with the nourseothricin resistance cassette containing FRTm1 sites (GAAGTTCCTATTCTCGAGAAAGTATAGGAACTTC) at both ends for recycling by Flp recombinase at the *cco1* locus. The nucleotide sequence of *idi1*<sup>HA</sup> is derived from pIdi1<sup>HA</sup>\_CbxR (pUMa3382). The flanking regions for the integration at the *cco1* locus are from pCco1Δ\_HygR (pUMa3281). The gene expression is under the control of the promoter *P<sub>rpl10</sub>* (1 kb upstream of the ORF of UMAG\_10842) and the terminator *T<sub>hsp70</sub>*. For cloning with *E. coli*, the plasmid contains a gene encoding β-lactamase enzyme for selection on ampicillin containing media. (This study)

### **pCnVS\_NatR<sup>FRTm2</sup> (pUMa4500)**

This plasmid is for producing dicodon-optimized CnVS with the nourseothricin resistance cassette containing FRTm2 sites (GAAGTTCCTATTCTCAAGAAAGTATAGGAACTTC) at both ends for recycling by Flp recombinase at the *upp3* locus. The flanking regions for the integration at the *upp3* locus is derived from pUpp3Δ\_HygR (pUMa1556). The gene expression is under the control of the promoter *P<sub>otef</sub>* and the terminator *T<sub>nos</sub>*. For cloning with *E. coli*, the plasmid contains a gene encoding β-lactamase enzyme for selection on ampicillin containing media. (This study)

### **pCnVSG\_NatR<sup>FRTm2</sup> (pUMa4356)**

This plasmid is for producing dicodon-optimized CnVS, which is N-terminally fused to eGfp with the nourseothricin resistance cassette containing FRTm2 sites (GAAGTTCCTATTCTCAAGAAAGTATAGGAACTTC) at both ends for recycling by Flp recombinase, at the *upp3* locus. The nucleotide sequence of the dicodon-optimized CnVS is from pCnVS\_NatR<sup>FRTm2</sup> (pUMa4500). The flanking regions for the integration at the *upp3* locus is derived from pUpp3Δ\_HygR (pUMa1556). The gene expression is under the control of the promoter *P<sub>otef</sub>* and the terminator *T<sub>nos</sub>*. For cloning with *E. coli*, the plasmid contains a gene encoding β-lactamase enzyme for selection on ampicillin containing media. (This study)

### **pCnVSG<sup>NES</sup>\_NatR<sup>FRTm2</sup> (pUMa4499)**

This plasmid is for producing dicodon-optimized CnVS, which is N-terminally fused to eGfp<sup>NES</sup> with the nourseothricin resistance cassette containing FRTm2 sites (GAAGTTCCTATTCTCAAGAAAGTATAGGAACTTC) at both ends for recycling by Flp recombinase, at the *upp3* locus. The nucleotide sequence of the dicodon-optimized CnVS is from pCnVS\_NatR<sup>FRTm2</sup> (pUMa4500). The nuclear export signal (NES) is from murine minute virus (MTKKFGTLTI; Engelsma et al., 2008). For cloning, oAB049 and oAB050 were annealed for the NES sequence. The flanking regions for the integration at the *upp3* locus is derived from pUpp3Δ\_HygR (pUMa1556). The gene expression is under the control of the promoter *P<sub>otef</sub>* and the terminator *T<sub>nos</sub>*. For cloning with *E. coli*, the plasmid contains

a gene encoding  $\beta$ -lactamase enzyme for selection on ampicillin containing media. More details are found in Appendix Figure 6.2A. (This study)

### **pCop6\_NatR<sup>FRTm2</sup> (pUMa4496)**

This plasmid is for producing dicodon-optimized Cop6 with the nourseothricin resistance cassette containing FRTm2 sites (GAAGTTCCTATTCTCAAGAAAGTATAGGAACTTC) at both ends for recycling by Flp recombinase, at the *upp3* locus. The flanking regions for the integration at the *upp3* locus is derived from pUpp3 $\Delta$ \_HygR (pUMa1556). The gene expression is under the control of the promoter  $P_{otef}$  and the terminator  $T_{nos}$ . For cloning with *E. coli*, the plasmid contains a gene encoding  $\beta$ -lactamase enzyme for selection on ampicillin containing media. (This study)

### **pCop6G\_NatR<sup>FRTm2</sup> (pUMa4089)**

This plasmid is for producing dicodon-optimized Cop6, which is N-terminally fused to eGfp with the nourseothricin resistance cassette containing FRTm2 sites (GAAGTTCCTATTCTCAAGAAAGTATAGGAACTTC) at both ends for recycling by Flp recombinase, at the *upp3* locus. The nucleotide sequence of the dicodon-optimized Cop6 is from pCop6\_NatR<sup>FRTm2</sup> (pUMa4496). The flanking regions for the integration at the *upp3* locus is derived from pUpp3 $\Delta$ \_HygR (pUMa1556). The gene expression is under the control of the promoter  $P_{otef}$  and the terminator  $T_{nos}$ . For cloning with *E. coli*, the plasmid contains a gene encoding  $\beta$ -lactamase enzyme for selection on ampicillin containing media. (This study)

### **pCop6G<sup>NES</sup>\_NatR<sup>FRTm2</sup> (pUMa4316)**

This plasmid is for producing dicodon-optimized Cop6, which is N-terminally fused to eGfp<sup>NES</sup> with the nourseothricin resistance cassette containing FRTm2 sites (GAAGTTCCTATTCTCAAGAAAGTATAGGAACTTC) at both ends for recycling by Flp recombinase, at the *upp3* locus. The nucleotide sequence of the dicodon-optimized Cop6 is from pCop6\_NatR<sup>FRTm2</sup> (pUMa4496). The nuclear export signal (NES) is from murine minute virus (MTKKFGTLTI; Engelsma et al., 2008). For cloning, oAB049 and oAB050 were annealed for the NES sequence. The flanking regions for the integration at the *upp3* locus is derived from pUpp3 $\Delta$ \_HygR (pUMa1556). For cloning with *E. coli*, the plasmid contains a gene encoding  $\beta$ -lactamase enzyme for selection on ampicillin containing media. More details are found in Appendix Figure 6.2B. (This study)

## 4.1.5 Strains

Table 4.7 List of *U. maydis* strains used in this study

Strain	Locus	Progenitor strain	Short description
AB33	<i>b</i>	FB2	<i>Pnar:bW2bE1</i> , production of active <i>b</i> heterodimer under control of the <i>P<sub>nar1</sub></i> promoter; strain grows filamentously upon changing the nitrogen source. (Brachmann, 2001).
AB33car2Δ_HygR	<i>car2</i>	AB33	Carrying a deletion of <i>car2</i> and possessing hygromycin B resistance.
AB33car2Δ/AacrB <sup>Myc</sup> _NatR	<i>car2</i>	AB33car2Δ_HygR	Carrying a deletion of <i>car2</i> and producing codon-optimized AaCrtB, which is C-terminally fused to 3× Myc tag at the <i>car2</i> locus. Possessing nourseothricin resistance.
AB33car2Δ/AacrB <sup>Myc</sup> _NatR/ car1Δ_HygR	<i>car2</i> <i>car1</i>	AB33car2Δ/AacrB <sup>Myc</sup> _NatR	Carrying deletions of <i>car2</i> and <i>car1</i> and producing codon-optimized AaCrtB, which is C-terminally fused to 3× Myc tag at the <i>car2</i> locus. Possessing nourseothricin and hygromycin B resistance.
AB33car2Δ/AacrB <sup>Myc</sup> _NatR/ aat1 <sup>HA</sup> _CbxR	<i>car2</i> <i>ip<sup>s</sup></i>	AB33car2Δ/AacrB <sup>Myc</sup> _NatR	Carrying a deletion of <i>car2</i> and co-producing codon-optimized AaCrtB, which is C-terminally fused to 3× Myc tag at the <i>car2</i> locus, and Aat1 N-terminally fused to 3× HA tag at the <i>ip<sup>s</sup></i> locus. Possessing nourseothricin and carboxin resistance.
AB33car2Δ/AacrB <sup>Myc</sup> _NatR/ hmg1 <sup>NA1-932HA</sup> _CbxR	<i>car2</i> <i>ip<sup>s</sup></i>	AB33car2Δ/AacrB <sup>Myc</sup> _NatR	Carrying a deletion of <i>car2</i> and co-producing codon-optimized AaCrtB, which is C-terminally fused to 3× Myc tag at the <i>car2</i> locus, and N-terminally truncated from aa 1 to 932 version of Hmg1, which is N-terminally fused to 3× HA tag at the <i>ip<sup>s</sup></i> locus. Possessing nourseothricin and carboxin resistance.
AB33car2Δ/AacrB <sup>Myc</sup> _NatR/ idi1 <sup>HA</sup> _CbxR	<i>car2</i> <i>ip<sup>s</sup></i>	AB33car2Δ/AacrB <sup>Myc</sup> _NatR	Carrying a deletion of <i>car2</i> and co-producing codon-optimized AaCrtB, which is C-terminally fused to 3× Myc tag at the <i>car2</i> locus, and Idi1 N-terminally fused to 3× HA tag at the <i>ip<sup>s</sup></i> locus. Possessing nourseothricin and carboxin resistance.
AB33car2Δ/AacrB <sup>Myc</sup> _NatR/ aat1G_CbxR	<i>car2</i> <i>ip<sup>s</sup></i>	AB33car2Δ/AacrB <sup>Myc</sup> _NatR	Carrying a deletion of <i>car2</i> and co-producing codon-optimized AaCrtB, which is C-terminally fused to 3× Myc tag at the <i>car2</i> locus, and Aat1 N-terminally fused to eGfp at the <i>ip<sup>s</sup></i> locus. Possessing nourseothricin and carboxin resistance.
AB33car2Δ/AacrB <sup>Myc</sup> _NatR/ hmg1 <sup>N1-932G</sup> _CbxR	<i>car2</i> <i>ip<sup>s</sup></i>	AB33car2Δ/AacrB <sup>Myc</sup> _NatR	Carrying a deletion of <i>car2</i> and co-producing codon-optimized AaCrtB, which is C-terminally fused to 3× Myc tag at the <i>car2</i> locus, and N-terminally truncated from aa 1 to 932 version of Hmg1, which is N-terminally fused to eGfp at the <i>ip<sup>s</sup></i> locus. Possessing nourseothricin and carboxin resistance.
AB33car2Δ/AacrB <sup>Myc</sup> _NatR/ idi1G_CbxR	<i>car2</i> <i>ip<sup>s</sup></i>	AB33car2Δ/AacrB <sup>Myc</sup> _NatR	Carrying a deletion of <i>car2</i> and co-producing codon-optimized AaCrtB, which is C-terminally fused to 3× Myc tag at the <i>car2</i> locus and Idi1 N-terminally fused to eGfp at the <i>ip<sup>s</sup></i> locus. Possessing nourseothricin and carboxin resistance.
AB33egfp_CbxR	<i>ip<sup>s</sup></i>	AB33	The <i>egfp</i> construct is ectopically integrated into the <i>ip<sup>s</sup></i> locus. Possessing nourseothricin and carboxin resistance (Koepeke, 2011).
AB33upa9mC_HygR/ egfp-skI_CbxR	<i>upa9</i> <i>ip<sup>s</sup></i>	AB33egfp-skI_CbxR	Co-producing eGfp containing SKL at the C-terminus at the <i>ip<sup>s</sup></i> locus and Upa9 C-terminally fused to eGfp at the <i>upa9</i> locus. Upa9 is the homolog of Pex3.
AB33pab1mC_HygR/ upa9G_NatR	<i>pab1</i> <i>upa9</i>	AB33pab1mC	Co-producing Pab1 C-terminally fused to mCherry at the <i>pab1</i> locus and Upa9 C-terminally fused to eGfp at the <i>upa9</i> locus. Possessing hygromycin B and carboxin resistance.
AB33car2Δ/AacrB <sup>Myc</sup>	<i>car2</i>	AB33car2Δ/AacrB <sup>Myc</sup> _NatR	Carrying a deletion of <i>car2</i> and producing codon-optimized AaCrtB, which is C-terminally fused to 3× Myc tag at the <i>car2</i> locus. Nourseothricin resistance gene cassette is recycled via FRTm7
AB33car2Δ/AacrB <sup>Myc</sup> / cco1Δ/HygR	<i>car2</i> <i>cco1</i>	AB33car2Δ/AacrB <sup>Myc</sup>	Carrying deletions of <i>car2</i> and <i>cco1</i> and producing codon-optimized AaCrtB, which is C-terminally fused to 3× Myc tag at the <i>car2</i> locus. Nourseothricin resistance gene cassette is recycled via FRTm7 and possessing hygromycin B resistance.



AB33car2Δ/AacrB <sup>Myc</sup> /cco1Δ/ idi1 <sup>HA</sup> _NatR	<i>car2</i> <i>cco1</i>	AB33car2Δ/AacrB <sup>Myc</sup> /cco1Δ _HygR	Carrying deletions of <i>car2</i> and <i>cco1</i> and co-producing codon-optimized AaCrtB, which is C-terminally fused to 3× Myc tag at the <i>car2</i> locus, and Idi1 N-terminally fused to 3× HA tag at the <i>cco1</i> locus. Possessing nourseothricin resistance.
AB33car2Δ/AacrB <sup>Myc</sup> /cco1Δ/ idi1 <sup>HA</sup>	<i>car2</i> <i>cco1</i>	AB33car2Δ/AacrB <sup>Myc</sup> /cco1Δ/ idi1 <sup>HA</sup> _NatR	Carrying deletions of <i>car2</i> and <i>cco1</i> and co-producing codon-optimized AaCrtB, which is C-terminally fused to 3× Myc tag at the <i>car2</i> locus, and Idi1 N-terminally fused to 3× HA tag at the <i>cco1</i> locus. Nourseothricin resistance gene cassette is recycled via FRTm1.
AB33car2Δ/AacrB <sup>Myc</sup> /cco1Δ/ idi1 <sup>HA</sup> /upp3Δ/HygR	<i>car2</i> <i>cco1</i>	AB33car2Δ/AacrB <sup>Myc</sup> /cco1Δ/ idi1 <sup>HA</sup>	Carrying deletions of <i>car2</i> , <i>cco1</i> , and <i>upp3</i> , and co-producing codon-optimized AaCrtB, which is C-terminally fused to 3× Myc tag at the <i>car2</i> locus, and Idi1 N-terminally fused to 3× HA tag at the <i>cco1</i> locus. Possessing hygromycin B resistance.
AB33upp3Δ/egfp_NatR	<i>upp3</i>	AB33upp3Δ_HygR	Carrying a deletion of <i>upp3</i> and producing eGfp at the <i>upp3</i> locus. Possessing nourseothricin resistance.
AB33car2Δ/AacrB <sup>Myc</sup> / upp3Δ_HygR	<i>car2</i> <i>upp3</i>	AB33car2Δ/AacrB <sup>Myc</sup>	Carrying deletions of <i>car2</i> and <i>upp3</i> and producing codon-optimized AaCrtB, which is C-terminally fused to 3× Myc tag at the <i>car2</i> locus. Possessing hygromycin B resistance
AB33car2Δ/AacrB <sup>Myc</sup> /upp3Δ/ CnVS_NatR	<i>car2</i> <i>upp3</i>	AB33car2Δ/AacrB <sup>Myc</sup> /upp3Δ _HygR	Carrying deletions of <i>car2</i> and <i>upp3</i> and co-producing codon-optimized AaCrtB, which is C-terminally fused to 3× Myc tag at the <i>car2</i> locus, and dicodon-optimized CnVS at the <i>upp3</i> locus. Possessing nourseothricin resistance.
AB33car2Δ/AacrB <sup>Myc</sup> /upp3Δ/ CnVSG_NatR	<i>car2</i> <i>upp3</i>	AB33car2Δ/AacrB <sup>Myc</sup> /upp3Δ _HygR	Carrying deletions of <i>car2</i> and <i>upp3</i> and co-producing codon-optimized AaCrtB, which is C-terminally fused to 3× Myc tag at the <i>car2</i> locus, and dicodon-optimized CnVS, which is N-terminally fused to eGfp at the <i>upp3</i> locus. Possessing nourseothricin resistance.
AB33car2Δ/AacrB <sup>Myc</sup> /upp3Δ/ CnVSG <sup>NES</sup> _NatR	<i>car2</i> <i>upp3</i>	AB33car2Δ/AacrB <sup>Myc</sup> /upp3Δ _HygR	Carrying deletions of <i>car2</i> and <i>upp3</i> and co-producing codon-optimized AaCrtB, which is C-terminally fused to 3× Myc tag at the <i>car2</i> locus, and dicodon-optimized CnVS, which is N-terminally fused to eGfp <sup>NES</sup> at the <i>upp3</i> locus. Possessing nourseothricin resistance.
AB33car2Δ/AacrB <sup>Myc</sup> /cco1Δ/ idi1 <sup>HA</sup> /upp3Δ/CnVSG <sup>NES</sup> _NatR	<i>car2</i> <i>cco1</i> <i>upp3</i>	AB33car2Δ/AacrB <sup>Myc</sup> /cco1Δ/ idi1 <sup>HA</sup> /upp3Δ_HygR	Carrying deletions of <i>car2</i> , <i>cco1</i> , and <i>upp3</i> and co-producing codon-optimized AaCrtB, which is C-terminally fused to 3× Myc tag at the <i>car2</i> locus, Idi1 N-terminally fused to 3× HA tag at the <i>cco1</i> locus, and dicodon-optimized CnVS, which is N-terminally fused to eGfp <sup>NES</sup> at the <i>upp3</i> locus. Possessing nourseothricin resistance.
AB33car2Δ/AacrB <sup>Myc</sup> /upp3Δ/ cop6_NatR	<i>car2</i> <i>upp3</i>	AB33car2Δ/AacrB <sup>Myc</sup> /upp3Δ _HygR	Carrying deletions of <i>car2</i> and <i>upp3</i> and co-producing codon-optimized AaCrtB, which is C-terminally fused to 3× Myc tag at the <i>car2</i> locus, and dicodon-optimized Cop6 at the <i>upp3</i> locus. Possessing nourseothricin resistance.
AB33car2Δ/AacrB <sup>Myc</sup> /upp3Δ/ cop6G_NatR	<i>car2</i> <i>upp3</i>	AB33car2Δ/AacrB <sup>Myc</sup> /upp3Δ _HygR	Carrying deletions of <i>car2</i> and <i>upp3</i> and co-producing codon-optimized AaCrtB, which is C-terminally fused to 3× Myc tag at the <i>car2</i> locus, and dicodon-optimized Cop6, which is N-terminally fused to eGfp at the <i>upp3</i> locus. Possessing nourseothricin resistance.
AB33car2Δ/AacrB <sup>Myc</sup> /upp3Δ/ cop6G <sup>NES</sup> _NatR	<i>car2</i> <i>upp3</i>	AB33car2Δ/AacrB <sup>Myc</sup> /upp3Δ _HygR	Carrying deletions of <i>car2</i> and <i>upp3</i> and co-producing codon-optimized AaCrtB, which is C-terminally fused to 3× Myc tag at the <i>car2</i> locus and dicodon-optimized Cop6, which is N-terminally fused to eGfp <sup>NES</sup> at the <i>upp3</i> locus. Possessing nourseothricin resistance.
AB33car2Δ/AacrB <sup>Myc</sup> /cco1Δ/ idi1 <sup>HA</sup> /upp3Δ/cop6G <sup>NES</sup> _NatR	<i>car2</i> <i>cco1</i> <i>upp3</i>	AB33car2Δ/AacrB <sup>Myc</sup> /cco1Δ/ idi1 <sup>HA</sup> /upp3Δ_HygR	Carrying deletions of <i>car2</i> , <i>cco1</i> , and <i>upp3</i> and co-producing codon-optimized AaCrtB, which is C-terminally fused to 3× Myc tag at the <i>car2</i> locus, Idi1 N-terminally fused to 3× HA tag at the <i>cco1</i> locus, and dicodon-optimized Cop6, which is N-terminally fused to eGfp <sup>NES</sup> at the <i>upp3</i> locus. Possessing nourseothricin resistance.

This table is derived from Lee et al., 2020a (Supplementary Table S1).

Table 4.8 Generation of *U. maydis* strains used in this study

Strain	Relevant genotype	UMa	Reference	Transformed plasmid (pUMa)	Locus	Progenitor strain
AB33	<i>a2 Pnar::bW2bE1</i>	133	Brachmann, 2001	pAB33	<i>b</i>	FB2
AB33car2Δ_HygR	<i>car2Δ</i>	2290	This study	pCar2Δ_HygR <sup>FRT</sup> (pUMa3287)	<i>car2</i>	AB33
AB33car2Δ/AacrB <sup>Myc</sup> _NatR	<i>car2Δ/AacrB</i>	2612	This study	pAacrB <sup>Myc</sup> _NatR <sup>FRTm7</sup> (pUMa3707)	<i>car2</i>	AB33car2Δ_HygR
AB33car2Δ/AacrB <sup>Myc</sup> _NatR/ <i>car1Δ_HygR</i>	<i>car2Δ/AacrB/ car1Δ</i>	3246	This study	pCar1Δ_HygR <sup>FRT</sup> (pUMa3286)	<i>car1</i>	AB33car2Δ/ AacrB <sup>Myc</sup> _NatR
AB33car2Δ/AacrB <sup>Myc</sup> _NatR/ <i>aat1<sup>HA</sup>_CbxR</i>	<i>car2Δ/AacrB/ aat1</i>	2706	This study	pAat1 <sup>HA</sup> _CbxR (pUMa3379)	<i>ip<sup>s</sup></i>	AB33car2Δ/ AacrB <sup>Myc</sup> _NatR
AB33car2Δ/AacrB <sup>Myc</sup> _NatR/ <i>hmg1<sup>NA1-932HA</sup>_CbxR</i>	<i>car2Δ/AacrB/ hmg1<sup>NA1-932</sup></i>	2707	This study	pHmg1 <sup>NA1-932</sup> _CbxR (pUMa3381)	<i>ip<sup>s</sup></i>	AB33car2Δ/ AacrB <sup>Myc</sup> _NatR
AB33car2Δ/AacrB <sup>Myc</sup> _NatR/ <i>idi1<sup>HA</sup>_CbxR</i>	<i>car2Δ/AacrB/ idi1</i>	2708	This study	pIdi1 <sup>HA</sup> _CbxR (pUMa3382)	<i>ip<sup>s</sup></i>	AB33car2Δ/ AacrB <sup>Myc</sup> _NatR
AB33car2Δ/AacrB <sup>Myc</sup> _NatR/ <i>aat1G_CbxR</i>	<i>car2Δ/AacrB/ aat1G</i>	3065	This study	pAat1G_CbxR (pUMa4230)	<i>ip<sup>s</sup></i>	AB33car2Δ/ AacrB <sup>Myc</sup> _NatR
AB33car2Δ/AacrB <sup>Myc</sup> _NatR/ <i>hmg1<sup>NA1-932G</sup>_CbxR</i>	<i>car2Δ/AacrB/ hmg1<sup>NA1-932</sup></i>	3066	This study	pHmg1 <sup>NA1-932G</sup> _CbxR (pUMa4231)	<i>ip<sup>s</sup></i>	AB33car2Δ/ AacrB <sup>Myc</sup> _NatR
AB33car2Δ/AacrB <sup>Myc</sup> _NatR/ <i>idi1G_CbxR</i>	<i>car2Δ/AacrB/ idi1G</i>	3067	This study	pIdi1G_CbxR (pUMa4232)	<i>ip<sup>s</sup></i>	AB33car2Δ/ AacrB <sup>Myc</sup> _NatR
AB33egfp_CbxR	<i>egfp</i>	2229	Koepeke, 2011	peGfp_CbxR (pUMa1139)	<i>ip<sup>s</sup></i>	AB33
AB33upa9mC_HygR/ <i>egfp-skl_CbxR</i>	<i>upa9mC/egfp-skl</i>	2386	This study	pUpa9mC_HygR (pUMa2722)	<i>upa9</i>	AB33egfp-skl_CbxR
AB33pab1mC_HygR/ <i>upa9G_NatR</i>	<i>pab1mC/upa9G</i>	1951	This study	pUpa9G_NatR (pUMa2938)	<i>upa9</i>	AB33pab1mC
AB33car2Δ/AacrB <sup>Myc</sup>	<i>car2Δ/AacrB</i>	2775	This study	pFLPexpC (pUMa1446)	<i>car2</i>	AB33car2Δ/ AacrB <sup>Myc</sup> _NatR
AB33car2Δ/AacrB <sup>Myc</sup> / <i>cco1Δ_HygR</i>	<i>car2Δ/AacrB/ cco1Δ</i>	2785	This study	pCco1Δ_HygR (pUMa3281)	<i>cco1</i>	AB33car2Δ/ AacrB <sup>Myc</sup>
AB33car2Δ/AacrB <sup>Myc</sup> / <i>cco1Δ/idi1<sup>HA</sup>_NatR</i>	<i>car2Δ/AacrB/ cco1Δ/idi1</i>	3025	This study	pIdi1 <sup>HA</sup> _NatR <sup>FRTm1</sup> (pUMa4082)	<i>cco1</i>	AB33car2Δ/AacrB <sup>Myc</sup> / cco1Δ_HygR
AB33car2Δ/AacrB <sup>Myc</sup> / <i>cco1Δ/idi1<sup>HA</sup></i>	<i>car2Δ/AacrB/ cco1Δ/idi1</i>	3077	This study	pFLPexpC (pUMa1446)	<i>cco1</i>	AB33car2Δ/AacrB <sup>Myc</sup> / cco1Δ/idi1 <sup>HA</sup> _NatR
AB33car2Δ/AacrB <sup>Myc</sup> / <i>cco1Δ/idi1<sup>HA</sup>/upp3Δ_HygR</i>	<i>car2Δ/AacrB/ cco1Δ/idi1/upp3Δ</i>	3131	This study	pUpp3Δ_HygR <sup>FRTm3</sup> (pUMa1556)	<i>upp3</i>	AB33car2Δ/AacrB <sup>Myc</sup> / cco1Δ/idi1 <sup>HA</sup>
AB33upp3Δ/egfp_NatR	<i>upp3Δ/egfp</i>	2179	This study	peGfp_NatR (pUMa3132)	<i>upp3</i>	AB33upp3Δ_HygR
AB33car2Δ/AacrB <sup>Myc</sup> / <i>upp3Δ_HygR</i>	<i>car2Δ/AacrB/ upp3Δ</i>	2884	This study	pUpp3Δ_HygR <sup>FRTm3</sup> (pUMa1556)	<i>upp3</i>	AB33car2Δ/AacrB <sup>Myc</sup>
AB33car2Δ/AacrB <sup>Myc</sup> / <i>upp3Δ/CnVS_NatR</i>	<i>car2Δ/AacrB/ upp3Δ/CnVS</i>	3194	This study	pCnVS_NatR <sup>FRTm2</sup> (pUMa4500)	<i>upp3</i>	AB33car2Δ/AacrB <sup>Myc</sup> / upp3Δ_HygR
AB33car2Δ/AacrB <sup>Myc</sup> / <i>upp3Δ/CnVSG_NatR</i>	<i>car2Δ/AacrB/ upp3Δ/CnVSG</i>	3104	This study	pCnVSG_NatR <sup>FRTm2</sup> (pUMa4356)	<i>upp3</i>	AB33car2Δ/AacrB <sup>Myc</sup> / upp3Δ_HygR
AB33car2Δ/AacrB <sup>Myc</sup> / <i>upp3Δ/CnVSG<sup>NES</sup>_NatR</i>	<i>car2Δ/AacrB/ upp3Δ/CnVSG<sup>NES</sup></i>	3192	This study	pCnVSG <sup>NES</sup> _NatR <sup>FRTm2</sup> (pUMa4499)	<i>upp3</i>	AB33car2Δ/AacrB <sup>Myc</sup> / upp3Δ_HygR
AB33car2Δ/AacrB <sup>Myc</sup> / <i>cco1Δ/idi1<sup>HA</sup>/upp3Δ/CnVSG<sup>NES</sup>_NatR</i>	<i>car2Δ/AacrB/ cco1Δ/idi1/ upp3Δ/CnVSG<sup>NES</sup></i>	3195	This study	pCnVSG <sup>NES</sup> _NatR <sup>FRTm2</sup> (pUMa4499)	<i>upp3</i>	AB33car2Δ/AacrB <sup>Myc</sup> / cco1Δ/idi1 <sup>HA</sup> / upp3Δ_HygR
AB33car2Δ/AacrB <sup>Myc</sup> / <i>upp3Δ/cop6_NatR</i>	<i>car2Δ/AacrB/ upp3Δ/cop6</i>	3193	This study	pCop6_NatR <sup>FRTm2</sup> (pUMa4496)	<i>upp3</i>	AB33car2Δ/AacrB <sup>Myc</sup> / upp3Δ_HygR
AB33car2Δ/AacrB <sup>Myc</sup> / <i>upp3Δ/cop6G_NatR</i>	<i>car2Δ/AacrB/ upp3Δ/cop6G</i>	2944	This study	pCop6G_NatR <sup>FRTm2</sup> (pUMa4089)	<i>upp3</i>	AB33car2Δ/AacrB <sup>Myc</sup> / upp3Δ_HygR
AB33car2Δ/AacrB <sup>Myc</sup> / <i>upp3Δ/cop6G<sup>NES</sup>_NatR</i>	<i>car2Δ/AacrB/ upp3Δ/cop6G<sup>NES</sup></i>	3078	This study	pCop6G <sup>NES</sup> _NatR <sup>FRTm2</sup> (pUMa4316)	<i>upp3</i>	AB33car2Δ/AacrB <sup>Myc</sup> / upp3Δ_HygR
AB33car2Δ/AacrB <sup>Myc</sup> / <i>cco1Δ/idi1<sup>HA</sup>/upp3Δ/cop6G<sup>NES</sup>_NatR</i>	<i>car2Δ/AacrB/ cco1Δ/idi1/ upp3Δ/cop6G<sup>NES</sup></i>	3148	This study	pCop6G <sup>NES</sup> _NatR <sup>FRTm2</sup> (pUMa4316)	<i>upp3</i>	AB33car2Δ/AacrB <sup>Myc</sup> / cco1Δ/idi1 <sup>HA</sup> / upp3Δ_HygR

This table is derived from Lee et al., 2020a (Supplementary Table S2).

**Table 4.9** List of additional strains used in this study

Strain	Relevant genotype	UMa	Reference
<i>S. cerevisiae</i> ESM356-1	<i>MAT<math>\alpha</math> ura3-52 leu2<math>\Delta</math>1 trp1<math>\Delta</math>63 his3<math>\Delta</math>200</i>	2193	Pereira et al., 2001
<i>C. glutamicum</i> wt	ATCC13032	2540	Abe et al., 1967
<i>E. coli</i> Top10	<i>F<sup>-</sup> mcrA<math>\Delta</math>(mrr-hsdRMS-mcrBC) <math>\phi</math>80lacZ<math>\Delta</math>M15 <math>\Delta</math>lacX74 recA1 araD139<math>\Delta</math>(ara-leu)7697 galU galK <math>\lambda^-</math> rpsL(Str<sup>R</sup>) endA1 nupG</i>	1027	Life Technologies

## 4.2 Methods

### 4.2.1 Molecular biology methods

Standard molecular biology techniques for cloning, such as DNA restriction digestion, ligation, purification, and electrophoretic separation were performed according to protocols (Sambrook et al., 1989; Sambrook and Russell, 2001). Kits and enzymes were used as the descriptions of the products by the manufacturers.

### Polymerase chain reaction (PCR)

Desired DNA fragments were amplified via polymerase chain reaction (PCR) as described (Saiki et al., 1985). Reactions were performed in a SensoQuest Labcycler (SensoQuest GmbH, Göttingen, Germany) or Eppendorf mastercycler® ep Gradient S Thermal Cycler (Eppendorf, Hamburg, Germany) with Phusion-HF DNA polymerase (Thermo Fisher Scientific, Waltham, MA, USA) according to the instructions. PCR programs were set up as below.

Standard Phusion-HF PCR reaction	
DNA (template)	50 ng
dNTPs	200 $\mu$ M
Oligonucleotide 1 (forward)	1 $\mu$ M
Oligonucleotide 2 (reverse)	1 $\mu$ M
5x Phusion-HF buffer	1x as final concentration of the reaction
DMSO	3% (v/v)
Phusion-HF DNA polymerase	1 U
ddH <sub>2</sub> O	Add as final volume 25 $\mu$ L or 50 $\mu$ L

**Table 4.10** Thermocycling conditions for PCR

Step		Temperature (°C)	Time
Initial denaturation		98	1 min
30-35 cycles	Denaturation	98	10 s
	Annealing	65	30 s
	Elongation	72	Based on amplicon size and DNA polymerase elongation speed
Final extension		72	8 min
Hold		4	To hold

### Golden Gate cloning

For efficient cloning, the Golden Gate cloning method described in (Terfrüchte et al., 2014) was used. This cloning strategy is based on a unique feature of type IIs restriction enzyme, whose recognition site is a few base pairs upstream of the hydrolysis site, such as *Bsa*I. It was successfully applied to generate plasmids for generating gene replacement mutants in *U. maydis*. For gene replacement at a specific locus, the upstream and downstream flanking regions were amplified by PCR. The storage vector (pStor) harbors the gene replacement module, which is the hygromycin B resistance cassette in this study (See 4.1.4). The destination vector (pDest) contains a LacZ operon where the gene replacement module flanked by the upstream and downstream flanks can be inserted. A one-pot reaction assembled the plasmid. *E. coli* top10 competent cells were transformed with 2 µL of the One-pot reaction product. The respective antibiotic and X-gal (5-bromo-4-chloro-3-indolyl-β-D-galactopyranoside) selections led to a successful cloning.

One-pot reaction
75 ng of storage vector (pStor)
75 ng of destination vector (pDest)
40 ng of each gene fragment
1 T4 DNA ligation buffer
0.75 µL T4 DNA ligase
0.5 µL <i>Bsa</i> I
Add ddH <sub>2</sub> O

**Table 4.11 Thermocycling conditions for One-pot reaction**

Temperature (°C)	Time	
37	2 min	50 cycles
16	5 min	
37	5 min	
50	5 min	
80	5 min	
16	To hold	

### Gibson Assembly®

Multiple DNA fragments were successfully assembled by the Gibson Assembly® method (Gibson et al., 2009). The assembly reaction starts from generating 3' single strands on each side of the DNA fragment by 5' exonuclease. Then, the complementary single strands of two neighboring DNA fragments can join together. DNA polymerase having a proofreading activity fills the empty bases, and DNA ligase joins the phosphate backbone between the two neighboring DNA fragments to seal the nicks (Gibson et al., 2009). PCR amplified the DNA fragments with oligonucleotides containing 5' extension with 20-40 base pairs overlapping sequence complementary to its neighboring DNA fragment. Each DNA fragment was mixed in Gibson Assembly® master mix and then incubated at 50°C for 1 h. *E. coli* top10 competent cells were transformed with 10 µL of the Gibson Assembly® product.

5× Isothermal reaction buffer for 6 mL
3 mL of 1 M Tris-HCl, pH 7.5
150 µL of 2 M MgCl <sub>2</sub>
60 µL of 100 mM dGTP
60 µL of 100 mM dATP
60 µL of 100 mM dTTP
60 µL of 100 mM dCTP
300 µL of 1 M DTT
1.5 g PEG-8000
300 µL of 100 mM NAD

Gibson Assembly® master mix
320 µL of 5× Isothermal reaction buffer
6.4 µL of 1 U/µL T5 exonuclease
20 µL of 2 U/µL Phusion DNA polymerase
160 µL of 40 U/µL Taq DNA ligase
Add 1.2 mL of ddH <sub>2</sub> O and then prepare 15 µL Aliquots

### Isolation of plasmid DNA from *E. coli*

In cloning procedure, transformed plasmids were amplified in *E. coli* Top10, and isolation of the large amounts of plasmids was performed using the boiling lysis method according to (Sambrook et al., 1989). The transformed *E. coli* cells were cultivated in 2 mL dYT supplemented with the respective antibiotics overnight at 37°C. The dense culture was centrifuged at 13,000 rpm for 2 min. The cell pellet was resuspended in 200 µL STET and 20 µL lysozyme to disrupt the cells. The disruption procedure was continued by incubation at 95°C for 1 min. Cell debris was pelleted at 13,000 for 10 min, and the supernatant was taken. The plasmid DNA in the supernatant was then precipitated when 20 µL 3 M Na<sup>2+</sup>-acetate (pH 4.8) and 500 µL 100% (v/v) isopropanol were added. The plasmid DNA was harvested at 13,000 rpm for 10 min and then washed in 200 µL 70% (v/v) ethanol. The plasmid DNA was dried at 50°C for 30 min. Afterward, the plasmid DNA was resuspended in 100 µL TE/RNase. As an alternative way to isolate plasmid DNA from *E. coli* for cloning purposes, Plasmid mini Kit (Macherey-Nagel, Düren, Germany) was used.

STET
10 mM Tris-HCl (pH 8.0)
1 mM Na <sub>2</sub> -EDTA
100 mM NaCl
5% (v/v) Triton X-100
Add ddH <sub>2</sub> O

Lysozyme
10 mg/mL lysozyme
Dissolve in 1× TE buffer

TE/RNase
20 µg/mL RNase A
Dissolve in 1× TE buffer

### Determination of DNA concentrations

The concentrations of DNA fragments or plasmids were photometrically determined by a Nanodrop 2000c spectral photometer (Thermo Fisher Scientific, Waltham, MA, USA). An OD<sub>260</sub> = 1 refers to a concentration of 50 µg/mL double-stranded DNA at 1 cm layer thickness. The purity was determined by calculating the A<sub>260</sub>/A<sub>280</sub> quotient with an optimum of 1.8.

### Sequencing plasmids

All generated plasmids were purified and then 250 ng of the plasmids were mixed with 3.2 pmol of the respective primer in 10 mM Tris/Cl, pH 8.5. The sequencing samples were sent to the Institute for Genetics in Ludwig Maximilian University München, Martinsried, Germany, to confirm the sequence.



### Isolation of genomic DNA from *U. maydis*

2 mL of *U. maydis* overnight culture in CM-glc was harvested at 13,000 rpm for 5 min, and isolation of genomic DNA from *U. maydis* was performed according to modified protocols (Bösch et al., 2016; Hoffman and Winston, 1987). The cell pellets were disrupted with approximately 200 µL of glass beads and 500 µL of ustilago lysis buffer mixed with 1× TE buffer (1:1 ratio) by shaking at 1,000 rpm for 15 min on a Vibrax® shaker (Ika). The resuspension was incubated at 65°C for 15 min to complete cell disruption. Afterward, the resuspension was cooled down on ice for 5 min. 100 µL of 8 M potassium acetate was added into the resuspension and inverted to mix. Subsequently, separation of the cell debris and supernatant was performed by centrifugation at 13,000 rpm for 15 min. 500 µL of the supernatant was taken and mixed with 400 µL of 100% (v/v) isopropanol for gDNA precipitation. The gDNA was harvested at 13,000 rpm for 15 min and washed in 500 µL of 70% (v/v) ethanol. Centrifugation was carried out at 13,000 rpm for 5 min to discard the supernatant and harvest the gDNA as a pellet. The residual ethanol was dried at 50°C for 30 min. Afterward, the pellet was resuspended in 50 µL of TE/RNase at 50°C for 30 min.

Ustilago lysis buffer	10× TE buffer
50 mM Tris-HCl (pH 7.5)	100 mM Tris-HCl (pH 7.9)
50 mM Na <sub>2</sub> -EDTA	10 mM Na <sub>2</sub> -EDTA
1% (w/v) SDS	Add ddH <sub>2</sub> O
Add ddH <sub>2</sub> O	

### Southern blot analysis

For Southern blot analysis, genomic DNAs (gDNAs) of *U. maydis* strains were isolated and cleaved with appropriate restriction endonucleases (e.g., *Bam*HI in the case of insertion at the *ip<sup>S</sup>* locus). The cleaved gDNA fragments were size-separated by electrophoresis (100 V, 3 h) on a 0.8% agarose gel. To break and depurinate the large gDNA fragments, the gDNA-containing agarose gel was incubated in 0.25 M HCl and then further denatured and renatured in denaturation solution (1.5 M NaCl, 0.4 M NaOH) and renaturation solution (1.5 M NaCl, 0.28 M Tris-HCl, 0.22 M Tris-Base) for 20 min each. The gDNA fragments were transferred to a nylon membrane (Hybond-N+ nylon membrane, GE Healthcare, USA) through a capillary blot using blotting solution (3.0 M NaCl, 0.3 M C<sub>6</sub>H<sub>5</sub>O<sub>7</sub>Na<sub>3</sub>\*2H<sub>2</sub>O, pH 7.0) for 12h. After the transfer, the gDNA fragments were cross-linked to the membrane by UV irradiation (120 mJ/cm<sup>2</sup>, 254 nm, Biolink UV-Crosslinker, Vilber-Lourmat, Eberhardzell, Germany). The prehybridization step was carried out in hybridization buffer (780 mM NaCl, 59.02 mM NaHPO<sub>4</sub>\*H<sub>2</sub>O, 5.2 mM Na<sub>2</sub>-EDTA\*2H<sub>2</sub>O, pH 7.4; 0.1% [w/v] BSA fraction V, 0.1% [w/v] Ficoll 400, 0.1% [w/v] polyvinylpyrrolidone, 5% [w/v] SDS) at 65°C for 30 min. For the detection of specific DNA fragments, a DNA probe was labeled with digoxigenin (PCR Dig Labeling Mix, Roche, Mannheim, Germany). In the case of integration at the *ip<sup>S</sup>* locus, a DNA fragment covering the open reading frame of the iron-sulfur protein *ip<sup>S</sup>* was amplified (888 base pair fragment; Loubradou et al., 2001). The double-stranded probe was denatured in 20 mL of hybridization buffer

at 98°C for 10 min. The membrane was hybridized with the denatured probe at 65°C for 12 h. To remove unbound probe, the membrane was incubated in 20 mL of membrane washing buffer I (300 mM NaCl, 22.7 mM NaHPO<sub>4</sub>\*H<sub>2</sub>O, 2 mM Na<sub>2</sub>-EDTA\*2H<sub>2</sub>O, pH 7.4, 0.1% [w/v] SDS), membrane washing buffer II (150 mM NaCl, 11.4 mM NaHPO<sub>4</sub>\*H<sub>2</sub>O, 1 mM Na<sub>2</sub>-EDTA\*2H<sub>2</sub>O, pH 7.4, 0.1% [w/v] SDS), and membrane washing buffer III (15 mM NaCl, 1.14 mM NaHPO<sub>4</sub>\*H<sub>2</sub>O, 0.1 mM Na<sub>2</sub>-EDTA\*2H<sub>2</sub>O, pH 7.4, 0.1% [w/v] SDS). Each washing step was carried out at 65°C for 15 min. Before adding  $\alpha$ -DIG antibody ( $\alpha$ -digoxigenin polyclonal antibody Fab fragments, Roche, Germany), which recognizes the digoxigenin-labeled probes, the membrane was incubated with DIG-wash solution (0.3% [v/v] Tween-20 in DIG wash buffer I: 0.1 M maleic acid, 0.15 M NaCl, pH 7.5) at room temperature for 5 min. To reduce unspecific binding of the  $\alpha$ -DIG antibody, the membrane was blocked with DIG wash buffer II (1% [w/v] skimmed milk powder in DIG wash buffer I) at room temperature for 1 h. The  $\alpha$ -DIG antibody was diluted (1:20,000) and incubated with the membrane at room temperature for 30 min. The membrane was washed twice in DIG wash solution for 15 min. Afterward, the membrane was equilibrated at room temperature with DIG wash buffer III (0.1 M Tris-HCl, 0.1 M NaCl, pH 9.5) for 5 min. Subsequently, the chemiluminescent substrate (1:100 CDP-Star, Roche, Germany in DIG wash buffer III) was added to the membrane. Resulting chemiluminescence was detected with a LAS4000 ImageQuant device (GE Healthcare, USA).

### 4.2.2 Microbiological methods

#### 4.2.2.1 Microbiological work with *E. coli*

*E. coli* cells were grown in 5 mL dYT liquid medium at 37°C, and a rotating wheel was used for overnight. If necessary, the medium was supplemented with 100  $\mu$ g/mL of ampicillin or 40  $\mu$ g/mL of gentamycin after cooling down. Single colony on selective agar plates was inoculated for the cultivation.

#### Determination of cell density of *E. coli* cultures

The cell density of liquid cultures was photometrically determined using a Novaspec II photometer (Pharmacia Biotech). The OD<sub>600</sub> (optical density at  $\lambda$  = 600 nm) of the cultures was measured. If necessary, the cultures were diluted in the respective culture medium. An OD<sub>600</sub> of 1 resembles  $1.0 \times 10^9$  cells/mL for *E. coli*.

#### Preparation of competent *E. coli*

The preparation of competent *E. coli* Top10 cells was followed (Cohen et al., 1972). 20 mL of *E. coli* Top10 overnight culture was inoculated in 1 L fresh dYT medium, and 10 mM MgCl<sub>2</sub> and 10 mM MgSO<sub>4</sub> were added. The culture was incubated at 37°C and shaken at 200 rpm for about 2 h until an OD<sub>600</sub> 0.6. Then, the cells were transferred into tubes to chill on ice for 30 min. Afterward, centrifugation at 3,000 rpm and 4°C for 8 min was carried out. The supernatant was removed, and

the cell pellet was resuspended with 330 mL of ice-cold RF1 solution before incubation on ice for 30 min. The cells were harvested at 3,000 rpm and 4°C for 8 min. The cell pellet was gently resuspended with 50 mL of ice-cold RF2 solution and then the cells were incubated on ice for 30 min. Each 100 µL aliquot was stored at -80°C.

RF1 solution for 1 L	RF2 solution for 1 L
12 g RbCl 9.9 g $\text{MnCl}_2 \times 4\text{H}_2\text{O}$ 30 mL of 1 M Potassium acetate 15 g $\text{CaCl}_2 \times 2\text{H}_2\text{O}$ 150 g 15% (v/v) glycerol Adjust pH 5.8 with glacial acetate and then filter for sterilization	20 mL of 0.5 M MOPS (pH 6.8) 1.2 g RbCl 11 g $\text{CaCl}_2 \times 2\text{H}_2\text{O}$ 150 g 15% (v/v) glycerol  Adjust pH 5.8 with glacial acetate and then filter for sterilization

### Transformation of *E. coli*

For transformation of *E. coli*, the heat shock method was used (Sambrook and Russell, 2001). 50 µL of the competent cells were mixed with 50-100 ng of plasmids, 10 µL Gibson Assembly® products, or 10 µL of ligation products. The suspension was incubated on ice for 10 min and then treated with a heat shock at 42°C for 45 s. Afterward, the suspension was incubated on ice for 2 min before adding 200 µL of dYT medium. The recovery was ensured by incubation at 37°C for 30-60 min (1,000 rpm, Vibrax®). Transformed cells were plated on antibiotic selection agar plates and incubated overnight at 37°C.

#### 4.2.2.2 Microbiological work with *U. maydis*

##### Protoplasting of *U. maydis*

Competent *U. maydis* cells were prepared as a modified protocol as previously described (Gillissen et al., 1992; Schulz et al., 1990). A 50 mL of CM-glc main culture was grown to an OD<sub>600</sub> of 0.7-0.9 at 28°C. The cells were harvested at 3,000 rpm for 5 min and then resuspended in 25 mL of SCS and spun down at 3,000 rpm for 5 min. Afterward, the cell pellet was gently resuspended in 4 mL of 12.5 mg/mL Glucanex solution (Trichoderma Lysing Enzymes, L1412, Merck) and incubated the suspension at room temperature until ca. 50% of the cell shapes became pinhead like after lysis of the cell wall. The Glucanex solution treatment step was immediately terminated by diluting the suspension with 10 mL of ice-cold SCS and centrifuged at 2,400 rpm, 4°C for 5 min. Continuously twice washing with 10 mL ice-cold SCS and once washing with 10 mL ice-cold STC were carried out. After harvesting the cell pellet again at 2,400 rpm, 4°C for 5 min, the cell pellet was gently resuspended with 1 mL ice-cold STS and stored at -80°C in 100 µL aliquots.

SCS for 1 L	STC for 1 L
<b>Solution 1:</b> 5.9 g tri-Na-citrate*2H <sub>2</sub> O 182.2 g sorbitol in 1 L of ddH <sub>2</sub> O <b>Solution 2:</b> 4.2 g citrate*H <sub>2</sub> O 182.2 g sorbitol in 1 L of ddH <sub>2</sub> O Titrate Solution 2 to Solution 1 to adjust pH 5.8 and then autoclave	500 mL of 1 M sorbitol solution 10 mL of 1 M Tris-HCl, pH 7.5 100 mL of 1 M CaCl <sub>2</sub> solution Add ddH <sub>2</sub> O and then autoclave

### Transformation of *U. maydis* protoplast

100 µL of *U. maydis* protoplast aliquot was thawed on ice for 10 min. Afterward, the protoplast was mixed with ca. 5 µg of linearized plasmids and 1 µL of heparin solution (10 mg/mL). The mixture was incubated on ice for 15 min and then supplemented with 500 µL of STC/PEG solution for another incubation on ice for 15 min. The total transformation mixture was gently plated on a two-layered RegLight-agar plate (Bösch et al., 2016), which contained an appropriate antibiotic in the bottom layer of the agar plate. After 5 days of incubation at 28°C, single colonies were isolated on CM-glc agar plates containing the appropriate antibiotic. Survived cells under the selection pressure were further tested in Southern blot analysis.

STC/PEG for 1 L
600 mL of STC
400 g polyethyleneglycol (PEG, MW 3350)
40 mL of 10% (w/v) SDS
Add ddH <sub>2</sub> O

**Table 4.12 Antibiotics used for transformation of *U. maydis* protoplast**

Antibiotic	Final concentration (µg/mL)
Carboxin	4
Hygromycin B	400
ClonNAT	300

### Recycling of a selection marker gene using the FLP-FRT system

The procedure of the recycling of a selection marker gene is followed by the protocol described in (Khrunyk et al., 2010). To recycle the selection marker gene cassette, which is flanked by FRT sites, from the genomic DNA of desired strains, *U. maydis* protoplasts were transformed with 250-500 ng of pFLPexpC (pUMa1446; see 4.1.4) according to the *U. maydis* transformation method. Importantly, the desired strains should not contain a carboxin resistance gene. The transformation plates were incubated at 28°C for 5-7 days until colonies were grown on a two-layered RegLight-agar plates containing 4 µg/mL of carboxin. Colonies were singled out on carboxin containing agar plates. Afterward, a single colony possessing carboxin resistance was inoculated in 20 mL CM liquid medium supplemented with carboxin and 1% (w/v) arabinose to induce a gene encoding Flp recombinase from the transformed plasmid. When the cell growth reached an OD<sub>600</sub> 1.0, the

culture was diluted to 1:1,000 and 1:10,000 in ddH<sub>2</sub>O for spreading 20  $\mu$ L and 100  $\mu$ L, respectively, on CM agar plates to obtain single colonies at 28°C for 2 days. Patching single colonies on CM-glc agar plates and CM agar plates supplemented with 2  $\mu$ g/mL of carboxin was carried out and then incubated at 28°C for 1-2 days. Only colonies grown on CM-glc agar plates were selected for liquid culture in 3 mL CM-glc medium. The loss of the transformed plasmid by the absence of carboxin in the medium was confirmed by growing the cells on CM-glc agar plates supplemented with 2  $\mu$ g/mL of carboxin. Finally, the confirmation of the removal of the selection marker gene by size comparison of the PCR products with genomic DNAs of the progenitor strain and the selection marker gene recycled strain.

### Standard cultivation conditions for *U. maydis*

*U. maydis* strains were incubated in complete medium supplemented with 1% (w/v) glucose (CM-glc) at 28°C shaking in baffled flasks with 200 rpm. To induce the filamentous form of laboratory strain AB33, the medium was exchanged from CM-glc to nitrate minimal medium supplemented with 1% glucose (NM-glc).

### Cultivation conditions for lycopene accumulation and sesquiterpenoid production in *U. maydis*

A pre-culture for 20 h was diluted in fresh CM-glc for a starting OD<sub>600</sub> of 0.25 in 500 mL volume non-baffled flask containing a total of 10 mL culture and incubated at 28°C, 200 rpm, and in white light as  $\beta$ -carotene was highly accumulated in this condition described in (Estrada et al., 2009). To trap the secreted sesquiterpenoids, 500  $\mu$ L of *n*-dodecane (D0968, TCI Deutschland GmbH, Eschborn, Germany) were added to the shaking culture.

### Determination of cell density of *U. maydis* cultures

The cell density of liquid cultures was photometrically determined using a Novaspec II photometer (Pharmacia Biotech). The OD<sub>600</sub> (optical density at  $\lambda$  = 600 nm) of the cultures was measured. If necessary, the cultures were diluted in the respective culture medium. An OD<sub>600</sub> of 1 resembles  $1.5 \times 10^7$  cells/mL for *U. maydis*.

### Fluorimetric measurements

A pre-culture was diluted to an OD<sub>600</sub> 0.5 in CM-glc for all *U. maydis* strains, and 1 mL of each culture was harvested at 13,000 rpm for 5 min at room temperature. The cell pellets were washed twice in double-distilled water and then pelleted again at 13,000 rpm for 5 min. Afterward, each cell pellet was resuspended in 1 mL of double-distilled water. 200  $\mu$ L of each sample was transferred into black 96-well plates (Greiner Bio-One, Kremsmünster, Austria) for measurements in an Infinite M200 plate reader (Tecan Group Ltd., Männedorf, Switzerland). As a blank, 200  $\mu$ L of double-distilled water was used. Within the microplate reader, measurements of OD<sub>600</sub> and fluorescence intensity were



performed. In the case of Gfp, an excitation wavelength of 483 nm and an emission wavelength of 535 nm were used. At least three independent biological experiments were performed with three technical replicates per strain.

### Fluorescence microscopy

To visualize the nucleus, cells were first fixed with 1% formaldehyde for 30 min on a rotary wheel at room temperature and then washed twice in PBS. Afterward, the DNA was stained with Hoechst 33342 dye (H3570, Thermo Fisher Scientific, Waltham, MA, USA). 10 mg/mL stock solution was diluted to 1:2000 in PBS, and the fixed cells were stained for 10 min on a rotary wheel at room temperature. Excess dye was washed three times with PBS. Microscopy was carried out as previously described (Baumann et al., 2016; Jankowski et al., 2019) using two systems: (i) a wide-field microscope set-up from Visitron Systems (Puchheim, Germany), Axio Imager M1 equipped with a Spot Pursuit CCD camera (Diagnostic Instruments, Sterling Heights, MI, USA) and the objective lens Plan Neofluar (40 ×, NA 1.3; 63 ×, NA 1.25; Carl Zeiss, Jena, Germany). The excitation of fluorescently labeled proteins was carried out using an HXP metal halide lamp (LEJ, Jena, Germany) in combination with a filter set for green fluorescent protein (ET470/40BP, ET495LP, and ET525/50BP) and Hoechst 33342 dye (HC387/11BP, BS409LP, and HC 447/ 60BP; AHF Analysentechnik, Tübingen, Germany). The microscopic system was controlled by MetaMorph software (Molecular Devices, version 7, Sunnyvale, CA, USA). The program was also used for image processing, including the adjustment of brightness and contrast. (ii) To record fluorescence signals localized in subcellular compartments with higher sensitivity, laser-based epifluorescence microscopy was performed on a Zeiss Axio Observer.Z1 equipped with CoolSNAP HQ2 CCD (Photometrics, Tuscon, AZ, USA) and ORCA-Flash4.0 V2 + CMOS (Hamamatsu Photonics Deutschland GmbH, Geldern, Germany) cameras. The microscopy set-up was the same as described above (Jankowski et al., 2019). For excitation, a VS-LMS4 Laser-Merge-System (Visitron Systems) combines solid-state lasers for excitation of Gfp (488 nm at 50 or 100 mW) was used. Videos were recorded with an exposure time of 150 ms, and 150 frames were taken. All videos and images were processed and analyzed using MetaMorph (Version 7.7.0.0, Molecular Devices). Kymographs were generated using a built-in plugin.

#### 4.2.2.3 Microbiological work with higher basidiomycete fungi

##### Fungal material collection and cultivation

Fruiting bodies of 35 different saprotrophic basidiomycete mushroom species were collected to rear in axenic cultures (Appendix Table 6.2), the generation of which by isolation from the fruiting bodies is exemplarily described with the fungus that served for production of basidiomycete ethyl acetate crude extract BE05, *Fistulina hepatica*. Basidiomes of *F. hepatica* were collected on August 18th 2013, from an oak tree stump in a deciduous forest on chalky soil dominated by *Fagus sylvatica* and *Quercus* spp. This forest is situated to the East of the German city of Jena about 300 m to the

Northeast from the Fürstenbrunnen, the spring of the creek Pennickenbach and about 1 km to the Southwest from the stony monument “Steinkreuz Ziegenhain” (50° 54′ 51.71″ N, 11° 38′ 23.36″ E). Dikaryotic mycelium of *F. hepatica* was isolated by sterile explanting of hyphal tufts onto potato dextrose agar (PDA, 413758.1210, AppliChem, Darmstadt, Germany) complemented with 100 µg/mL ampicillin and 50 µg/mL chloramphenicol from freshly harvested *F. hepatica* fruiting bodies which were torn open sterily. Primary cultures were grown at 25°C in the dark until hyphal outgrowth from the fruiting body explants (after about a week). Clean-up subcultures were made by transferring hyphal tufts, which were taken from the edge of uncontaminated areas where hyphal outgrowth had occurred and grown for one week under the same conditions. After one additional round of subcultivation from such a clean-up subculture showing no sign of contamination, the culture characteristics of the pure culture of *F. hepatica* were assessed under the microscope. Mycelial cultures of *F. hepatica* were maintained on PDA and preserved as mineral oil-covered stocks at 4°C in the dark at the Department of Mycology (Goethe University Frankfurt, Frankfurt am Main, Germany). To prepare those, *F. hepatica* mycelium was grown for two weeks at 25°C in the dark on Corn meal agar (CMA, 42347-500G-F, Merck, Munich, Germany) glass vial slants and then overlaid by sterile mineral oil (J217-500ML, VWR, Radnor, PA, USA) which had before been allowed to clear back from turbidity after autoclaving for one week.

PDA for 1 L	CMA for 1 L
39 g PDA, 413758.1210, AppliChem Add ddH <sub>2</sub> O and then autoclave	17 g CMA, 42347-500G-F, Merck Add ddH <sub>2</sub> O and then autoclave

### Morphological identification via microscopy

To confirm the morphological identification, microscopy of the mycelium culture on PDA at 25°C for 4 weeks was carried out as described before (Baumann et al., 2016, Jankowski et al., 2019) using a wide-field microscope set-up from Visitron Systems (Puchheim, Germany), Axio Imager M1 equipped with a Spot Pursuit CCD camera (Diagnostic Instruments, Sterling Heights, MI, USA) and the objective lens Plan Neofluar (40 ×, NA 1.3; 63 ×, NA 1.25; Carl Zeiss, Jena, Germany). The microscopic system was controlled by MetaMorph software (Molecular Devices, version 7, Sunnyvale, CA, USA). The program was also used for image processing, including the adjustment of brightness and contrast.

### Antifungal and antibacterial assays

The antifungal and antibacterial assays were performed using the agar diffusion (Kirby-Bauer) method applying a protocol described previously (Harwoko et al., 2019). *Ustilago maydis* AB33 (Brachmann et al., 2001) and *Saccharomyces cerevisiae* ESM356-1 (Pereira et al., 2001) were pre-cultured in CM medium supplemented with 10 g/L glucose (Holliday 1974; Banuett and Herskowitz 1989) and YPD, respectively. Cultivation of fungi was performed at 28°C shaking in baffled flasks with 200 rpm. The Gram-positive bacterium *Corynebacterium glutamicum* ATCC13032

## Materials and Methods

(Abe et al., 1967) and *Escherichia coli* K-12 derivate Top10 (Life Technologies, Carlsbad, CA, USA) were pre-cultured in LB medium by shaking in baffled flasks with 200 rpm at 28°C and 37°C, respectively. 500 µL of diluted overnight cultures to an OD<sub>600</sub> of 0.5 was then inoculated on LB agar plates. Sterile 5 mm diameter Whatman filter paper disks (GE Healthcare Life Sciences, Munich, Germany) were placed on the agar plates. For the antifungal assay, each dried fungal extract, a subfraction of the dried fungal extract, or pure feldin compound (100 µg) was dissolved in DMSO to impregnate the disks. In the case of the antibacterial assay, different amounts (100 µg, 200 µg, and 500 µg) of dried basidiomycete ethyl acetate crude extract BE05 were dissolved in DMSO to impregnate the disks. 200 µg nourseothricin (clonNAT, AB-102L, Jena Bioscience, Jena, Germany) was used as the positive control, while DMSO was used as negative control. To observe antifungal activity, inoculated agar plates were incubated at 28°C for 48 h. In the case of the antibacterial activity assay, the inoculated agar plates were incubated at 28°C (*C. glutamicum*) or 37°C (*E. coli*) for 48 h. Afterward, the growth inhibition zone surrounding the disk was recorded photographically. Three independent biological experiments ( $n=3$ ) were carried out.

YPD for 1 L
20 g peptone 10 g yeast extract 24 g agar for YPD agar Add 950 mL of ddH <sub>2</sub> O and then autoclave After cooling, add 50 mL sterile 40% (w/v) glucose

LB for 1 L
10 g tryptone 5 g yeast extract 10 g NaCl 20 g agar for LB agar Add ddH <sub>2</sub> O and then autoclave

### 4.2.3 Biochemical methods

#### Protein extraction from *U. maydis*

A culture of 20 mL growing to an OD<sub>600</sub> of ca. 2 was harvested by centrifugation (13,000 rpm for 10 min at room temperature). Cell pellets were frozen in liquid nitrogen and then disrupted in a pebble mill (MM400, Retsch GmbH, Hann, Germany) using a frequency of 30 Hz three times for 1 min with two steal beads. Afterward, urea buffer (8 M urea, 50 mM Tris-HCl, pH 8) supplemented with protease inhibitors (1 tablet of complete protease inhibitor per 20 mL; Roche, Mannheim, 0.1 M PMSF, and 0.5 M benzamidine) was used for resuspension at 4°C. Cell debris was pelleted by centrifugation at 13,000 rpm for 15 min at 4°C.

Lysis buffer for 20 mL
9.6 g urea 1 tablet of cOMplete EDTA-free protease inhibitor (Roche) 0.1 M PMSF 0.5 M benzamidine 50 mM Tris-HCl, pH 8 Add ddH <sub>2</sub> O

### Determination of protein concentration by Bradford assay

Protein concentrations of *U. maydis* cell extracts were determined with the Bradford method (Bradford, 1976). A bovine serum albumin (BSA) standard curve was made with different concentrations ranging from 0 µg/mL to 200 µg/mL in ddH<sub>2</sub>O. For the preparation of samples, 10 µL of the supernatant of *U. maydis* cell extracts was diluted in ddH<sub>2</sub>O with 1:5 diluted Bradford solution (Protein Assay Dye, BioRad, Hercules, CA, USA). The absorbance was measured at 595 nm in an Infinite M200 plate reader (Tecan Group Ltd., Männedorf, Switzerland).

### SDS-Polyacrylamide gel electrophoresis (SDS-PAGE)

To separate proteins according to their molecular weight (MW), SDS-PAGE was used as described (Laemmli, 1970). 10% SDS gels were prepared with the Mini-Protean series (BioRad, Hercules, CA, USA). For denaturation of protein samples, the samples were diluted with 3× Laemmli buffer and incubated at 95°C for 10 min. Afterward, the samples were shortly spun down. The samples were loaded in SDS gels to run at 50 mA per gel.

3× Laemmli buffer for 1 L
300 mL Tris-HCl (0.5 M stock, pH 6.8)
60 g SDS
300 mg glycerol
150 mL β-mercapto-ethanol
300 mg bromophenol blue
Add ddH <sub>2</sub> O

1× SDS running buffer
25 mM Tris, pH 8.4
192 mM glycine
0.1% (w/v) SDS
Add ddH <sub>2</sub> O

Separation gel (for 2 gels)
6.75 mL 1M Tris-HCl (pH 8.8)
5.8 mL ddH <sub>2</sub> O
6 mL 30% (w/w) acrylamide/bis-acrylamide
90 µL 20% (w/v) SDS
450 µL 50% (v/v) glycerol
90 µL 10% (w/v) APS
18 µL TEMED

Stacking gel (for 2 gels)
1.2 mL 0.5 M Tris-HCl (pH 6.8)
0.8 mL 30% (w/w) acrylamide/bis-acrylamide
2.8 mL ddH <sub>2</sub> O
24 µL 20% (w/v) SDS
24 µL 10% (w/v) APS
4.8 µL TEMED

### Western blot analysis

After SDS-PAGE proteins were transferred to nitrocellulose membranes (Amersham Protran 0.45 NC Western blotting membrane, GE Healthcare Life Sciences, Munich, Germany) using a semi-dry Western blot chamber (846-015-200, Biometra, Göttingen, Germany). Two layers of Whatman® filter papers (Whatmann, Maidstone, UK) were soaked in Anode buffer 1 and placed on the anode of the chamber. Another one layer of Whatman® filter paper soaked in Anode buffer 2 was placed on it. The nitrocellulose membrane was laid on the Whatman® filter paper. The stacking gel of the SDS gel was placed on the membrane and then bubbles were removed. Finally, 3 layers of Whatman® filter paper soaked in Cathode buffer covered the SDS gel. The transfer was performed at 45 mA per membrane for 90 min. The membrane was incubated in 5% (w/v) skimmed milk powder blocking solution overnight at room temperature. Afterward, Epitope-tagged proteins were detected using

different primary antibodies produced in mouse,  $\alpha$ -Gfp (monoclonal, Roche, Freiburg, Germany; 1:1,000 dilution),  $\alpha$ -HA (monoclonal, Roche; 1:4,000 dilution),  $\alpha$ -Myc (monoclonal, Merck; 1:5,000 dilution) and  $\alpha$ -actin (monoclonal antibody raised against actin from chicken gizzard, MP Biomedicals, Eschwege, Germany; 1:500 dilution). The primary detection was carried out at 4°C overnight. After washing three times in TBST for each 15 min and 1 time in TBS for 5 min, secondary  $\alpha$ -mouse IgG-HRP conjugate (Promega, Mannheim, Germany; 1:4,000 dilution) was used for detection for 1 h at room temperature. The developing step was performed with Amersham ECL prime detection reagent and a LAS4000 chemiluminescence imager (both GE Healthcare Life Sciences).

Anode buffer 1 for 1L	Anode buffer 2 for 1L
300 mM Tris-HCl, pH 10.4 15% (v/v) methanol Add ddH <sub>2</sub> O	30 mM Tris-HCl, pH 10.4 15% (v/v) methanol Add ddH <sub>2</sub> O

Cathode buffer for 1L	TBS or TBST
25 mM Tris-HCl, pH 9.4 15% (v/v) methanol 40 mM 6-aminohexanoic acid Add ddH <sub>2</sub> O	20 mM Tris-HCl 136 mM NaCl Added ddH <sub>2</sub> O and adjusted pH 7.6 0.05% (v/v) Tween-20 is added for TBST

### Lycopene extraction and quantification

Lycopene extraction was adopted and modified as published (Ukibe et al., 2008). Cell pellets of a 10 mL culture after 48 h of incubation were washed in double-distilled water before disruption in 100% (v/v) acetone together with glass beads by shaking twice at a frequency of 30 Hz for 15 min in a pebble mill (MM400, Retsch GmbH, Haan, Germany). Afterward, each suspension was heated for 10 min at 65°C to extract lycopene. Then, the color of the cell debris turned to white, and the acetone phase became yellowish as extracted lycopene was dissolved in the acetone phase. The acetone was dried entirely overnight at room temperature, and samples were re-dissolved in 1 mL 100% (v/v) *n*-hexane. To remove cell debris, centrifugation at 13,000 rpm for 10 min was performed twice. The lycopene extraction process was carried out at low light conditions as the lycopene is sensitive to light, causing the *cis-trans* photoisomerization (Butnariu, 2016). A commercial reference of lycopene was purchased (SMB00706, Merck, Darmstadt, Germany) to compare absorbance wavelengths with lycopene extracts. Absorbance scanning was carried out in a UV-Vis spectrophotometer (Genesys 10S UV-Vis, Thermo Fisher Scientific, Waltham, MA, USA) recording from 350 nm to 700 nm. In addition, the determination of lycopene in the extract was performed according to lycopene specific absorption wavelengths, 444, 471, and 503 nm. For the quantification of lycopene, the maximum absorption ( $\lambda_{\max}$ ) at 503 nm was determined, and titer was assessed using molecular extinction coefficient 172,000 M<sup>-1</sup>cm<sup>-1</sup> of lycopene in *n*-hexane (Fish et al., 2002).



### Analysis of sesquiterpenoids using GC-MS

For the analysis of (+)-valencene and  $\alpha$ -cuprenene, 10 mL of cells grown to an OD<sub>600</sub> of approximately 6 were harvested after 48 h. To trap the secreted sesquiterpenoids, 500  $\mu$ L of *n*-dodecane (D0968, TCI Deutschland GmbH, Eschborn, Germany) were added to the shaking culture. To ensure phase separation, the cell suspension was centrifuged twice at 13,000 rpm for 10 min. The *n*-dodecane phase-containing sesquiterpenoids was analyzed using a GC/MS-QP2010 (Shimadzu, Kyoto, Japan) equipped with an FS-Supreme-5 column (30 m  $\times$  0.25 mm  $\times$  0.25  $\mu$ m; CS-Chromatographie Service GmbH, Langerwehe, Germany). The GC-MS conditions were adopted from a previous study (Schulz et al., 2015). Temperatures of the injector and interface were set at 250°C and 285°C, respectively. The carrier gas was helium, and its velocity was set to 30 cm sec<sup>-1</sup>. 1  $\mu$ L of the sample was injected with a split ratio of 10. The column temperature was sequentially changed and maintained at 130°C for 3 min, ramped to 260°C at a rate of 10°C min<sup>-1</sup>, held at 260°C for 1 min, ramped to 300°C at a rate of 40°C min<sup>-1</sup> and held at 300°C for 1 min. In the case of (+)-valencene, a purchased reference compound (75056, Merck) was diluted as 50  $\mu$ M and 200  $\mu$ M in *n*-dodecane samples of the negative control. The retention time and fragmentation pattern of the mass spectrum obtained with the *U. maydis* sample were compared with the reference compounds. In addition, the fragmentation patterns of (+)-valencene and  $\alpha$ -cuprenene were compared with the previously reported data (Agger et al., 2009; Troost et al., 2019).

### Quantification of sesquiterpenoid production with GC-FID

To determine product titers of (+)-valencene and  $\alpha$ -cuprenene, *n*-dodecane samples were subjected to the Agilent 6890N gas chromatograph equipped with a (5%-phenyl)-methylpolysiloxane HP-5 column (length, 30 m; inside diameter, 0.32 mm; film thickness, 0.25  $\mu$ m; Agilent Technologies, Ratingen, Germany) and a flame ionization detector (FID). Both heterologously produced sesquiterpenoid samples and standard calibration samples were diluted in ethyl acetate (Rodriguez et al., 2014). Temperatures of the injector and FID were set to 240°C and 250°C, respectively. Each sample had a volume of 1  $\mu$ L and was injected splitless with helium as a carrier gas. The column temperature was sequentially changed: starting at 100°C for 5 min, ramped at 10°C min<sup>-1</sup> to 180°C and then at 20°C min<sup>-1</sup> to 300°C. The signals of heterologously produced (+)-valencene, which were absent in the negative control samples, were confirmed by comparison of retention time to a commercial reference of (+)-valencene purchased (75056, Merck). To create a (+)-valencene standard curve, different concentrations of the commercial (+)-valencene were prepared in ethyl acetate ranging from 0  $\mu$ M to 300  $\mu$ M. To estimate the titer of  $\alpha$ -cuprenene, the chemically similar reference compound  $\beta$ -caryophyllene was used (22075, Merck) because  $\alpha$ -cuprenene is not commercially available to correlate putative  $\alpha$ -cuprenene signals, which were absent in the negative control samples, to compound amounts. In the case of  $\beta$ -caryophyllene standard curve, concentrations ranging from 0  $\mu$ M to 1000  $\mu$ M of the commercial  $\beta$ -caryophyllene were prepared in

ethyl acetate. As an accurate concentration determination, the purities of the commercial (+)-valencene and  $\beta$ -caryophyllene were considered to calculate the standard curve samples.

### Secondary metabolite extraction from higher basidiomycete fungi

Four weeks old mycelial cultures on PDA of each strain of the 35 basidiomycete species employed in the present study (Appendix Table 6.2) were extracted in their entirety. For bioactive compound isolation, this step was repeated for *F. hepatica* on a large scale. The plates were sliced and soaked in pure ethyl acetate shaking overnight at 150 rpm. The extraction procedure was performed twice, and the ethyl acetate extract was filtrated through filter paper (Munktell & Filtrak GmbH, Bärenstein, Germany). Ethyl acetate was then evaporated at 40°C and 180 mbar using a rotary evaporator equipped with a cooling system working at 4°C. Further removal of residual organic solvent in vacuum yielded basidiomycete ethyl acetate crude extract of each strain from Appendix Table 6.2. In the case of *F. hepatica*, about 3 g of brown ethyl acetate crude extract was obtained.

### Liquid chromatography/mass spectrometry for bioactivity-guided isolation

Fractionation and subfractionation of the crude extract and isolation of pure substances were carried out on preparative and semipreparative Agilent LC-MS 1260 Infinity II coupled to a DAD and a single quadrupole detector. The crude extract was resuspended in methanol and then subjected to the preparative HPLC with a C18 column (30 × 250 mm, 10  $\mu$ m) using an acetonitrile/water gradient (0.1% formic acid) 0-18 min, 5-100%, 40 mL min<sup>-1</sup> to afford eight fractions. Fraction 8.2 (29.5 mg) containing the bioactive compound was subjected to semipreparative HPLC with a phenyl column (9.8 × 250 mm, 5  $\mu$ m) using an acetonitrile/water gradient (0.1% formic acid) 0-10 min, 45-60%, 3 mL min<sup>-1</sup> to afford six subfractions. Subfraction 8.2.6 (5.8 mg) mainly containing the target compound was further purified by the semipreparative HPLC with a C18 column (9.8 × 250 mm, 5  $\mu$ m) using 45% acetonitrile/water isocratic elution (0.1% formic acid), 3 mL min<sup>-1</sup> to afford feldin (2.0 mg), from which, beforehand, a small subsample (0.3 mg) had been sidelined and dissolved in DMSO for an immediate bioactivity test against *S. cerevisiae* before NMR. The rest of the 2.0 mg feldin retrieved after NMR was used for another round of bioactivity-testing against *S. cerevisiae*.

### NMR spectroscopy for structure elucidation of feldin

1D and 2D NMR spectra were recorded on a 500 MHz NMR spectrometer for <sup>1</sup>H and 125 MHz for <sup>13</sup>C. Chemical shifts ( $\delta$ ) were given on parts per million (ppm) scale and referenced to the solvent signals. Coupling constants were expressed in Hertz (Hz).

#### 4.2.4 Bioinformatics

The KEGG database (Kyoto Encyclopedia of Genes and Genomes, Kanehisa and Goto, 2000; <https://www.genome.jp/kegg/>) was used to identify candidates of the mevalonate pathway enzymes in *U. maydis* (Figure 2.1; Table 2.1). For verification, amino acid sequences were compared to known

enzymes from well-studied eukaryotes like *S. cerevisiae*, *H. sapiens*, and *A. thaliana* using BLASTP (Altschul et al., 1990; <https://blast.ncbi.nlm.nih.gov/blast/>). Clustal Omega and GeneDoc 2.6 were used for multiple amino acid sequence alignments and graphical representation (Figure 2.2-9; Larkin et al., 2007; Nicholas et al., 1997). Domain structure was analyzed with SMART (Simple Modular Architecture Research Tool; analysis performed in April 2020; Schultz et al., 1998; Letunic and Bork, 2018).

### 4.2.5 Computer programs

#### Nucleic and amino acid analysis

Clone Manager 9 (Sci Ed Central Software, Cary, NC, USA)

BLASTP (<https://blast.ncbi.nlm.nih.gov/Blast.cgi>)

Clustal Omega (<http://www.clustal.org/omega/>)

GeneDoc 2.6 (<http://www.psc.edu/biomed/genedoc>)

#### Literature research and sequence information

NCBI - National Centre for Biotechnology Information (<http://www.ncbi.nlm.nih.gov/>)

KEGG database - Kyoto Encyclopedia of Genes and Genomes (<https://www.genome.jp/kegg/>)

SMART - Simple Modular Architecture Research Tool (<http://smart.embl-heidelberg.de/>)

Dicodon usage optimizer (<http://dicodon-optimization.appspot.com/>)

#### Operation of special devices and data analysis

i-control™ Microplate Reader Software (Tecan Trading AG, Männedorf, Switzerland)

ImageQuant LAS4000 Control Software (GE Healthcare, Chicago, IL, USA)

MetaMorph software (Molecular Devices, San Jose, CA, USA)

#### Data analysis, writing, and graphics

MetaMorph (Version 7.7.0.0, Molecular Devices, San Jose, CA, USA)

Microsoft Office 2016 (Microsoft Corporation, Redmond, WA, USA)

Prism 5 (Version 5.04, GraphPad Software San Diego, CA, USA)

Canvas 12 (ACD Systems of America, WA, USA)

## 5 References

- Abe, S., Takayama, K., Kinoshita, S., 1967. Taxonomical studies on glutamic acid producing bacteria. The Journal of General and Applied Microbiology 13, 279-301.
- Agger, S., Lopez-Gallego, F., Schmidt-Dannert, C., 2009. Diversity of sesquiterpene synthases in the basidiomycete *Coprinus cinereus*. Molecular Microbiology 72, 1181-1195.
- Ahmed, M., Barley, G. C., Hearn, M. T. W., Jones, E. R. H., Thaller, V., Yates, J. A., 1974. Natural acetylenes. Part XLIII. Polyacetylenes from cultures of the fungus *Fistulina pallida* (berk. and rev.) Journal of the Chemical Society, Perkin Transactions, 1981-1987.
- Ajikumar, P. K., Xiao, W. H., Tyo, K. E., Wang, Y., Simeon, F., Leonard, E., Mucha, O., Phon, T. H., Pfeifer, B., Stephanopoulos, G., 2010. Isoprenoid pathway optimization for taxol precursor overproduction in *Escherichia coli*. Science (New York, N.Y.) 330, 70-74.
- Alberti, F., Khairudin, K., Venegas, E., Davies, J.A., Hayes, P.M., Willis, C.L., Bailey, A.M., Foster, G.D., 2017. Heterologous expression reveals the biosynthesis of the antibiotic pleuromutilin and generates bioactive semi-synthetic derivatives. Nature Communications 8, 1831.
- Altschul, S. F., Gish, W., Miller, W., Myers, E. W., Lipman, D. J., 1990. Basic local alignment search tool. Journal of Molecular Biology 215, 403-410.
- Arnone, A., Cardillo, R., Nasini, G., 1986. Structures of melleolides B-D, three antibacterial sesquiterpenoids from *Armillaria mellea*. Phytochemistry 25, 471-474.
- Asadollahi, M. A., Maury, J., Schalk, M., Clark, A., Nielsen, J., 2010. Enhancement of farnesyl diphosphate pool as direct precursor of sesquiterpenes through metabolic engineering of the mevalonate pathway in *Saccharomyces cerevisiae*. Biotechnology and Bioengineering 106, 86-96.
- Avalos, J., Limón, M. C., 2015. Biological roles of fungal carotenoids. Current Genetics 61, 309-324.
- Avalos, J., Pardo-Medina, J., Parra-Rivero, O., Ruger-Herreros, M., Rodríguez-Ortiz, R., Hornero-Méndez, D., Limón, M. C., 2017. Carotenoid biosynthesis in *Fusarium*. Journal of Fungi (Basel, Switzerland) 3.
- Aylett, C. H., Ban, N., 2017. Eukaryotic aspects of translation initiation brought into focus. Philosophical transactions of the Royal Society of London. Series B, Biological Sciences 372.
- Ayté, J., Gil-Gómez, G., Haro, D., Marrero, P. F., Hegardt, F. G., 1990. Rat mitochondrial and cytosolic 3-hydroxy-3-methylglutaryl-CoA synthases are encoded by two different genes. Proc. Natl. Acad. Sci. U. S. A. 87, 3874-3878.
- Baldovini, N., Delasalle, C., Joulain, D., 2010. Phytochemistry of the heartwood from fragrant *Santalum* species: a review. Flavour Fragr. J. 26, 7-26.
- Banuett, F., Herskowitz, I., 1989. Different alleles of *Ustilago maydis* are necessary for maintenance of filamentous growth but not for meiosis. Proc. Natl. Acad. Sci. U. S. A. 86, 5878-5882.
- Bäuerle, J., Anke, T., Jente, R., Bosold, F., 1982. Antibiotics from Basidiomycetes. XVI. Antimicrobial and cytotoxic polyines from *Mycena viridimarginata* Karst. Archives of Microbiology 132, 194-196.
- Baumann, S., Zander, S., Weidtkamp-Peters, S., Feldbrügge, M., 2016. Live cell imaging of septin dynamics in *Ustilago maydis*. Methods in Cell Biology 136, 143-159.
- Becht, P., Vollmeister, E., Feldbrügge, M., 2005. Role for RNA-binding proteins implicated in pathogenic development of *Ustilago maydis*. Eukaryotic Cell 4, 121-133.

- Becker, J., Hosseinpour Tehrani, H., Gauert, M., Mampel, J., Blank, L. M., Wierckx, N., 2020. An *Ustilago maydis* chassis for itaconic acid production without by-products. *Microbial Biotechnology* 13, 350-362.
- Beekwilder, J., van Houwelingen, A., Cankar, K., van Dijk, A. D., de Jong, R. M., Stoop, G., Bouwmeester, H., Achkar, J., Sonke, T., Bosch, D., 2014. Valencene synthase from the heartwood of Nootka cypress (*Callitropsis nootkatensis*) for biotechnological production of valencene. *Plant Biotechnol. J* 12, 174-182.
- Benencia, F., Courrèges, M. C., 1999. Antiviral activity of sandalwood oil against herpes simplex viruses-1 and -2. *Phytomedicine* 6, 119-123.
- Bera, R., Dey, A., Chakrabarty, D., 2015. Synthesis, Characterization, and drug release study of acrylamide-co-itaconic acid based smart hydrogel. *Polym Eng Sci* 55, 113-122.
- Berendsen, R. L., Baars, J. J., Kalkhove, S. I., Lugones, L. G., Wösten, H. A., Bakker, P. A., 2010. *Lecanicillium fungicola*: causal agent of dry bubble disease in white-button mushroom. *Molecular Plant Pathology* 11, 585-595.
- Berthelot, K., Estevez, Y., Deffieux, A., Peruch, F., 2012. Isopentenyl diphosphate isomerase: A checkpoint to isoprenoid biosynthesis. *Biochimie* 94, 1621-1634.
- Betancourt, T., Pardo, J., Soo, K., Peppas, N. A., 2010. Characterization of pH-responsive hydrogels of poly(itaconic acid-g-ethylene glycol) prepared by UV-initiated free radical polymerization as biomaterials for oral delivery of bioactive agents. *Journal of Biomedical Materials Research. Part A* 93, 175-188.
- Béthune, J., Jansen, R. P., Feldbrügge, M., Zarnack, K., 2019. Membrane-associated RNA-binding proteins orchestrate organelle-coupled translation. *Trends Cell Biol* 29, 178-188.
- Blacklock, B. J., Scheffler, B. E., Shepard, M. R., Jayasuriya, N., Minto, R. E., 2010. Functional diversity in fungal fatty acid synthesis: the first acetylenase from the Pacific golden chanterelle, *Cantharellus formosus*. *The Journal of Biological Chemistry* 285, 28442-28449.
- Blair, J. M., Webber, M. A., Baylay, A. J., Ogbolu, D. O., Piddock, L. J., 2015. Molecular mechanisms of antibiotic resistance. *Nature Reviews. Microbiology* 13, 42-51.
- Boh, B., Berovic, M., Zhang, J., Zhi-Bin, L., 2007. *Ganoderma lucidum* and its pharmaceutically active compounds. *Biotechnology Annual Review* 13, 265-301.
- Bohlmann, F., Knoll, K.-H., 1978. New acetylenic compounds from *Emilia* species. *Phytochemistry* 17, 557-558.
- Bölker, M., 2001. *Ustilago maydis*-a valuable model system for the study of fungal dimorphism and virulence. *Microbiology* 147, 1395-1401.
- Bölker, M., Basse, C. W., Schirawski, J., 2008. *Ustilago maydis* secondary metabolism-from genomics to biochemistry. *Fungal Genetics and Biology* 45 Suppl 1, S88-93.
- Bölker, M., Urban, M., Kahmann, R., 1992. The *a* mating type locus of *U. maydis* specifies cell signaling components. *Cell* 68, 441-450.
- Bollinger, P., 1965. Ueber die Konstitution und Konfiguration der Lagopodine A, B und C. Zürich: ETH Zürich.
- Bösch, K., Frantzeskakis, L., Vraneš, M., Kämper, J., Schipper, K., Göhre, V., 2016. Genetic manipulation of the plant pathogen *Ustilago maydis* to study fungal biology and plant microbe interactions. *Journal of Visualized Experiments* 115, 54522.
- Boucher, Y., Kamekura, M., Doolittle, W. F., 2004. Origins and evolution of isoprenoid lipid biosynthesis in archaea. *Molecular Microbiology* 52, 515-527.



- Brachmann, A., 2001. Die frühe Infektionsphase von *Ustilago maydis*: Genregulation durch das bW/bE- Heterodimer. PhD Dissertation (LMU, München, Germany).
- Brachmann, A., König, J., Julius, C., Feldbrügge, M., 2004. A reverse genetic approach for generating gene replacement mutants in *Ustilago maydis*. *Molecular Genetics and Genomics* 272, 216-226.
- Brachmann, A., Weinzierl, G., Kämper, J., Kahmann, R., 2001. Identification of genes in the bW/bE regulatory cascade in *Ustilago maydis*. *Molecular Genetics and Genomics* 272, 216-226.
- Bradford, M. M., 1976. A rapid and sensitive method for the quantitation of microgram quantities of protein utilizing the principle of protein-dye binding. *Analytical Biochemistry* 72, 248-254.
- Britton, G., 1995. Structure and properties of carotenoids in relation to function. *FASEB Journal* 9, 1551-1558.
- Brown, G. D., Denning, D. W., Gow, N. A., Levitz, S. M., Netea, M. G., White, T. C., 2012. Hidden killers: human fungal infections. *Science Translational Medicine* 4, 165rv113.
- Brych, A., Mascarenhas, J., Jaeger, E., Charkiewicz, E., Pokorny, R., Bölker, M., Doehlemann, G., Batschauer, A., 2016. White collar 1-induced photolyase expression contributes to UV-tolerance of *Ustilago maydis*. *Microbiologyopen* 5, 224-243.
- Bu'Lock, J. D., Darbyshire, J., 1976. Lagopodin metabo-lites and artefacts in cultures of *Coprinus*. *Phytochemistry* 15, 2004.
- Bu, X., Sun, L., Shang, F., Yan, G., 2017. Comparative metabolomics profiling of engineered *Saccharomyces cerevisiae* lead to a strategy that improving  $\beta$ -carotene production by acetate supplementation. *PLoS One* 12, e0188385.
- Burdock, G. A., Carabin, I. G., 2008. Safety assessment of sandalwood oil (*Santalum album* L.). *Food and Chemical Toxicology* 46, 421-432.
- Busta, L., Yim, W. C., LaBrant, E. W., Wang, P., Grimes, L., Malyszka, K., Cushman, J. C., Santos, P., Kosma, D. K., Cahoon, E. B., 2018. Identification of genes encoding enzymes catalyzing the early steps of carrot polyacetylene biosynthesis. *Plant Physiology* 178, 1507-1521.
- Butnariu, M., 2016. Methods of analysis (extraction, separation, identification and quantification) of carotenoids from natural products. *J. Ecosys. Ecograph.* 6, 193.
- Campos Ziegenbein, F., Hanssen, H. P., König, W. A., 2006. Secondary metabolites from *Ganoderma lucidum* and *Spongiporus leucomallellus*. *Phytochemistry* 67, 202-211.
- Cankar, K., van Houwelingen, A., Goedbloed, M., Renirie, R., de Jong, R. M., Bouwmeester, H., Bosch, D., Sonke, T., Beekwilder, J., 2014. Valencene oxidase CYP706M1 from Alaska cedar (*Callitropsis nootkatensis*). *FEBS Letters* 588, 1001-1007.
- Cano-Canchola, C., Acevedo, L., Ponce-Noyola, P., Flores-Martínez, A., Flores-Carreón, A., Leal-Morales, C. A., 2000. Induction of lytic enzymes by the interaction of *Ustilago maydis* with *Zea mays* tissues. *Fungal Genetics and Biology* 29, 145-151.
- Caraballo, C., Jaimes, F., 2019. Organ dysfunction in sepsis: an ominous trajectory from infection to death. *The Yale Journal of Biology and Medicine* 92, 629-640.
- Carrascosa, J. L., Llorca, O., Valpuesta, J. M., 2001. Structural comparison of prokaryotic and eukaryotic chaperonins. *Micron*. 32, 43-50.
- Celmer, W. D., Solomons, I. A., 1952. The structure of the antibiotic mycomycin. *Journal of the American Chemical Society* 74, 1870-1871.
- Chen, H., Zhu, C., Zhu, M., Xiong, J., Ma, H., Zhuo, M., Li, S., 2019. High production of valencene in *Saccharomyces cerevisiae* through metabolic engineering. *Microbial Cell Factories* 18, 195.

- Chen, Y., Siewers, V., Nielsen, J., 2012. Profiling of cytosolic and peroxisomal acetyl-CoA metabolism in *Saccharomyces cerevisiae*. PloS One 7, e42475.
- Chen, Y., Xiao, W., Wang, Y., Liu, H., Li, X., Yuan, Y., 2016. Lycopene overproduction in *Saccharomyces cerevisiae* through combining pathway engineering with host engineering. Microbial Cell Factories 15, 113.
- Chen, Y., Zhang, Y., Siewers, V., Nielsen, J., 2015. Ach1 is involved in shuttling mitochondrial acetyl units for cytosolic C2 provision in *Saccharomyces cerevisiae* lacking pyruvate decarboxylase. FEMS Yeast Research 15, fov015.
- Clastre, M., Papon, N., Courdavault, V., Giglioli-Guivarc'h, N., St-Pierre, B., Simkin, A. J., 2011. Subcellular evidence for the involvement of peroxisomes in plant isoprenoid biosynthesis. Plant Signaling & Behavior 6, 2044-2046.
- Cohen, S. N., Chang, A. C., Hsu, L., 1972. Nonchromosomal antibiotic resistance in bacteria: genetic transformation of *Escherichia coli* by R-factor DNA. Proc. Natl. Acad. Sci. U. S. A. 69, 2110-2114.
- Cole, R. J., Jarvis, B. B., Schweikert, M. A., 2003. Handbook of Secondary Fungal Metabolites. Academic Press, San Diego.
- Collins, C., Keane, T. M., Turner, D. J., O'Keeffe, G., Fitzpatrick, D. A., Doyle, S., 2013. Genomic and proteomic dissection of the ubiquitous plant pathogen, *Armillaria mellea*: toward a new infection model system. Journal of Proteome Research 12, 2552-2570.
- Costa-de-Oliveira, S., Rodrigues, A. G., 2020. *Candida albicans* antifungal resistance and tolerance in bloodstream infections: the triad yeast-host-antifungal. Microorganisms 8, 154.
- Costa, R., De Grazia, S., Grasso, E., Trozzi, A., 2015. Headspace-solid-phase microextraction-gas chromatography as analytical methodology for the determination of volatiles in wild mushrooms and evaluation of modifications occurring during storage. Journal of Analytical Methods in Chemistry 2015, 951748.
- Couturier, M., Navarro, D., Olivé, C., Chevret, D., Haon, M., Favel, A., Lesage-Meessen, L., Henrissat, B., Coutinho, P. M., Berrin, J. G., 2012. Post-genomic analyses of fungal lignocellulosic biomass degradation reveal the unexpected potential of the plant pathogen *Ustilago maydis*. BMC Genomics 13, 57.
- Croteau, R., Ketchum, R. E., Long, R. M., Kaspera, R., Wildung, M. R., 2006. Taxol biosynthesis and molecular genetics. Phytochemistry Reviews 5, 75-97.
- Croxen, R., Goosey, M. W., Keon, J. P., Hargreaves, J. A., 1994. Isolation of an *Ustilago maydis* gene encoding 3-hydroxy-3-methylglutaryl-coenzyme A reductase and expression of a C-terminal-truncated form in *Escherichia coli*. Microbiology (Reading, England) 140 ( Pt 9), 2363-2370.
- Dahl, R. H., Zhang, F., Alonso-Gutierrez, J., Baidoo, E., Batth, T. S., Redding-Johanson, A. M., Petzold, C. J., Mukhopadhyay, A., Lee, T. S., Adams, P. D., Keasling, J. D., 2013. Engineering dynamic pathway regulation using stress-response promoters. Nature Biotechnology 31, 1039-1046.
- Dawid, C., Dunemann, F., Schwab, W., Nothnagel, T., Hofmann, T., 2015. Bioactive C<sub>17</sub>-polyacetylenes in carrots (*Daucus carota* L.): current knowledge and future perspectives. Journal of Agricultural and Food Chemistry 63, 9211-9222.
- de Carvalho, C. C. C. R., Caramujo, M. J., 2017. Carotenoids in aquatic ecosystems and aquaculture: A colorful business with implications for human health. Frontiers in Marine Science 4.
- De Carvalho, J. C., Magalhaes, A. I., Soccol, C. R., 2018. Biobased itaconic acid market and research trends - is it really a promising chemical? Chim Oggi - Chem Today 36, 56-58.

- de Mattos-Shipley, K. M. J., Foster, G. D., Bailey, A. M., 2017. Insights into the classical genetics of *Clitopilus passeckerianus* - the pleuromutilin producing mushroom. *Frontiers in Microbiology* 8, 1056.
- DeBose-Boyd, R. A., 2008. Feedback regulation of cholesterol synthesis: sterol-accelerated ubiquitination and degradation of HMG CoA reductase. *Cell Res.* 18, 609-621.
- Dejong, J. M., Liu, Y., Bollon, A. P., Long, R. M., Jennewein, S., Williams, D., Croteau, R. B., 2006. Genetic engineering of taxol biosynthetic genes in *Saccharomyces cerevisiae*. *Biotechnology and Bioengineering* 93, 212-224.
- Doehlemann, G., Wahl, R., Vranes, M., de Vries, R. P., Kämper, J., Kahmann, R., 2008. Establishment of compatibility in the *Ustilago maydis*/maize pathosystem. *Journal of Plant Physiology* 165, 29-40.
- Donald, K. A., Hampton, R. Y., Fritz, I. B., 1997. Effects of overproduction of the catalytic domain of 3-hydroxy-3-methylglutaryl coenzyme A reductase on squalene synthesis in *Saccharomyces cerevisiae*. *Applied and Environmental Microbiology* 63, 3341-3344.
- Dörfer, M., Gressler, M., Hoffmeister, D., 2019. Diversity and bioactivity of *Armillaria* sesquiterpene aryl ester natural products. *Mycological Progress* 18, 1027-1037.
- Douglas, L. M., Konopka, J. B., 2016. Plasma membrane organization promotes virulence of the human fungal pathogen *Candida albicans*. *Journal of Microbiology (Seoul, Korea)* 54, 178-191.
- Drews, A., Kraume, M., 2005. Process improvement by application of membrane bioreactors. *Chem Eng. Res. Desgin* 83.
- Drews, A., Kraume, M., 2007. On maintenance models in severely and long-term limited membrane bioreactor cultivations. *Biotechnology and Bioengineering* 96, 892-903.
- Dwivedi, C., Guan, X., Harmsen, W. L., Voss, A. L., Goetz-Parten, D. E., Koopman, E. M., Johnson, K. M., Valluri, H. B., Matthees, D. P., 2003. Chemopreventive effects of alpha-santalol on skin tumor development in CD-1 and SENCAR mice. *Cancer Epidemiol Biomarkers Prev.* 12, 151-156.
- Engels, B., Heinig, U., Grothe, T., Stadler, M., Jennewein, S., 2011. Cloning and characterization of an *Armillaria gallica* cDNA encoding protoilludene synthase, which catalyzes the first committed step in the synthesis of antimicrobial melleolides. *Journal of Biological Chemistry* 286, 6871-6878.
- Engelsma, D., Valle, N., Fish, A., Salomé, N., Almendral, J. M., Fornerod, M., 2008. A supraphysiological nuclear export signal is required for parvovirus nuclear export. *Mol. Biol. Cell.* 19, 2544-2552.
- Estrada, A. F., Brefort, T., Mengel, C., Díaz-Sánchez, V., Alder, A., Al-Babili, S., Avalos, J., 2009. *Ustilago maydis* accumulates beta-carotene at levels determined by a retinal-forming carotenoid oxygenase. *Fungal Genetics and Biology* 46, 803-813.
- Fan, Y., Solomon, P., Oliver, R. P., Brown, L. S., 2011. Photochemical characterization of a novel fungal rhodopsin from *Phaeosphaeria nodorum*. *Biochimica et Biophysica Acta* 1807, 1457-1466.
- Feldbrügge, M., Kämper, J., Steinberg, G., Kahmann, R., 2004. Regulation of mating and pathogenic development in *Ustilago maydis*. *Current Opinion in Microbiology* 7, 666-672.
- Feldbrügge, M., Kellner, R., Schipper, K., 2013. The biotechnological use and potential of plant pathogenic smut fungi. *Applied Microbiology and Biotechnology* 97, 3253-3265.
- Fish, W. W., Perkins-Veazie, P., Collins, J. K., 2002. A quantitative assay for lycopene that utilizes reduced volumes of organic solvents. *J. Food Comp. Anal.* 15, 309-317.

- Fleischmann, C., Scherag, A., Adhikari, N. K., Hartog, C. S., Tsaganos, T., Schlattmann, P., Angus, D. C., Reinhart, K., 2016. Assessment of global incidence and mortality of hospital-treated sepsis. Current estimates and limitations. *American Journal of Respiratory and Critical Care Medicine* 193, 259-272.
- Flor-Weiler, L. B., Behle, R. W., Stafford, K. C., 3rd, 2011. Susceptibility of four tick species, *Amblyomma americanum*, *Dermacentor variabilis*, *Ixodes scapularis*, and *Rhipicephalus sanguineus* (Acari: Ixodidae), to nootkatone from essential oil of grapefruit. *Journal of Medical Entomology* 48, 322-326.
- Floudas, D., Held, B. W., Riley, R., Nagy, L. G., Koehler, G., Ransdell, A. S., Younus, H., Chow, J., Chiniquy, J., Lipzen, A., Tritt, A., Sun, H., Haridas, S., LaButti, K., Ohm, R. A., Kues, U., Blanchette, R. A., Grigoriev, I. V., Minto, R. E., Hobbett, D. S., 2015. Evolution of novel wood decay mechanisms in Agaricales revealed by the genome sequences of *Fistulina hepatica* and *Cylindrobasidium torrendii*. *Fungal Genetics and Biology* 76, 78-92.
- Fong, N. J., Burgess, M. L., Barrow, K. D., Glenn, D. R., 2001. Carotenoid accumulation in the psychrotrophic bacterium *Arthrobacter agilis* in response to thermal and salt stress. *Applied Microbiology and Biotechnology* 56, 750-756.
- Frey-Klett, P., Burlinson, P., Deveau, A., Barret, M., Tarkka, M., Sarniguet, A., 2011. Bacterial-fungal interactions: hyphens between agricultural, clinical, environmental, and food microbiologists. *Microbiology and Molecular Biology Reviews* 75, 583-609.
- Fritsche, K., Berg, M. V. D., Boer, W. D., Beek, T. A. V., Raaijmakers, J. M., Veen, J. A. V., Leveau, J. H. J., 2014. Biosynthetic genes and activity spectrum of antifungal polyynes from *Collimonas Fungivorans* Ter331. *Environmental Microbiology* 16, 1334-1345.
- Frohwitter, J., Heider, S. A., Peters-Wendisch, P., Beekwilder, J., Wendisch, V. F., 2014. Production of the sesquiterpene (+)-valencene by metabolically engineered *Corynebacterium glutamicum*. *J. Biotechnol.* 191, 205-213.
- Fu, Z., Wang, M., Potter, D., Miziorko, H. M., Kim, J. J., 2002. The structure of a binary complex between a mammalian mevalonate kinase and ATP: insights into the reaction mechanism and human inherited disease. *The Journal of Biological Chemistry* 277, 18134-18142.
- Galdieri, L., Zhang, T., Rogerson, D., Lleshi, R., Vancura, A., 2014. Protein acetylation and acetyl coenzyme a metabolism in budding yeast. *Eukaryotic Cell* 13, 1472-1483.
- García-Cabeza, A. L., Marín-Barrios, R., Moreno-Dorado, F. J., Ortega, M. J., Massanet, G. M., Guerra, F. M., 2014. Allylic oxidation of alkenes catalyzed by a copper-aluminum mixed oxide. *Organic Letters* 16, 1598-1601.
- García-Martínez, J., Brunk, M., Avalos, J., Terpitz, U., 2015. The CarO rhodopsin of the fungus *Fusarium fujikuroi* is a light-driven proton pump that retards spore germination. *Scientific Reports* 5, 7798.
- Garrod, B., Lewis, B. G., 1979a. Location of the antifungal compound faltarindiol in carrot root tissue. *Transactions of the British Mycological Society* 72, 515-517.
- Garrod, B., Lewis, B. G., 1979b. Studies on the mechanism of action of the antifungal compound faltarindiol. *New Phytologist* 83, 463-471.
- Gavira, C., Höfer, R., Lesot, A., Lambert, F., Zucca, J., Werck-Reichhart, D., 2013. Challenges and pitfalls of P450-dependent (+)-valencene bioconversion by *Saccharomyces cerevisiae*. *Metabolic Engineering* 18, 25-35.
- Geiser, E., Reindl, M., Blank, L. M., Feldbrügge, M., Wierckx, N., Schipper, K., 2016. Activating intrinsic carbohydrate-active enzymes of the smut fungus *Ustilago maydis* for the degradation of plant cell wall components. *Applied and Environmental Microbiology* 82, 5174-5185.



- Ghosh, A., 2014. Small heat shock proteins (HSP12, HSP20 and HSP30) play a role in *Ustilago maydis* pathogenesis. FEMS Microbiology Letters 361, 17-24.
- Gibson, D. G., Young, L., Chuang, R. Y., Venter, J. C., Hutchison, C. A., 3rd, Smith, H. O., 2009. Enzymatic assembly of DNA molecules up to several hundred kilobases. Nat. Methods 6, 343-345.
- Gillissen, B., Bergemann, J., Sandmann, C., Schroeder, B., Bölker, M., Kahmann, R., 1992. A two-component regulatory system for self/non-self recognition in *Ustilago maydis*. Cell 68, 647-657.
- Griffith, G. W., Easton, G. L., Detheridge, A., Roderick, K., Edwards, A., Worgan, H. J., Nicholson, J., Perkins, W. T., 2007. Copper deficiency in potato dextrose agar causes reduced pigmentation in cultures of various fungi. FEMS Microbiology Letters 276, 165-171.
- Gruchattka, E., Hädicke, O., Klamt, S., Schütz, V., Kayser, O., 2013. In silico profiling of *Escherichia coli* and *Saccharomyces cerevisiae* as terpenoid factories. Microbial Cell Factories 12, 84.
- Guerin, M., Huntley, M. E., Olaizola, M., 2003. *Haematococcus* astaxanthin: applications for human health and nutrition. Trends in Biotechnology 21, 210-216.
- Guevarra, E. D., Tabuchi, T., 1990. Accumulation of itaconic, 2-hydroxyparaconic, itatartaric, and malic acids by strains of the genus *Ustilago*. Agricultural and Biological Chemistry 54, 2353-2358.
- Guimaraes, S. C., Schuster, M., Bielska, E., Dagdas, G., Kilaru, S., Meadows, B. R., Schrader, M., Steinberg, G., 2015. Peroxisomes, lipid droplets, and endoplasmic reticulum "hitchhike" on motile early endosomes. The Journal of Cell Biology 211, 945-954.
- Hammer, S. K., Avalos, J. L., 2017. Harnessing yeast organelles for metabolic engineering. Nature Chemical Biology 13, 823-832.
- Hartley, A. J., de Mattos-Shiple, K., Collins, C. M., Kilaru, S., Foster, G. D., Bailey, A. M., 2009. Investigating pleuromutilin-producing *Clitopilus* species and related basidiomycetes. FEMS Microbiology Letters 297, 24-30.
- Hartmann, M. A., 2003. Sterol metabolism and function in higher plants. In G Daum, ed, Lipid Metabolism and Membrane Biogenesis. Springer, Heidelberg, PP 183-211.
- Harwoko, H., Daletos, G., Stuhldreier, F., Lee, J., Wesselborg, S., Feldbrugge, M., Muller, W. E. G., Kalscheuer, R., Ancheeva, E., Proksch, P., 2019. Dithiodiketopiperazine derivatives from endophytic fungi *Trichoderma harzianum* and *Epicoccum nigrum*. Natural Product Research 18, 1-9.
- Haskins, R. H., 1950. Biochemistry of the Ustilaginales: I. Preliminary cultural studies of *Ustilago zeae*. Can. J. Res. 28, 213-223.
- He, J., Shen, Y., Jiang, J. S., Yang, Y.-N., Feng, Z.-M., Zhang, P.-C., Yuan, S.-P., Hou, Q., 2011. New polyacetylene glucosides from the florets of *Carthamus tinctorius* and their weak anti-inflammatory activities. Carbohydrate Research 346, 1903-1908.
- He, M., Zhao, R., Hyde, K. D., Begerow, D., Kemler, M., Yurkov, A., McKenzie, E. H. C., Raspé, O., Kakishima, M., Sánchez-Ramírez, S., Vellinga, E. C., Halling, R., Papp, V., Zmitrovich, I. V., Buyck, B., Ertz, D., Wijayawardene, N. N., Cui, B., Schoutteten, N., Liu, X., Li, T., Yao, Y., Zhu, X., Liu, A., Li, G., Zhang, M., Ling, Z., Cao, B., Antonín, V., Boekhout, T., da Silva, B. D. B., De Crop, E., Decock, C., Dima, B., Dutta, A. K., Fell, J. W., Geml, J., Ghobad-Nejhad, M., Giachini, A. J., Gibertoni, T. B., Gorjón, S. P., Haelewaters, D., He, S., Hodgkinson, B. P., Horak, E., Hoshino, T., Justo, A., Lim, Y. W., Menolli, N., Mešić, A., Moncalvo, J., Mueller, G. M., Nagy, L. G., Nilsson, R. H., Noordeloos, M., Nuytinck, J., Orihara, T., Ratchadawan, C., Rajchenberg, M., Silva-Filho, A. G. S., Sulzbacher, M. A., Tkáčec, Z., Valenzuela, R., Verbeken, A., Vizzini, A., Wartchow, F., Wei, T., Weiß, M., Zhao, C., Kirk, P. M., 2019. Notes, outline and divergence times of Basidiomycota. Fungal Diversity 99, 105-367.



- He, Q., Liu, Y., 2005. Molecular mechanism of light responses in *Neurospora*: from light-induced transcription to photoadaptation. *Genes & Development* 19, 2888-2899.
- Hennicke, F., Cheikh-Ali, Z., Liebisch, T., Maciá-Vicente, J. G., Bode, H. B., Piepenbring, M., 2016. Distinguishing commercially grown *Ganoderma lucidum* from *Ganoderma lingzhi* from Europe and East Asia on the basis of morphology, molecular phylogeny, and triterpenic acid profiles. *Phytochemistry* 127, 29-37.
- Hewald, S., Josephs, K., Bölker, M., 2005. Genetic analysis of biosurfactant production in *Ustilago maydis*. *Applied and Environmental Microbiology* 71, 3033-3040.
- Hewald, S., Linne, U., Scherer, M., Marahiel, M. A., Kämper, J., Bölker, M., 2006. Identification of a gene cluster for biosynthesis of mannosylerythritol lipids in the basidiomycetous fungus *Ustilago maydis*. *Applied and Environmental Microbiology* 72, 5469-5477.
- Hoffman, C. S., Winston, F., 1987. A ten-minute DNA preparation from yeast efficiently releases autonomous plasmids for transformation of *Escherichia coli*. *Gene* 57, 267-272.
- Holliday, R., 1974. Molecular aspects of genetic exchange and gene conversion. *Genetics* 78, 273-287.
- Hu, Y., Zhou, Y. J., Bao, J., Huang, L., Nielsen, J., Krivoruchko, A., 2017. Metabolic engineering of *Saccharomyces cerevisiae* for production of germacrene A, a precursor of beta-elemene. *Journal of Industrial Microbiology & Biotechnology* 44, 1065-1072.
- Hümbelin, M., Thomas, A., Lin, J., Li, J., Jore, J., Berry, A., 2002. Genetics of isoprenoid biosynthesis in *Paracoccus zeaxanthinifaciens*. *Gene* 297, 129-139.
- Hung, L. V. M., Moon, J. Y., Ryu, J. Y., Cho, S. K., 2019. Nootkatone, an AMPK activator derived from grapefruit, inhibits KRAS downstream pathway and sensitizes non-small-cell lung cancer A549 cells to adriamycin. *Phytomedicine* 63, 153000.
- Hunter, G. L. K., Brogden, W. B., 1965a. Analysis of the terpene and sesquiterpene hydrocarbons in some citrus oils. *J. Food Sci.* 30, 383-387.
- Hunter, G. L. K., Brogden, W.B., 1965b. Conversion of valencene to nootkatone. *J. Food Sci.* 30, 876-878.
- Hyde, K. D., Xu, J., Rapior, S., Jeewon, R., Lumyong, S., Niego, A. G. T., Abeywickrama, P. D., Aluthmuhandiram, J. V. S., Brahmananage, R. S., Brooks, S., Chaiyasen, A., Chethana, K. W. T., Chomnunti, P., Chepkirui, C., Chuankid, B., de Silva, N. I., Doilom, M., Faulds, C., Gentekaki, E., Gopalan, V., Kakumyan, P., Harishchandra, D., Hemachandran, H., Hongsanant, S., Karunarathna, A., Karunarathna, S. C., Khan, S., Kumla, J., Jayawardena, R. S., Liu, J., Liu, N., Luangharn, T., Macabeo, A. P. G., Marasinghe, D. S., Meeks, D., Mortimer, P. E., Mueller, P., Nadir, S., Nataraja, K. N. and S. Nontachaiyapoom, O'Brien, M., Penkhrue, W., Phukhamsakda, C., Ramanan, U. S., Rathnayaka, A. R., Sadaba, R. B., Sandargo, B., Samarakoon, B. C., Tennakoon, D. S., Siva, R., Sriprom, W., Suryanarayanan, T. S., Sujarit, K., Suwannarach, N., Suwunwong, T., Thongbai, B., Thongklang, N., Wei, D., Wijesinghe, S. N., Winiski, J., Yan, J., Yasanthika, E., Stadler, M., 2019. The amazing potential of fungi: 50 ways we can exploit fungi industrially. *Fungal Diversity* 97, 1-136.
- Hynes, M. J., Murray, S. L., 2010. ATP-citrate lyase is required for production of cytosolic acetyl coenzyme A and development in *Aspergillus nidulans*. *Eukaryotic Cell* 9, 1039-1048.
- Ichinose, H., Wariishi, H., 2013. High-level heterologous expression of fungal cytochrome P450s in *Escherichia coli*. *Biochemical and Biophysical Research Communications* 438, 289-294.
- Ignea, C., Cvetkovic, I., Loupassaki, S., Kefalas, P., Johnson, C. B., Kampranis, S. C., Makris, A. M., 2011. Improving yeast strains using recyclable integration cassettes, for the production of plant terpenoids. *Microbial Cell Factories* 10, 4.

- Ignea, C., Pontini, M., Motawia, M. S., Maffei, M. E., Makris, A. M., Kampranis, S. C., 2018. Synthesis of 11-carbon terpenoids in yeast using protein and metabolic engineering. *Nat. Chem. Biol.* 14, 1090-1098.
- Ivanova, V., Kolarova M., Aleksieva, K., Schlegel R., Schumann P., Graefe, U., 2013. Octadeca-8,11-dienoic acid methylester, a new fatty acid metabolite from *Fistulina hepatica*. *Journal of Modern Medicinal Chemistry* 1, 43-48.
- Jankowski, S., Pohlmann, T., Baumann, S., Muntjes, K., Devan, S. K., Zander, S., Feldbrügge, M., 2019. The multi PAM2 protein Upa2 functions as novel core component of endosomal mRNA transport. *EMBO reports* 20, e47381.
- Jaspers, N. G., Raams, A., Kelner, M. J., Ng, J. M., Yamashita, Y. M., Takeda, S., McMorris, T. C., Hoeijmakers, J. H., 2002. Anti-tumour compounds illudin S and Irofulven induce DNA lesions ignored by global repair and exclusively processed by transcription- and replication-coupled repair pathways. *DNA Repair (Amst)* 1, 1027-1038.
- Jiang, Z., Kempinski, C., Chappell, J., 2016. Extraction and analysis of terpenes/terpenoids. *Current Protocols in Plant Biology* 1, 345-358.
- Jirovetz, L., Buchbauer, G., Denkova, Z., Stoyanova, A., Murgov, I., Gearon, V., Birkbeck, S., Schmidt, E., Geissler, M., 2006. Comparative study on the antimicrobial activities of the different sandalwood essential oils of various origin. *Flavour Fragr. J.* 21, 465-468.
- Jones, E. R. H., Lowe, G., Shannon, P. V. R., 1966. Natural acetylenes. Part XX. Tetra-acetylenic and other metabolites from *Fistulina hepatica*(Huds) Fr. *Journal of the Chemical Society C: Organic*, 139-144.
- Kaffenberger, J. T., Schilling, J. S., 2015. Comparing lignocellulose physiochemistry after decomposition by brown rot fungi with distinct evolutionary origins. *Environmental Microbiology* 17, 4885-4897.
- Kahmann, R., Kämper, J., 2004. *Ustilago maydis*: how its biology relates to pathogenic development. *New Phytologist* 164, 31-42.
- Kai, K., Sogame, M., Sakurai, F., Nasu, N., Fujita, M., 2018. Collimonins A-D, unstable polyynes with antifungal or pigmentation activities from the fungus-feeding bacterium *Collimonas fungivorans* Ter331. *Organic Letters* 20, 3536-3540.
- Kämper, J., Kahmann, R., Bölker, M., Ma, L. J., Brefort, T., Saville, B. J., Banuett, F., Kronstad, J. W., Gold, S. E., Müller, O., Perlin, M. H., Wösten, H. A., de Vries, R., Ruiz-Herrera, J., Reynaga-Peña, C. G., Snetselaar, K., McCann, M., Pérez-Martín, J., Feldbrügge, M., Basse, C. W., Steinberg, G., Ibeas, J. I., Holloman, W., Guzman, P., Farman, M., Stajich, J. E., Sentandreu, R., González-Prieto, J. M., Kennell, J. C., Molina, L., Schirawski, J., Mendoza-Mendoza, A., Greilinger, D., Münch, K., Rössel, N., Scherer, M., Vranes, M., Ladendorf, O., Vincon, V., Fuchs, U., Sandroock, B., Meng, S., Ho, E. C., Cahill, M. J., Boyce, K. J., Klose, J., Klosterman, S. J., Deelstra, H. J., Ortiz-Castellanos, L., Li, W., Sanchez-Alonso, P., Schreier, P. H., Häuser-Hahn, I., Vaupel, M., Koopmann, E., Friedrich, G., Voss, H., Schlüter, T., Margolis, J., Platt, D., Swimmer, C., Gnirke, A., Chen, F., Vysotskaia, V., Mannhaupt, G., Güldener, U., Münsterkötter, M., Haase, D., Oesterheld, M., Mewes, H. W., Mauceli, E. W., DeCaprio, D., Wade, C. M., Butler, J., Young, S., Jaffe, D. B., Calvo, S., Nusbaum, C., Galagan, J., Birren, B. W., 2006. Insights from the genome of the biotrophic fungal plant pathogen *Ustilago maydis*. *Nature* 444, 97-101.
- Kampranis, S. C., Makris, A. M., 2012. Developing a yeast cell factory for the production of terpenoids. *Comput. Struct. Biotechnol. J.* 3, e201210006.
- Kanehisa, M., Goto, S., 2000. KEGG: kyoto encyclopedia of genes and genomes. *Nucleic Acids Res.* 28, 27-30.

- Kavanagh, K. L., Guo, K., Dunford, J. E., Wu, X., Knapp, S., Ebetino, F. H., Rogers, M. J., Russell, R. G., Oppermann, U., 2006. The molecular mechanism of nitrogen-containing bisphosphonates as antiosteoporosis drugs. *Proc. Natl. Acad. Sci. U. S. A.* 103, 7829-7834.
- Keller, N. P., 2019. Fungal secondary metabolism: regulation, function and drug discovery. *Nature Reviews Microbiology* 17, 167-180.
- Kettering, M., Sterner, O., Anke, T., 2004. Antibiotics in the chemical communication of fungi. *Zeitschrift für Naturforschung* 59, 816-823.
- Khrunyk, Y., Münch, K., Schipper, K., Lupas, A. N., Kahmann, R., 2010. The use of FLP-mediated recombination for the functional analysis of an effector gene family in the biotrophic smut fungus *Ustilago maydis*. *New Phytol.* 187, 957-968.
- Kim, H. K., Kim, R. R., Oh, J. H., Cho, H., Varshavsky, A., Hwang, C. S., 2014. The N-terminal methionine of cellular proteins as a degradation signal. *Cell* 156, 158-169.
- Kirti, K., Amita, S., Priti, S., Kumar, A. M., Jyoti, S., 2014. Colorful world of microbes: carotenoids and their applications. *Advances in Biology* 2014, 837891.
- Kitamoto, D., S. Akiba, C., Hioki, C., Tabuchi, T., 1990. Extracellular accumulation of mannosylerythritol lipids by a strain of *Candida antarctica*. *Agric. Biol. Chem* 54, 31-36.
- Kjer, J., Debbab, A., Aly, A. H., Proksch, P., 2010. Methods for isolation of marine-derived endophytic fungi and their bioactive secondary products. *Nature Protocols* 5, 479-490.
- Klement, T., Milker, S., Jäger, G., Grande, P. M., Domínguez de María, P., Büchs, J., 2012. Biomass pretreatment affects *Ustilago maydis* in producing itaconic acid. *Microbial Cell Factories* 11, 43.
- Kleofas, V., Sommer, L., Fraatz, M.A., Zorn, H., Rühl, M., 2014. Fruiting body production and aroma profile analysis of *Agrocybe aegerita* cultivated on different substrates. *Nat. Resour.* 05, 233.
- Knudsen, H., Vesterholt, J., 2008. *Funga Nordica*. Nordsvamp, 966 p.
- Kobaisy, M., Abramowski, Z., Lerner, L., Saxena, G., Hancock, R. E. W., Towers, G. H. N., Doxsee, D., Stokes, R. W., 1997. Antimycobacterial polyynes of Devil's Club (*Oplopanax horridus*), a North American native medicinal plant. *Journal of Natural Products* 60, 1210-1213.
- Koehn, F. E., Carter, G. T., 2005. The evolving role of natural products in drug discovery. *Nature reviews. Drug Discovery* 4, 206-220.
- Koepke, J., Kaffarnik, F., Haag, C., Zarnack, K., Luscombe, N. M., König, J., Ule, J., Kellner, R., Begerow, D., Feldbrügge, M., 2011. The RNA-binding protein Rrm4 is essential for efficient secretion of endochitinase Cts1. *Mol. Cell. Proteomics* 10, M111.011213.
- Konovalov, D. A., 2014. Polyacetylene compounds of plants of the *Asteraceae* family (review). *Pharmaceutical Chemistry Journal* 48, 615-633.
- Kovacs, W. J., Faust, P. L., Keller, G. A., Krisans, S. K., 2001. Purification of brain peroxisomes and localization of 3-hydroxy-3-methylglutaryl coenzyme A reductase. *European Journal of Biochemistry* 268, 4850-4859.
- Kovacs, W. J., Krisans, S., 2003. Cholesterol biosynthesis and regulation: role of peroxisomes. *Advances in Experimental Medicine and Biology* 544, 315-327.
- Kovacs, W. J., Olivier, L. M., Krisans, S. K., 2002. Central role of peroxisomes in isoprenoid biosynthesis. *Progress in Lipid Research* 41, 369-391.
- Kovacs, W. J., Tape, K. N., Shackelford, J. E., Duan, X., Kasumov, T., Kelleher, J. K., Brunengraber, H., Krisans, S. K., 2007. Localization of the pre-squalene segment of the isoprenoid biosynthetic pathway in mammalian peroxisomes. *Histochemistry and Cell Biology* 127, 273-290.

- Kriegelsteiner, G. J., 2000. Die Grosspilze Baden-Württembergs. Bd. 1: Allgemeiner Teil, Ständerpilze: Gallert-Rinden-, Stachel- und Porenpilze. [in German] E. Ulmer, 629 p.
- Kris-Etherton, P. M., Hecker, K. D., Bonanome, A., Coval, S. M., Binkoski, A. E., Hilpert, K. F., Griel, A. E., Etherton, T. D., 2002. Bioactive compounds in foods: their role in the prevention of cardiovascular disease and cancer. *The American Journal of Medicine* 113 Suppl 9B, 71s-88s.
- Krivoruchko, A., Zhang, Y., Siewers, V., Chen, Y., Nielsen, J., 2015. Microbial acetyl-CoA metabolism and metabolic engineering. *Metabolic Engineering* 28, 28-42.
- Kronstad, J. W., Leong, S. A., 1990. The b mating-type locus of *Ustilago maydis* contains variable and constant regions. *Genes & Development* 4, 1384-1395.
- Kuenz, A., Krull, S., 2018. Biotechnological production of itaconic acid-things you have to know. *Applied Microbiology and Biotechnology* 102, 3901-3914.
- Kuhnt, D., Anke, T., Besl, H., Bross, M., Herrmann, R., Mocek, U., Steffan, B., Steglich, W., 1990. Antibiotics from basidiomycetes. XXXVII. New inhibitors of cholesterol biosynthesis from cultures of *Xerula melanotricha* Dörfelt. *The Journal of Antibiotics* 43, 1413-1420.
- Künzler, M., 2018. How fungi defend themselves against microbial competitors and animal predators. *PLoS Pathogens* 14, e1007184.
- Lackner, G., Bohnert, M., Wick, J., Hoffmeister, D., 2013. Assembly of melleolide antibiotics involves a polyketide synthase with cross-coupling activity. *Chemistry & Biology* 20, 1101-1106.
- Laemmli, U. K., 1970. Cleavage of structural proteins during the assembly of the head of bacteriophage T4. *Nature* 227, 680-685.
- Lange, B. M., Rujan, T., Martin, W., Croteau, R., 2000. Isoprenoid biosynthesis: the evolution of two ancient and distinct pathways across genomes. *Proc. Natl. Acad. Sci. U. S. A.* 97, 13172-13177.
- Lanver, D., Müller, A. N., Happel, P., Schweizer, G., Haas, F. B., Franitza, M., Pellegrin, C., Reissmann, S., Altmüller, J., Rensing, S. A., Kahmann, R., 2018. The biotrophic development of *Ustilago maydis* studied by RNA-seq analysis. *The Plant Cell* 30, 300-323.
- Larkin, M. A., Blackshields, G., Brown, N. P., Chenna, R., McGettigan, P. A., McWilliam, H., Valentin, F., Wallace, I. M., Wilm, A., Lopez, R., Thompson, J. D., Gibson, T. J., Higgins, D. G., 2007. Clustal W and Clustal X version 2.0. *Bioinformatics* 23, 2947-2948.
- Lechner, D., Stavri, M., Oluwatuyi, M., Pereda-Miranda, R., Gibbons, S., 2004. The anti-staphylococcal activity of *Angelica dahurica* (Bai Zhi). *Phytochemistry* 65, 331-335.
- Lee, J., Hilgers, F., Loeschke, A., Jaeger, K.-E., Feldbrügge, M., 2020a. *Ustilago maydis* serves as a novel production host for the synthesis of plant and fungal sesquiterpenoids. *Frontiers in Microbiology* 11, 1655.
- Lee, J., Shi, Y., Grün, P., Gube, M., Feldbrügge, M., Bode, H. B., Hennicke, F., 2020b, Identification of feldin, an antifungal polyine from the beefsteak fungus *Fistulina hepatica*. *Biomolecules* 10, 1502.
- Letunic, I., Bork, P., 2018. 20 years of the SMART protein domain annotation resource. *Nucleic Acids Res.* 46, D493-d496.
- Li, C., Swofford, C. A., Sinskey, A. J., 2020. Modular engineering for microbial production of carotenoids. *Metabolic Engineering Communications* 10, e00118.
- Li, J., Zhang, J., Chen, H., Chen, X., Lan, J., Liu, C., 2013. Complete mitochondrial genome of the medicinal mushroom *Ganoderma lucidum*. *PloS One* 8, e72038.



- Linnemannstöns, P., Prado, M. M., Fernández-Martín, R., Tudzynski, B., Avalos, J., 2002. A carotenoid biosynthesis gene cluster in *Fusarium fujikuroi*: the genes *carB* and *carRA*. *Molecular Genetics and Genomics* 267, 593-602.
- Liu, G. S., Li, T., Zhou, W., Jiang, M., Tao, X. Y., Liu, M., Zhao, M., Ren, Y. H., Gao, B., Wang, F. Q., Wei, D. Z., 2020. The yeast peroxisome: A dynamic storage depot and subcellular factory for squalene overproduction. *Metabolic Engineering* 57, 151-161.
- Liu, J., Zhai, Y., Zhang, Y., Zhu, S., Liu, G., Che, Y., 2018. Heterologous biosynthesis of the fungal sesquiterpene trichodermol in *Saccharomyces cerevisiae*. *Frontiers in Microbiology* 9, 1773.
- Lombard, J., Moreira, D., 2011. Origins and early evolution of the mevalonate pathway of isoprenoid biosynthesis in the three domains of life. *Molecular Biology and Evolution* 28, 87-99.
- Lopez-Gallego, F., Agger, S. A., Abate-Pella, D., Distefano, M. D., Schmidt-Dannert, C., 2010. Sesquiterpene synthases Cop4 and Cop6 from *Coprinus cinereus*: catalytic promiscuity and cyclization of farnesyl pyrophosphate geometric isomers. *Chembiochem* 11, 1093-1106.
- Loubradou, G., Brachmann, A., Feldbrügge, M., Kahmann, R., 2001. A homologue of the transcriptional repressor Ssn6p antagonizes cAMP signalling in *Ustilago maydis*. *Molecular Microbiology* 40, 719-730.
- Lv, X., Wang, F., Zhou, P., Ye, L., Xie, W., Xu, H., Yu, H., 2016. Dual regulation of cytoplasmic and mitochondrial acetyl-CoA utilization for improved isoprene production in *Saccharomyces cerevisiae*. *Nature Communications* 7, 12851.
- Maassen, N., Panakova, M., Wierckx, N., Geiser, E., Zimmermann, M., Bölker, M., Kliner, U., Blank, L. M., 2014. Influence of carbon and nitrogen concentration on itaconic acid production by the smut fungus *Ustilago maydis*. *Eng. Life Sci.* 14, 129-134.
- Macek, B., Forchhammer, K., Hardouin, J., Weber-Ban, E., Grangeasse, C., Mijakovic, I., 2019. Protein post-translational modifications in bacteria. *Nature Reviews. Microbiology* 17, 651-664.
- Magiorakos, A. P., Srinivasan, A., Carey, R. B., Carmeli, Y., Falagas, M. E., Giske, C. G., Harbarth, S., Hindler, J. F., Kahlmeter, G., Olsson-Liljequist, B., Paterson, D. L., Rice, L. B., Stelling, J., Struelens, M. J., Vatopoulos, A., Weber, J. T., Monnet, D. L., 2012. Multidrug-resistant, extensively drug-resistant and pandrug-resistant bacteria: an international expert proposal for interim standard definitions for acquired resistance. *Clinical Microbiology and Infection* 18, 268-281.
- Maoka, T., 2020. Carotenoids as natural functional pigments. *Journal of Natural Medicines* 74, 1-16.
- Matheny, P. B., Curtis, J. M., Hofstetter, V., Aime, M. C., Moncalvo, J. M., Ge, Z. W., Slot, J. C., Ammirati, J. F., Baroni, T. J., Bougher, N. L., Hughes, K. W., Lodge, D. J., Kerrigan, R. W., Seidl, M. T., Aanen, D. K., DeNitis, M., Daniele, G. M., Desjardin, D. E., Kropp, B. R., Norvell, L. L., Parker, A., Vellinga, E. C., Vilgalys, R., Hibbett, D. S., 2006. Major Clades of Agaricales: a Multilocus Phylogenetic Overview. *Mycologia* 98, 982-995.
- McGarvey, D. J., Croteau, R., 1995. Terpenoid metabolism. *The Plant cell* 7, 1015-1026.
- McWilliams, A., 2018. The global market for carotenoids. BCC Research: Wellesley, MA, USA.
- Melillo, E., Setroikromo, R., Quax, W. J., Kayser, O., 2013. Production of  $\alpha$ -cuprenene in *Xanthophyllomyces dendrorhous*: a step closer to a potent terpene biofactory. *Microbial Cell Factories* 12, 13.
- Mendoza-Mendoza, A., Berndt, P., Djamei, A., Weise, C., Linne, U., Marahiel, M., Vranes, M., Kämper, J., Kahmann, R., 2009. Physical-chemical plant-derived signals induce differentiation in *Ustilago maydis*. *Molecular Microbiology* 71, 895-911.
- Meng, X., Liu, H., Xu, W., Zhang, W., Wang, Z., Liu, W., 2020. Metabolic engineering *Saccharomyces cerevisiae* for de novo production of the sesquiterpenoid (+)-nootkatone. *Microbial Cell Factories* 19, 21.



- Mickymaray, S., 2019. Efficacy and mechanism of traditional medicinal plants and bioactive compounds against clinically important pathogens. *Antibiotics* (Basel, Switzerland) 8.
- Minto, R. E., Blacklock, B. J., 2008. Biosynthesis and function of polyacetylenes and allied natural products. *Progress in Lipid Research* 47, 233-306.
- Miziorko, H. M., 2011. Enzymes of the mevalonate pathway of isoprenoid biosynthesis. *Archives of Biochemistry and Biophysics* 505, 131-143.
- Mojzita, D., Rantasalo, A., Jäntti, J., 2019. Gene expression engineering in fungi. *Current Opinion in Biotechnology* 59, 141-149.
- Montañés, F. M., Pascual-Ahuir, A., Proft, M., 2011. Repression of ergosterol biosynthesis is essential for stress resistance and is mediated by the Hog1 MAP kinase and the Mot3 and Rox1 transcription factors. *Molecular Microbiology* 79, 1008-1023.
- Montero-Lobato, Z., Ramos-Merchante, A., Fuentes, J. L., Sayago, A., Fernández-Recamales, Á., Martínez-Espinosa, R. M., Vega, J. M., Vilchez, C., Garbayo, I., 2018. Optimization of growth and carotenoid production by *Haloferax mediterranei* using response surface methodology. *Marine Drugs* 16.
- Moon, H. J., Jeya, M., Kim, I. W., Lee, J. K., 2010. Biotechnological production of erythritol and its applications. *Applied Microbiology and Biotechnology* 86, 1017-1025.
- Moser, S., Pichler, H., 2019. Identifying and engineering the ideal microbial terpenoid production host. *Applied Microbiology and Biotechnology* 103, 5501-5516.
- Mueller, O., Kahmann, R., Aguilar, G., Trejo-Aguilar, B., Wu, A., de Vries, R. P., 2008. The secretome of the maize pathogen *Ustilago maydis*. *Fungal Genetics and Biology* 45 Suppl 1, S63-70.
- Müller, M. J., Stachurski, S., Stoffels, P., Schipper, K., Feldbrügge, M., Büchs, J., 2018. Online evaluation of the metabolic activity of *Ustilago maydis* on (poly)galacturonic acid. *J. Biol. Eng.* 12, 34.
- Müntjes, K., Philipp, M., Hüsemann, L., Heucken, N., Weidtkamp-Peters, S., Schipper, K., Zurbriggen, M. D., Feldbrügge, M., 2020. Establishing polycistronic expression in the model microorganism *Ustilago maydis*. *Frontiers in Microbiology* 11.
- Nicholas, K. B., Nicholas, H. B. J., Deerfield, D. W., 1997. GeneDoc: Analysis and visualization of genetic variation. *Embnew. news* 4, 14.
- Nielsen, J., Keasling, J. D., 2016. Engineering cellular metabolism. *Cell* 164, 1185-1197.
- Nikaido, H., 2009. Multidrug resistance in bacteria. *Annual Review of Biochemistry* 78, 119-146.
- Niklitschek, M., Alcaíno, J., Barahona, S., Sepúlveda, D., Lozano, C., Carmona, M., Marcoleta, A., Martínez, C., Lodato, P., Baeza, M., Cifuentes, V., 2008. Genomic organization of the structural genes controlling the astaxanthin biosynthesis pathway of *Xanthophyllomyces dendrorhous*. *Biological Research* 41, 93-108.
- Nofiani, R., de Mattos-Shiple, K., Lebe, K.E., Han, L.-C., Iqbal, Z., Bailey, A.M., Willis, C.L., Simpson, T.J., Cox, R.J., 2018. Strobilurin biosynthesis in basidiomycete fungi. *Nature Communications* 9, 3940.
- Obuchi, T., Kondoh, H., Watanabe, N., Tamai, M., Omura, S., Yang, J. S., Liang, X. T., 1990. Armillaric acid, a new antibiotic produced by *Armillaria mellea*. *Planta Medica* 56, 198-201.
- Ogawara, H., 2020. Possible drugs for the treatment of bacterial infections in the future: anti-virulence drugs. *The Journal of Antibiotics*.
- Ohm, R. A., de Jong, J. F., Lugones, L. G., Aerts, A., Kothe, E., Stajich, J. E., de Vries, R. P., Record, E., Levasseur, A., Baker, S. E., Bartholomew, K. A., Coutinho, P. M., Erdmann, S., Fowler, T. J., Gathman, A. C., Lombard, V., Henrissat, B., Knabe, N., Kües, U., Lilly, W. W.,

- Lindquist, E., Lucas, S., Magnuson, J. K., Piumi, F., Raudaskoski, M., Salamov, A., Schmutz, J., Schwarze, F. W., vanKuyk, P. A., Horton, J. S., Grigoriev, I. V., Wösten, H. A., 2010. Genome sequence of the model mushroom *Schizophyllum commune*. *Nature Biotechnology* 28, 957-963.
- Okabe, M., Lies, D., Kanamasa, S., Park, E. Y., 2009. Biotechnological production of itaconic acid and its biosynthesis in *Aspergillus terreus*. *Applied Microbiology and Biotechnology* 84, 597-606.
- Olgeiser, L., Haag, C., Boerner, S., Ule, J., Busch, A., Koepke, J., König, J., Feldbrügge, M., Zarnack, K., 2019. The key protein of endosomal mRNP transport Rrm4 binds translational landmark sites of cargo mRNAs. *EMBO Reports* 20.
- Olivier, L. M., Kovacs, W., Masuda, K., Keller, G. A., Krisans, S. K., 2000. Identification of peroxisomal targeting signals in cholesterol biosynthetic enzymes. AA-CoA thiolase, hmg-coa synthase, MPPD, and FPP synthase. *Journal of Lipid Research* 41, 1921-1935.
- Olivier, L. M., Krisans, S. K., 2000. Peroxisomal protein targeting and identification of peroxisomal targeting signals in cholesterol biosynthetic enzymes. *Biochimica et biophysica acta* 1529, 89-102.
- Ondeyka, J. G., Zink, D. L., Young, K., Painter, R., Kodali, S., Galgoci, A., Collado, J., Tormo, J. R., Basilio, A., Vicente, F., Wang, J., Singh, S. B., 2006. Discovery of bacterial fatty acid synthase inhibitors from a *Phoma* species as antimicrobial agents using a new antisense-based strategy. *Journal of Natural Products* 69, 377-380.
- Orban, A., Hennicke, F., Rühl, M., 2020. Volatilomes of *Cyclocybe aegerita* during different stages of monokaryotic and dikaryotic fruiting. *Biological Chemistry*.
- Orsi, E., Beekwilder, J., van Gelder, D., van Houwelingen, A., Eggink, G., Kengen, S. W. M., Weusthuis, R. A., 2020. Functional replacement of isoprenoid pathways in *Rhodobacter sphaeroides*. *Microbial Biotechnology* 13, 1082-1093.
- Ouyang, X., Cha, Y., Li, W., Zhu, C., Zhu, M., Li, S., Zhuo, M., Huang, S., Li J., 2019. Stepwise engineering of *Saccharomyces cerevisiae* to produce (+)-valencene and its related sesquiterpenes. *RSC Adv.* 9, 30171–30181.
- Özaydin, B., Burd, H., Lee, T. S., Keasling, J. D., 2013. Carotenoid-based phenotypic screen of the yeast deletion collection reveals new genes with roles in isoprenoid production. *Metabolic Engineering* 15, 174-183.
- Paddon, C. J., Westfall, P. J., Pitera, D. J., Benjamin, K., Fisher, K., McPhee, D., Leavell, M. D., Tai, A., Main, A., Eng, D., Polichuk, D. R., Teoh, K. H., Reed, D. W., Treynor, T., Lenihan, J., Fleck, M., Bajad, S., Dang, G., Dengrove, D., Diola, D., Dorin, G., Ellens, K. W., Fickes, S., Galazzo, J., Gaucher, S. P., Geistlinger, T., Henry, R., Hepp, M., Horning, T., Iqbal, T., Jiang, H., Kizer, L., Lieu, B., Melis, D., Moss, N., Regentin, R., Secrest, S., Tsuruta, H., Vazquez, R., Westblade, L. F., Xu, L., Yu, M., Zhang, Y., Zhao, L., Lievense, J., Covello, P. S., Keasling, J. D., Reiling, K. K., Renninger, N. S., Newman, J. D., 2013. High-level semi-synthetic production of the potent antimalarial artemisinin. *Nature* 496, 528–532.
- Pan, Y., Lowary, T. D., Tykwinski, R. R., 2009. Naturally occurring and synthetic polyyne glycosides. *Canadian Journal of Chemistry* 87, 1565-1582.
- Panzer, S., Brych, A., Batschauer, A., Terpitz, U., 2019. Opsin 1 and Opsin 2 of the corn smut fungus *Ustilago maydis* are green light-driven proton pumps. *Frontiers in Microbiology* 10, 735.
- Parish, C. A., Huber, J., Baxter, J., González, A., Collado, J., Platas, G., Diez, M. T., Vicente, F., Dorso, K., Abruzzo, G., Wilson, K., 2004. A new ene-triptyc antibiotic from the fungus *Baeospora myosura*. *Journal of Natural Products* 67, 1900-1902.
- Pegler, D. N., 2002. Useful fungi of the world: the Ling-zhi – the mushroom of immortality. *Mycologist* 16, 100–101.

- Pereira, G., Tanaka, T. U., Nasmyth, K., Schiebel, E., 2001. Modes of spindle pole body inheritance and segregation of the Bfa1p-Bub2p checkpoint protein complex. *The EMBO Journal* 20, 6359-6370.
- Peretó, J., López-García, P., Moreira, D., 2005. Phylogenetic analysis of eukaryotic thiolases suggests multiple proteobacterial origins. *Journal of Molecular Evolution* 61, 65-74.
- Polakowski, T., Stahl, U., Lang, C., 1998. Overexpression of a cytosolic hydroxymethylglutaryl-CoA reductase leads to squalene accumulation in yeast. *Applied Microbiology and Biotechnology* 49, 66-71.
- Prado-Cabrero, A., Scherzinger, D., Avalos, J., Al-Babili, S., 2007. Retinal biosynthesis in fungi: characterization of the carotenoid oxygenase CarX from *Fusarium fujikuroi*. *Eukaryotic cell* 6, 650-657.
- Prado, M. M., Prado-Cabrero, A., Fernández-Martín, R., Avalos, J., 2004. A gene of the opsin family in the carotenoid gene cluster of *Fusarium fujikuroi*. *Current Genetics* 46, 47-58.
- Ram, S., Mitra, M., Shah, F., Tirkey, S. R., Mishra, S., 2020. Bacteria as an alternate biofactory for carotenoid production: A review of its applications, opportunities and challenges. *Journal of Functional Foods* 67, 103867.
- Ramos-Valdivia, A. C., van der Heijden, R., Verpoorte, R., 1997. Isopentenyl diphosphate isomerase: a core enzyme in isoprenoid biosynthesis. A review of its biochemistry and function. *Natural Product Reports* 14, 591-603.
- Rapier, S., Breheret, S., Talou, T., Pelissier, Y., Milhau, M., Bessiere, J. M., 1998. Volatile components of fresh *Agrocybe aegerita* and *Tricholoma sulfureum*. *Cryptogam. Mycol.* 19, 15-23.
- Regué, A., Bassié, L., de-Miguel, S., Colinas, C., 2019. Environmental and stand conditions related to *Fistulina hepatica* heart rot attack on *Castanea sativa*. *Forest Pathology* 49, e12517.
- Renault, H., Bassard, J. E., Hamberger, B., Werck-Reichhart, D., 2014. Cytochrome P450-mediated metabolic engineering: current progress and future challenges. *Current Opinion in Plant Biology* 19, 27-34.
- Reumann, S., Babujee, L., Ma, C., Wienkoop, S., Siemsen, T., Antonicelli, G. E., Rasche, N., Lüder, F., Weckwerth, W., Jahn, O., 2007. Proteome analysis of *Arabidopsis* leaf peroxisomes reveals novel targeting peptides, metabolic pathways, and defense mechanisms. *The Plant Cell* 19, 3170-3193.
- Reyes, L. H., Gomez, J. M., Kao, K. C., 2014. Improving carotenoids production in yeast via adaptive laboratory evolution. *Metabolic Engineering* 21, 26-33.
- Ro, D. K., Paradise, E. M., Ouellet, M., Fisher, K. J., Newman, K. L., Ndungu, J. M., Ho, K. A., Eachus, R. A., Ham, T. S., Kirby, J., Chang, M. C., Withers, S. T., Shiba, Y., Sarpong, R., Keasling, J. D., 2006. Production of the antimalarial drug precursor artemisinic acid in engineered yeast. *Nature* 440, 940-943.
- Rodríguez-Sáiz, M., Paz, B., De La Fuente, J. L., López-Nieto, M. J., Cabri, W., Barredo, J. L., 2004. *Blakeslea trispora* genes for carotene biosynthesis. *Applied and Environmental Microbiology* 70, 5589-5594.
- Rodriguez, S., Denby, C. M., Van Vu, T., Baidoo, E. E., Wang, G., Keasling, J. D., 2016. ATP citrate lyase mediated cytosolic acetyl-CoA biosynthesis increases mevalonate production in *Saccharomyces cerevisiae*. *Microbial Cell Factories* 15, 48.
- Rodriguez, S., Kirby, J., Denby, C. M., Keasling, J. D., 2014. Production and quantification of sesquiterpenes in *Saccharomyces cerevisiae*, including extraction, detection and quantification of terpene products and key related metabolites. *Nature Protocols* 9, 1980-1996.

- Roemer, T., Krysan, D. J., 2014. Antifungal drug development: challenges, unmet clinical needs, and new approaches. Cold Spring Harbor Perspectives in Medicine 4.
- Ron, E. Z., Rosenberg, E., 2001. Natural roles of biosurfactants. Environmental Microbiology 3, 229-236.
- Ruiz-Sola, M., Rodríguez-Concepción, M., 2012. Carotenoid biosynthesis in *Arabidopsis*: a colorful pathway. The Arabidopsis Book 10, e0158.
- Saiki, R. K., Scharf, S., Faloona, F., Mullis, K. B., Horn, G. T., Erlich, H. A., Arnheim, N., 1992. Enzymatic amplification of beta-globin genomic sequences and restriction site analysis for diagnosis of sickle cell anemia. 1985. Biotechnology (Reading, Mass.) 24, 476-480.
- Saini, R. K., Keum, Y. S., 2019. Microbial platforms to produce commercially vital carotenoids at industrial scale: an updated review of critical issues. Journal of Industrial Microbiology & Biotechnology 46, 657-674.
- Sambrook, J., Fritsch, E. F., Maniatis, T., 1989. Molecular cloning: A laboratory manual. New York, NY: Cold Spring Harbor Laboratory Press.
- Sambrook, J., Russell, D. , 2001. Molecular cloning: A laboratory manual. Cold Spring Harbor Laboratory Press, Cold Spring Harbor, New York.
- Sandargo, B., Chepkirui, C., Cheng, T., Chaverra-Munoz, L., Thongbai, B., Stadler, M., Huttel, S., 2019. Biological and chemical diversity go hand in hand: Basidiomycota as source of new pharmaceuticals and agrochemicals. Biotechnology Advances 37, 107344.
- Sandmann, G., 2009. Evolution of carotene desaturation: the complication of a simple pathway. Archives of Biochemistry and Biophysics 483, 169-174.
- Sanz, C., Rodríguez-Romero, J., Idnurm, A., Christie, J. M., Heitman, J., Corrochano, L. M., Eslava, A. P., 2009. Phycomyces MADB interacts with MADA to form the primary photoreceptor complex for fungal phototropism. Proc. Natl. Acad. Sci. U. S. A. 106, 7095-7100.
- Sanz, C., Velayos, A., Álvarez, M. I., Benito, E. P., Eslava, A. P., 2011. Functional analysis of the *Phycomyces carRA* gene encoding the enzymes phytoene synthase and lycopene cyclase. PLoS One 6, e23102.
- Sapir-Mir, M., Mett, A., Belausov, E., Tal-Meshulam, S., Frydman, A., Gidoni, D., Eyal, Y., 2008. Peroxisomal localization of *Arabidopsis* isopentenyl diphosphate isomerases suggests that part of the plant isoprenoid mevalonic acid pathway is compartmentalized to peroxisomes. Plant Physiology 148, 1219-1228.
- Sarkari, P., Reindl, M., Stock, J., Müller, O., Kahmann, R., Feldbrügge, M., Schipper, K., 2014. Improved expression of single-chain antibodies in *Ustilago maydis*. J. Biotechnol. 191, 165-175.
- Sauter, H., Steglich, W., Anke, T., 1999. Strobilurins: evolution of a new class of active substances. Angewandte Chemie (International ed. in English) 38, 1328-1349.
- Schempp, F. M., Drummond, L., Buchhaupt, M., Schrader, J., 2018. Microbial cell factories for the production of terpenoid flavor and fragrance compounds. Journal of Agricultural and Food Chemistry 66, 2247-2258.
- Scherer, M., Heimel, K., Starke, V., Kämper, J., 2006. The Clp1 protein is required for clamp formation and pathogenic development of *Ustilago maydis*. The Plant Cell 18, 2388-2401.
- Schilling, J. S., Kaffenberger, J. T., Liew, F. J., Song, Z., 2015. Signature wood modifications reveal decomposer community history. PLoS One 10, e0120679.
- Schlingmann, G., Milne, L., Pearce, C. J., Borders, D. B., Greenstein, M., Maiese, W. M., Carter, G. T., 1995. Isolation, characterization and structure of a new allenic polyine antibiotic produced by fungus LL-07F275. The Journal of Antibiotics 48, 375-379.



- Schmidt-Dannert, C., 2015. Biosynthesis of terpenoid natural products in fungi. *Advances in Biochemical Engineering/Biotechnology* 148, 19-61.
- Scholtmeijer, K., Cankar, K., Beekwilder, J., Wösten, H. A., Lugones, L. G., Bosch, D., 2014. Production of (+)-valencene in the mushroom-forming fungus *S. commune*. *Applied Microbiology and Biotechnology* 98, 5059-5068.
- Schultz, J., Milpetz, F., Bork, P., Ponting, C. P., 1998. SMART, a simple modular architecture research tool: identification of signaling domains. *Proc. Natl. Acad. Sci. U. S. A.* 95, 5857-5864.
- Schulz, B., Banuett, F., Dahl, M., Schlesinger, R., Schäfer, W., Martin, T., Herskowitz, I., Kahmann, R., 1990. The *b* alleles of *U. maydis*, whose combinations program pathogenic development, code for polypeptides containing a homeodomain-related motif. *Cell* 60, 295-306.
- Schulz, S., Girhard, M., Gaßmeyer, S. K., Jäger, V. D., Schwarze, D., Vogel, A., Urlacher, V. B., 2015. Selective enzymatic synthesis of the grapefruit flavor (+)-nootkatone. *ChemCatChem* 7, 601-604.
- Sharon-Asa, L., Shalit, M., Frydman, A., Bar, E., Holland, D., Or, E., Lavi, U., Lewinsohn, E., Eyal, Y., 2003. Citrus fruit flavor and aroma biosynthesis: isolation, functional characterization, and developmental regulation of *Cstps1*, a key gene in the production of the sesquiterpene aroma compound valencene. *The Plant Journal* 36, 664-674.
- Shi, B., Ma, T., Ye, Z., Li, X., Huang, Y., Zhou, Z., Ding, Y., Deng, Z., Liu, T., 2019. Systematic metabolic engineering of *Saccharomyces cerevisiae* for lycopene overproduction. *Journal of Agricultural and Food Chemistry* 67, 11148-11157.
- Shiao, M. S., 2003. Natural products of the medicinal fungus *Ganoderma lucidum*: occurrence, biological activities, and pharmacological functions. *Chem. Rec.* 3, 172-180.
- Shiba, Y., Paradise, E. M., Kirby, J., Ro, D. K., Keasling, J. D., 2007. Engineering of the pyruvate dehydrogenase bypass in *Saccharomyces cerevisiae* for high-level production of isoprenoids. *Metabolic Engineering* 9, 160-168.
- Simkin, A. J., Guirimand, G., Papon, N., Courdavault, V., Thabet, I., Ginis, O., Bouzid, S., Giglioli-Guivarc'h, N., Clastre, M., 2011. Peroxisomal localisation of the final steps of the mevalonic acid pathway in planta. *Planta* 234, 903-914.
- Spellig, T., Böcker, M., Lottspeich, F., Frank, R. W., Kahmann, R., 1994. Pheromones trigger filamentous growth in *Ustilago maydis*. *The EMBO Journal* 13, 1620-1627.
- Stadler, M., Hoffmeister, D., 2015. Fungal natural products-the mushroom perspective. *Frontiers in Microbiology* 6, 127.
- Stalpers, J. A., Vlug, I., 1983. *Confistulina*, the anamorph of *Fistulina hepatica*. *Canadian Journal of Botany* 61, 1660-1666.
- Steussy, C. N., Robison, A. D., Tetrack, A. M., Knight, J. T., Rodwell, V. W., Stauffacher, C. V., Sutherland, A. L., 2006. A structural limitation on enzyme activity: the case of HMG-CoA synthase. *Biochemistry* 45, 14407-14414.
- Stock, J., Sarkari, P., Kreibich, S., Brefort, T., Feldbrügge, M., Schipper, K., 2012. Applying unconventional secretion of the endochitinase Cts1 to export heterologous proteins in *Ustilago maydis*. *J. Biotechnol.* 161, 80-91.
- Stöckli, M., Morinaka, B. I., Lackner, G., Kombrink, A., Sieber, R., Margot, C., Stanley, C. E., deMello, A. J., Piel, J., Künzler, M., 2019. Bacteria-induced production of the antibacterial sesquiterpene lagopodin B in *Coprinopsis cinerea*. *Molecular Microbiology* 112, 605-619.
- Stoffels, P., Müller, M. J., Stachurski, S., Terfrüchte, M., Schröder, S., Ihling, N., Wierckx, N., Feldbrügge, M., Schipper, K., Büchs, J., 2020. Complementing the intrinsic repertoire of *Ustilago maydis* for degradation of the pectin backbone polygalacturonic acid. *J. Biotechnol.* 307, 148-163.



- Subramaniam, S., Selvaduray, K. R., Radhakrishnan, A. K., 2019. Bioactive compounds: natural defense against cancer?. *Biomolecules* 9.
- Subramanian, V., Yadav, J. S., 2008. Regulation and heterologous expression of P450 enzyme system components of the white rot fungus *phanerochaete chrysosporium*. *Enzyme and Microbial Technology* 43, 205-213.
- Suffness, M., 1995. *Taxol : science and applications*. CRC Press, Boca Raton.
- Szabó, Z., Tönnis, M., Kessler, H., Feldbrügge, M., 2002. Structure-function analysis of lipopeptide pheromones from the plant pathogen *Ustilago maydis*. *Molecular Genetics and Genomics* 268, 362-370.
- Tayrov, A., Azevedo, S., Herzog, R., Vogt, E., Arzt, S., Lüthy, P., Müller, P., Rühl, M., Hennicke, F., Künzler, M., 2019. Heterologous production and functional characterization of ageritin, a novel type of ribotoxin highly expressed during fruiting of the edible mushroom *Agrocybe aegerita*. *Applied and Environmental Microbiology* 85, e01549-01519.
- Teichmann, B., Linne, U., Hewald, S., Marahiel, M. A., Bölker, M., 2007. A biosynthetic gene cluster for a secreted cellobiose lipid with antifungal activity from *Ustilago maydis*. *Molecular Microbiology* 66, 525-533.
- Teichmann, B., Liu, L., Schink, K. O., Bölker, M., 2010. Activation of the ustilagic acid biosynthesis gene cluster in *Ustilago maydis* by the C<sub>2</sub>H<sub>2</sub> zinc finger transcription factor Rua1. *Applied and Environmental Microbiology* 76, 2633-2640.
- Terakita, A., 2005. The opsins. *Genome Biology* 6, 213.
- Terfrüchte, M., Joehnk, B., Fajardo-Somera, R., Braus, G. H., Riquelme, M., Schipper, K., Feldbrügge, M., 2014. Establishing a versatile Golden Gate cloning system for genetic engineering in fungi. *Fungal Genetics and Biology* 62, 1-10.
- Terfrüchte, M., Reindl, M., Jankowski, S., Sarkari, P., Feldbrügge, M., Schipper, K., 2017. Applying unconventional secretion in *Ustilago maydis* for the export of functional nanobodies. *International Journal of Molecular Sciences* 18.
- Terfrüchte, M., Wewetzer, S., Sarkari, P., Stollewerk, D., Franz-Wachtel, M., Macek, B., Schlepütz, T., Feldbrügge, M., Büchs, J., Schipper, K., 2018. Tackling destructive proteolysis of unconventionally secreted heterologous proteins in *Ustilago maydis*. *J. Biotechnol.* 284, 37-51.
- Thompson, S. L., Krisans, S. K., 1990. Rat liver peroxisomes catalyze the initial step in cholesterol synthesis. The condensation of acetyl-CoA units into acetoacetyl-CoA. *The Journal of Biological Chemistry* 265, 5731-5735.
- Tran, A., 2019. The N-end rule pathway and Ubr1 enforce protein compartmentalization via P2-encoded cellular location signals. *Journal of Cell Science* 132.
- Trikka, F. A., Nikolaidis, A., Athanasakoglou, A., Andreadelli, A., Ignea, C., Kotta, K., Argiriou, A., Kampranis, S. C., Makris, A. M., 2015. Iterative carotenogenic screens identify combinations of yeast gene deletions that enhance sclareol production. *Microbial Cell Factories* 14, 60.
- Troost, K., Loeschcke, A., Hilgers, F., Özgür, A. Y., Weber, T. M., Santiago-Schübel, B., Svensson, V., Hage-Hülsmann, J., Habash, S. S., Grundler, F. M. W., Schleker, A. S. S., Jaeger, K. E., Drepper, T., 2019. Engineered *Rhodobacter capsulatus* as a phototrophic platform organism for the synthesis of plant sesquiterpenoids. *Frontiers in Microbiology* 10, 1998.
- Tsuge, N., Mori, T., Hamano, T., Tanaka, H., Shin-ya, K., Seto, H., 1999. Cinnatriacetins A and B, new antibacterial triacetylene derivatives from the fruiting bodies of *Fistulina hepatica*. *The Journal of Antibiotics* 52, 578-581.
- Tyers, M., Wright, G. D., 2019. Drug combinations: a strategy to extend the life of antibiotics in the 21st century. *Nature reviews. Microbiology* 17, 141-155.

- Ukibe, K., Katsuragi, T., Tani, Y., Takagi, H., 2008. Efficient screening for astaxanthin-overproducing mutants of the yeast *Xanthophyllomyces dendrorhous* by flow cytometry. *FEMS Microbiology Letters* 286, 241-248.
- Varshavsky, A., 1996. The N-end rule: functions, mysteries, uses. *Proc. Natl. Acad. Sci. U. S. A.* 93, 12142-12149.
- Varshavsky, A., 2011. The N-end rule pathway and regulation by proteolysis. *Protein Science* 20, 1298-1345.
- Varshavsky, A., 2019. N-degron and C-degron pathways of protein degradation. *Proc. Natl. Acad. Sci. U. S. A.* 116, 358-366.
- Vaz, J. A., Barros, L., Martins, A., Morais, J. S., Vasconcelos, M. H., Ferreira, I. C. F. R., 2011. Phenolic profile of seventeen Portuguese wild mushrooms. *LWT - Food Science and Technology* 44, 343-346.
- Velayos, A., Blasco, J. L., Alvarez, M. I., Iturriaga, E. A., Eslava, A. P., 2000a. Blue-light regulation of phytoene dehydrogenase (*carB*) gene expression in *Mucor circinelloides*. *Planta* 210, 938-946.
- Velayos, A., Eslava, A. P., Iturriaga, E. A., 2000b. A bifunctional enzyme with lycopene cyclase and phytoene synthase activities is encoded by the *carRP* gene of *Mucor circinelloides*. *European Journal of Biochemistry* 267, 5509-5519.
- Vellai, T., Vida, G., 1999. The origin of eukaryotes: the difference between prokaryotic and eukaryotic cells. *Proceedings. Biological Sciences* 266, 1571-1577.
- Vollmeister, E., Schipper, K., Baumann, S., Haag, C., Pohlmann, T., Stock, J., Feldbrügge, M., 2012. Fungal development of the plant pathogen *Ustilago maydis*. *FEMS Microbiology Reviews* 36, 59-77.
- Voynova, N. E., Rios, S. E., Miziorko, H. M., 2004. *Staphylococcus aureus* mevalonate kinase: isolation and characterization of an enzyme of the isoprenoid biosynthetic pathway. *Journal of Bacteriology* 186, 61-67.
- Walsh, C. T., Schonbrunn, A., Lockridge, O., Massey, V., Abeles, R. H., 1972. Inactivation of a flavoprotein, lactate oxidase, by an acetylenic substance. *Journal of Biological Chemistry* 247, 6004-6006.
- Wang, C., Zhao, S., Shao, X., Park, J. B., Jeong, S. H., Park, H. J., Kwak, W. J., Wei, G., Kim, S. W., 2019. Challenges and tackles in metabolic engineering for microbial production of carotenoids. *Microbial Cell Factories* 18, 55.
- Wang, J., Holden, D. W., Leong, S. A., 1988. Gene transfer system for the phytopathogenic fungus *Ustilago maydis*. *Proc. Natl. Acad. Sci. U. S. A.* 85, 865-869.
- Wang, M., Wang, D., Zhang, Q., Chai, J., Peng, Y., Cai, X., 2017a. Identification and cytochemical immunolocalization of acetyl-CoA acetyltransferase involved in the terpenoid mevalonate pathway in *Euphorbia helioscopia* laticifers. *Bot Stud* 58, 62.
- Wang, Y., Pang, J., Zheng, Y., Jiang, P., Gong, W., Chen, X., Chen, D., 2017b. Genetic manipulation of the bifunctional gene, *carRA*, to enhance lycopene content in *Blakeslea trispora*. *Biochemical Engineering Journal* 119, 27-33.
- Wang, Z., Wang, J., Li, N., Li, J., Trail, F., Dunlap, J. C., Townsend, J. P., 2018. Light sensing by opsins and fungal ecology: NOP-1 modulates entry into sexual reproduction in response to environmental cues. *Molecular Ecology* 27, 216-232.
- Werner, N., Gómez, M., Baeza, M., Cifuentes, V., Alcaíno, J., 2016. Functional characterization of thiolase-encoding genes from *Xanthophyllomyces dendrorhous* and their effects on carotenoid synthesis. *BMC Microbiology* 16, 278.

- White, T. C., Holleman, S., Dy, F., Mirels, L. F., Stevens, D. A., 2002. Resistance mechanisms in clinical isolates of *Candida albicans*. *Antimicrobial Agents and Chemotherapy* 46, 1704-1713.
- Wierckx, N., Agrimi, G., Lübeck, P. S., Steiger, M. G., Mira, N. P., Punt, P. J., 2020. Metabolic specialization in itaconic acid production: a tale of two fungi. *Current opinion in Biotechnology* 62, 153-159.
- Willke, T., Vorlop, K. D., 2001. Biotechnological production of itaconic acid. *Applied Microbiology and Biotechnology* 56, 289-295.
- Winterberg, B., Uhlmann, S., Linne, U., Lessing, F., Marahiel, M. A., Eichhorn, H., Kahmann, R., Schirawski, J., 2010. Elucidation of the complete ferrichrome A biosynthetic pathway in *Ustilago maydis*. *Molecular Microbiology* 75, 1260-1271.
- Withers, S. T., Keasling, J. D., 2007. Biosynthesis and engineering of isoprenoid small molecules. *Applied Microbiology and Biotechnology* 73, 980-990.
- Wu, S., Krings, U., Zorn, H., Berger, R. G., 2005. Volatile compounds from the fruiting bodies of beefsteak fungus *Fistulina hepatica* (Schaeffer: Fr.) Fr. *Food Chemistry* 92, 221-226.
- Wu, S., Zorn, H., Krings, U., Berger, R. G., 2007. Volatiles from submerged and surface-cultured beefsteak fungus, *Fistulina hepatica*. *Flavour and Fragrance Journal* 22, 53-60.
- Xiao, H., Zhong, J. J., 2016. Production of useful terpenoids by higher-fungus cell factory and synthetic biology approaches. *Trends in Biotechnology* 34, 242-255.
- Xu, X., Cao, X., Yang, J., Chen, L., Liu, B., Liu, T., Jin, Q., 2019. Proteome-wide identification of lysine propionylation in the conidial and mycelial stages of *Trichophyton rubrum*. *Frontiers in Microbiology* 10, 2613.
- Ye, L., Lv, X., Yu, H., 2016. Engineering microbes for isoprene production. *Metabolic Engineering* 38, 125-138.
- Yee, D. A., DeNicola, A. B., Billingsley, J. M., Creso, J. G., Subrahmanyam, V., Tang, Y., 2019. Engineered mitochondrial production of monoterpenes in *Saccharomyces cerevisiae*. *Metabolic Engineering* 55, 76-84.
- Zarnack, K., Feldbrügge, M., 2010. Microtubule-dependent mRNA transport in fungi. *Eukaryotic cell* 9, 982-990.
- Zarnack, K., Maurer, S., Kaffarnik, F., Ladendorf, O., Brachmann, A., Kämper, J., Feldbrügge, M., 2006. Tetracycline-regulated gene expression in the pathogen *Ustilago maydis*. *Fungal Genetics and Biology* 43, 727-738.
- Zhang, C., Chen, X., Orban, A., Shukal, S., Birk, F., Too, H. P., Rühl, M., 2020. *Agrocybe aegerita* serves as a gateway for identifying sesquiterpene biosynthetic enzymes in higher fungi. *ACS Chemical Biology* 15, 1268-1277.
- Zhang, C., Hong, K., 2020. Production of terpenoids by synthetic biology approaches. *Frontiers in Bioengineering and Biotechnology* 8, 347.
- Zhang, F., Vierock, J., Yizhar, O., Fenno, L. E., Tsunoda, S., Kianianmomeni, A., Prigge, M., Berndt, A., Cushman, J., Polle, J., Magnuson, J., Hegemann, P., Deisseroth, K., 2011. The microbial opsin family of optogenetic tools. *Cell* 147, 1446-1457.
- Zhao, R.-L., Li, G.-J., Sánchez-Ramírez, S., Stata, M., Yang, Z.L., Wu, G., Dai, Y. C., He, S. H., Cui, B. K., Zhou, J. L., Wu, F., He, M. Q., Moncalvo, J. M., Hyde, K. D., 2017. A six-gene phylogenetic overview of *Basidiomycota* and allied phyla with estimated divergence times of higher taxa and a phyloproteomics perspective. *Fungal Diversity* 84, 43-74.
- Zheng, W., Sun, F., Bartlam, M., Li, X., Li, R., Rao, Z., 2007. The crystal structure of human isopentenyl diphosphate isomerase at 1.7 Å resolution reveals its catalytic mechanism in isoprenoid biosynthesis. *Journal of Molecular Biology* 366, 1447-1458.

- Zhou, L., Obhof, T., Schneider, K., Feldbrügge, M., Nienhaus, G. U., Kämper, J., 2018. Cytoplasmic transport machinery of the SPF27 homologue Num1 in *Ustilago maydis*. *Scientific Reports* 8, 3611.
- Zhu, B. C., Henderson, G., Chen, F., Maistrello, L., Laine, R. A., 2001. Nootkatone is a repellent for Formosan subterranean termite (*Coptotermes formosanus*). *Journal of Chemical Ecology* 27, 523-531.
- Zhu, X., Li, X., Chen, Z., 2020. Inhibition of anticancer growth in Retinoblastoma cells by naturally occurring sesquiterpene nootkatone is mediated via autophagy, endogenous ROS production, cell cycle arrest and inhibition of NF-κB signalling pathway. *Journal of B.U.ON.* 25, 427-431.
- Zigmantas, D., Hiller, R. G., Sundstrom, V., Polivka, T., 2002. Carotenoid to chlorophyll energy transfer in the peridinin-chlorophyll-a-protein complex involves an intramolecular charge transfer state. *Proc. Natl. Acad. Sci. U. S. A.* 99, 16760-16765.

## 6 Appendix

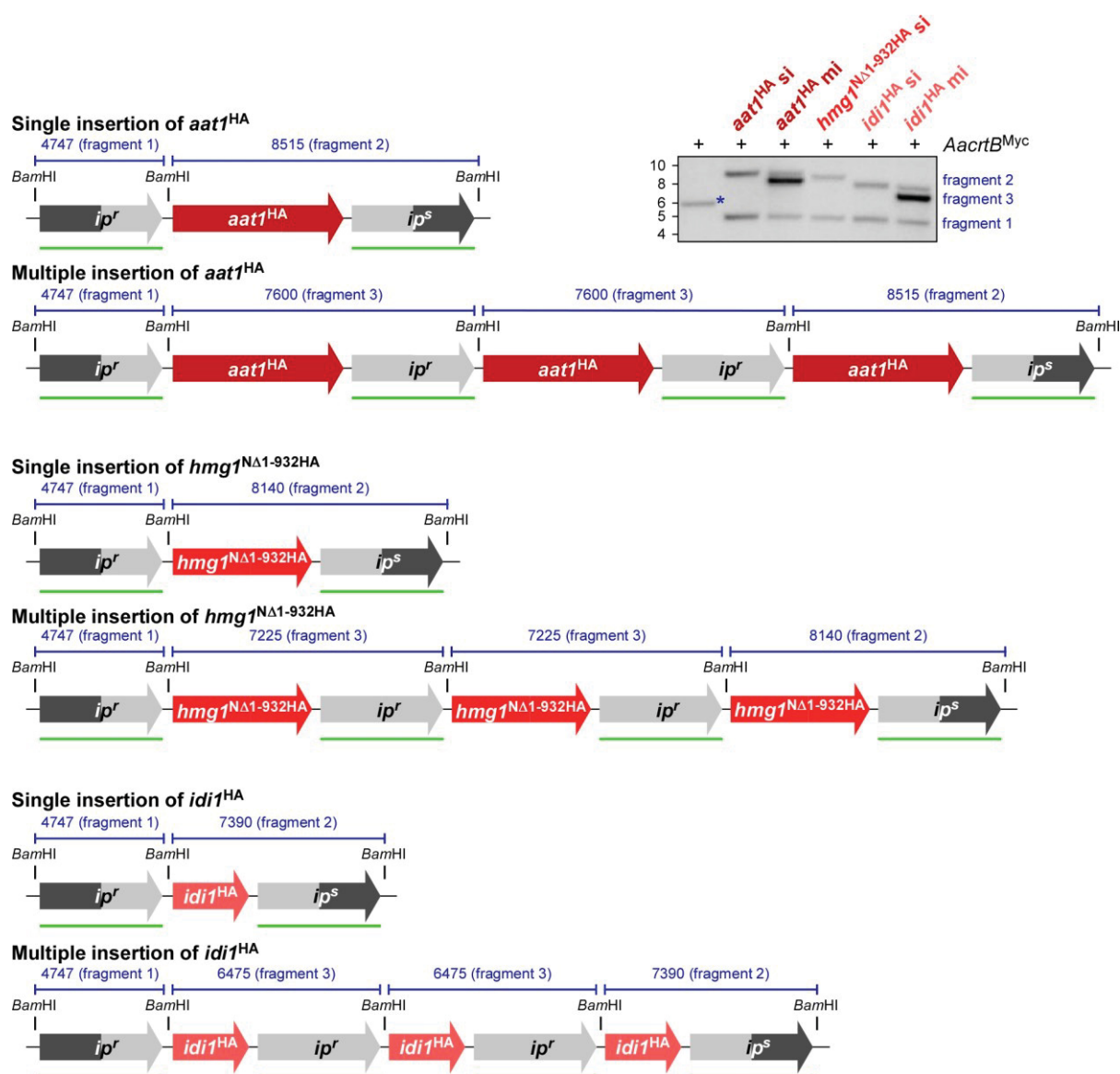


**Figure 6.1 Graphical representation of the genetic modification at the *ip<sup>s</sup>* locus encoding an iron-sulfur protein conferring carboxin resistance for genetic engineering of the mevalonate pathway.**

The expected gene structure for *aat1*<sup>HA</sup>, *hmg1*<sup>NΔ1-932</sup>, and *idi1*<sup>HA</sup> are given. Single and multiple insertions are compared. For the sake of clarity, the Southern blot shown in Figure 2.11B is given in the right upper corner. The wild type (*wt*) version encoding a sensitive version *ip<sup>s</sup>* is given in dark grey. The corresponding resistant version is given in light grey (*ip<sup>r</sup>*). The expected fragments are given in blue. Note that due to the repetition during multiple insertions, the intensity of fragment 3 is always the strongest. The probe used for hybridization is indicated as a green line. This figure is derived from Lee et al., 2020a (Supplementary Figure S2C).



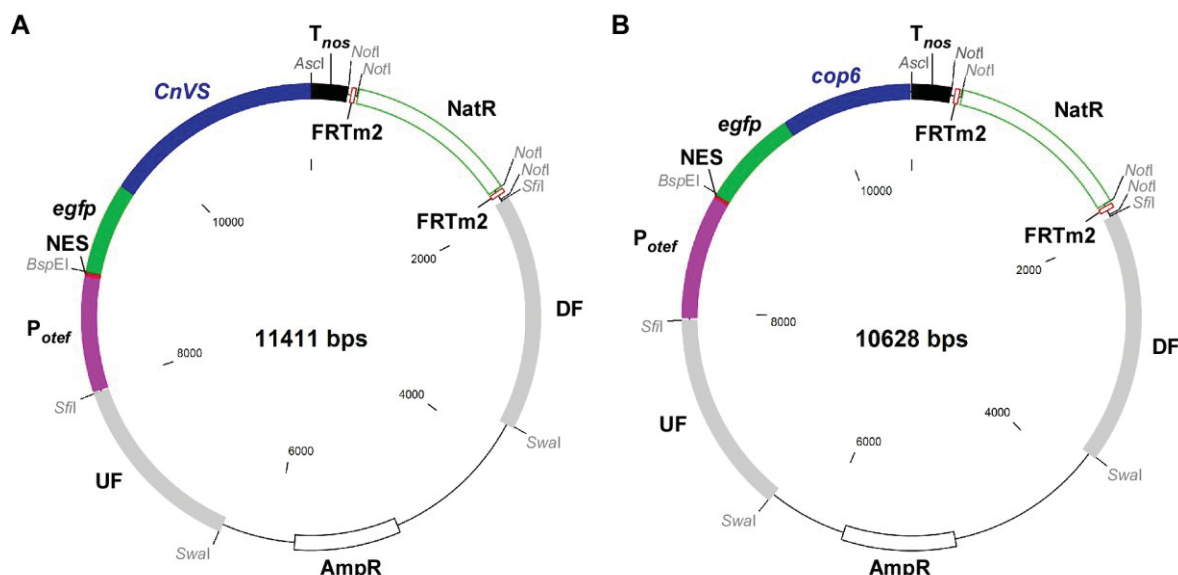


**Figure 6.2 Plasmid maps for the expression of heterologous genes encoding plant and fungal sesquiterpenoid synthases in *U. maydis*.**

(A) Plasmid (pUMa4499) for the heterologous production of (+)-valencene synthase CnVS from *C. nootkatensis*. The heterologous gene encoding CnVS (closed blue box) was dicodon optimized. CnVS is N-terminally fused to eGFP<sup>NES</sup> (closed green and red boxes). The nuclear export signal (NES; closed red box) is from murine minute virus (MTKKFGTLTI; Engelsma et al., 2008). The expression of the construct is under control of the constitutively active promoter  $P_{otef}$  (closed magenta box) and the transcriptional termination is facilitated by  $T_{nos}$  (closed black box). UF and DF (closed grey boxes) are the flanking regions for homologous recombination at the *upp3* locus. The flanking regions are exchangeable with *SfiI* restriction enzyme cutting sites. For plasmid linearization to transform into a protoplast of *U. maydis* strain, *SwaI* restriction enzyme cutting sites were used. AmpR (open white box) represents an ampicillin resistance gene encoding  $\beta$ -lactamase enzyme for cloning. The NatR resistance cassette (open green box) is flanked by FRTm2 sites (open red boxes) for recycling by Flp recombinase (Khrunyk et al., 2010). The expression of the nourseothricin resistance gene derived from *S. noursei* is under the control of  $P_{gap1}$  derived from UMAG\_00343 and the transcription termination is facilitated by  $T_{cyc1}$  from *S. cerevisiae* (Brachmann, 2001). (B) Plasmid (pUMa4136) for the heterologous production of  $\alpha$ -cuprenene synthase Cop6 from *C. cinerea*. The heterologous gene encoding Cop6 (closed blue box) was dicodon optimized. Cop6 is N-terminally fused to eGFP<sup>NES</sup> (closed green and red boxes). The nuclear export signal (NES; closed red box) is from murine minute virus (MTKKFGTLTI; Engelsma et al., 2008). The expression of the construct is under control of the constitutively active promoter  $P_{otef}$  (closed magenta box) and the transcriptional termination is facilitated by  $T_{nos}$  (closed black box). UF and DF (closed grey boxes) are the flanking regions for homologous recombination at the *upp3* locus. The flanking regions are exchangeable with *SfiI* restriction enzyme cutting sites. For plasmid linearization to transform into a protoplast of *U. maydis* strain, *SwaI* restriction enzyme cutting sites were used. AmpR (open white box) represents an ampicillin resistance gene encoding  $\beta$ -lactamase enzyme for cloning. The NatR resistance cassette (open green box) is flanked by FRTm2 sites (open red boxes) for recycling by Flp recombinase (Khrunyk et al., 2010). The expression of the nourseothricin resistance gene derived from *S. noursei* is under the control of  $P_{gap1}$  derived from UMAG\_00343 and the transcription termination is facilitated by  $T_{cyc1}$  from *S. cerevisiae* (Brachmann, 2001).

Table 6.1 Codon optimized DNA sequences for expression in *U. maydis*.

<b>Phytoene synthase AaCrtB from <i>Agrobacterium aurantiacum</i></b>
ATGTCGGACCTGGTTCTTACGTCTACCGAAGCTATTACACAAGGCTCGCAGTCGTTTCGCTACAGCGGCGAAGCTTATGC CTCCTGGCATCCGCGACGATACAGTCATGCTCTATGCGTGGTGCCGTCATGCTGATGACGTGATTGATGGTCAGGCGCT CGGAAGCCGTCGCCGAGGCGGTGAACGACCCACAAGCTCGCCTTGATGGACTCCGCGCAGACACCCTGGCCGCCCTTC AGGGTGATGGTCCGGTGACCCCTCCATTTGCTGCATTGCGAGCCGTGGCAGCAGACACGATTTCTCAAGCGTGCG CTATGGATCTCATTGAGGGTTTCGCAATGGATGTTGAGGCTCGTGATTACCGTACACTCGACGACGTGCTGGAGTACAG CTATCATGTTGCCGAATTGTCGGCGTCATGATGCCCCGAGTCATGGGTGTCGCGATGATCCTGTGTTGGACCGAGC CTGTGACCTGGGTCTGGCATTCCAGCTGACAAATATCGCACGCGACGTATCGACGACGCTCGAATTGGACGATGCTAC CTTCCAGGAGACTGGCTGGACCAAGCGGGCGCACGAGTGGACGGACCAAGTCCAAGCCCAGAGCTTTACACCGTCATT TTGCGTCTGTTGGACGCGAGCCGAATTGTATTACGCCTCTGCACGAGTTGGCTTGGCAGATTTGCCCTCCGCGATGCGCGT GGAGCATCGCCGCTGCACTCCGCATCTATCGTGCCATTGGACTGCGTATCCGCAAAGGAGGACCAGAGGCATACCGTC AACGTATTTCCACTTCCAAAGCTGCTAAAATTGGACTCCTGGGCAATTGGCGGCTGGGACGTTGCACGACGCCGCTCCC CGGCGCGGGTGTACGCCCAAGGCTGTGGACTCGACCGCACCATGCATAG
<b>(+)-valencene synthase CnVS from <i>Callitropsis nootkatensis</i></b>
ATGGCCGAGATGTTCAACGGCAACTCGAGCAACGACGGCTCGTCGTGTATGCCCGTCAAGGACGCGCTGCGCCGCAC CGGCAACCACCACCCCAACCTCTGGACCGACGACTTTATCCAGTCGCTCAACTCGCCCTACTCGGACTCGTCGTACCAC AAGCACCGCGAGATCCTCATCGACGAGATCCGCGACATGTTCTCCAACGGCGAGGGCGACGAGTTCGGTGTGCTCGAG AACATCTGGTTCTGCGACGTCTCCAGCGTCTCGGCATCGACCGCACTTCCAGGAGGATCAAGACGGCGCTCGAC TACATCTACAAGTTCTGGAACACGATTTCGATCTTTGGCGACCTCAACATGGTCGCTCTCGGTTTCCGCATCTCGCTCT CAACCGCTACGTCGCTTCGAGCGACGTCTTCAAGAAGTTCAAGGGCGAGGAGGGTCAGTTCTCGGGCTTCGAGTCGTC CGACCAGGACGCCAAGCTCGAAATGATGCTCAACCTGTACAAGGCTTCCGAGCTCGACTTCCCCGACGAGGACATTCT CAAGGAGGCGCGTGCTTTTGTTCGATGTACCTCAAGCACGTATCAAGGAGTACGGTGACATCCAGGAGAGCAAGAA CCCGCTGCTCATGGAGATCGAGTACACCTTCAAGTACCCTTGGCGTTGGCGTCTGCCCGCTCTCGAGGCGTGGAACCTT ATCCACATCATGCGTCAGCAGGACTGCAACATCTCGCTCGCCAACAACCTCTACAAGATCCCCAAGATCTACATGAAAAA GATCCTCGAGCTCGCCATCCTCGACTTCAACATCCTCCAGTCGCAGCACCAGCAGAGATGAAGCTCATCTCGACCTGG TGGAAGAACTCGTCGGCCATCCAGCTCGACTTTTCCGTCAACCGCCACATCGAGTCGTAATCTGGTGGGCTCGCCCC TCTTCGAGCCCGAGTTCTCGACGTGCCGTCATCAACTGCACCAAGCTCTCGACCAAGATGTTCTCTCGACGACATCTA CGACACCTACGGCACCGCTCGAAGAGCTCAAGCCCTTACCACACGCTCACCCGCTGGGACGTCTCGACCGTCGACAA CCACCCCGACTACATGAAGATCGCCTTCAACTTTAGCTACGAGATCTACAAGGAGATCGCCTCGGAAGCTGAGCGCAAG CACGGTCTTTTGTCTACAAGTACCTCCAGTCGTGCTGGAAGTCGTACATCGAGGCGTACATGCAGGAGGCCGAGTGG ATCGCGACAACCACTGCTGGTTTCGACGAGTACCTCATGAACGGTGTCAAGTCGTGGGTATGCGCATCCTCATGA TTCACGCGCTCATCCTCATGGACACGCCGCTCTCCGACGAGATTCTCGAACAGCTCGACATCCCTTCGTGCAAGTCGCA GGCTCTGCTCTCGCTCATACGCGTCTCGTCGACGACGTCAAGGACTTTGAAGACGAGCAGGCGCATGGCGAGATGGC TTCGTGATCGAGTGCTACATGAAGGACAACCACGGTTCGACGCGCGAGGATGCGCTCAACTACCTCAAGATCCGCAT CGAGTCGTGCGTCCAGGAGCTCAACAAGGAGTTGCTCGAGCCCTCGAACATGCACGGCTCGTTCCGCAACCTCTACCT CAACGTCGGCATGCGTGTCTCTTTCATGCTCAACGACGGTGACCTTTCACCCACTCGAACCCGAAGGAGATCCAG GACGCCATACCAAGTTCTTTGTCGAGCCCATCATCCCCTGA
<b>The fungal <math>\alpha</math>-cuprenene synthase Cop6 from <i>Coprinopsis cinerea</i></b>
ATGCCTGCTGCTCTGCCCTACAACGTCTCGCGCGACAACAAGTGGGATATCAAGAAGATCATCCAGGACTTTTTCAAGC GCTGCGATGTGCCCTACCAGGTATCCCTACGACACCGAGCTCTGGAACGCCTGCCTCAAGCGTGCCAAGGAGAAGG GCTACCCCGTCGAGCCCGACTCGCCCATGTGCTCTACCGCAGCTTCAAGGTGCGGTGTCGTCATCACGCGCACCTCGT ACGGTACATCCAGGACTACGAGATCCTCATCTGGGTCCGACCTTACCAGCCTTTGTCACCTACGCCGACGACGCTT CCAGGAGGACATCCAGCACCTCCACAGCTTCGCTCGCACCTTCTCCAGAACGAAAAGCAGCAGGATCCCGTCCGTCGA GGCCTTTGCCAGTTTCTGCGCGAGTCGTGATCCGATTCTCGCACTTTGTGCGCAACACCGTCTGCTCGTGGCGCT GCGCTTCATGATGTGATCGCGCTCGAGTTCGAGGGTCAGAACGTCTCGGTCTCGACCGAGGCGCGTGAGTACCCTGG CTACATCCGCATCCTCTCGGGTCTCTCGGACATCTACGCGCTTTCGCCCTTCCCATGGACCTGCCGCGTTCCACCTAC ATCCAGGCCCTTCCCCGAGCAGATCGACTACATCAACGGCACCAACGACCTGCTCTGTTCTACAAGGAGGAGCTCGACT GCGAGACCGTCAACTTTATCTCGGCCGCTGCCACCTCGCAGCAGGTGAGCAAGCTCGAGGTGCTGCGCAACGCCGCC GAGAAGGCCGCTACTCGTACGACGTCTGTCGTAACGTGCTCAAGCCCTACCCCGAGGCGCTTGGCGCCTGGAAGTC GTTTGCTCGCGGCTTCTGCTACTTCCACACCTCGTCGCCACGCTACCGTCTCGGCGAGATGTTCCACGACTTTGAGCAC GACCTCGTCTGCAAGTGCGCCTCGTGACCGAGATCTGA

This table is derived from Lee et al., 2020a (Supplementary Table S5).

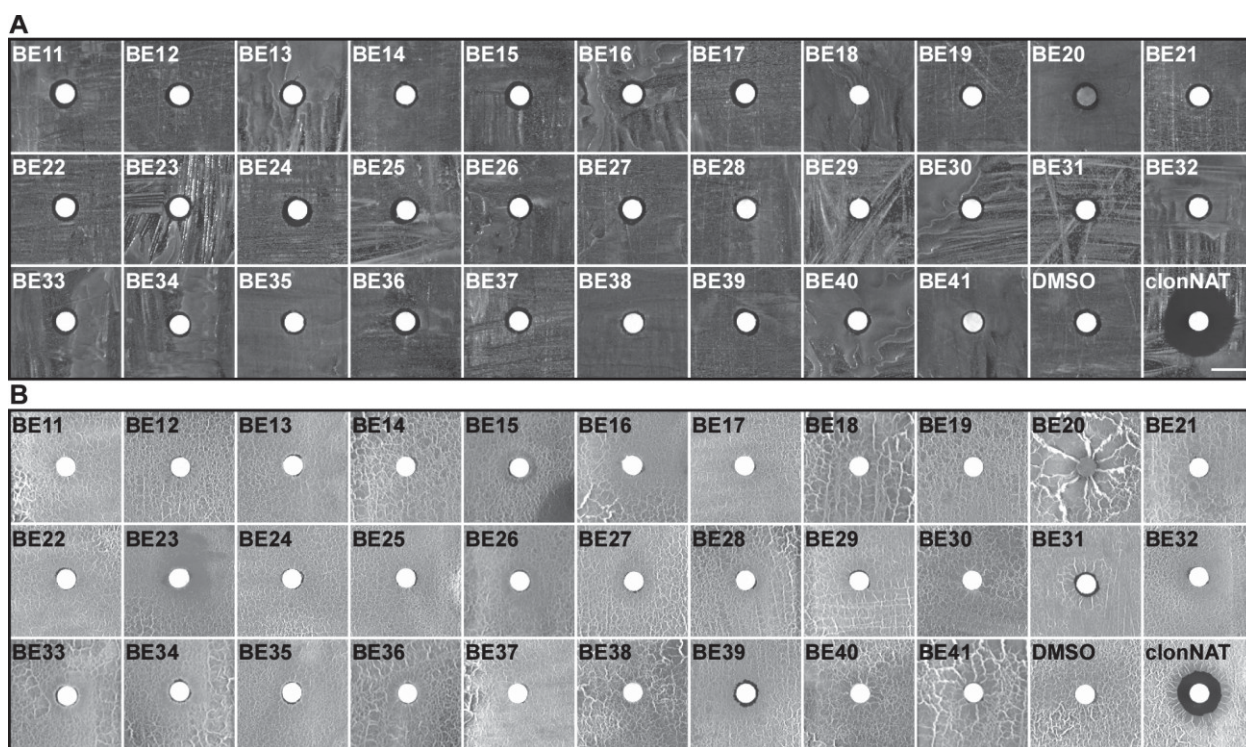


**Figure 6.3 Bioactivity test basidiomycete crude extracts.**

Bioactivity against *S. cerevisiae* (A) and *U. maydis* (B). 100 µg of each basidiomycete crude extract (BE11-BE41) was dissolved in DMSO to impregnate the filter paper disk. DMSO was used instead of such an extract as negative control and 200 µg of clonNAT dissolved in ddH<sub>2</sub>O was used as the positive control, respectively. The size bar represents 1 cm. Three independent biological experiments ( $n=3$ ) were carried out. This figure is derived from Lee et al., 2020b (Supplementary Figure S1).

**Table 6.2 Basidiomycete mushroom strain extracts (BE01-41) for bioactivity test against *S. cerevisiae* and *U. maydis*.**

Extract No.	Species	Strain-ID	Collector's ID	Medium	DNA status	Geographic and ecological data
BE01	<i>Armillaria ostoyae</i>	P089	MG091007_08	PDA	WT, dikaryon	2009-10-07, Göttingen, Kerstlingeröder Feld, under <i>Pinus nigra</i> , terricolous (tc), leg., det. Dr. M. Gube
BE02	<i>Armillaria cf. ostoyae</i>	P145	MG100927_01	PDA	WT, dikaryon	2010-09-27, Grobsdorf, Nordhalde, lignicolous (lc), stump of <i>Tilia</i> sp., mixed forest, about 1,2 km S Grobsdorf, leg., det. Dr. M. Gube
BE03	<i>Coprinopsis atramentaria</i>	P125	MG131118_01	PDA	WT, dikaryon	2013-11-18, Jena, Beutenbergcampus, half buried softwood, lc, leg., det. Dr. M. Gube
BE04	<i>Coprinopsis picacea</i>	P106	MG131125_01	PDA	WT, dikaryon	2013-11-25, Göttingen, municipal forest, about 1 km W of Göttingen-Herberhausen, <i>Fagus sylvatica</i> forest, tc, leg., det. Dr. M. Gube
BE05	<i>Fistulina hepatica</i>	P052	FH130818_01	PDA	WT, dikaryon	2013-08-18, Jena, 1 km SW of "Steinkreuz Ziegenhain", <i>Fagus sylvatica</i> forest, lc, stump of <i>Quercus</i> sp., leg., det. Dr. F. Hennicke
BE06	<i>Flammulina velutipes</i>	P111	MG091201_01	PDA	WT, dikaryon	2009-12-01, Jena, Cospedaer Grund, lc, <i>Fraxinus excelsior</i> stump, leg., det. Dr. M. Gube
BE07	<i>Fomes fomentarius</i>	P116	MG120305_02	PDA	WT, dikaryon	2012-03-05, Jonsdorf, Weißer Stein, lc, on <i>Betula pendula</i> wood, leg., det. Dr. M. Gube
BE08	<i>Pleurotus dryinus</i>	P090	MG091118_01	PDA	WT, dikaryon	2009-11-18, Dederstedt, lc, living stem of <i>Fraxinus excelsior</i> , leg., det. Dr. habil. H. Dörfelt

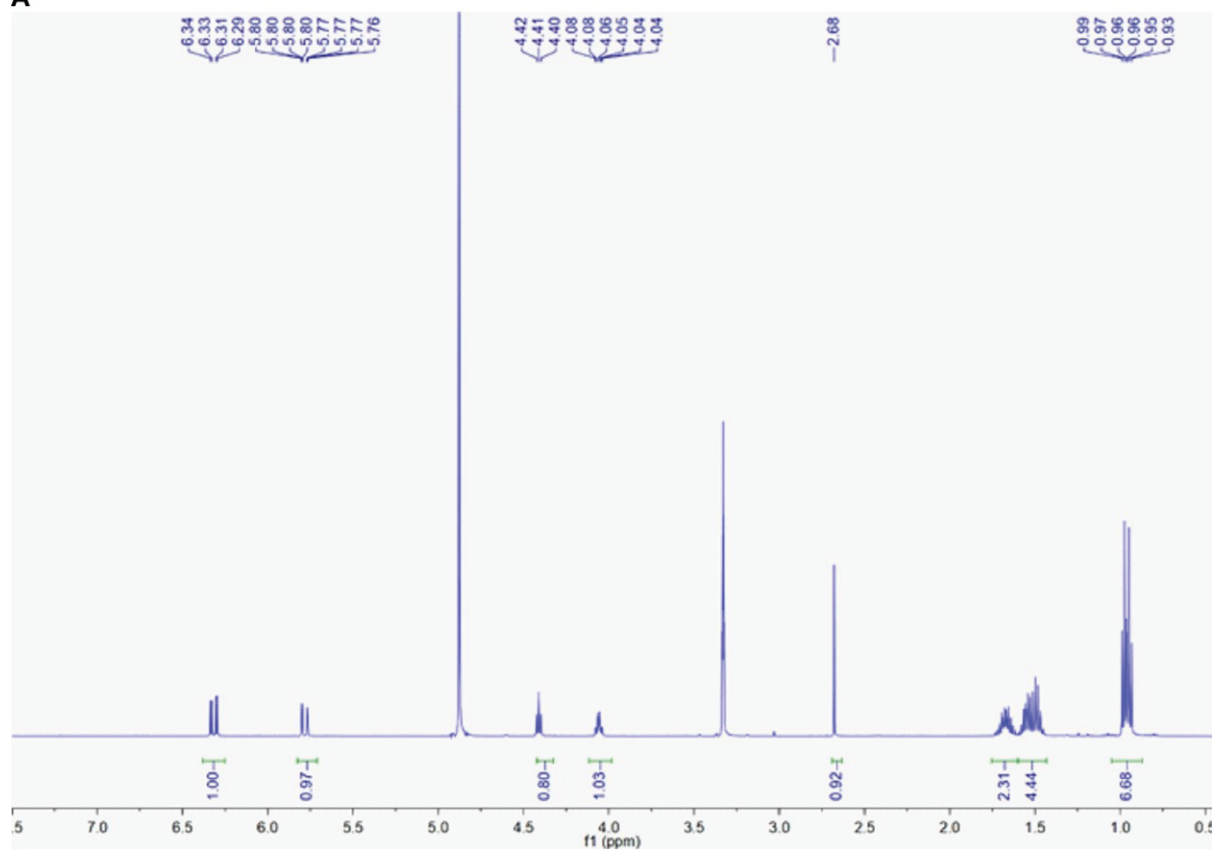
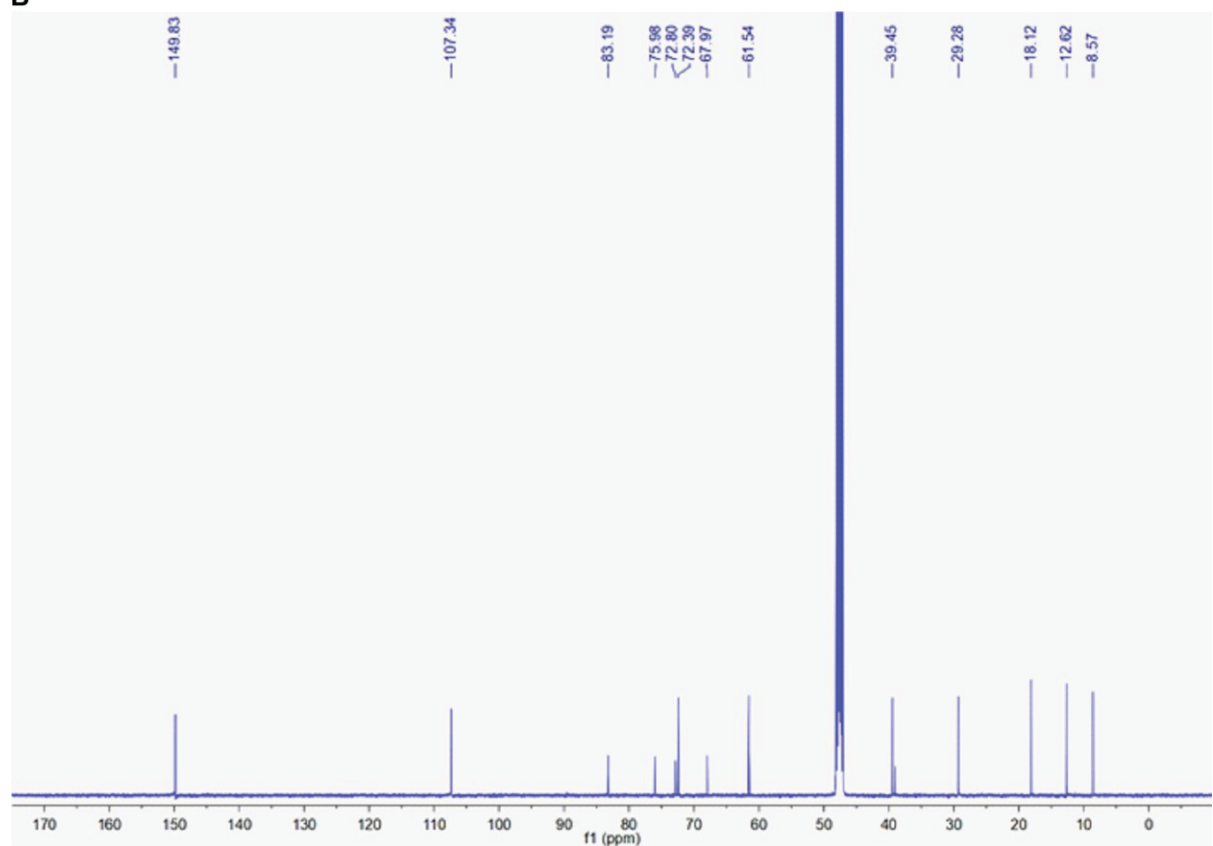
BE09	<i>Pleurotus cf. pulmonarius</i>	P046	FH130913_01	PDA	WT, dikaryon	2013-09-13, Oberursel (Hohe Mark), Taunus, mixed <i>Fagus sylvatica</i> forest, lc, on <i>Fagus sylvatica</i> wood, leg., det. Dr. F. Henniecke
BE10	<i>Pleurotus ostreatus</i>	P118	MG120730_01	PDA	WT, dikaryon	2012-07-30, Bad Karlshafen, Hannoversche Klippen, about 1,5 km NW Bad Karlshafen, lc, <i>Fagus sylvatica</i> wood, leg., det. Dr. M. Gube
BE11	<i>Agaricus arvensis</i>	P151	MG090923_04	PDA	WT, dikaryon	2009-09-23, Kauern, Nordhalde, about 1 km S of Grobsdorf, mixed forest, terricolous (tc), leg., det. Dr. M. Gube
BE12	<i>Agaricus augustus</i>	P096	MG100812_01	PDA	WT, dikaryon	2010-08-12, Maria Laach, about 2.5 km NE of Maria Laach, mixed <i>Fagus sylvatica</i> forest, tc, leg., det. Dr. M. Gube
BE13	<i>Agaricus augustus</i>	P148	MG131025_01	PDA	WT, dikaryon	2013-10-25, Göttingen, Brüder-Grimm-Allee, tc, under <i>Tilia</i> sp., leg., det. Dr. M. Gube
BE14	<i>Auricularia auricula-judae</i>	P093	MG091207_01	PDA	WT, dikaryon	2009-12-07, Jena, Mühlital, lignicolous (lc), <i>Sambucus nigra</i> wood, leg., det. Dr. M. Gube
BE15	<i>Bovista nigrescens</i>	P123	MG130923_01	PDA	WT, dikaryon	2013-09-23, Rothesütte, about 500 m SE of Rothesütte, tc, pasture, leg., det. Dr. M. Gube
BE16	<i>Clitocybe geotropa</i>	P149	MG131202_01	PDA	WT, dikaryon	2013-12-02, Göttingen, municipal forest, close to Göttingen-Herberhausen, beech forest, tc, leg., det. Dr. M. Gube
BE17	<i>Clitocybe odorata</i>	P053	FH130907_01	PDA	WT, dikaryon	2013-09-07, Morgenröthe (MTB:5540/24, 630-640 m above sea level), tc, needle litter (leg. P. Wagner & K. Schneider, det. C. Morgner)
BE18	<i>Galerina marginata</i>	P057	FH130913_05	PDA	WT, dikaryon	2013-09-13, Oberursel (Hohe Mark), Taunus, mixed <i>Fagus sylvatica</i> forest, lc, <i>Picea abies</i> wood, leg., det. Dr. F. Henniecke
BE19	<i>Ganoderma lucidum</i>	P095	MG100717_01	PDA	WT, dikaryon	2010-07-17, Königsfeld/SW, about 500 m N of Königsfeld, lc, stump of <i>Quercus</i> sp., leg., det. Dr. M. Gube
BE20	<i>Gloeophyllum odoratum</i>	P124	MG131104_01	PDA	WT, dikaryon	2013-11-04, Jena, Mühlital, lc, <i>Picea abies</i> stump, leg., det. Dr. M. Gube
BE21	<i>Hypholoma fasciculare</i>	P099	MG100907_06	PDA	WT, dikaryon	2010-09-07, Grobsdorf, Nordhalde, about 750 m SE of Grobsdorf, in mixed forest, lc, <i>Quercus</i> sp. stump, (leg., det. M. Gube, AG Kothe)
BE22	<i>Hypholoma sublateralium</i>	P169	MG140217_05	PDA	WT, dikaryon	2014-02-17, Closewitz, 200 m S of Closewitz, <i>Quercus</i> spp. forest, lc, on stump of <i>Quercus</i> sp., leg., det. Dr. M. Gube
BE23	<i>Inonotus obliquus</i>	P150	MG140106_01	PDA	WT, dikaryon	2014-01-06, Oybin, Töpfer/Brandhöhe, lc, on <i>Betula pendula</i> wood, leg., det. Dr. M. Gube
BE24	<i>Kuehneromyces mutabilis</i>	P050	FH130913_02	PDA	WT, dikaryon	2013-09-13, Oberursel (Hohe Mark), Taunus, mixed <i>Fagus sylvatica</i> forest, lc, on <i>Fagus sylvatica</i> wood, leg., det. Dr. F. Henniecke
BE25	<i>Langermannia gigantea</i>	P051	FH130817_01	PDA	WT, dikaryon	2013-08-17, southern Bad Berka, tc, garden lawn, leg., det. Dr. F. Henniecke
BE26	<i>Lycoperdon excipuliforme</i>	P122	MG130912_01	PDA	WT, dikaryon	2013-09-12, Grobsdorf, about 800 m S of Grobsdorf, tc, under scattered individuals of <i>Betula pendula</i> , leg., det. Dr. M. Gube
BE27	<i>Lycoperdon molle</i>	P154	MG100812_04	PDA	WT, dikaryon	2010-08-12, Maria Laach, Laacher-See-Haus, about 1.3 km SE of Maria Laach, tc, on a path in a beech forest, leg., det. Dr. M. Gube
BE28	<i>Macrolepiota procera</i>	P097	MG100816_03	PDA	WT, dikaryon	2010-08-16, Maria Laach, about 2.5 km NE of Maria Laach, mixed <i>Fagus sylvatica</i> forest, tc, leg., det. Dr. M. Gube
BE29	<i>Macrolepiota procera</i>	P130	MG090925_01	PDA	WT, dikaryon	2009-09-25, Kauern, Nordhalde, about 1.2 km S of Grobsdorf, mixed forest, tc, leg., det. Dr. M. Gube
BE30	<i>Marasmius oreades</i>	P144	MG100908_03	PDA	WT, dikaryon	2010-09-08, Grobsdorf, Nordhalde, tc, grassy forest margin, about 1 km S of Grobsdorf, leg., det. Dr. M. Gube



BE31	<i>Marasmius scorodoni</i>	P055	FH130913_03	PDA	WT, dikaryon	2013-09-13, Oberursel (Hohe Mark), Taunus, mixed <i>Fagus sylvatica</i> forest, tc, <i>Fagus sylvatica</i> leaf litter, leg., det. Dr. F. Henniecke
BE32	<i>Megacollihya platyphylla</i>	P026	T1509	PDA	WT, dikaryon	2013-05-27, Taunus, experimental plot of Dr. M. Piepenbring (Goethe University Frankfurt, Germany), tc, leaf litter, leg., det. Dr. F. Henniecke
BE33	<i>Pleurotus ostreatus</i>	P114	MG110802_02	PDA	WT, dikaryon	2011-08-02, Maria Laach, Laacher-See-Haus, about 1.3 km SE Maria Laach, lc, on <i>Fagus sylvatica</i> wood, leg., det. Dr. M. Gube
BE34	<i>Pleurotus ostreatus</i>	P119	MG130823_01	PDA	WT, dikaryon	2013-08-23, Rosdorf, Kiessee, lc, on wood of <i>Salix</i> sp., leg., det. Dr. M. Gube
BE35	<i>Pleurotus ostreatus</i>	P128	MG140106_03	PDA	WT, dikaryon	2014-01-06, Hainewalde, near graveyard, lc, stump of <i>Populus x canadensis</i> , leg., det. Dr. M. Gube
BE36	<i>Polyporus brumalis</i>	P117	MG120305_01	PDA	WT, dikaryon	2012-03-05, Göttingen, municipal forest, about 1.5 km SW of Göttingen-Herberhausen, mixed beech forest, lc, wood litter of <i>Tilia</i> sp., leg., det. Dr. M. Gube
BE37	<i>Polyporus tuberaster</i>	P036	FH130818_02	PDA	WT, dikaryon	2013-08-18, Jena, about 300 m S of "Steinkreuz Ziegenhain", <i>Fagus sylvatica</i> forest, lc, on soft wood, leg., det. Dr. F. Henniecke
BE38	<i>Sarcomyxa serotina</i>	P126	MG131125_04	PDA	WT, dikaryon	2013-11-25, Göttingen, municipal forest, about 800 m W of Göttingen-Herberhausen, mixed <i>Fagus sylvatica</i> forest, lc, stump of <i>Fagus sylvatica</i> , leg., det. Dr. M. Gube
BE39	<i>Stropharia aeruginosa</i>	P102	MG101006_02	PDA	WT, dikaryon	2010-10-06, Jenaprießnitz, Tännicht, tc, <i>Fagus sylvatica</i> forest, leg., det. Dr. M. Gube
BE40	<i>Trametes gibbosa</i>	P129	Pr13Gr4	PDA	WT, dikaryon	2013-03-17, Jena, Mühlital, about 1.3 km SW of Cospeda, wood of <i>Fagus sylvatica</i> , leg., det. Dr. M. Gube (within a students' practical of the University of Jena, Germany)
BE41	<i>Tricholomopsis rutilans</i>	P056	FH130913_04	PDA	WT, dikaryon	2013-09-13, Oberursel (Hohe Mark), Taunus, mixed <i>Fagus sylvatica</i> forest, lc, <i>Fagus sylvatica</i> wood (?), leg., det. Dr. F. Henniecke

This table is derived from Lee et al., 2020b (Table 1).



**A****B**



E

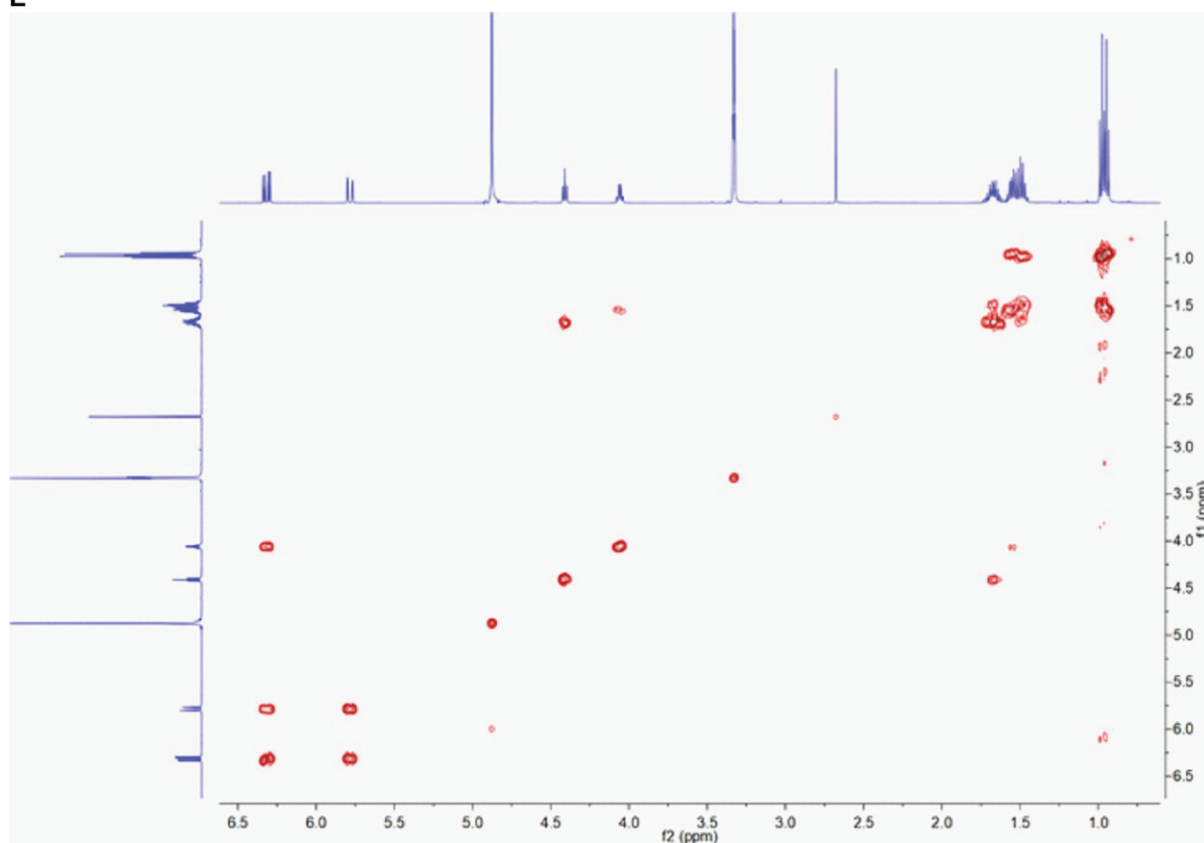


**Figure 6.4 NMR spectra of feldin.**

(A)  $^1\text{H}$  NMR spectrum of feldin in  $\text{MeOH-}d_4$ . (B)  $^{13}\text{C}$  NMR spectrum of feldin in  $\text{MeOH-}d_4$ . (C) HSQC spectrum of feldin in  $\text{MeOH-}d_4$ . (D) HMBC spectrum of feldin in  $\text{MeOH-}d_4$ . (E)  $^1\text{H-}^1\text{H}$  COSY spectrum of feldin in  $\text{MeOH-}d_4$ . This figure is derived from Lee et al., 2020b (Supplementary Figure S3-7).

## Author contributions

Parts of this dissertation were submitted for publications.

- Lee, J., Hilgers, F., Loeschke, A., Jaeger, K. E., Feldbrügge, M., 2020, *Ustilago maydis* serves as a novel production host for the synthesis of plant and fungal sesquiterpenoids. *Frontiers in Microbiology* 11, 1655.

J. Lee performed the experiments in this publication as follows.

- The generation of plasmids and strains (see Materials and Methods)
- Bioinformatics analysis (Figure 2.1; Table 2.1; Figure 2.2-9)
- Lycopene extraction and quantification (Figure 2.10; Figure 2.11D; Figure 2.12; Figure 2.14D; Figure 2.16D)
- Fluorimetric measurements (Figure 2.13A; Figure 2.14A; Figure 2.16A)
- Southern blot analysis (Figure 2.11A-B; Appendix Figure 6.1)
- Western blot analysis (Figure 2.11C; Figure 2.13B; Figure 2.14B, Figure 2.16B)
- Fluorescence microscopy (Figure 2.13C-D; Figure 2.14C; Figure 2.16C)
- The heterologous production of (+)-valencene and  $\alpha$ -cuprenene in *U. maydis* and quantification of the titers (Figure 2.14; Figure 2.15; Figure 2.16; Figure 2.17).

J. Lee, Dr. A. Loeschke, Prof. Dr. K. E. Jaeger, and Prof. Dr. M. Feldbrügge designed and planned the study.

J. Lee, F. Hilgers, Dr. A. Loeschke, Prof. Dr. K. E. Jaeger, and Prof. Dr. M. Feldbrügge analyzed the data. J. Lee and Prof. Dr. M. Feldbrügge designed and revised the manuscript for the publication (Lee et al., 2020a). Prof. Dr. M. Feldbrügge directed the project. All authors contributed to the article and approved the submitted version.

J. Lee quantified the heterologous production of (+)-valencene and  $\alpha$ -cuprenene with F. Hilgers and Dr. A. Loeschke (Institute of Molecular Enzyme Technology, Heinrich-Heine-University Düsseldorf, Forschungszentrum Jülich GmbH, Jülich, Germany) who supported GC-FID analysis (Figure 2.15C-E; Figure 2.17C-D). In addition, Dr. K. Müntjes helped with microscopic analysis (Figure 2.13C-D; Figure 2.14C; Figure 2.16C) and provided a control strain expressing *gfp* (UMa2179; see Table 4.7-8). Dr. S. Jankowski generated Gfp-SKL (UMa2386; see Table 4.7-8) and Pex3-Gfp (UMa1951; see Table 4.7-8) strains for peroxisomal localization studies. K. Hußnätter provided information on the promoter  $P_{rpl40}$ . B. D. Anderson studied additional ribosomal promoters with RISE-DAAD scholarship. Prof. Dr. V. D. Urlacher and A. Kokorin (Institute of Biochemistry II, Heinrich-Heine-University Düsseldorf, Düsseldorf, Germany) supported the GC-MS analysis (Figure 2.15A-B; Figure 2.17A-B).

- Lee, J., Shi, Y., Grün, P., Gube, M., Feldbrügge, M., Bode, H. B., Hennicke, F., 2020, Identification of feldin, an antifungal polyine from the beefsteak fungus *Fistulina hepatica*. Biomolecules 10, 1502.

J. Lee performed the experiments in this publication as follows.

- Characterization of *F. hepatica* via microscopy (Figure 2.19C-D)
- Large scale cultivation of *F. hepatica*
- Extraction and fractionation of *F. hepatica* crude extract
- Isolation of feldin from *F. hepatica* crude extract
- Bioactivity test (Figure 2.18; Figure 2.20A-B; Appendix Figure 6.3)

J. Lee, Dr. Y. Shi, P. Grün, Dr. M. Gube, Prof. Dr. M. Feldbrügge, Prof. Dr. H. B. Bode, and Dr. F. Hennieke designed and planned the study. J. Lee, Dr. Y. Shi, P. Grün, Dr. M. Gube, Prof. Dr. M. Feldbrügge, Prof. Dr. H. B. Bode, and Dr. F. Hennieke analyzed the data. Prof. Dr. M. Feldbrügge, Prof. Dr. H. B. Bode, and Dr. F. Hennieke directed the project. In addition, Dr. F. Hennieke (Department of Geobotany, Ruhr-University Bochum, Bochum, Germany) performed the Isolation and characterization of *F. hepatica* (Figure 2.19), and coordinated the fungal strain collection at the Department of Mycology of the Goethe University with Prof. Dr. M. Piepenbring (Goethe University Frankfurt, Frankfurt am Main, Germany) and Dr. M. Gube (Soil Science of Temperate Ecosystems, Georg-August University Göttingen, Göttingen, Germany; Appendix Table 6.2). The initial mushroom extraction (Appendix Table 6.2), extraction and fractionation of *F. hepatica* crude extract, isolation of feldin, and structure elucidation of feldin (Figure 2.20C; Table 2.2; Appendix Figure 6.4) were conducted in cooperative work with Prof. Dr. H. B. Bode, Dr. Y. Shi, and Peter Grün (Institute of Molecular Biosciences, Goethe University Frankfurt, Frankfurt am Main, Germany).

This declaration is intended to clarify the use of figures and sections from the publications.



## Additional contributions

Additional publications were achieved during this doctoral research, but the information is not included in this thesis.

J. Lee collaborated with Prof. Dr. P. Proksch, Dr. F. Pan, and Dr. H. Harwoko (Institute for Pharmaceutical Biology and Biotechnology, Heinrich-Heine-University Düsseldorf, Düsseldorf, Germany) for the discovery of noble bioactive compounds from fungi. For the following publications, J. Lee conducted the antifungal assays against *S. cerevisiae* and *U. maydis* with fungal secondary metabolites and determined their minimum inhibitory concentration (MIC) values.

- Harwoko, H., Daletos, G., Stuhldreier, F., **Lee, J.**, Wesselborg, S., Feldbrügge, M., Müller, W. E. G., Kalscheuer, R., Ancheeva, E., Proksch, P., 2019, Dithiodiketopiperazine derivatives from endophytic fungi *Trichoderma harzianum* and *Epicoccum nigrum*. Nat. Prod. Res. 1-9
- Pan, F., El-Kashef, D. H., Kalscheuer, R., Müller, W. E. G., **Lee, J.**, Feldbrügge, M., Mándi, A., Kurtán, T., Liu, Z., Wu, W., Proksch, P., 2020, Cladosins L-O, new hybrid polyketides from the endophytic fungus *Cladosporium sphaerospermum* WBS017. Eur. J. Med. Chem. 191, 112159
- Harwoko, H., **Lee, J.**, Hartmann, R., Mándi, A., Kurtán, T., Müller, W. E. G., Feldbrügge, M., Kalscheuer, R., Ancheeva, E., Daletos, G., Frank, M., Liu, Z., Proksch, P., 2020, Azacoccones F–H, new flavipin-derived alkaloids from an endophytic fungus *Epicoccum nigrum* MK214079. Fitoterapia, 104698

## Acknowledgement

The work was funded by the Deutsche Forschungsgemeinschaft under Germany's Excellence Strategy EXC-2048/1 - Project ID 39068111. The scientific activities of the Bioeconomy Science Center were financially supported by the Ministry of Culture and Science within the framework of the NRW Strategieprojekt BioSC (No. 313/323-400-002 13).

First of all, I would like to thank Prof. Dr. M. Feldbrügge for giving me the chance to study the topics of my Ph.D. thesis at Institute for Microbiology of Heinrich-Heine-University Düsseldorf.

I acknowledge lab members and BioSC FocusLab CombiCom project members for valuable discussion. I am grateful to Dr. L. Bismar, Dr. F. Hennicke, and Dr. T. Drepper for continuous support. B. D. Anderson assisted the project within the framework of a RISE-DAAD scholarship.

I furthermore express my sincere gratitude to Prof. Dr. Meike Piepenbring (Goethe University Frankfurt, Frankfurt am Main, Germany) for giving me access to the fungal strain collection at the Department of Mycology of the Goethe University where the culture of *Fistulina hepatica* P052 is maintained. I also thank Prof. Dr. Erika Kothe (Institute of Microbiology, Friedrich Schiller University Jena, Jena, Germany) for her support of Dr. M. Gube's sampling activities of basidiomycete mushrooms, not least at the former uranium mining site in Eastern Thuringia (near Ronneburg), and the permission of including the thereof isolated strains in this study. In addition, I cordially thank Dr. H. Dörfelt (Institute of Microbiology, Friedrich Schiller University Jena, Jena, Germany) for providing me a strain of *Pleurotus dryinus* and Dr. F. Surup (HZI Braunschweig, Braunschweig, Germany) for providing me information about polyines.

I specially thank Prof. Dr. P. Proksch and Dr. H. Harwoko (Institute for Pharmaceutical Biology and Biotechnology, Heinrich-Heine-University Düsseldorf, Düsseldorf, Germany), Prof. Dr. H. B. Bode and Peter Grün (Institute of Molecular Biosciences, Goethe University Frankfurt, Frankfurt am Main, Germany) for inspiring me and instructing me how to study fungal bioactive compounds.

Here, I wish to thank Prof. Dr. Cheong Gang-Won, Prof. Dr. V. F. Wendisch, Prof. Dr. J. Frunzke, and especially Prof. Dr. M. Feldbrügge for their kind guidance to develop my scientific career.

I also like to thank my family. My mother always gives me unconditional love and encourages me to study what I want to study. My brother has become a good friend since my childhood and inspired me to have curiosity in nature. I thank D. Kalens, G. Skinner, and their families for their supports to have a dream.

## Lee, Jungho

Date of birth June 5th, 1989  
Place of birth Daegu, South Korea  
Nationality South Korea

## Education

10/2016-present	Doctoral candidate, Biology, Institute for Microbiology, Heinrich-Heine-University Düsseldorf, Düsseldorf, Germany
4/2015-9/2016	M.Sc. International Master program of Biology, Heinrich-Heine-University Düsseldorf, Düsseldorf, Germany
1/2011-11/2011	Language course. Completed Level 5 of 5, Tutorium in Intensive English, University of Illinois at Chicago, Chicago, IL, USA
3/2008-8/2012	B.Sc. Biochemistry, Gyeongsang National University, Jinju, South Korea

## Additional education courses

BioSC International Online Summer School 2020, From plants to pilot plant – Holistic process development in a sustainable bioeconomy, Virtual events at Forschungszentrum Jülich / RWTH Aachen / Campus Klein-Altendorf Bonn, Germany
BioBased1x: Biobased Products for a Sustainable (Bio)economy DelftXRWTHx, an online learning initiative of Delft and RWTH Aachen
Good Scientific Practice for (Post) Doctoral Researchers iGRAD, Heinrich-Heine-University Düsseldorf, Düsseldorf, Germany
BioSC Analytics workshop for the Young Researchers of CombiCom IBOC, Forschungszentrum Jülich, Jülich, Germany

## Work experience

10/2016-09/2020	<b>Research topic:</b> The biosynthesis of plant and fungal sesquiterpenoids in <i>Ustilago maydis</i> and discovery of a bioactive compound from <i>Fistulina hepatica</i> Institute for Microbiology, Heinrich-Heine-University Düsseldorf, Düsseldorf, Germany Advisor: Prof. Dr. Michael Feldbrügge
11/2015-7/2016	<b>Research topic:</b> Construction of genetic toggle switches for application in <i>Corynebacterium glutamicum</i> Institute of Bio- and Geosciences 1, IBG-1: Biotechnology, Forschungszentrum Jülich, Jülich, Germany Advisor: Prof. Dr. Julia Frunzke
5/2015-8/2015 (12weeks)	<b>Research topic:</b> Co-cultivation of <i>Corynebacterium glutamicum</i> and <i>Ustilago maydis</i> Institute of Microbiology, Heinrich-Heine-University Düsseldorf, Düsseldorf, Germany Advisors: Prof. Dr. Michael Feldbrügge and Prof. Dr. Julia Frunzke
4/2014-2/2015	<b>Research topic:</b> Improvement of putrescine and GABA production by <i>Corynebacterium glutamicum</i> The Wendisch Lab, Genetics of Prokaryotes, University of Bielefeld, Bielefeld, Germany Advisor: Prof. Dr. Volker F. Wendisch

10/2013- 1/2014	<b>Research topic:</b> Ectopic expression and functions of olfactory receptors Laboratory of Sensory Biology, Department of Brain Science, Daegu Gyeongbuk Institute of Science & Technology (DGIST), Daegu, South Korea Advisor: Prof. Dr. JaeHyung Koo
3/2009- 12/2010	<b>Research topic:</b> Characterization of heat shock proteins from <i>Thermococcus kodakarensis</i> KOD1 Structural Biochemistry Laboratory, Department of Biochemistry, Gyeongsang National University, Jinju, South Korea Advisor: Prof. Dr. Cheong Gang-Won

### Presentations (conference contributions)

Talk	Fruiting body development and chemical defense in basidiomycetes, Florian Hennicke and <b>Jungho Lee</b> , 3rd Boletus-Tagung/ Vortrags- und Exkursionstagung der ThAM, Bad Blankenburg, Germany
Talk	Establishing <i>Ustilago maydis</i> as a basidiomycete production platform for sesquiterpene production via pathway engineering, 30th Fungal Genetics Conference, Asilomar, CA, USA
Talk	Establishing <i>Ustilago maydis</i> as a basidiomycete production platform for the production of novel bioactive compounds, <i>Ustilago</i> -Smut Convergence Workshop, Asilomar, CA, USA
Poster	Establishing the basidiomycete <i>Ustilago maydis</i> as a production platform for novel bioactive compounds, Peter Stoffels, <b>Jungho Lee</b> , Marta Rodríguez Estévez, Helge. B. Bode, Florian Hennicke, Michael Feldbrügge, and Kerstin Schipper, 4th International BioSC Symposium, Cologne, Germany
Poster	Identification of novel bioactive compounds from basidiomycetes for production in <i>Ustilago maydis</i> , <b>Lee, J.</b> , Harwoko, H., Proksch, P., Bode, H.B., Feldbrügge, M., and Hennicke, F., 30th Fungal Genetics Conference, Asilomar, CA, USA
Poster	Establishing <i>Ustilago maydis</i> as a basidiomycete production platform for sesquiterpene production via pathway engineering, <b>Lee, J.</b> , Hennicke, F., and Feldbrügge, M., 30th Fungal Genetics Conference, Asilomar, CA, USA
Poster	Establishing a basidiomycete host for sesquiterpene production and Identification of future target compounds in <i>Ustilago maydis</i> , <b>Jungho Lee</b> , Harwoko Harwoko, Carl Haag, Helge B. Bode, Peter Proksch, Florian Hennicke, and Michael Feldbrügge, 3rd International BioSC Symposium, Bonn, Germany
Poster	Establishing a basidiomycete host for sesquiterpene production and identification of future target compounds in <i>Ustilago maydis</i> , <b>Jungho Lee</b> , Carl Haag, and Michael Feldbrügge, 2nd international BioSC Symposium, Cologne, Germany
Poster	Establishing a basidiomycete host for sesquiterpene production and identification of future target compounds in <i>Ustilago maydis</i> , <b>Jungho Lee</b> , Carl Haag, and Michael Feldbrügge, 2nd International Bioeconomy Congress, Stuttgart-Hohenheim, Germany
Poster	Identification of the biological role of the RNA-binding protein Khd4 during pathogenic development of the plant pathogen <i>Ustilago maydis</i> , <b>Jungho Lee</b> , Carl Haag, Evelyn Vollmeister, and Michael Feldbrügge, DGHM & VAAM conference 2017, Würzburg, Germany

## Publications

<p><b>Lee, J.</b>, Shi, Y., Grün, P., Feldbrügge, M., Bode, H. B., Hennicke, F., 2020, Identification of feldin, an antifungal polyine from the beefsteak fungus <i>Fistulina hepatica</i>. <i>Biomolecules</i> 10, 1502.</p>
<p><b>Lee, J.</b>, Hilgers, F., Loeschke, A., Jaeger, K. E., Feldbrügge, M., 2020, <i>Ustilago maydis</i> serves as a novel production host for the synthesis of plant and fungal sesquiterpenoids. <i>Frontiers in Microbiology</i> 11, 1655</p>
<p>Harwoko, H., <b>Lee, J.</b>, Hartmann, R., Mándi, A., Kurtán, T., Müller, W. E. G., Feldbrügge, M., Kalscheuer, R., Ancheeva, E., Daletos, G., Frank, M., Liu, Z., Proksch, P., 2020, Azacoccones F–H, new flavipin-derived alkaloids from an endophytic fungus <i>Epicoccum nigrum</i> MK214079. <i>Fitoterapia</i>, 104698</p>
<p>Pan, F., El-Kashef, D. H., Kalscheuer, R., Müller, W. E. G., <b>Lee, J.</b>, Feldbrügge, M., Mándi, A., Kurtán, T., Liu, Z., Wu, W., Proksch, P., 2020, Cladosins L–O, new hybrid polyketides from the endophytic fungus <i>Cladosporium sphaerospermum</i> WBS017. <i>Eur. J. Med. Chem.</i> 191, 112159</p>
<p>Harwoko, H., Daletos, G., Stuhldreier, F., <b>Lee, J.</b>, Wesselborg, S., Feldbrügge, M., Müller, W. E. G., Kalscheuer, R., Ancheeva, E., Proksch, P., 2019, Dithiodiketopiperazine derivatives from endophytic fungi <i>Trichoderma harzianum</i> and <i>Epicoccum nigrum</i>. <i>Nat. Prod. Res.</i> 1–9</p>
<p>Construction of genetic toggle switches for application in <i>Corynebacterium glutamicum</i>. Master thesis, 2016</p>
<p>Structural and Functional Characterization of Thioredoxin reductase (TrxR) from <i>Thermococcus kodakarensis</i> KOD1. Bachelor thesis, 2010</p>